Examination Committee
Prof. dr. Ann Dumoulin (Chair, Ghent University)
Prof. dr. ir. Arne Verliefde (Ghent University)
Prof. dr. ir. Frederik Ronsse (Ghent University)
dr. Sylvie Gillot (Irstea)
Prof. dr. Carlos M. López Vázquez (UNESCO-IHE)
dr. ir. Stefan Weijers (Waterschap de Dommel)

Promotor
Prof. dr. ir. Ingmar Nopens
Department of Mathematical Modelling, Statistics and Bioinformatics
BIOMATH research group: Model-based analysis and optimisation of bioprocesses
Faculty of Bioscience Engineering
Ghent University

Dean
Prof. dr. ir. Guido Van Huylenbroeck

Rector
Prof. dr. Anne De Paepe

Youri Amerlinck

Model refinements in view of wastewater treatment plant optimization: improving the balance in sub-model detail.

Thesis submitted in fulfillment of the requirements
for the degree of Doctor (PhD) in Applied Biological Sciences

Dutch translation of the title:
Model verfijningen met het oog op de optimalisatie van waterzuiveringsinstallaties: het verbeteren van het evenwicht in detail van de model onderdelen.

Please refer to this work as follows:
Amerlinck, Y., 2015. Model refinements in view of wastewater treatment plant optimization: improving the balance in sub-model detail. PhD thesis, Ghent University, Belgium.

ISBN: 978-90-5989-834-9

Acknowledgements

"Eppur si muove!"
Galileo Galilei

"And yet she moves", Galileo Galilei purportedly muttered after torturers forced him to recant his theory that the earth orbits the sun. I guess Galilei and my admiration of stars and other stellar objects, is certainly the person that finally drew my interest towards science. Physics, chemistry and mathematics were adsorbed easily and following my interests I started and finished my studies as industrial engineer chemistry with option environment. After graduating, working at the industrial wastewater treatment plant of Levi Strauss gave me the opportunity to run a 60 m^3/h 'pilot plant' where I really learned the practical side of wastewater treatment processes, mechanics, electronics and control. I even got to disassemble and assemble pumps finally understanding what the pump courses were about.
When one door shuts another opens and so, in 1999, I got to start at HEMMIS. There and later at MOSTforWATER, I was introduced in a whole new wonderful world. Combining the expertise of information technology and water, i.e. the world of mathematical modelling. With Peter, at that time still in BIOMATH, I found an enthusiastic tutor and mentor with at least a million of ideas. During those years the idea grew of doing something more with this knowledge building up and when Ingmar gave me the opportunity to join BIOMATH, I didn't hesitate to jump into this new adventure.
Starting on the ADD Control project, with which I was already familiar gave me the perfect platform to integrate. Following up on the work of Webbey with the practical input from Gorka made it possible to make a giant leap forward. In those early days at the university Katrijn and Femke helped me a lot finding my way in the maze of the university (administrative) network.
After this first project, I could step into the Kallisto project with Waterboard de Dommel, modelling the WWTP of Eindhoven. The Kallisto project was a great innovative project with practical applications of mathematical modelling. The perfect playground so to say. With its enormous collection of data the modelling of the WWTP presented a lot of opportunities but also a lot of challenges (when the

results started deviating again from the measurements and delaying another dead line). I'm really grateful that after the Kallisto project Waterboard de Dommel decided to continue the collaboration with BIOMATH as such supporting my research, both financially as content wise. It was great having all those discussions with the water technologists (Tony, Victor, Peter, Oscar…) in Eindhoven and Boxtel.
At BIOMATH I got to learn and work together with some wonderful colleagues (Andreia, Ashish, Chaïm, Daan, Elena, Giacomo, Ivaylo, Jose, Katrijn, Lieven, Marina, Mehul, Michael, Niels, Severine, Sophie, Stijn, Stijn (Van Hulle), Thomas, Timothy, Tinne, Usman, Wim and Wouter), both on the job as outside. All of them contributed somehow to this work, i.e. assisting in the measurement campaigns, discussing results, helping out with matlab or python. In general the faculty has been a nice environment to work but also to meet great people (too many to mention one by one). I also guided quite a number of thesis students (Ellen, Faezeh, Giacomo, Hélène, Nazia and Veerle) who provided me with a lot of data feeding the models. In the final stage, Sebastiaan and Chris (University of Kwazulu-Natal) helped me a lot to find my way in the PHREEQ-C software.
In the end it was also great (and a challenge) to have a reading committee (Arne, Frederik, Sylvie, Carlos and Stefan) that took the time (I know 300 pages is not trivial) to read and critically comment on this work.

To all of you that I mentioned and those I unwillingly forgot: Thanks for all support!

Youri
Ghent, September 2015

For Sofie, Jarne, Matti and Lore;-)

Table of contents

List of abbreviations

1D	1-dimensional
AC	Alternating current
Al	Aluminium
AN01	Anaerobic tank section 1
AN02	Anaerobic tank section 2
AN03	Anaerobic tank section 3
AN04	Anaerobic tank section 4
ANN	Artificial Neural Network
AOTR	Actual oxygen transfer rate
ASM	Activated sludge model
ASM1	Activated sludge model number 1
ASM2	Activated sludge model number 2
ASM2d	Activated sludge model number 2d
ASM3	Activated sludge model number 3
ATU	Allylthiourea
bCOD	Biodegradable chemical oxygen demand
BEP	Best Efficiency Point
BOD	Biochemical oxygen demand
BOD_5	5-day biochemical oxygen demand
BOD_{10}	10-day biochemical oxygen demand
BSM	Benchmark simulation model
BSM1	Benchmark simulation model number 1
BSM2	Benchmark simulation model number 2
BT01	Aeration tank section 1
BT02	Aeration tank section 2
BT03	Aeration tank section 3
BT04	Aeration tank section 4
BT05	Aeration tank section 5
BT06	Aeration tank section 6
Ca	Calcium

CA	Cascade overflow from the activated sludge towards the SST
CFD	Computational fluid dynamics
COD	Chemical oxygen demand
COD_S	Soluble chemical oxygen demand
COD_T	Total chemical oxygen demand
COD_X	Particulate chemical oxygen demand
CSO	Combined sewer overflows
CSTR	Completely stirred tank reactor
DAF	Dissolved air flotation
DO	Dissolved oxygen
DP	Discrete phase
DT01	Denitrification tank section 1
DT02	Denitrification tank section 2
DWP	Diffuser dynamic wet pressure
EBPR	Enhanced biological phosphorus removal
EE	Elementary Effects
EHV-1	Version 1 of the Eindhoven WWTP model
EHV-2	Version 2 of the Eindhoven WWTP model
EHV-3	Version 3 of the Eindhoven WWTP model
EHV-4	Version 4 of the Eindhoven WWTP model
EHV-5	Version 5 of the Eindhoven WWTP model
EHV-6	Version 6 of the Eindhoven WWTP model
EHV-7	Version 7 of the Eindhoven WWTP model
EHV-8	Version 8 of the Eindhoven WWTP model
EHV-9	Version 9 of the Eindhoven WWTP model
EHV-10	Version 10 of the Eindhoven WWTP model
Fe	Iron
FIM	Fisher Information Matrix
GMP	Good modelling practice
G_F-L_S	Flowing gas – static liquid respirometric assay
G_S-L_S	Static gas – static liquid respirometric assay
HSA	German design rules
ICP-OES	Inductively coupled plasma optical emission spectrometry
IGV	Inlet Guide Vane
ISS	Inorganic suspended solids
IUWS	Integrated urban water system
K	Potassium

LCC	Linear correlation coefficient
Max	Maximum
MBR	Membrane bioreactor
Mg	Magnesium
Min	Minimum
MLSS	Mixed liquor suspended solids
Modified UCT	Modified University of Cape Town plant configuration
Na	Sodium
NH_4	Ammonium
NO_3	Nitrate
NRC	Normalized regression coefficient
OED	Optimal experimental design
OP	Operating point
$OP_{throttling}$	Operating point for outlet throttling control
OP_{VFD}	Operating point for VFD control
ORC	Ordinary regression coefficient
OT	Outlet Throttling
OTR	Oxygen transfer rate
OTE	Oxygen transfer efficiency
OUR	Oxygen uptake rate
OUR_{end}	Endogenous oxygen uptake rate
OUR_{ex}	Exogenous oxygen uptake rate
P_{Part}	Particulate phosphorus
PAO	Phosphate accumulating organisms
PBM	Population balance model
PCC	Partial correlation coefficient
PD	Positive displacement
PDD	Particle density distribution
PDE	Partial differential equation
PE	Population equivalent
PID	Proportional integral derivative
PO_4	Phosphate
PST	Primary sedimentation tank
PSD	Particles size distribution
PSVD	Particle settling velocity distribution
P&ID	Piping and instrumentation diagram
R	The universal gas constant
RAS	Return Activated Sludge
RMSE	Root mean square error

SCADA	Supervisory control and data acquisition
SOTE	Standard oxygen transfer efficiency
SPC	Semi-partial correlation coefficient
SRC	Standardized regression coefficient
SRT	Sludge retention time
SS	Suspended solids
SSE	Sum of squared errors
SST	Secondary sedimentation tank
Stdev	Standard deviation
STOWA	Acronym for Foundation for Applied Water Research in the Netherlands
tLCC	t-statistics of the linear correlation coefficient
tPCC	t-statistics of the partial correlation coefficient
tSPC	t-statistics of the semi-partial correlation coefficient
tSRC	t-statistics of the standardized regression coefficient
ThCOD	Theoretical chemical oxygen demand
TIS	Tanks-in-series
TKN	Total Kjeldahl nitrogen
TN	Total nitrogen
TP	Total phosphorus
TSS	Total suspended solids
UV-VIS	Ultraviolet-visible
VFA	Volatile fatty acids
VFD	Variable frequency drive
ViCAs	Vitesses de Chute en Assainissement (Effluent Settling Velocity)
VIF	Variance inflation factor
VOF	Volume of fluid
VSS	Volatile suspended solids
WDD	Waterschap de Dommel – Waterboard the Dommel
WFD	Water Framework Directive
WWTP	Wastewater treatment plant

Notation ASM fractions

S_B	Readily biodegradable COD
S_{VFA}	Fermentation products, considered to be acetate
S_F	Fermentable organic matter
S_U	Unbiodegradable soluble COD

S_{O2}	Dissolved oxygen
S_{NHx}	Ammonium plus ammonia nitrogen
S_{NOx}	Nitrate plus nitrite nitrogen
S_{N2}	Dissolved nitrogen gas
S_{PO4}	Phosphate
S_{Alk}	Alkalinity
XC_B	Slowly biodegradable COD
X_U	Unbiodegradable particulate COD
X_{Ig}	Particulate inorganic matter
X_{ANO}	Autotrophic nitrifying organisms
X_{OHO}	Ordinary heterotrophic organisms
X_{PAO}	Phosphorus accumulating organisms
$X_{PAO,Stor}$	Cell internal storage product of PAOs
$X_{PAO,PP}$	Stored polyphosphates in PAOs
X_{MEP}	Metal-phosphates
X_{MEOH}	Metal-hydroxides
X_{TSS}	Total suspended solids

PART I

Restoring the balance in the Eindhoven WWTP model

Chapter 1

General introduction

"Everything must be made as simple as possible. But not simpler."
Albert Einstein

1.1. SYMBOLS

n_p	Number of parameters in the model (-)
n_{sv}	Number of state variables in the model (-)
n_{tp}	Number of transformation processes in the model (-)
n_{TIS}	Number of tanks-in-series in the model (-)
$N_{C,A}$	Measure of complexity as proposed in this work (-)
$N_{C,G}$	Measure of complexity as proposed by Gujer (2006) (-)
$N_{Classes}$	Number of particle classes in the model (-)

1.2. CONCEPT

In the European Union, the Water Framework Directive (WFD) enforces a good ecological and chemical status of all surface waters, which is to be accomplished by 2015. Many surface waters throughout Europe still do not meet the WFD requirements due to discharges of combined sewer overflows (CSO) and effluents of wastewater treatment plants (WWTP). Mathematical models provide a valuable tool for guiding the decisions towards meeting the requirements set forth by the WFD.

One of the main challenges for the optimization of wastewater treatment plants, today, is the proper evaluation of all important performance indicators such as effluent quality (including priority pollutants), energy consumption and greenhouse

gas emissions. In order to come to an optimal solution, all relevant aspects need to be considered, as such reducing the uncertainty in the model outcome. It is generally acknowledged that the largest uncertainties are located in the description of influent, hydraulics, gas-liquid mass transfers and primary and secondary settling. A global sensitivity analysis performed by Benedetti et al. (2008) demonstrates that the importance of the biokinetic parameters is outweighed by the other parameters. The aeration parameters (oxygen transfer coefficients in the different tanks) are ranked as the second most important for predicting effluent ammonium concentration. In addition the aeration parameters are also important for the calculation of the operational cost, for which the primary sedimentation model parameter was the most important one.

Regardless this importance of the different sub-processes, WWTP models, to date, show a clear unbalance in the modelling of the different sub-processes, i.e. the models consist of highly detailed biokinetic models (Barker and Dold, 1997; Henze et al., 2000) but often lack detail of other critical processes carrying a considerable uncertainty. This unbalance can be quantified using an estimation of the complexity of the models (Table 1.1). Gujer (2006) proposed a comprehensive equation based on the number of state variables, transformation processes and locations (Equation 1.1). This equation, however, neglects the complexity that may be included in a single transformation process. For this reason an alternative equation was proposed here, replacing the number of transformation processes with the total number of parameters (Equation 1.2).

$$N_{C,G} = n_{sv} \cdot n_{tp} \cdot n_{TIS} \quad (1.1)$$

Where $N_{C,G}$ is a measure of complexity as proposed by Gujer (2006) [-], n_{sv} is the number of different state variables (components) considered [-], n_{tp} is the number of transformation processes in the model [-] and n_{TIS} is the number of tanks-in-series applied [-] to give an identification of the spatial resolution (i.e. the number of locations for which information is provided).

$$N_{C,A} = n_{sv} \cdot n_{p} \cdot n_{TIS} \quad (1.2)$$

Where $N_{C,A}$ is an adapted measure of complexity [-], n_p is the number of different parameters considered [-].

Considering the calculated complexity it is clear that the bio-kinetic models are overly complex compared to the other sub-process models (Table 1.1). The only model that seems to restore the balance is the particle settling velocity distribution (PSVD) model.

Table 1.1. Overview of the model complexity for the models of the different sub-processes WWTP models. Information of the biokinetic models is retrieved from Hauduc et al. (2013) and for the other sub-processes from this work.

Models	Refs	n_{tp}	n_{sv}	n_p	n_{TIS}	$N_{C,S}$	$N_{C,A}$
Activated sludge models							
ASM1	Henze et al. (2000)	8	13	26	12	1248	**4056**
ASM2d	Henze et al. (2000)	21	19	74	12	4788	**16872**
Barker & Dold	Barker and Dold (1997)	36	19	81	12	8208	**18468**
Aeration models							
kLa based		1	1	2	2	2	**4**
Rosso et al.	Rosso et al. (2005)	2 (5)	2	25	2	8 (20)	**100**
Primary sedimentation tank							
Ideal separation		1	1	2	1	1	**2**
Tay	(Tay, 1982)	1	1	3	1	1	**3**
Modified Tay	This work (section 6.4.3.1)	1	2	5	1	4	**10**
PSVD	This work (section 6.4.3.2)	3	10[(1)]	15[(2)]	20[(3)]	600[(4)]	**3000[(5)]**
Secondary sedimentation tank							
Ideal separation		1	1	2	1	1	**2**
Takacs	(Takács et al., 1991)	3	1	10	10	30	**100**
Bürger –Diehl	(Bürger et al., 2011)	4	1	14	20[(3)]	80[(6)]	**280[(7)]**
Aeration energy							
BSM1	Copp et al. (2002)	1	1	3	2	2	**6**
Dynamic	This work (Chapter 8)	1	1	23	2	2	**46**
Pumping energy							
BSM1	Copp et al. (2002)	1	1	1	6	6	**6**
Dynamic	This work (Chapter 9)	1	1	28	6	6	**168**

[(1)] $2 \times N_{Classes}$;[(2)] $5+2x\ N_{Classes}$;[(3)] N_{Layers} ;[(4)] $6 \times N_{Classes} \times N_{Layers}$;[(5)] $N_{Layers} \times (10 \times N_{Classes} + 4 \times N_{Classes}^2)$; [(6)] $4 \times N_{Layers}$; [(7)] $14 \times N_{Layers}$.

Belia et al. (2009) name the different levels of uncertainty as quantifiable uncertainty, scenario uncertainty, recognized ignorance and total ignorance. Here, quantifiable uncertainty is uncertainty that can be quantified and described in a statistical sense and can be attributed. On the other hand scenario uncertainty can be described with qualitative estimations of possible outcomes. The third level, recognized ignorance, is the state where fundamental uncertainty is acknowledged and, finally, total ignorance is defined as the state where a deep level of uncertainty exists. It is unknown what is unknown. Considering this uncertainty in the decision making process is crucial. In some cases it might be fair to settle for recognized ignorance, as long as it is being considered in the decision process, but total ignorance is unacceptable.

Restoring the balance in the WWTP models basically comes down to move from total ignorance towards quantifiable or scenario uncertainty. Moving away from total ignorance is pursued by incorporating more detail in the important processes. As such, the objective of this work is to include more detail in the sub-process models for influent characterization, primary sedimentation, oxygen transfer

(aeration) and energy consumption (aeration blowers and pumps) and showing its impact on the results and calibration of the biokinetic model.
On a side note, it has to be mentioned that uncertainty closely relates to the objectives of the modelling project and in some cases a simplification/reduction of the biokinetic model can be an option to restore the balance. E.g. if only NH4 removal and related oxygen consumption is studied a reduction from an overly complex model to an 'simpler' ASM1 model could give acceptable results as well.

1.3. OUTLINE

The PhD thesis consists of 6 major parts totalling in total 12 chapters. Three of these major parts address the sub processes for which more detail has been applied in the models to come to a more balanced modelling approach for the whole WWTP. A fifth part addresses the simulation methodology and tools applied. The first part introduces the concept of restoring the balance in the sub-models and the last part draws conclusions about the progress and future perspectives.

Part I: Restoring the balance in the Eindhoven WWTP model
Chapter 1 describes the unbalance in the different sub-models applied in whole treatment plant models and demonstrates the need for restoring the balance. **Chapter 2** gives a description of the WWTP of Eindhoven and the reference model that has been applied to compare the different models studied in this thesis.

Part II: Influent characterization
Evaluating the performance of a wastewater treatment plant (WWTP) requires a good characterization of the biodegradable substrate entering the plant. As is generally acknowledged, the wastewater characterization under rain or storm weather conditions is significantly altered. In **chapter 3** some hurdles regarding a better exploration of the impact of dilute wastewater conditions using respirometric assays are described and discussed.

Part III: Primary sedimentation
Primary sedimentation is a complex process involving flocculation, gravitational settling and drag. Gravitational settling in primary sedimentation tanks mainly occurs in the discrete particle settling and flocculent settling types, of which the behaviour is independent of the particle concentration but depends on the particle size distribution (and particle density distribution). A literature review on

modelling of primary sedimentation was conducted and the findings were reported in **chapter 4**.
In order to evaluate the performance of the primary sedimentation tanks at the WWTP of Eindhoven data was collected comprising of routinely collected data and data from 3 measurement campaigns. **Chapter 5** reports on the data analysis and possible correlations and the preparation of the data for the application within the modelling of the primary sedimentation in view of integration with the whole plant model.
Chapter 6 presents the results of the four different modelling approaches applied to explain different observations made during the data collection at the treatment plant and the integration with the whole treatment plant model.

Part IV: Aeration and energy consumption
Aerobic conversion is one of the most important steps applied in many WWTPs. Within these aerobic conversions, the oxygen transfer is often the rate limiting step. Even though the high importance, WWTP models often lack detail on the aeration part. In order to provide more information on the performance and behaviour of the oxygen transfer and to increase the level of detail in the models applied an extensive measurement campaign with off-gas tests was performed at the WWTP of Eindhoven. **Chapter 7** reports on the results of the off-gas tests and its implications in view of modelling the activated sludge process.
In addition, aeration is the largest energy consumer at wastewater treatment plants and **chapter 8** describes the development, calibration and application of a new dynamic model for a more accurate prediction of aeration energy costs in activated sludge systems, equipped with submerged air distributing diffusers (producing coarse or fine bubbles) connected via piping to blowers.
Pumping is the second largest energy consumer at wastewater treatment plants. To enable optimisation of pumping power consumption an accurate prediction of pumping costs at wastewater treatment plants is needed. In **chapter 9**, a generic dynamic model for a more accurate calculation of pumping energy consumption is proposed. The model is based on a description of the pump curve and the system curve. The model has been demonstrated for variable frequency drive controlled pumps. The model can also be used, but has not been validated, for throttling controlled pumps.

Part V: Simulation methodology
Mathematical modelling is state of the art practice in optimization of wastewater treatment plants. Notwithstanding this increased popularity, many questions remain regarding the fine tuning or calibration of the models. A calibration methodology

focusing on the restoration of the balance in the different sub-models of the WWTP of Eindhoven model is proposed. **Chapter 10** sheds light on the application of this calibration procedure for the wastewater treatment plant of Eindhoven.

Chapter 11 demonstrates an extremely simple yet effective colour-based evaluation method for system analysis, dealing with large data sets generated through the numerous simulations. The tool facilitates the search for specific information in these data sets, which is not always a trivial task especially when this information is hidden in intermediate variables that are not easily accessible.

Despite all the tremendous efforts put in modelling of the WWTP, uncertainty will always be inherent to the application of models. **Chapter 12** summarises how the interaction with the different stakeholders during a model based optimisation study proved to be really valuable for all parties and increased the acceptance of the modelling results, as such reducing the uncertainty of the decisions taking process.

Chapter 2

The WWTP of Eindhoven

"We are all in the gutter, but some of us are looking at the stars."
Oscar Wilde

2.1. SYMBOLS

a_1	Empirical parameters for chemical phosphate removal (-)
a_2	Empirical parameters for chemical phosphate removal (-)
a_{spec}	diffuser specific area (m²)
A_{Clar}	Surface area of the clarifier (-)
A	Calibration parameter of aeration model (-)
B	Calibration parameter of aeration model (-)
C_0	Dissolved oxygen concentration in the aerated tank (g O_2/m^3)
C_{sT}	Standard oxygen saturation concentration (g O_2/m^3)
C_s^*	Oxygen saturation concentration (g O_2/m^3)
C_{TSS}	Concentration of suspended solids (mg/l)
$C_{TSS,In}$	Influent concentration of suspended solids (mg/l)
d_{comp}	Compression function (m²/dl)
d_{disp}	Dispersion function (m²/dl)
f	Correction factor for averaging over the entire depth (-)
$f_{ns,XCOD}$	Non-settleable fraction for the particulate COD (-)
$f_{ns,XIg}$	Non-settleable fraction for the particulate inorganic fraction (-)
$f_{Out,DW}$	Fraction of the incoming flow rate going to the effluent (-)
H	Depth of the tank (m)
k_La	Oxygen transfer coefficient (1/d)

Me^0	Concentration of dosed metal (-)
N_d	Number of diffusers (-)
OTE	Oxygen transfer efficiency (%)
p_{atm}	Atmospheric pressure at standard conditions (101325 Pa)
p_{site}	Atmospheric pressure at test site (Pa)
$p_{w,site}$	Saturated water vapor pressure at test site (Pa)
$p_{w,std}$	Saturated water vapour pressure at standard temperature (2300 Pa)
P_{In}	Influent phosphate concentration (mol/l)
P_{Out}	Effluent phosphate concentration (mol/l)
Q_{Air}	Airflow rate (m^3/d)
Q_{In}	Incoming flow rate (m^3/d)
$Q_{In,DW}$	Average incoming flow rate during dry weather conditions (m^3/d)
$Q_{N,Air}$	Normalized airflow rate (1/d)
r	Stoichiometric coefficient of metals (-)
S	Suspended solids concentration in the effluent (mg/l)
S_0	Suspended solids concentration in the influent (mg/l)
t_r	hydraulic retention time (d)
T	Temperature of the water (°C)
T_A	half-removal time (d)
$T_{A,XCOD}$	half-removal time for the particulate COD (d)
$T_{A,XIg}$	half-removal time for the particulate inorganic fraction (d)
V_{Clar}	Volume of the primary sedimentation tank (m^3)
X_r	inlet mole fraction of oxygen (-)
Y_i	inlet mole fraction of oxygen (-)
Z	Diffuser submergence depth (m)
αSOTE	Product of α-factor and standard oxygen transfer efficiency (%)
β	Oxygen saturation concentration correction factor (-)
ρ_{Air}	Density of air (kg/m^3)
ρ_s	Density of the sludge (kg/m^3)
θ	temperature correction factor (-)
χ	Ratio of SRT over normalized air flow rate (-)

2.2. WATER BOARD THE DOMMEL

Waterboard The Dommel (WDD) is a Waterboard governing an area in the southern part of the Netherlands. The serviced area, including the city of Eindhoven, is about 1510 km² and has about 840000 inhabitants. WDD governs 8 municipal wastewater treatment plants and one sludge treatment facility (www.dommel.nl). In this area, the main river is the Dommel, which is a relatively small and sensitive river flowing through the city of Eindhoven from the Belgian border (South) into the river Meuse (North), receiving discharges from the 750,000 PE wastewater treatment plant (WWTP) of Eindhoven and from over 200 combined sewer overflows (CSOs) in 10 municipalities. In summer time, the WWTP effluent equals the base flow of 1.5 m^3/s of the Dommel River just upstream the WWTP. This contribution accounts for about 50% (during dry weather) and sometimes up to 90% (during rain weather) of the total flow in the river. Taking into account as well that when a storm event occurs an almost immediate effect occurs at the WWTP. I.e. the high flow rate arrives at the plant almost instantaneously and combined with the still present high dry weather concentration it causes an extremely high load. Whereas it takes more time for the CSOs to occur, i.e. the sewer first fills up. At that time the concentrations of pollutants has decreased and the CSO spills contain less pollution. The combination of these phenomena causes a significant stress from the WWTP upon the eco system.

The Dommel River does not yet meet the requirements of the European Union WFD. According to Waterboard the Dommel, which is managing the river basin including wastewater treatment, dissolved oxygen (DO) depletion, ammonia peaks and seasonal average nutrient concentration levels are the main water quality issues to be addressed (Weijers et al. 2012). These issues set forth the requirements for the model. i.e. the model has to be able to describe both dry weather and rain weather performance. Dry weather performance is required in view of describing the seasonal nutrient concentration levels and rain weather performance is required in view of the DO depletion and ammonia peaks.

2.3. PLANT DESCRIPTION

With a treatment capacity of 750,000 population equivalents (PE), the WWTP of Eindhoven (The Netherlands) is the largest treatment plant of Waterboard De Dommel and the third largest in The Netherlands. The WWTP of Eindhoven

receives wastewater from ten municipalities comprising many urban areas (Schilperoort, 2011). The entire system comprises an area of about 23 km in east-west direction and about 28 km in north-south direction (≈ 600 km2) in and around the city of Eindhoven. From this served area, three wastewater flows from three distinct catchment areas arrive at the influent pumping station of the WWTP (Figure 2.1). The three flows are respectively wastewater from the municipality of Eindhoven, wastewater from the municipalities Son en Breugel and Nuenen and wastewater from seven municipalities south of Eindhoven (Schilperoort, 2011). The latter flow also comprises the reject water from the sludge treatment facility in Mierlo.

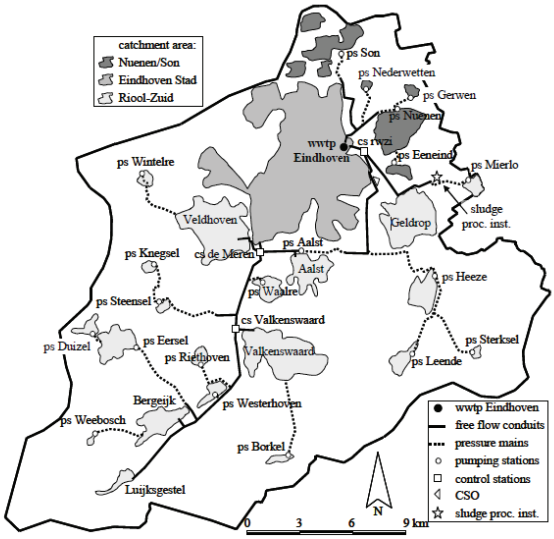

Figure 2.1. Area served by the WWTP of Eindhoven (Schilperoort, 2011).

At the WWTP of Eindhoven, the incoming wastewater is treated in three parallel lanes with a total plant maximum hydraulic load of 26,250 m^3/h (Figure 2.2). An extra 8,750 m^3/h can be treated, first mechanically and then it passes a pre-settling tank before it is discharged in the river Dommel or treated in the biological step when the hydraulic load would again drop below 26,250 m^3/h.

The water enters the plant in three influent pits, which are followed by coarse screens before the water flows into the influent pumping station, from where the wastewater is pumped up by Archimedes screws and released over fine screens into two parallel sand traps. After the sand traps the wastewater is distributed over three parallel circular primary sedimentation tanks (PST), each of which are completely covered in order to avoid odour nuisance. Downstream the primary sedimentation tanks the water is mixed again in an intermediate tank before it is pumped to the biological tanks.

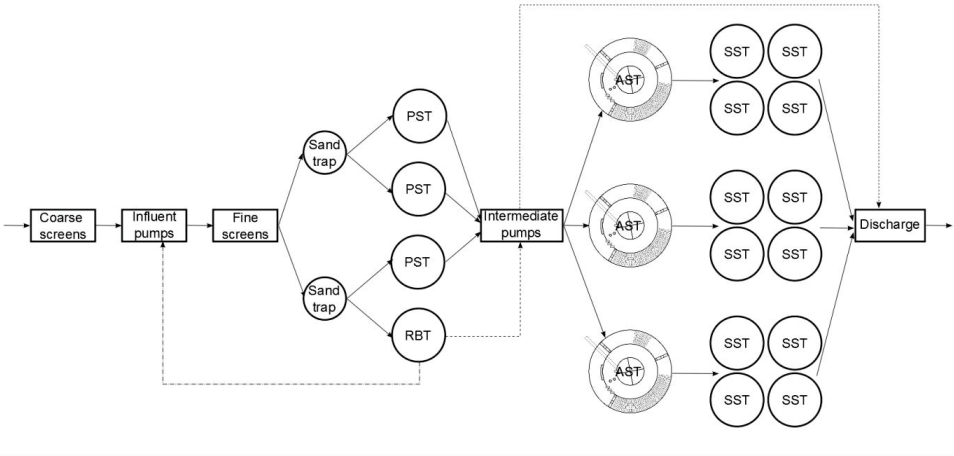

Figure 2.2. Schematic layout of the WWTP of Eindhoven, redrafted from Reitsma et al. (2007).

The WWTP has a modified UCT configuration (Tchobanoglous et al., 2004) and has 7 meter deep biological tanks (Figure 2.3). The inner ring is an anaerobic tank, the middle ring is an anoxic tank and the outer ring is a partially aerated tank. The aeration is provided by plate aerators in two separate aeration packages: a so-called summer package, which provides the aeration under normal dry weather conditions, and a so-called winter package, which provides aeration when the first package is not sufficient, mainly under rain weather conditions and cold temperatures. The airflow of the summer package is controlled by an ammonium (NH_4)-dissolved oxygen (DO) cascade feedback controller.

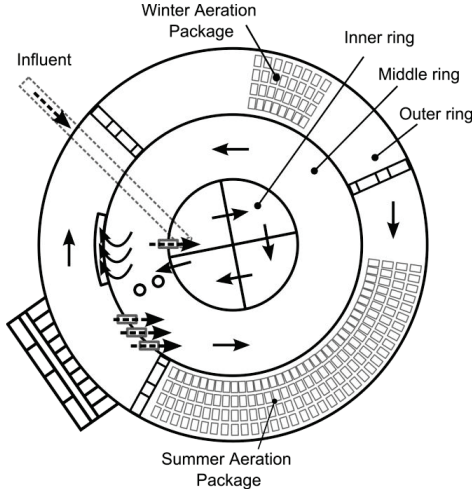

Figure 2.3. The circular modified UCT configuration of the activated sludge tanks at the WWTP of Eindhoven.

The mixed liquor of each of the biological tanks flows over in four secondary clarifiers. An extra 8,750 m^3/h can be treated mechanically and passes a pre-settling tank or rain buffer tank before it is discharged in the river Dommel or sent to the influent pumping station when the hydraulic load again drops below 26,250 m^3/h.

2.4. MODEL VERSIONS OF THE WWTP OF EINDHOVEN

2.4.1. Evolution of the Eindhoven WWTP model

Over the years several versions of a process model of the plant were set up and calibrated using WEST (mikebyDHI). With the first version EHV-1 (Table 2.1), the results of activated sludge models (ASM) were compared with the results of the semi-dynamic Excel-sheet based design tool HSA (Böhnke, 1989), which was used to design the WWTP. The Eindhoven WWTP model was implemented taking into account the reduced level of complexity used in the HSA approach. This meant that:

- only 1 treatment line was modelled, with its volume equal to the entire volume of the plant (in HSA the volume plays no role, it is all about sludge mass);
- each zone (inner, middle and outer ring) was modelled with only 1 completely stirred tank reactor CSTR (i.e. possible plug flow behaviour is ignored).
- The volume and flow data were determined by HSA and translated into ASM2d.
- The respective volumes of the outer ring are determined by the percentage specified in the HSA aerobic model (this percentage refers to the volumes of the middle and outer ring). This percentage varies over time with temperature. At lower temperatures nitrification slows down and thus additional aerobic volume is provided (winter package). Four different temperatures were adopted in HSA.

EHV-1 showed some flaws, mainly because of the fact that HSA's simplicity was mimicked. EHV-2 therefore uses a more realistic approach to model the biological tanks. This was necessary in order to obtain better predictions of NH_4 and NO_3 in the outer ring. EHV-2 accounts for plug flow behaviour, i.e. each zone was modelled with multiple CSTRs in series. The model comprised 4 tanks for the inner

ring (mimicking the baffled compartments), 4 tanks for the middle ring (arbitrary assumption) and 8 tanks for the outer ring (assuring the representation of aerobic and anoxic zones). The carrousel behaviour in both middle and outer rings was also reflected in the configuration. No improvement in the results for NH_4 and NO_3 were seen in EHV-2 and the general behaviour of the system was similar to EHV-1. Hence it was necessary to implement all controllers as described in the design manual of the plant in version EHV-3. These controls include: Recycle A (anaerobic recycle from middle ring to inner ring), Recycle B (nitrate recycle from outer ring to middle ring), dissolved oxygen (DO) control and the Return Activated Sludge (RAS) control.

Model versions EHV-1 to 3 were used for steady state evaluations. Model version EHV-4 was developed for dynamic evaluations, as dynamic data for the influent from an S::CAN probe became available. It was also decided to use the logged data on operational settings, such as aeration (airflow rate) and recycle flow rates as model inputs. In this way the calibration of the biokinetic part and the controllers was decoupled. Based on the high degree of mixing, the number of CSTRs used in the outer ring was reduced from 8 to 6. Although calculations using the Peclet number and an empirical formula derived by Thomas et al. (1989) indicated 5 CSTRs an additional CSTR is foreseen in order to account for the different (inlet, outlet, recycle and aeration) zones. The aeration model was upgraded from a mere oxygen transfer coefficient (k_La) based model to a model calculating oxygen transfer from the airflow rate taking into account a dependence of total suspended solids (TSS). The aeration model was initially developed for MBRs (Maere et al., 2011) but recalibrated for the WWTP of Eindhoven. In version EHV-5 the number of CSTRs in the middle ring was reduced from 4 to 2. The better description of the mixing behaviour gave another (slight) improvement in the simulation results. The model was then upgraded, in the frame of a global sensitivity analysis study, to version EHV-6. This version included a storm tank model, a primary sedimentation tank model (a point settler model), a more detailed implementation of the controllers and a model of the cascade, which provides re-aeration, in between the activated sludge tanks and the secondary clarifiers. In version EHV-7 a new model for the aeration, based on the work of Rosso et al. (2005), was implemented (Cierkens et al., 2012). In the EHV-8 version of the model more attention was given to the wet weather behaviour. Hereto the primary sedimentation tank PST model was upgraded to a model taking into account the effect of the hydraulic retention time on the removal efficiency (Tay, 1982). The model of the secondary sedimentation tank was upgraded from the Takacs model (Takács et al., 1991) to a model with a more sound mathematical structure allowing improved prediction of the sludge blanket height (by including compression settling) and underflow

concentration during wet weather (Bürger et al., 2012). Also more detail (e.g. wet weather rules) in the modelling of the controllers was introduced. Finally, a model for chemical phosphorus removal was added. This model was based on the model of Briggs (de Haas et al., 2000), which describes an empirical relation between the metal dosing and the chemical phosphorus removal. The version of the model EHV-8 performed well, during dry weather, on all considered parameters (Suspended solids, dissolved oxygen, and ammonium concentrations) except for nitrate concentrations. In version EHV-9 this was tackled by upgrading the model of the primary sedimentation taking into account different removal efficiencies for the different suspended fractions, based on the results of a measurement campaign performed on the PSTs. This resulted in a higher COD concentration entering the activated sludge tanks, improving the nitrate removal.

Table 2.1. Increasing detail in the sub-models over the different versions of the WWTP Eindhoven model.

Version	Description
EHV-1	Based on HSA
EHV-2	Adaptation of the model to include plug flow behaviour
EHV-3	Simple algorithms are used for the controllers
EHV-4	Aeration model (dependence to TSS) was implemented in ASM2d (Maere et al., 2011)
EHV-5	Mixing behaviour was tested changing the number of tanks in series for the middle ring
EHV-6	Controllers (Aeration, sludge wastage, recycles) were implemented
EHV-7	New Aeration model including dependence to SRT and Airflow (Rosso et al., 2005)
EHV-8	New models for PST (Tay, 1982), SST (Bürger et al., 2012) and Chemical P removal.
EHV-9	New model for the PST (extension of the Tay model)

2.4.2. MODEL VERSION EHV-10

This section illustrates the WWTP of Eindhoven model version (EHV-10), which is developed within the framework of the project leading to this thesis. For the final write up, having the need for a reference model, it was used as the starting point for comparison. The EHV-10 version is an upgrade of EHV-9, compliant with WEST2014 (mikebydhi), mainly intended as the starting point for the new developments. A detailed description is given in Appendix A.

Actually, EHV-10 consists of two models of the WWTP. The first model uses input files (based on online measurement data) to mimic the most important control actions, without implementing those explicitly. The goal of this model is model calibration, in particular the process models such as the primary sedimentation tank, aeration or biochemical model. Using online measurements avoids a bias caused by the control actions, i.e. the controllers attempt to correct for the imperfect model of the physical system, on the normal behaviour of the plant. In

the second model those control actions are implemented explicitly, i.e. the online data (input files) are replaced by models of the controllers. The second model is used within the integrated urban water system model of Eindhoven (Benedetti et al., 2013; Langeveld et al., 2013a). Given the complexity of the integrated model, some complexity of the WWTP model is sacrificed. This work will focus on the first model and is really intended to improve the detailed description of the plant behaviour under dry and wet weather conditions.

PART II

Influent characterization

Chapter 3

Investigation of influent fractionation under diluted wastewater conditions

"I have not failed. I've just found 10,000 ways that won't work."
Thomas A. Edison

3.1. ABSTRACT

Evaluating the performance of a wastewater treatment plant (WWTP) requires a good characterization of the biodegradable substrate entering the plant. As is generally acknowledged, the wastewater characteristics under rain or storm weather conditions vary significantly. A measuring campaign was set up and samples were analysed using respirometric assays. In this chapter some hurdles regarding a better exploration of the impact of dilute wastewater conditions using respirometric assays are described and discussed. The dependence of the heterotrophic yield on different substrates severely hampers the evaluation of the respirograms under dilute wastewater conditions. In addition, the low load conditions limit the application of the assays due to insufficient sensitivity of the experiment and uncontrolled oxygen inputs. The results clearly demonstrate the need for further research in order to allow for a proper evaluation of WWTP performance under rain and storm weather conditions.

3.2. SYMBOLS

$bCOD_R$	bCOD in the reactor (mg/l)
$bCOD_{WW}$	bCOD in the wastewater (mg/l)
k_La	gas-liquid oxygen transfer coefficient (1/d)

Q_{In}	Influent flow rate (m^3/d)
Q_{Out}	Effluent flow rate (m^3/d)
S_{O2}	Dissolved oxygen concentration in the reactor (mg/l)
$S_{O2,Eq}$	Equilibrium dissolved oxygen concentration (mg/l)
$S_{O2,In}$	Influent dissolved oxygen concentration (mg/l)
$S_{O2,Sat}$	Dissolved oxygen concentration at saturation (mg/l)
S_0	Initial substrate concentration (mg/l)
t_{final}	Endpoint of the integration interval (min)
t_x	chosen end point (min)
t_0	Chosen starting point (min)
t_{98}	Response time after which 98% of the signal is reached
V_R	Liquid volume in the reactor (m^3)
V_{WW}	Volume wastewater added (m^3)
X_0	Initial biomass concentration (mg/l)
Y_{OHO}	Heterotrophic biomass Yield (mg cell COD/mg COD)
Y_{obs}	Observed biomass Yield (mg cell COD/mg COD)
ΔO_2	Change in oxygen concentration (mg/l)
Δt_S	Time to degrade the biodegradable matter in the wastewater (min)
Δt_x	Time interval (t_x-t_0) for the linear part in the semi-logarithmic plot (min)

3.3. INTRODUCTION

Any (model based) design or optimization study of biological wastewater treatment plants (WWTP) requires a determination of the biological degradability of the carbonaceous substrate, expressed as chemical oxygen demand (COD). The inert particulate COD affects the sludge production, whereas the inert soluble COD is a major fraction of the effluent COD (Choubert et al., 2013). Furthermore, the biological degradable carbonaceous substrate (bCOD) determines largely the oxygen demand and its variation clearly affects denitrification, enhanced biological phosphorus removal and high rate activated sludge performance as all these processes depend on the input of bCOD and therefore a good characterisation is crucial for their design and operation. In addition, the available oxygen supply at a WWTP is regularly limiting for nitrification during storm events. An accurate

estimation of the oxygen demand related to the bCOD allows for a better appraisal of the available capacity for the nitrification.

Temporal (daily, seasonal and weather dependent) variation in flow rates and loading is an acknowledged phenomenon at WWTPs (Henze, 2008; Tchobanoglous et al., 2004) and heavily influences the performance of the WWTP. However, the corresponding temporal variation in biological degradable (carbonaceous) substrate (bCOD) and its ratio over total COD, has received far less attention. Choubert et al. (2013) showed examples where, during dry weather, the readily biodegradable COD (S_B) fraction varies between 5 and 25% of the total COD over a period of a few hours. Lagarde et al. (2005) sampled two different types of sewers during several rain weather days. The analysis revealed variations in total COD concentrations from 220 to 515 mg/l. The readily biodegradable fraction ranged between 24% and 32% of the total COD, while the slowly biodegradable fraction ranged from 40% to 49%.

For the determination of bCOD, respirometric tests have been applied varying in either measurement variables or in substrate to biomass ratio (S/X) (Choubert et al., 2013). Choubert et al. (2013) further elaborate on the various protocols, of which the most typical are (i) respirometric monitoring of the oxygen uptake rate for a few hours with a low substrate to biomass ratio (S/X) (Sperandio et al., 2001; Vanrolleghem et al., 2003), (ii) ultimate biochemical oxygen demand (BOD) tests monitoring the total oxygen uptake for 10 days with a high S/X ratio (Roeleveld and van Loosdrecht, 2002), or (iii) monitoring the COD uptake versus time (total and soluble) for 30 days with a high S/X ratio (Lesouef et al., 1992; Orhon et al., 1997; Stricker et al., 2003).

Despite the increased attention, still no measurement campaign has demonstrated the (fast) dynamics occurring under rain and storm water conditions with regard to the biodegradable COD fraction. Understanding these variations requires extensive measurement campaigns. As described above Lagarde et al. (2005) investigated the use of respirometry for influent fractionation for samples collected under various rain conditions. However, the total COD concentration for their samples lies between 220 and 515mg COD/l, which is in the high range, considering that Bixio et al. (2000) reported an average total COD value of about 300 mg COD/l for the WWTP of Ghent.

In order to evaluate the performance of a WWTP under rain or storm weather conditions it is crucial to have a clear view on the quantity of biodegradable substrate entering the plant. The quantity of biodegradable substrate in the wastewater is known to be varying significantly. In order to quantify these variations separate samples were collected and a measurement campaign was set up in rain weather conditions.

This chapter highlights some of the hurdles encountered when setting up a measurement campaign for determining the wastewater fractionation under rain or storm weather conditions. In order to quantify the possible variations in influent fractions a measurement campaign was set up. The samples collected were consecutively analysed using respirometric assays. The respirometric assays were assessed for the impact of low COD and bCOD concentrations and possible improvements are proposed. Furthermore, the experiments and improvements are verified for their applicability in high frequency (e.g. hourly composite samples) measurement campaigns.

3.4. MATERIALS AND METHODS

The respirometric analysis applied in this work comprises of measuring the dissolved oxygen concentration and subsequently deriving the oxygen uptake rate (OUR) in order to determine the biodegradable COD fraction in the wastewater. The respirometer consists of a titrimetric and a respirometric unit (Figure 3.1).

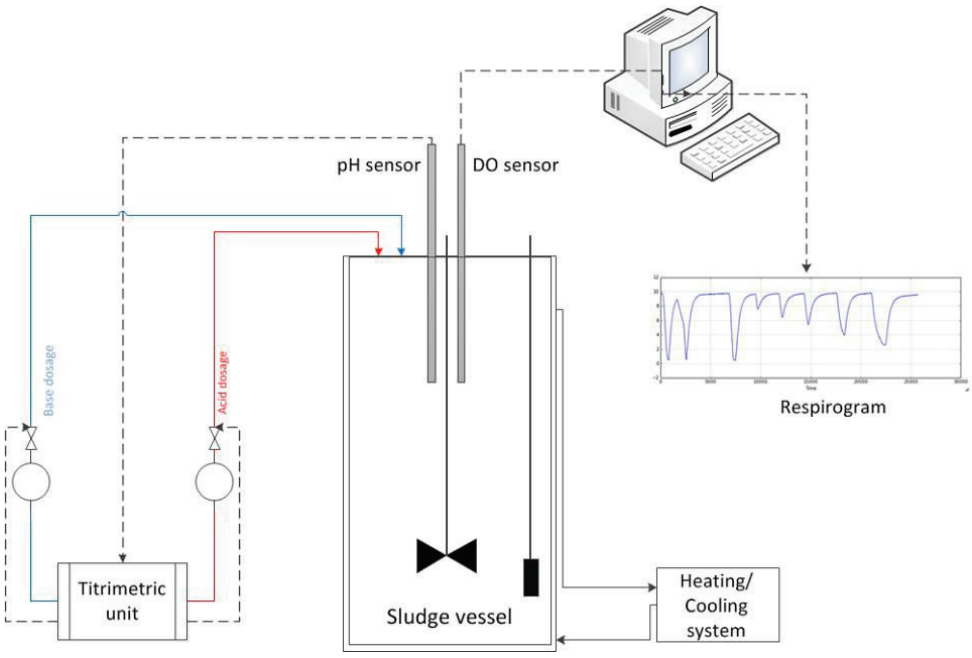

Figure 3.1. General flow scheme of the respirometer

The respirometric unit consists of a 2L double-glass vessel, kept at a constant temperature of 20°C by means of a cooling system (Lauda Alpha RA8; VWR),

which pumps water through the heat-jacked reactors. The sludge is constantly mixed at a speed of 100 rpm and aerated with the aid of an aeration stone at a constant airflow rate.
The titrimetric unit is composed of one 1L acid mariotte bottle, one 2L base mariotte bottle, one Gilson pump (Minipuls 3; Analis) and two solenoid valves that dose the titrimetric solution to the reactor. The Gilson pump continuously recycles the acid solution (1M HCl) and the base solution (1M NaOH). The solenoid valve is opened when the pH in the reactor deviates more than 0.1 units from the pH set point (7.5) and base or acid is consequently dosed to the reactor. The acid and base dosage system is calibrated by collecting and weighing the volume of acid and base dosed during a fixed number (35) of subsequent pulses.
LabView (National Instruments, USA) is used for monitoring, control and data acquisition of the respirometer. Dissolved oxygen and pH are measured using a Led dissolved oxygen (LDO) probe (LnPro68701/12/220; Mettler Toledo, Elscolab) and pH probe (GA405-DXK-S8/120 PN: 104054287; Mettler Toledo, Elscolab). The probes are connected respectively to an oxygen transmitter (M400 Type 2) and a pH transmitter (Knick Stratos 2401). Communication between the transmitters and labview is based on 4-20 mA signals. Before starting a respirometric assay, the pH probe and LDO probe and their communication to the transmitters are calibrated. The LDO probe has an accuracy of 1% (with a minimum of 8 ppb) and a response time after which 98% of the signal has been reached (t_{98}) of less than 20 seconds.

3.4.1. Respirometric assays

Several types of respirometric assays exist and can be classified according to the behaviour of both the liquid and gas phase (Spanjers et al., 1998; Young and Cowan, 2004). In this research the flowing gas – static liquid(G_F-L_S) method and the static gas – static liquid (G_S-L_S) method are applied.
At the start of both assays, the reactor is filled with 1.9 liter of mixed liquor, which was aerated overnight until endogenous respiration was reached, collected from the biological tank from either the WWTP of Eindhoven (operated by Waterboard de Dommel) or the WWTP of Roeselare (operated by Aquafin NV). Nitrification is inhibited by adding allylthiourea (ATU) to the reactor at a concentration of 10 mg/L. Finally the reactor is operated depending on the selected method and a wastewater sample is added. The OUR is calculated (Equation 3.1) by making a general mass balance for dissolved oxygen over the liquid phase (Spanjers et al., 1998):

$$\frac{d(V_L \cdot S_{O2})}{dt} = Q_{In} \cdot S_{O2,In} - Q_{Out} \cdot S_{O2} + V_R \cdot k_L a \cdot \left(S_{O2,Sat} - S_{O2}\right) - V_R \cdot OUR \qquad (3.1)$$

where V_R is the liquid volume in the reactor [m³], Q_{In} and Q_{Out} are the incoming and outgoing flow rate respectively [m³/d], $S_{O2,In}$ is the dissolved oxygen concentration in the incoming flow [mg/l], S_{O2} is the measured dissolved oxygen concentration in the reactor (assuming completely mixed conditions) [mg/l], k_La is the gas-liquid oxygen transfer coefficient [1/d] and $S_{O2,Sat}$ is the dissolved oxygen concentration at saturation (at a certain temperature) [mg/l].

Upon the addition of wastewater, the microorganisms will start oxidizing the bCOD, thereby using dissolved oxygen, which results in an increase in the oxygen uptake rate (OUR), i.e. the exogenous respiration (OUR_{ex}) adds on to the endogenous respiration (OUR_{end}). Once bCOD is depleted, oxygen demand for aerobic respiration decreases and reaeration gains in importance again. This results in an increase in DO and simultaneously a decrease in OUR until the original endogenous level is reached (Nopens, 2010; Orhon and Okutman, 2003; Vanrolleghem et al., 1999).

Integrating the surface under the OUR curve provides the total amount of oxygen consumed at the expense of all degraded substrate (Figure 3.2). From the amount of oxygen consumed the bCOD is calculated (Equation 3.2), for which knowledge of the heterotrophic biomass Yield (Y_{OHO}) is indispensable (Barnett et al., 1998; Petersen, 2000; Vanrolleghem et al., 1999). For municipal wastewater a value of 0.67 gCOD/gCOD for Y_{OHO} is deemed appropriate and generally accepted (Fall et al., 2011; Kappeler and Gujer, 1992).

$$bCOD_R = \frac{1}{(1-Y_{OHO})} \int_0^{t_{final}} OUR \, dt \qquad (3.2)$$

where $bCOD_R$ is the bCOD in the reactor [mg/l] and t_{final} is the endpoint of the integration interval, i.e. the time instant for which the endogenous state is reached again [min]. The concentration of biodegradable COD in the wastewater ($bCOD_{WW}$) is then determined by taking into account a dilution factor (Equation 3.3).

$$bCOD_{WW} = bCOD_R \frac{V_R}{V_{WW}} \qquad (3.3)$$

where $bCOD_{WW}$ is the biodegradable COD in the wastewater [mg/l], V_R is the liquid volume (activated sludge plus wastewater) in the reactor (after addition of the wastewater) [m³] and V_{WW} is the volume of the wastewater used in the experiment [m³] (Gatti et al., 2010; Orhon and Okutman, 2003; Vanrolleghem et al., 1999).

The bCOD is composed of two major fractions, i.e. the readily biodegradable substrate (S_B) and the slowly biodegradable substrate (XC_B). In some respirograms a separation of both fractions can be segregated (Figure 3.3). However, the isolation of both fractions, based on the shoulder in the respirogram is not always

straightforward. This is due to the difficulty in determining the infliction point indicating the beginning of the shoulder.

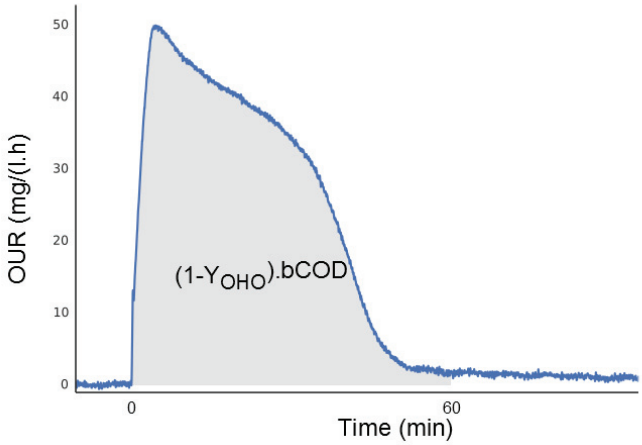

Figure 3.2. Calculation of bCOD from the OUR curve obtained from the addition of 0.25l of wastewater taken before the PST into 1.9 l of mixed liquor of the WWTP of Eindhoven.

The readily biodegradable fraction is composed of small molecules, such as volatile fatty acids, carbohydrates, alcohols, peptones and amino acids that can be directly metabolized (Henze, 1992). The S_B fraction is degraded rapidly, resulting in a fast respirometric response (Vanrolleghem et al., 1999). The concentration of S_B is calculated using equation 3.2 and 3.3 but limiting to the surface above the first shoulder in the OUR curve (Figure 3.3).

The slowly biodegradable substrate (XC_B) fraction is composed of high-molecular weight compounds made up of soluble, colloidal and particulate COD fractions (Henze, 1992). These compounds need to be hydrolysed to low-molecular weight compounds (S_B) by extracellular enzymes produced by bacteria prior to further degradation as they cannot pass the cell membrane as such (Pasztor et al., 2008). The degradation of these compounds results in a slower respirometric response than for S_B because the hydrolysis rate is significantly lower than the oxidation rate of S_B (Petersen, 2000). The concentration of XC_B in the wastewater can be determined in a similar way as for S_B (Kappeler and Gujer, 1992; Sollfrank and Gujer, 1991), using equations 3.2 and 3.3 but limiting to the surface under the first shoulder in the OUR curve (Figure 3.3).

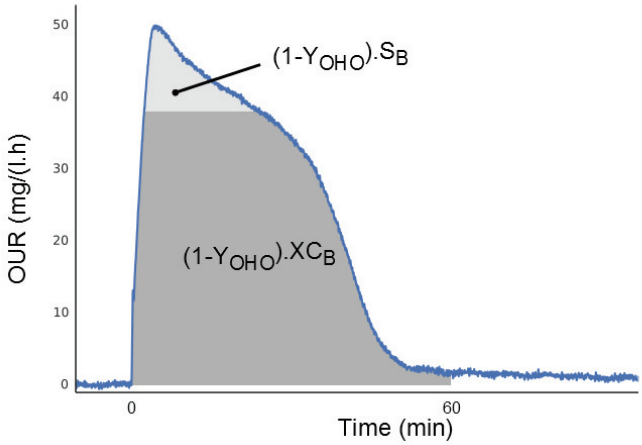

Figure 3.3. Calculation of S_B and XC_B from the OUR curve obtained from the addition of 0.25l of wastewater taken before the PST into 1.9 l of mixed liquor of the WWTP of Eindhoven.

3.4.1.1. The flowing gas – static liquid(G_F-L_S) respirometric assay

During the flowing gas – static liquid(G_F-L_S) method the batch reactor is continuously aerated (flowing gas) while the liquid is kept in the reactor (static liquid)(Spanjers et al., 1998). For this assay the following consecutive steps are proposed: (i) the determination of the equilibrium dissolved oxygen concentration in mixed liquor ($S_{O2,Eq}$), (ii) the estimation of the oxygen transfer coefficient (k_La) and (iii) the measurement of the exogenous oxygen uptake rate (OUR_{ex}).

The first step is the determination of the equilibrium dissolved oxygen concentration in mixed liquor ($S_{O2,Eq}$). $S_{O2,Eq}$ represents the equilibrium between oxygen transfer and endogenous respiration and is determined by aerating the mixed liquor in the reactor for approximately 30 min until a stable equilibrium concentration of dissolved oxygen is obtained.

The second step is the estimation of the oxygen transfer coefficient (k_La) based on a dynamic gassing out method (Figure 3.4). First, the aeration is stopped until a dissolved oxygen concentration of approximately 1.5 mg/L is reached (Bandyopadhyay and Humphrey, 2009). Then the aeration is started again and the k_La is calculated from the re-aeration curve (Equation 3.5).

$$\frac{dS_{O2}}{dt} = k_La \times \left(S_{O2,Eq} - S_{O2}\right) \quad (3.4)$$

$$\frac{\ln(S_{O2,Eq}-S_{O2,tx})-\ln(S_{O2,Eq}-S_{O2,t0})}{\Delta t_x} = -k_La \quad (3.5)$$

where Δt_x is the time interval (t_x-t_0) for the linear part in the semi-logarithmic plot [min], t_0 is the chosen starting point [min] and t_x the chosen end point [min]. By

plotting ln($S_{O2,Eq}$ - $S_{O2,tx}$) versus time, k_La [1/min] can be deduced as the negative slope of this curve.

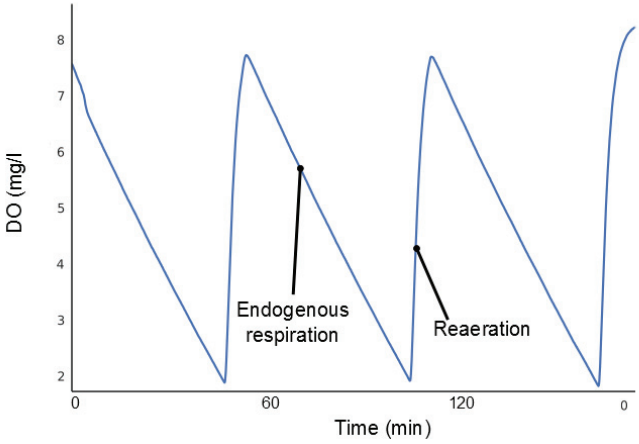

Figure 3.4. Dynamic gassing out method with three repetitions for the determination of k_La.

Gas flow, bubble size, reactor dimensions, stirring of mixed liquor (turbulence and sludge flocculation state), temperature of mixed liquor, and air pressure have a major influence on k_La. Therefore the following conditions must be ensured during the subsequent experiments (Ros et al., 1988): (i) a constant airflow through the whole experiment, (ii) a reactor with known volume and shape has to be used for all measurements, (iii) constant stirring must be provided and (iv) a constant temperature of mixed liquor during the measurements.

The third step, finalising the respirometric assay, is the determination of the exogenous OUR by adding a specific volume of substrate (in this work wastewater) to the mixed liquor and measuring the dynamic response of dissolved oxygen concentration. Based on the latter the OUR profile (Figure 3.3) can be derived from equation 3.6.

$$\frac{dS_{O2}}{dt} + OUR_{ex} = k_L a \times \left(S_{O2,eq} - S_{O2}\right) \quad (3.6)$$

3.4.1.2. The static gas – static liquid (GS-LS) respirometric assay

During G_SL_S of respirometric assays aeration in the batch reactor is stopped (static gas) before dosing the sample while the liquid is kept and only stirred in the reactor (static liquid)(Spanjers et al., 1998). For this assay the following consecutive steps are performed: (i) aerating the mixed liquor in the reactor until a dissolved oxygen concentration of about 8 mg/l is reached, (ii) stopping the aeration and monitoring the (endogenous) respiration rate until the oxygen concentration has dropped about

1.5 mg/l and (iii) dosing the substrate and monitoring of the total oxygen uptake rate (OUR), which is the sum of both endogenous and exogenous respiration.
During this type of assay the mass balance of equation 3.1 reduces to equation 3.7 (Drtil et al., 1993; Gernaey et al., 2001a).

$$\frac{dS_{O2}}{dt} = -OUR \qquad (3.7)$$

During phase I, oxygen is utilized at a constant rate, which is determined by the endogenous activity or respiration (OUR_I) of the microorganisms in the activated sludge (Figure 3.5). At a certain time, a known volume of substrate is added to the batch reactor resulting in a temporary increase in respiration rate (OUR_{II}) due to substrate degradation, i.e. exogenous activity (phase II). The increased respiration can be noticed by an increased slope in the DO curve. If the substrate is completely degraded and removed (phase III), the respiration returns to the endogenous activity (OUR_{III}), with the same slope in the DO curve as before the substrate addition.

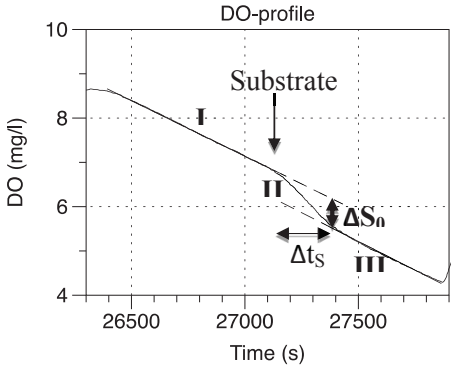

Figure 3.5. DO-profile obtained after addition of 13.6 mg of sodium acetate trihydrate to 1.9 l of mixed liquor of the WWTP of Roeselare.

According to Vanrolleghem (2002) the differential term in equation 3.7 can be approximated with a finite difference term resulting in the following derivation for bCOD (equation 3.8), which will be referred to as direct parameter abstraction method.

$$bCOD_{WW} = \frac{(OUR_{II} - OUR_I)\Delta t_S}{1 - Y_{OHO}} \frac{V_R}{V_{WW}} \qquad (3.8)$$

Where $bCOD_{WW}$ is the biodegradable COD in the wastewater [mg/l] and Δt_S is the time needed to degrade the biodegradable matter present in the wastewater [min].
For the direct parameter abstraction method, in order to calculate the confidence intervals on the calculations, the combined standard uncertainties are calculated using the summation in quadrature method (BIPM et al., 1993). Multiplying the combined standard uncertainty with a coverage factor of 2 (for a confidence level

of 95%) yields the expanded uncertainty, which can be used as estimate to the confidence intervals.

3.4.1.3. Automatic parameter estimation for dynamic process models

As an alternative to the direct parameter abstraction method, as described above, a model based evaluation, using dynamic process models including activated sludge models (Henze et al., 2000), is evaluated as well. The model was implemented in the WEST (mikebyDHI) taking into account the respirometer configuration. The configuration (Figure 3.6) reflects the actual set-up and consists of a sample container, 2 timers and respirometer. The first timer controls the timing and volume of the sample dosed in the respirometer, whereas the second timer controls the aeration. The biological reactions in the respirometer are dynamically modeled based on activated sludge models (ASM). Either ASM1 or ASM3 (Henze et al., 2000) were selected.

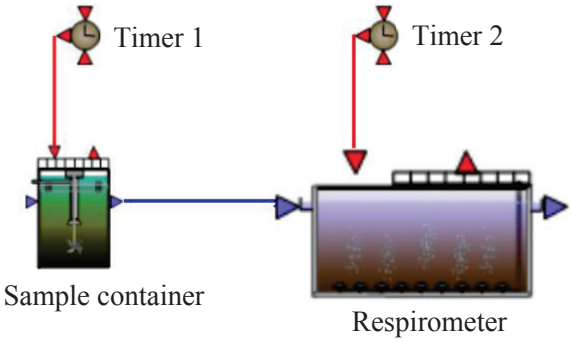

Figure 3.6. Configuration of the respirometer in WEST (mikebyDHI)

To fit the model to the experimental data sets, automatic parameter estimation experiments are performed. During parameter estimation a unique set of model parameters, resulting in the best fit of the model prediction to the experimental data, is searched for. This is achieved by minimization of an objective function, which is the root mean square error (RMSE) between simulation data and measured oxygen profiles. Two different optimisation algorithms are used, namely the simplex method (Nelder and Mead, 1965b) or the Praxis method (Brent, 1973). In first instance, for the G_SL_S respirometric assays, the initial values describing the endogenous respiration behaviour of the respirometer are estimated on the oxygen profiles before the addition of the wastewater sample. In second instance, the concentration of biodegradable COD in the sample is estimated with the total curve. In last instance the uncertainty bounds on the estimated parameters are

determined using the inverse of the Fisher Information Matrix (FIM) (Donckels, 2009).

3.4.2. Wastewater fractionation according to STOWA

In order to quantify the removal efficiency for the different activated sludge model (ASM) components as used in the remainder of the whole plant model of the WWTP of Eindhoven, the wastewater before and after the primary sedimentation tanks is fractionated according to the STOWA protocol (Roeleveld and van Loosdrecht, 2002).
For the activated sludge model n°2d (ASM2d) the carbon fractions are defined in COD (Henze et al., 2000). The total COD (COD_T) is the sum of the different carbonaceous components (Equation 3.9).

$$COD_T = S_{VFA} + S_F + S_U + XC_B + X_U + X_{PAO} + X_{OHO} + X_{ANO} \quad (3.9)$$

The COD fractions are divided into soluble (S) and particulate (X) components and a further division is made on the biodegradability, subscript B for biodegradable or subscript U for non-biodegradable (Corominas et al., 2010). In this study, the different COD fractions are calculated (Equation 3.10-3.17) from the physical-chemical analyses as proposed by STOWA (Roeleveld and van Loosdrecht, 2002).

$$S_U = 0.9 \cdot COD_{Eff,S} \quad (3.10)$$

Where S_U is the concentration of inert soluble COD [mg/l] and $COD_{Eff,S}$ is the effluent soluble COD[mg/l].

$$S_B = COD_{Inf,S} - S_U \quad (3.11)$$

Where S_B is the concentration of readily biodegradable COD [mg/l] and $COD_{Inf,S}$ is the influent soluble COD [mg/l].

$$S_B = S_{VFA} + S_F \quad (3.12)$$

Where S_{VFA} is the concentration of volatile fatty acids [mg/l] and S_F is the concentration of fermentation products [mg/l].

$$XC_B = bCOD - S_B \quad (3.13)$$

Where XC_B is the concentration of slowly biodegradable COD [mg/l] and bCOD is the biodegradable COD [mg/l].

$$X_U = COD_{Inf,T} - S_U - S_B - XC_B - X_{OHO} - X_{ANO} - X_{PAO} - X_{PAO,Stor} \quad (3.14)$$

Where X_U is the concentration of inert particulate COD [mg/l], X_{OHO} is the concentration of heterotrophic organisms [mg/l], X_{ANO} is the concentration of nitrifying organisms [mg/l], X_{PAO} is the concentration of phosphate accumulating organisms [mg/l], $X_{PAO,Stor}$ is the concentration of cell internal storage products of the X_{PAO} [mg/l] and $COD_{Inf,T}$ is the influent total COD [mg/l]. The concentrations of X_{ANO}, X_{PAO} and $X_{PAO,Stor}$ are typically considered to be negligible, which reduces equation 3.14 to equation 3.15.

$$X_U = COD_{Inf,T} - S_U - S_B - XC_B - X_{OHO} \quad (3.15)$$

The influent ($COD_{Eff,S}$) and effluent soluble COD ($COD_{Inf,S}$) concentration are, after flocculation and filtration through a 0.45 µm filter, determined with a spectrophotometer with HACH-LANGE kits for COD (LCK 614 – LCK 414). The total influent COD concentration ($COD_{Inf,T}$) as well is determined with the spectrophotometer with HACH-LANGE kits for COD (LCK 314 – LCK 514).

The biodegradable COD is determined by applying a constant ratio with respect to the total BOD (Equation 3.16), which is estimated in combination with the first order rate constant of BOD versus time from a 10-day BOD test (Equation 3.17).

$$bCOD = \frac{1}{1-0.15} \cdot BOD_T \quad (3.16)$$

Where BOD_T is total BOD [mg/l].

$$BOD_T = \frac{1}{1-e^{-k_{BOD} \cdot t}} \cdot BOD_t \quad (3.17)$$

Where BOD_t is the BOD at time t [mg/l].

3.5. RESULTS AND DISCUSSION

3.5.1. Dependence on the yield of heterotrophs

Respirometric assays according to the G_FL_S method, with dosing of acetate as readily biodegradable substrate, were performed in triplicate in two identical respirometers. The respirometers were filled with activated sludge collected at the WWTP of Eindhoven and 250 ml of a solution of sodium acetate trihydrate with a concentration of 92 mg COD/l was dosed. The calculated S_B fraction equals to a concentration of 52.9 mg/l (with a standard deviation of 8.6%) for the first respirometer and to 61.2 mg/l (with a standard deviation of 8.3%) for the second respirometer.

The underestimation of the S_B fraction, well below the dosed COD concentration, might be attributed by a real heterotrophic yield that is different from the default heterotrophic yield of 0.67 g COD/g COD as used in the evaluation. To confirm the possible difference in the yield, it has been recalculated based on the experimental data, according to equation 3.18 (Majone et al., 1999; Strotmann et al., 1999). The recalculated yield amounts to 0.795 g COD/g COD (with a standard deviation of 2.9 %), which proves to be significantly higher than the default yield value.

$$Y_{obs} = 1 - \frac{\Delta O_2}{COD_{deg}} \quad (3.18)$$

Where Y_{obs} is the observed yield [mg cell COD/mg COD], ΔO_2 is the change in oxygen concentration [mg/l] and COD_{deg} is the COD removed.

Respirometric assays, similar to the assays with acetate, were performed with glucose. For this respirometric assay, the activated sludge was collected at the WWTP of Roeselare and 250 ml of a solution of glucose with a concentration of 213.5 mg COD/l was dosed in quadruplicate. After calculation of the concentration of biodegradable substrate with the default value for Y_{OHO} of 0.67 g COD/ g COD, a concentration of only 59.6 mg COD/l (with a standard deviation of 7.7%) was obtained. Recalculating the yield according to equation 3.18, provides a value of 0.91 g COD/g COD (with a standard deviation of 0.8%).

High yield values for the heterotrophic bacteria have also been reported by Guisasola et al. (2005) (0.666, 0.726, 0.757 and 0.792 g COD/g COD). They attribute the high yield values to excessively available substrate and extensive storage. The storage of polymers (usually, polysaccharides and lipids) can be caused by a feast and famine regime, which is present at the WWTP of Eindhoven, the origin of the sludge. As such arguing for the dependence of Y_{OHO} on (the history of) the biomass. Dircks et al. (1999) reported higher values for the heterotrophic yield for different substances, 0.72 g COD/g COD for acetate and 0.91 g COD/g COD for glucose. Goel et al. (1999) also reported high Y_{OHO} values for the degradation of glucose (0.9 g COD/ g COD). Moreover, McCarty et al. (2007) clearly demonstrated the variability of Y_{OHO}, in a dataset on yields for different individual substrates, which they used for the calibration of their thermodynamic electron equivalents model for bacterial yield prediction. From the dataset the yield was calculated to range from 0.37 for methanol up to 0.65 for formate (gCOD cell/gCOD substrate). In a global sensitivity analysis, Cosenza et al. (2014) used, based on a literature review, a variance of the yield ranging from 0.38 up to 0.75 (gCOD cell/gCOD substrate).

As can be clearly deduced from equations 3.2 and 3.18, the yield of heteroptrophs is indispensable to determine the biodegradable COD from respirograms. The value of Y_{OHO} is important as a variation of 10% leads to a change of 18% in estimation of the biodegradable fraction (Spérandio and Paul, 2000). However, as explained above, the yield of heterotrophs has a considerable variability related to both the (history of the) biomass and to the substrate consumed.

Depending on the length of the previous dry weather period and the intensity and length of the rain event the content of organic particulate matter changes significantly during the course of the rain events (Stumwohrer et al., 2003). Boogaard et al. (2014) listed stormwater quality data retrieved from a database based on data monitoring projects and compared them with data from the US and other European countries. The quality data is significantly different from dry weather data. Also typical ratios differ considerably compared to dry weather. The dry weather COD over BOD_5 ratio mean value (2.06) reported by Rieger et al.

(2012) is smaller than the ratio (5.61 for the Netherlands, 6.23 for Europe and 6.11 for the USA) calculated from the storm weather data presented by Boogaard et al. (2014). This higher ratio may be attributed to the scouring of deposited sludge, which may have undergone sludge stabilisation reactions resulting in less organic biodegradable matter.
As the wastewater matrix changes the yield factor is also likely to change. As a consequence there is a need to determine this yield factor for the wastewater composition during storm events. This however is beyond the scope of this work but has a strong recommendation for future projects. However, this additional experiment lengthens the procedure for determining the influent fractionation and may become a bottleneck when a measurement campaign is set up requiring a high sampling frequency.

3.5.2. Low load conditions

At the WWTP of Roeselare, influent wastewater samples were taken Monday mornings around 9 am on March 24th, April 7th and April 14th of 2014. All the samples were analysed the next two days in the lab (Table 3.1). All three days were dry weather days. However, the first day and in a lesser extent the second and third day flow rates surpassed the normal dry weather flow considerably. The increased flow rate is probably contributed to the high infiltration rate caused by the extreme rain events in February and March of 2014. The possibility of high infiltration rates was confirmed by consulting the ground water levels at the Flemish subsoil database (https://dov.vlaanderen.be). The total COD (COD_T) is within the same range for the three days although it shows a moderate increase with decreasing flow rates, which could strengthen the hypothesis of the dilution by infiltration. BOD_{10} proves to be weaker the first day indicating a lower biodegradability, which is confirmed by the wastewater fractionation.
The first two days the biodegradable fraction (bCOD) determined by respirometry is substantially lower than the bCOD determined with the STOWA method (Hulsbeek et al., 2002). The last day the difference between the methods is reasonably small. This indicates that the physical-chemical fractionation methods tend to estimate higher fractions of biodegradable matter in case of low biodegradability, conditions which seems to occur in rain weather or under a large infiltration. This could indicate that some of the biodegradable matter is only degraded in the BOD_{10} tests, which are applied in the STOWA protocol, and not in the short term respirometry experiments. In addition, the ratio of readily biodegradable substrate determined by respirometry (S_B) to the total wastewater COD ranges between 5.9 - 8.5%. For the slowly biodegradable substrate (XC_B),

this ratio ranges between 2.2 - 20.3%. These low ratios may also be attributed to the high infiltration rate caused by the extreme rain events in February and March of 2014.

Table 3.1. Influent fractionation and ratios in respect to total COD of influent at the WWTP of Roeselare for sampling during dry weather days (Monday mornings around 9 am on March 24th , April 7th and April 14th of 2014). The raw data can be found in Appendix B.

Date	Method	Unit	24/03/14		07/04/14		14/04/14	
			Mean	Stdev[2] %	Mean	Stdev[2] %	Mean	Stdev[2] %
Q^1	Logged	m^3/h	974	N.A.	730	N.A.	680	N.A.
COD_T	chemical	mg/l	196	0.8	205	2	221	6
BOD_5[3]	respirometry	mg/l	40.2	0.0	59.2	2	58.5	3
BOD_{10}[3]	respirometry	mg/l	50.7	0.0	69.8	2	70.4	3
bCOD	respirometry	mg/l	22.4	21	19.3	12	63.7	16
bCOD	STOWA[4]	mg/l	59.2	0.3	82.8	0.7	86.4	4
S_B	respirometry	mg/l	11.6	22	14.7	13	18.8	12
S_B	STOWA[4]	mg/l	34.9	1	29.1	17	33.6	9
XC_B	respirometry	mg/l	10.8	20	4.6	44	44.9	17
XC_B	STOWA[4]	mg/l	24.3	1	53.7	4	52.8	12
$bCOD/COD_T$[5]	calculation	%	11.4	21	9.4	12	28.9	16
S_B/ COD_T[5]	calculation	%	5.9	22	7.1	13	8.5	13
XC_B/ COD_T[5]	calculation	%	5.5	20	2.2	44	20.3	17

[1] Instantaneous value at the time of sampling.
[2] Standard deviation in %
[3] BOD is performed in duplicate, while the other analysis were done in triplicate.
[4] Physical-chemical fractionation method according to the STOWA protocol (Hulsbeek et al., 2002).
[5] Ratios calculated based on the results of the respirometry tests.

Wastewater samples obtained on February 25th and March 3th at the WWTP of Roeselare were taken during wet weather conditions and analysed using respirometric assays according to the G_FL_S method (the raw data can be found in

Appendix B). After determination of the k_La, 250 ml of wastewater sample was added. As can be seen in Figure 3.7, the DO-profile (left) shows the expected drop of DO immediately after the addition the wastewater sample. However, instead of an enduring decrease, the DO unexpectedly starts increasing again up to a level higher than the previous equilibrium DO concentration.

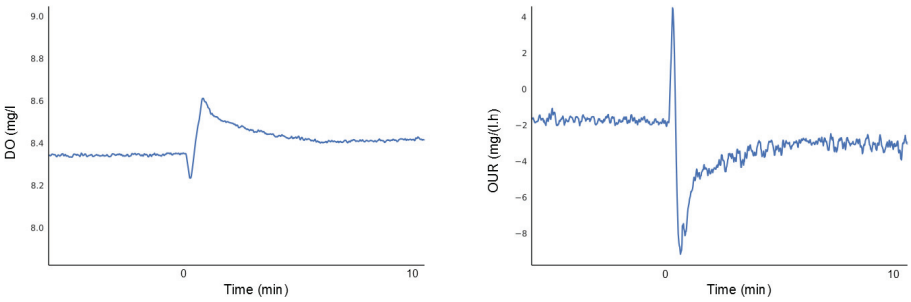

Figure 3.7 DO-profile (left) and OUR-profile (right) after the addition of 250 ml of a dilute PST influent to a batch reactor containing 2.0 l activated sludge (with 10 mg/l ATU to block nitrification)

To eliminate the possibility that the organisms in the activated sludge did not have enough essential nutrients, limiting the degradation of the biodegradable substrate, sodium phosphate and ammonia sulphate were added to the activated sludge. However, after adding these nutrients the same respirometric response was observed upon addition of the wastewater samples. Another possible cause for the low bCOD values could be the presence of toxic components in either the sludge or the wastewater. To check for the possible presence of toxic components, acetate and diluted synthetic wastewater were dosed to the batch reactor. This resulted in a fast respirometric response (results not shown) for both substrates implying the absence of toxic components.

COD measurements of the wastewater samples taken during wet weather conditions yielded a COD concentration ranging between 31.2 mg/l and 179.0 mg/l. In addition five-day BOD measurements were performed, resulting in a BOD_5 value ranging between 30.3 mg/l and 43.7 mg/l indicating a low presence of biodegradable substrate in these wastewater samples. In comparison, samples obtained during dry weather conditions had a BOD_5 value ranging between 58.5 mg/l and 145 mg/l. Apparently, the dilute wastewater samples contain mainly COD fractions that cannot be degraded during the short-term respirometric experiments.

Due to this large unbiodegradable COD fractions, the respirometric test meets its limits in regard to its sensitivity. I.e. the rate of oxygen consumption of the microorganisms in the activated sludge during substrate degradation does not exceed the oxygen supply, resulting in DO and OUR-profiles as shown in Figure

3.5. Therefore, the aeration was lowered to the minimal aeration rate (0.5 l/min) to reduce the oxygen supply. In an attempt to further decrease the oxygen supply, the aeration stone was removed to create larger air bubble sizes, resulting in a lower specific area for mass transfer and less efficient oxygen transfer. However, the same respirometric profile was still observed indicating that the oxygen supply was not reduced sufficiently.
The technical specifications of the dissolved oxygen probes may also play a role in the observed behaviour. The main factor playing a role in the dissolved oxygen probes used here is the response time (t_{98}), which amounts to about 20 seconds. The profile may display a time lag but will represent the same trend as the real dissolved oxygen profile.

3.5.3. Uncontrolled oxygen input

Another phenomenon witnessed during the tests is the unexpected increase in DO concentration after the dosing of the sampled wastewater (Figure 3.8). This increase in oxygen concentration is probably caused by an increased oxygen input during the addition of the sample. Gas flow, bubble size, reactor dimensions, stirring of mixed liquor (turbulence), temperature of mixed liquor, and air pressure have a major influence on oxygen transfer and the k_La. Due to the relatively large sample volume that is added, temporary swirls are created in the reactor, creating air-bubbles and a temporary higher oxygen transfer. As such, the conditions, which must be ensured during the subsequent experiments to justify the assumption of a constant k_La (Ros et al., 1988), are not met.

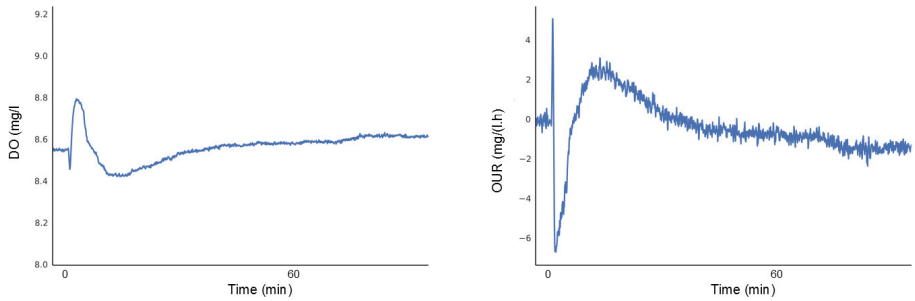

Figure 3.8. Effect of the oxygen increase on the DO-profile (left) and the OUR-profile (right) obtained after addition of 250.0 ml of PST influent (266.0 mg COD/l) to a batch reactor containing 1.9 l activated sludge (with 10 mg/l ATU to block nitrification).

In order to test this hypothesis of the higher oxygen transfer, 250 ml of distilled wastewater was added to the reactor, to check if the same profile would be obtained. Upon addition of the sample, an immediate drop followed by a rapid

increase in DO concentration is observed (Figure 3.9). Because there is no biodegradable substrate present in the distilled water, the DO concentration goes slowly back to the saturated DO concentration, while a faster decrease in DO concentration is observed in Figure 3.8 due to the degradation of biodegradable matter present in the wastewater sample.

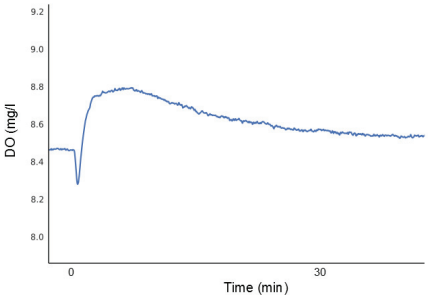

Figure 3.9. DO-profile obtained after addition of 250 ml of distilled water to a batch reactor containing 1.9 l activated sludge (with 10 mg/l ATU to block nitrification).

This phenomenon of uncontrolled increased oxygen input is probably only witnessed because of the low biodegradable COD fractions. With higher fractions the phenomenon would completely vanish in the more pronounced biodegradation reactions. Furthermore, the phenomenon complicates the evaluation of the respirogram using the direct parameter abstraction method.

Another explanation for the observed behaviour could be that the samples contain substantially higher dissolved oxygen concentrations than the reactor (i.e. significantly higher than 8 mg/l). In the case of the wastewater this is rather unlikely as the collected wastewater was stored in closed barrels (20 l) with little or no headspace. In addition the wastewater was stored overnight (at 4°C), which may cause some of the oxygen to be depleted before the whole sample reaches 4°C.

3.5.4. Changing the initial substrate concentration to biomass concentration

Since the respirometric protocol yielded extremely low results on bCOD for dilute wastewater samples, several attempts were made to improve the respirometric response upon addition of the water samples. First of all, the initial substrate concentration to initial biomass concentration (S_0/X_0) was adapted. A low S_0/X_0 results in a tall and narrow curve due the fast utilization of the biodegradable substrate, while a high S_0/X_0 gives a low and wide OUR-curve (Ekama et al., 1986). In order to evaluate the effect several S_0/X_0 combinations were examined.

First a batch test was performed with diluted sludge to create a higher S_0/X_0 ratio (0.011 g COD/g VSS). 1.0 l of activated sludge was diluted with 1.0 l of distilled water. To mimic the wastewater composition under rain weather condition, influent of the PST was diluted with effluent of the WWTP. Despite the higher S_0/X_0 ratio, the DO-profile and OUR (Figure 3.10) remain narrow and low, when dosing 250 ml of the diluted wastewater (125.3 mg COD/l) to the batch reactor containing the diluted sludge (Flowing gas–static liquid method). A total biodegradable substrate concentration of 13.2 mg/l is obtained, consisting of 9.7 mg/l readily biodegradable substrate and 3.5 mg/l slowly biodegradable substrate, which is still a meagre fraction of the total dosed COD.

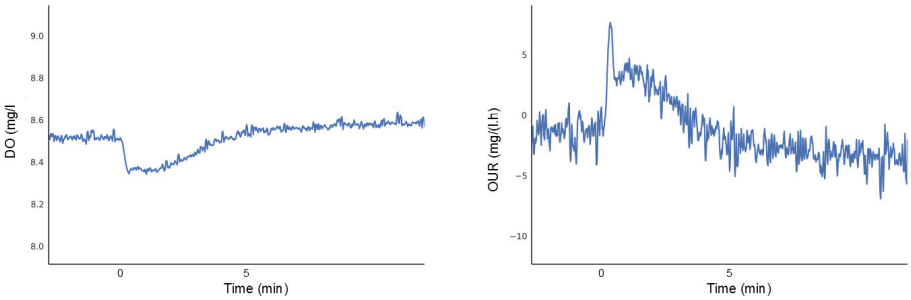

Figure 3.10. DO-profile (left) and OUR-profile (right) obtained after the addition of 250 ml of a 125.3 mg COD/l wastewater solution to a batch reactor containing 1.9 l diluted activated sludge (with 10 mg/l ATU to block nitrification)

A drawback of performing experiments with diluted sludge is the long time necessary for determining the k_La value. Normally it takes approximately 40 minutes to determine one k_La value, but with diluted sludge it takes 1h40 minutes (about 5h for a triplicate determination). Due to this elongated procedure, this method hampers the application for high-measuring frequencies (e.g. for hourly composite samples).

Another test was performed creating an even higher S_0/X_0 ratio (0.038 g C0D/g VSS) through adding 0.40l of dilute wastewater (103.7 mg COD/l) to the batch reactor containing 0.50 l of activated sludge. After addition of the wastewater sample, the exogenous respiration rate reaches a maximum of 40.4 mg/l/h and then decreases to a value lower than the endogenous respiration rate. Thereafter OUR_{ex} increases again to OUR_{end} (Figure 3.11). Due to the addition of 400 ml to 500 ml of sludge, the total reactor volume almost doubles upon addition of the sample. The air bubbles can stay longer in the mixed liquor and there is a strong dilution of the activated sludge. These factors possibly change the oxygen transfer (k_La), resulting in an error in the calculated OUR values. A better OUR-profile could be obtained, if the change in k_La value and oxygen transfer would be accounted for in the

calculation of the OUR value, for which dynamic process models seem to be appropriate. However, these models suffer from identifiability issues (Guisasola et al., 2005) and may require additional measurements during the respirometric tests (Gernaey et al., 2002).

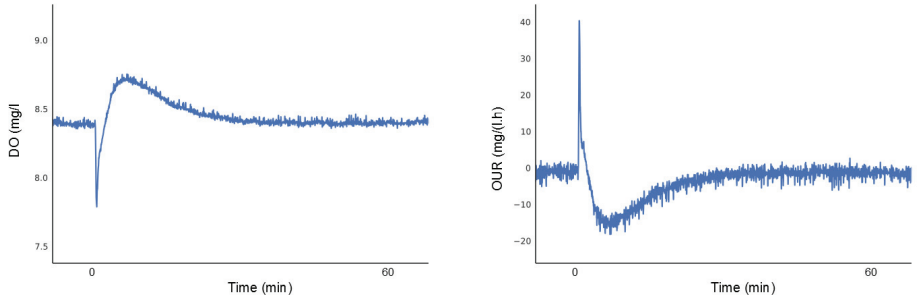

Figure 3.11. DO-profile (a) and OUR-profile (b) obtained after the addition of 400 ml of a 103.7 mg COD/l wastewater solution to a batch reactor containing 500.0 ml concentrated activated sludge (with 10 mg/l ATU to block nitrification)

3.5.5. Reducing oxygen input

In order to further reduce the oxygen input for the analysis of the diluted wastewater samples, the aeration was stopped before the addition of the sample, i.e. the principle of static gas - static liquid respirometric assays. The method is validated on the basis of an experiment dosing about 0.1 mol of sodium acetate trihydrate ($CH_3COONa.3H_2O$) and the theoretical COD for the sample was calculated (5.6 mg/l). The experimental results were analysed using the direct parameter abstraction method and also using a dynamic model based on either ASM1 or ASM3 (Table 3.2).

The direct parameter abstraction method, using the default heterotrophic yield (0.67 g COD/g COD), provides a slightly too low estimate for the biodegradable COD (4.7 mg/l vs. a ThCOD of 5.6 mg/l). Applying the higher yield (0.795 g COD/g COD), as associated to the degradation of acetate before, provides a too high estimate (7.6 mg/l).

Estimating bCOD with the ASM1 model, using the default yield (0.67 g COD/g COD), also provides a reasonable estimate (4.9 mg/l vs. a ThCOD of 5.6 mg/l). Although the use of dynamic models is assumed to be hampered by identifiability issues (Gernaey et al., 2002; Orhon et al., 2007), the uncertainty bounds are relatively small. The offset in the values could be attributed to an incorrect Y_{OHO} value or the fact that not all acetate has been degraded. Applying the methods that could indicate the occurrence of storage, i.e. the higher Y_{OHO} value (0.795 g COD/g COD) determined before and the use of ASM3, overestimate the bCOD

(respectively 7.4 and 7.7 mg/l vs. a ThCOD of 5.6 mg/l) similar as with the direct parameter abstraction method. This possibly indicates that storage of readily biodegradable substrate is not significant, which is contradictory to the flowing gas- static liquid experiment.

Table 3.2. concentration of biodegradable substrate bCOD after addition of sodium acetate trihydrate determined using static gas-static liquid respirometry.

Method	Note	Quantity	Value
Sample	$CH_3COONa.3H_2O$	Dry weight ThCOD	13.6±0.1 mg/l 5.6±0.1 mg/l
Direct parameter abstraction	Y_{OHO}=0.67 Y_{OHO}=0.795	bCOD bCOD	4.7±0.3 mg/l 7.6±0.3 mg/l
ASM1	Y_{OHO}=0.67 Y_{OHO}=0.795	bCOD bCOD	4.9±0.2 mg/l 7.4±0.3 mg/l
ASM3	Y_{OHO}=0.63	bCOD	7.7±0.4 mg/l

After the validation of the method, the experiment was repeated with 250 ml of dilute wastewater sample (52.7 mg COD/l). During this method, there is no aeration, so the oxygen decrease due to substrate degradation should be visible upon addition of the sample. However, no increase in respiration rate due to substrate degradation was observed (Figure 3.12, left). Moreover an increase in DO concentration was observed after sample addition. The same increase in DO concentration upon addition of 250 ml of distilled water is observed (Figure 3.12, right). Similar as in the flowing gas-static liquid method, this increase in DO-concentration could be caused due to the sample addition, creating swirls in the reactor, inducing reaeration.

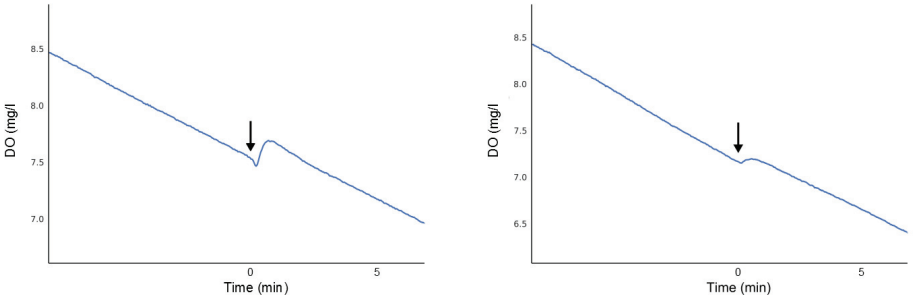

Figure 3.12. DO-profile obtained after addition of (left) 250 ml of PST influent (57.3 mg COD/l) and (right) 250 ml of distilled water to 1.9 l active sludge (arrow indicating the addition of the substrate).

To evaluate the minimum biodegradable substrate concentration leading to an increased respiration rate after sample addition, dilute wastewater samples with different COD concentrations were made. Table 3.3 shows the obtained results. For the dilute wastewater sample with a COD concentration of 52.4 mg/l, no increased

respiration rate upon addition of the sample was visible. For the other samples, with a higher COD concentration, a visible respirometric response was observed. After calculation of the biodegradable substrate concentration, a very low value is obtained. The calculated concentrations of the biodegradable substrate in the wastewater sample are probably an underestimation of the real biodegradable substrate concentrations, as was the case with acetate.

Table 3.3. concentration of biodegradable substrate bCOD in dilute wastewater sample determined with static gas-static liquid respirometry

COD of sample (mg/l)	bCOD (mg/l)	Stdev (%)	bCOD /COD_T (%)	Stdev (%)
52.4	B.D[(1)]	B.D[(1)]	B.D[(1)]	B.D[(1)]
80.2	4.1	83.2	5.1	4.2
110.5	9.1	25.9	8.2	2.1
158.9	12.5	28.8	7.9	2.3

[(1)] Below detection limit.

Due to the above observations, a parameter estimation experiment was performed in WEST (mikebyDHI). The same configuration was used as described for acetate. For the determination of the endogenous state of the activated sludge in the batch reactor, an additional experiment was performed, during which the activated sludge was aerated for 3 hours. The initial biomass concentration of the heterotrophs and the k_La were estimated, so that the simulated conditions of endogenous respiration were matching to the real experimental conditions of endogenous respiration. It was noticed that the longer the experiment continued the estimated biomass concentration in the respirometer increased from 0.98 g/l to 4.28 g/l. Indeed, the longer the experiment lasted, the lower (more negative) the slope of the curves were. At the beginning of the experiment the endogenous respiration rate is 0.0018 mg/l.s, while at the end of the experiment (approximately 4h later) the endogenous respiration rate is 0.0079 mg/l.s. This increase in respiration rate cannot only be caused by the growth of biomass due to substrate addition. Another possible explanation is the presence of slowly biodegradable substrate present in the wastewater samples, which could not be degraded in the short time frame. So this means, that the microorganisms in the batch reactor are not in the endogenous state because they are still degrading slowly biodegradable substrate. However, endogenous conditions of activated sludge in the beginning of the test are crucial for a correct determination of the biodegradable substrate present in a dosed sample. Waiting until the slowly biodegradable substrate is degraded before the aeration is turned on again is not an option because of oxygen limitations. Alternatively, oxygen limitation can be avoided by a regular reaeration of the batch reactor.

3.5.6. General discussion

The work described shows the need for further investigation of respirometric assays, in particular for the application for storm water characterisation. The research should either be directed into more sensitive assays, taking special care to avoid uncontrolled (and undesired) oxygen input, or into the possibility of concentrating the wastewater, e.g. by means of membrane filtration. For the latter, special attention needs to be addressed to the effect of the pore size of the filters for the characterisation.

In order to obtain more sensitive assays special care should be given to the assumptions made. One of these assumptions is the k_La considered to be constant. Many factors play a role in the k_La, including the surfactants. These surfactants degrade during the assay and as such alter the k_La. Possible approaches to account for changes in the kLa are either the elimination of the dependence on the kLa (e.g. using alternating aeration or hybrid respirometers (Vanrolleghem and Spanjers, 1998)) or a more rigorous evaluation of the respirograms (e.g. using dynamic activated sludge models).

A second issue that needs to be addressed in future research is the determination of the yield factor. A question that arises is whether the fractionation method or the model should be adapted. I.e. the model could address more components groups of which the yield is more stable. Fractionation methods could then heavily rely on more chemical techniques such as gas or liquid chromatography combined with the detection methods mass spectrometry or UV-VIS spectrophotometry.

Additionally, one should consider the modelling of the primary sedimentation tanks (as addressed in Part IV). For the modelling of primary sedimentation tanks particle size is important. However, the borderline distinguishing between particulate and soluble, is different from (biokinetic) modelling studies, where 0.1 μm (or 0.45 μm after flocculation) is applied (Roeleveld and van Loosdrecht, 2002), and other studies. In contrast with modelling studies, other studies, consider particles below 1 nm as dissolved components (Dulekgurgen et al., 2006; Sophonsiri and Morgenroth, 2004).

3.6. CONCLUSIONS

In order to evaluate the performance of a WWTP under rain or storm weather conditions it is crucial to have a clear view on the quantity of biodegradable substrate entering the plant. In order to quantify the variations in biodegradable substrate separate samples were collected and a measurement campaign was set up

in rain weather conditions. Several factors hamper the application of the respirometric assays to quantify the biodegradable COD.

Firstly the dependence on the yield of heterotrophs is demonstrated in accordance with previously published values. An accurate estimation of the yield factor is important as a 10% variation leads to a change of 18% in the estimation of the biodegradable COD. Moreover, the changing yield factor for different substrates is important for the evaluation under rain and storm water conditions as these conditions alter the wastewater characteristics drastically. This observation of altered wastewater characteristics should be considered in further model developments.

Secondly, the low load conditions, confront the respirometric assay with its limitations. Attempts changing the initial substrate concentration to biomass concentration were not successful. Moreover, diluting the sludge enlarged the necessary time to perform the assays. Another option to improve the sensitivity of the assays, but also not entirely successful, was to attempt eliminating the oxygen input by applying the static gas - static liquid respirometric assay.

The evaluation of the respirometric assays using the direct parameter abstraction method proves to be delicate under these extreme conditions. The evaluation using dynamic models based on activated sludge models proves to be promising but needs to address the issues of identifiability. In addition further studies could investigate the possibility of concentrating the wastewater samples by membrane filtration.

This work is another step in the better exploration of the impact of dilute wastewater conditions on biodegradable substrate fraction in wastewater.

PART III

Primary Sedimentation

Chapter 4

Theoretical background and modelling of primary sedimentation tanks

"Names and attributes must be accommodated to the essence of things, and not the essence to the names, since things come first and names afterwards."
Galileo Galilei

4.1. ABSTRACT

Primary sedimentation tanks are often used as a preliminary step in wastewater treatment plants in order to reduce the load (50 to 70% of the suspended solids and 25 to 40% of the biochemical oxygen demand) on the subsequent (biological) treatment steps. Primary sedimentation is a complex process involving flocculation, gravitational settling and drag. Gravitational settling in primary sedimentation tanks mainly occurs in the discrete particle settling and flocculent settling types, of which the behaviour is independent of the particle concentration but depends on the particle size distribution (and particle density distribution). A literature review on modelling of primary sedimentation was conducted and it was found that most modelling efforts are based on empirical relations, which are not able to describe the high scatter present in primary sedimentation tank removal efficiency data. A limited number of computational fluid dynamic models, which describe the hydraulic profile carefully but are too complex to apply within a whole plant modelling context, have been proposed as well. For integration in a whole plant model, phenomenological models such as the model of Bachis et al. (Bachis et al., 2012) are promising as they provide sufficient detail to model the impact of particle velocity distributions. Possible improvements are the integration within a rigorous discretization scheme as proposed by Bürger et al. (2011) and the differentiation

between organic and inorganic matter as this is crucial for the succeeding biological treatment.

4.2. SYMBOLS

a	regression coefficient (Silva et al., 2014) (-)
b	regression coefficient (Silva et al., 2014) (mg/l)
a	regression coefficient (Christoulas et al., 1998) (d/m)
b	regression coefficient (Christoulas et al., 1998) (g/m³)
a	regression constant (Voshel and Sak, 1968) (m³/(s.m²))
a_{sc}	Scouring parameter (-)
a_t	Series of uncorrelated independent ‘‘shocks’’ in a stochastic model (-)
B	Back shift operator (-)
B	Intermediate variable (Ribes et al., 2002) (-)
A	Surface area of the tank (m²)
A_c	Cross sectional area of the clarifier (m²)
A_p	Cross-sectional or projected area of particles in direction of the flow (m²)
B	Width of the basin (m)
c	regression coefficient (Christoulas et al., 1998) (d/m)
C	Concentration of suspended solids in the sedimentation tank (mg/l)
C_D	Drag coefficient (-)
C_{In}	Influent concentration (mg/l)
C_{Eff}	Effluent concentration of the component (mg/l)
$COD_{In,t-1}$	Influent COD concentration at time t minus 1 (mg/l)
COD_{Total}	Total COD (mg/l)
$COD_{particulate}$	Particulate COD (mg/l)
COD_X	Particulate COD (mg/l)
d_p	Particle diameter (m)
$d_{p,c}(t_{In})$	Particle diameter of particles reaching the critical settling velocity (m)
d_s	Diameter of the sand particle (m)
$E(v_s)$	Fraction of particles with settling velocity v_s (-)
E_c	Removal efficiency for organic matter as COD (-)
E_f	Intermediate variable, function of the Froude number (-)

E_r	Removal efficiency (%)
E_s	Removal efficiency for suspended solids (-)
E_x	Longitudinal turbulent diffusion coefficient (-)
f	Darcy-Weisbach friction factor (-)
f_{corr}	Dimensionless correction factor (Otterpohl and Freund, 1992) (-)
f_{ns}	Fraction of non-settleable solids (-)
f_s	Fraction of settleable solids (-)
f_R	Fraction removed (-)
f_X	Mean fraction of particulate COD (-)
F_d	Drag force (kg.m/s²)
F_G	Gravitational force (kg.m/s²)
F^i_{Floc}	Source/sink term to shear-induced flocculation (-)
F_r	Froude number (-)
F_x	Additional forces (N)
$F(t_{In};v_s)$	Removal fraction of suspended solids entering the basin at time t_{In} with a settling velocity v_s (-)
F_{pr}	fraction of particles with velocity v_p smaller or equal than v_c (-)
g	Gravitational acceleration (9.81 m/s²)
h(t)	Water depth in the basin at time t (m)
h_0	Depth of the settling zone [m]
h_c	Calculated height (Ribes et al., 2002) (m)
h_f	Height of the feed (m)
h_p	Height of the particle in the inlet zone [m]
$h_{p,t}$	Distance from the water surface for the particle (m)
h_t	Calculated height (Ribes et al., 2002) (m)
H_{Av}	Mean depth of the basin (m)
k	Scouring parameter (-)
L	Length of the basin (m)
m	regression constant (Voshel and Sak, 1968) (-)
m_p	Mass of the particle (kg)
n	regression constant (Voshel and Sak, 1968) (-)
n_i	Number of particles in the i^{th} velocity range (-)
N_{hpnu}	number of hours per new unit (24 hours per day, 1/60 hours per minute, 1/3600 hours per second)
OR	Overflow rate ($m^3/m^2.s$)
q	surface overflow rate (m/d)
Q_{hl}	Hydraulic loading ($m^3/(s.m^2)$)

Q	Flow rate (m^3/h)
Q_{In}	Influent flow rate (m^3/s)
$Q_{In,t-1}$	Influent flow rate at time t minus 1 (m^3/h)
Q_{Out}	Effluent flow rate (m^3/s)
Q_τ	the average flow for the residence time (m^3/h)
r	Distance measured from the centre of the basin [m]
r_0	Radius of the settling and inlet zone [m]
r_h	Settling parameter characteristic of the hindered settling zone (m^3/g)
r_i	Radius of the inlet zone [m]
r_p	Settling parameter characteristic of the low solids concentration (m^3/g)
R_{SS}	Suspended solids removal (%)
Re	Reynolds number (-)
Re_p	Particle Reynolds number (-)
$R_{Out}(t_{In})$	Removed fraction of particles entering at time t_{In} (-)
S	Influent suspended solids concentration (mg/l)
S_0	Effluent suspended solids concentration (mg/l)
S_i	Influent suspended solids concentration (mg/l)
SG	Specific gravity (-)
SG_p	Specific gravity of the particle (-)
SVI	sludge volume index (ml/g)
t	Current time (h)
t_{In}	Time at which the particles enter the basin (s)
t_{Out}	Time at which the particles leaves the basin (s)
t_s	Settling time (s)
t_r	hydraulic retention time (min)
T	Temperature (°C)
T_A	Half-removal time (min)
TSS_{Eff}	TSS effluent concentration (mg/l)
$TSS_{In,t-1}$	Influent TSS concentration at time t minus 1 (mg/l)
u	the new unit of time (s, min or d)
$v(h,t)$	vertical flow velocity in the basin at height h and at time t (m/s)
v_0	Theoretical maximum settling velocity (m/d)
v'_0	Practical maximum settling velocity (m/d)
v_{Av}	Mean flow velocity (m/s)
v_c	Critical settling velocity (m/s)
v_f	Fluid velocity (m/h)

v_H	Horizontal velocity that will just produce scour (m/s)
$v_{n,i}$	Average velocity of particles in the i^{th} velocity range (m/s)
v_p	Particle settling velocity (m/s)
v_s	Particle settling velocity (m/s)
v_s	Settling velocity (Takács et al., 1991) (m/s)
v_s	Settling velocity of the sand particle (m/s)
$v_{s,c}$	Critical settling velocity (m/s)
V	Volume of the PST (m³)
V_p	Volume of the particle (m/s)
W	Suspended solids concentration of the feed (mg/l)
x_c	Critical concentration (mg/l)
x_s	Longitudinal location of the particle (m)
X_f	Feed or influent solids concentration (mg/l)
X_{In}	Influent suspended solids concentration (mg/l)
X_j	Suspended solids concentration in layer j (mg/l)
X_{Min}	Minimum attainable suspended solids concentration below which no settling occurs (mg/l)
X_{Out}	Effluent suspended solids concentration (mg/l)
X_{pr}	Fraction of particles removed (-)
X_r	Removed fraction (-)
z_s	Vertical position of the particle (m)
$\alpha, \beta, \gamma, \lambda$	Correlation parameters (Lessard and Beck, 1988) (-)
α_i	Single volume fraction of class i (-)
β_i	proportionality constant (Liu and Garcia, 2011) (-)
$\delta_{2,1}$	First order term of the denominator of the second transfer function (-)
ε	Turbulence energy dissipation rate (m²/s³)
η_{COD}	Efficiency of the COD removal (%)
η_X	Efficiency of the particulate COD removal (%)
μ	Dynamic viscosity (N.s/m²)
ν	Kinematic viscosity (m²/s)
ρ_c	Density of the component (g/m³)
ρ_p	Density of the particle (g/m³)
ρ_w	Density of water (g/m³)
$\rho_{w,4}$	Density of pure water at 4°C (g/m³)
τ	Hydraulic retention time (h)
τ_{nu}	Hydraulic retention time in the new unit (u)

φ_1	First order term of the auto-regressive operator of the stochastic model (-)
φ_2	Second order term of the auto-regressive operator of the stochastic model (-)
$\omega_{1,0}$	Zero order term of the numerator of the first transfer function (-)
$\omega_{2,0}$	Zero order term of the numerator of the second transfer function (-)
Ω	compression factor (-)

4.3. INTRODUCTION

Primary sedimentation is often used as a preliminary step in wastewater treatment plants in order to reduce the load on the subsequent (biological) treatment steps. The load is approximately reduced with 50 to 70% of the suspended solids and 25 to 40% of the biochemical oxygen demand (BOD) (Tchobanoglous et al., 2004). As such the primary sedimentation tanks (PST) allow for saving on aeration energy required for the aerobic removal of chemical oxygen demand (COD). In addition, the primary sludge has a higher energetic potential than waste activated sludge, which is an important asset to consider in the evaluation of resource recovery potential. Cao and Pawlowski (2012) reported a production of 61.0 m³ biogas per 100 kg of primary sludge opposed to 24.4 m³ per 100 kg of waste activated sludge. On the other hand primary sedimentation alters the wastewater composition and removes COD that might be necessary for biological nutrient removal and biological phosphate removal. Actually, the fact that the PST changes the wastewater characteristics through the sedimentation process is often overlooked (Tchobanoglous et al., 2004), as such affecting the consecutive biological treatment. This effect on the biological treatment requires a thorough evaluation of the primary sedimentation tank on the influent ASM fractions (see chapter 3).
Due to the advantages and disadvantage of primary sedimentation, the use of PSTs is still under debate. Bixio et al. (2000) identified the combination of primary clarifiers and anaerobic digestion of the excess sludge as having the least potential impact on the environment and the most advantages in terms of transportation and provision of integral power generation. However, in another study, Bixio et al. (2002) argued that primary clarification has a negative impact on the life cycle costs of the WWTP. Certain studies consider removing, reducing or bypassing, in case of storm events (Niemann and Orth, 2001), the PSTs also in view of new

treatment schemes such as the high rate activated sludge process (Boehnke et al., 1998). Other studies discuss the replacement of the PSTs by more efficient technologies, such as microsieves (Remy et al., 2014) or dissolved air flotation units (Amerlinck et al., 2014).

The clearly case-dependent evaluation of primary sedimentation tanks calls for a thorough description and modelling of the process. Despite the significant impact on the overall WWTP performance and cost effectiveness, characterisation and modelling of primary settlers has been neglected pretty much to date and very few efforts have been made for its optimisation and modelling (Bachis et al., 2014). A simple Web of Science search (on 5/5/2015) for "primary & sedimentation & wastewater" produced 230 hits, a search for "primary & sedimentation & wastewater & model" gave 54 hits only and a search for "primary & settling & tank & model" resulted in 48 hits, demonstrating the moderate scrutiny primary sedimentation received to date.

It has been neglected either because primary settling is not considered very influential for modelling purposes, or because the simple models proposed earlier were considered sufficiently robust to describe the primary settling tanks (PSTs) behaviour (Otterpohl and Freund, 1992). As a consequence, removal efficiencies of PSTs for the different COD fractions of wastewater have rarely been reported in literature, although they are extremely important for the determination of the organic loading to be treated in the succeeding biological treatment process (Tchobanoglous et al., 2004). To some extent this lack of attention can be explained by the limited operational control opportunities on primary clarifiers (Lessard and Beck, 1988).

Improved primary settler models are also essential ingredients of whole WWTP descriptions (Bachis et al., 2014). In this respect, Choubert *et al.* (2013) stated that based on combined expertise of modellers (Phillips et al., 2009) and sensitivity analysis (Petersen et al., 2002) profound effects, of which the following are impacted by primary sedimentation, of wastewater characterisation on modelling outputs (Henze *et al*. 2000) have been proven:

- Sludge production is influenced by the estimated inert particulate COD.
- Oxygen demand is influenced by the estimated total biodegradable COD.
- Anoxic denitrification rate and anaerobic phosphorus release are influenced by the estimated readily biodegradable COD.
- Effluent COD is influenced by the estimated inert soluble COD.

The primary sedimentation tanks are highly dynamic systems with complex mechanisms governing the removal of particles and as such they can be hardly described based on simple average removal efficiencies.
In the remainder of this chapter an overview is given on the theoretical description of primary sedimentation and of the most important primary sedimentation models. Finally the different types of models and their applicability within the whole plant model of the WWTP of Eindhoven, which is mainly based on process models such as the activated sludge models (ASM) (Henze et al., 2000), are discussed.

4.4. THEORETICAL DESCRIPTION OF PRIMARY SEDIMENTATION

4.4.1. Wastewater characterisation

Gravitational settling is governed by the difference of the weight of the particle and the buoyancy force (the upward force created by the displaced fluid) the particle creates. Both forces are quantified by the mass of respectively the particle and the displaced fluid. As such, gravitational settling is based on the density difference between particle and displaced fluid, i.e. the wastewater. Random environmental factors (heat flux and wind action) and inlet conditions often cause drastic changes to the density and velocity field (e.g. short circuiting and circulating flows), which in turn can cause major variations in suspended solids removal (Christoulas et al., 1998).

Although no references where found addressing the density of the wastewater, it can be assumed to be close to that of water. Table 4.1 lists densities for different aqueous solutions. The density of aqueous solutions containing salts or organics likely to occur in wastewater do slightly vary from that of pure water. However, the deviations are small, even for concentrations higher than the ones encountered in typical wastewaters.

Table 4.1. Densities and specific gravities (reference to the density of water at 4°C) for different aqueous solutions (Perry et al., 1997).

Component	Specific gravity -	Density kg/m³
Water (4°C)	1.00	999.97
Water (15°C)	1.00	999.10
Water (20°C)	1.00	998.20
Water (25°C)	1.00	997.05
Ammonium chloride 2% (20°C)	1.00	1004.50
Calcium chloride 2% (20°C)	1.01	1014.80
Ferric Sulfate 2% (17.5°C)	1.02	1015.70
Magnesium sulfate 2% (20°C)	1.02	1018.60
Potassium carbonate 2% (20°C)	1.02	1016.30
Sodium carbonate 2% (20°C)	1.02	1019.00
Sodium chloride 2% (25°C)	1.01	1011.12
Acetone 2% (20°C)	1.00	995.72
Acetic acid 2% (20°C)	1.00	999.60
Ethanol 2% (20°C)	0.99	994.53
Glycerol 2% (20°C)	1.00	1003.00

Wastewater contains a broad range of particulate pollutants, which may be organic (food residues, micro-organisms, cellulose fibres…) or inorganic (sand, salts…) from nature. Sand, having a specific gravity (equation 4.1) between 1.40 and 1.70 (density between 1400 and 1700 kg/m³) is clearly one of the denser particles occurring in wastewater (Table 4.2). Only minerals and rubble masonry are demonstrating higher specific gravities. However, the rubble masonry are likely to settle in a grid chamber before the primary sedimentation tanks. In respect to the minerals, their specific gravities are determined on dense particles. However, the minerals formed and precipitating in wastewater are presumably more porous in nature and as such they will have lower densities (and specific gravities).

$$SG = \frac{\rho_c}{\rho_{w,4}} \qquad (4.1)$$

Where SG is the specific gravity of the component [-], ρ_c is the density of the component [g/m³], $\rho_{w,4}$ is the density of pure water at 4°C [g/m³].

Municipal wastewater contains particles ranging from small colloids up to very large particles (Figure 4.2). Sophonsiri and Morgenroth (2004) reported a uniform distribution of number of particles over the studied range (0.001 µm to 1000 µm). Dulekgurgen et al. (2006) evidenced particle sizes encountered in wastewater in the range of 2 nm up to more than about 2 µm (Figure 4.1).

Table 4.2. Specific gravities and densities of different components possibly occurring in municipal wastewater.

Group	Component	Specific gravity -		Density kg/m³		References
		Min	Max	Min	Max	
Various	Biomass	1.02	1.06	1020.00	1056.00	(Schuler and Jang, 2007)
	Starch	1.53		1529.96		(Perry et al., 1997)
	Fats	0.90	0.97	899.97	969.97	(Perry et al., 1997)
	Cellulose	1.59	1.58	1592.00	1583.00	(Mwaikambo and Ansell, 2001)
	Cotton	1.47	1.50	1469.96	1499.96	(Perry et al., 1997)
	Wool	1.32		1319.96		(Perry et al., 1997)
	Paper	0.70	1.15	699.98	1149.97	(Perry et al., 1997)
Excavated	Earth	1.20		1199.97		(Perry et al., 1997)
	Clay	1.00		999.97		(Perry et al., 1997)
	Sand	1.40	1.70	1399.96	1699.95	(Perry et al., 1997)
Rubble Masonry	Bluestone	2.20	2.50	2199.94	2499.93	(Perry et al., 1997)
	Granite	1.30	2.60	1299.96	2599.93	(Perry et al., 1997)
	Limestone	2.00	2.70	1999.94	2699.92	(Perry et al., 1997)
	Marble	2.30	2.70	2299.94	2699.92	(Perry et al., 1997)
	Sandstone	1.90	2.50	1899.95	2499.93	(Perry et al., 1997)
Minerals	Chalk (calcite)	1.80	2.80	1799.95	2799.92	(Perry et al., 1997)
	Gypsum, alabaster	2.30	2.80	2299.94	2799.92	(Perry et al., 1997)
	Magnesite	3.00		2999.92		(Perry et al., 1997)
	phosphate rock, apatite	3.20		3199.91		(Perry et al., 1997)
	hydroxyapatite	3.14	3.21	3139.91	3209.91	(Anthony et al., 2009)
	Goethite	4.28		4279.88		(Anthony et al., 2009)
	Hematite	5.26		5259.85		(Anthony et al., 2009)
	Lepidocrocite	4.00		3999.89		(Anthony et al., 2009)
	Maghemite	4.86		4859.86		(Anthony et al., 2009)
	Magnetite	5.18		5174.86		(Anthony et al., 2009)
	Sand	2.00	2.65	1999.94	2650.00	(Perry et al., 1997; Takamatsu et al., 2009)

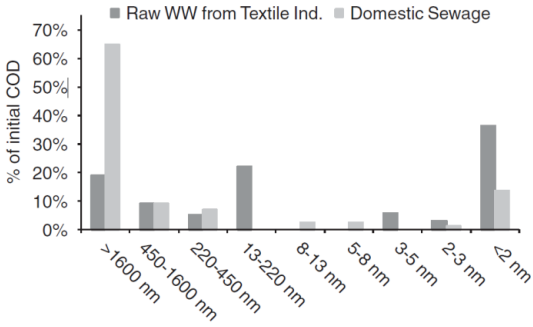

Figure 4.1. Percent distribution of COD fractions for textile wastewater and domestic sewage (Dulekgurgen et al., 2006).

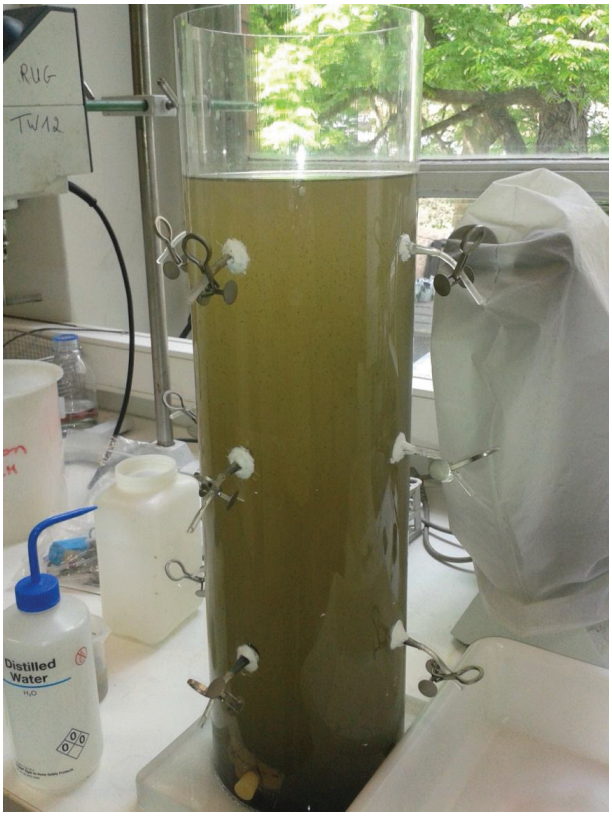

Figure 4.2. Settling column test for discrete settling on wastewater from the WWTP of Roeselare (Belgium) showing the discrete particles in the wastewater.

In sedimentation tanks, even though the mean flow velocities are relatively low compared to other processes, the Reynolds number is sometimes high enough to cause turbulent flow. In fact turbulent flow in clarifiers is caused by mixing of the influent with the flow in the tank (Matko et al., 1996) and mainly exist in the inlet section.

The discrete settling velocity of particles depends also on the flow pattern around the particle, not to be confused with the general flow pattern. A laminar flow around the particle will result in a larger drag coefficient (Equation 4.11) than turbulent flow (Equation 4.14). The flow pattern around the particle depends largely on its settling velocity, i.e. the higher the velocity the more turbulence is introduced. Using sand as an upper boundary for the settling velocity of particles, Figure 4.3 demonstrates that the flow patterns around particles in primary sedimentation are rarely turbulent.

From equation 4.2 (Tchobanoglous et al., 2004), a relation between the particle size and the settling velocity, for a constant Reynolds number (Re) can be derived (Figure 4.3).

$$Re = \frac{v_p \cdot d_p \cdot \rho_w}{\mu} = \frac{v_p \cdot d_p}{\nu} \quad (4.2)$$

Where μ is the dynamic viscosity [N.s/m²], ν is the kinematic viscosity [m²/s], v_p is the velocity of the particle [m/s], d_p is the diameter of the particle [m] and ρ_w is the density of water [g/m³].

The laminar region, for flows around the particle, unfolds below a Reynolds number Re equal to about 1. On the other side, the turbulent particle flow region stretches out above an Re equal to about 2000 (Tchobanoglous et al., 2004). The transitional region spans in between. Perry et al. (1997) define the boundaries of the zones slightly different, i.e. the laminar flow regime for Re smaller than 0.1 and the turbulent flow regime for Re larger than 1000.

Pragmatic boundaries for typical conditions in a primary sedimentation tank are based on a maximal particle diameter and settling velocities. As first boundary, a safe maximum particle diameter is deduced doubling the maximum diameter (1000 μm or 1 mm) reported by Sophonsiri and Morgenroth (2004). As second boundary, assuming sand as fast settling particles, the sand settling velocity, calculated according to equations 4.3-4.5, can be considered as an upper limit. Considering this demarcated area of feasible primary sedimentation tank conditions, it mainly covers the laminar and transitional regions for flow around the particle.

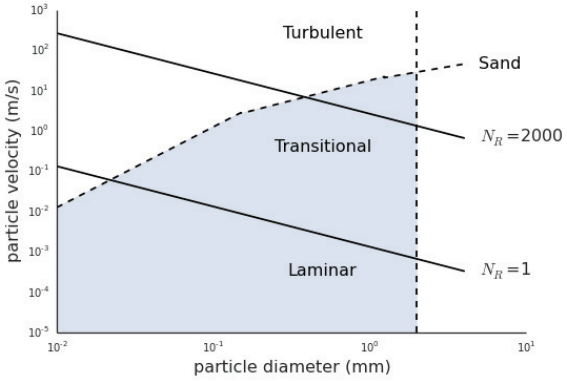

Figure 4.3. Laminar, transitional and turbulent flows around the particles for different particle diameters and settling velocities calculated according to Tchobanoglous et al. (2004). The grey area confines typical primary sedimentation tank conditions, for which the boundaries are based on settling velocities of sand (Yoshikawa et al., 2013) and a maximum particle diameter based on the observation of Sophonsiri and Morgenroth (2004).

Yoshikawa et al. (2013) estimated the settling velocities of sand particles from theoretical formulas (Equations 4.3-4.5) derived from Stokes' law using the particle diameter and the relative density.

$d_s < 0.015\,, v_s = 12295.5 \cdot d_s^2$ (4.3)

$0.015 \leq d_s < 0.124\,, v_s = 175.8 \cdot d_s$ (4.4)

$0.124 \leq d_s < 0.531\,, v_s = 82.4 \cdot d_s^{0.667}$ (4.5)

4.4.2. Types of sedimentation

During the sedimentation process, suspended particles heavier than water are separated by gravitational settling (Tchobanoglous et al., 2004).

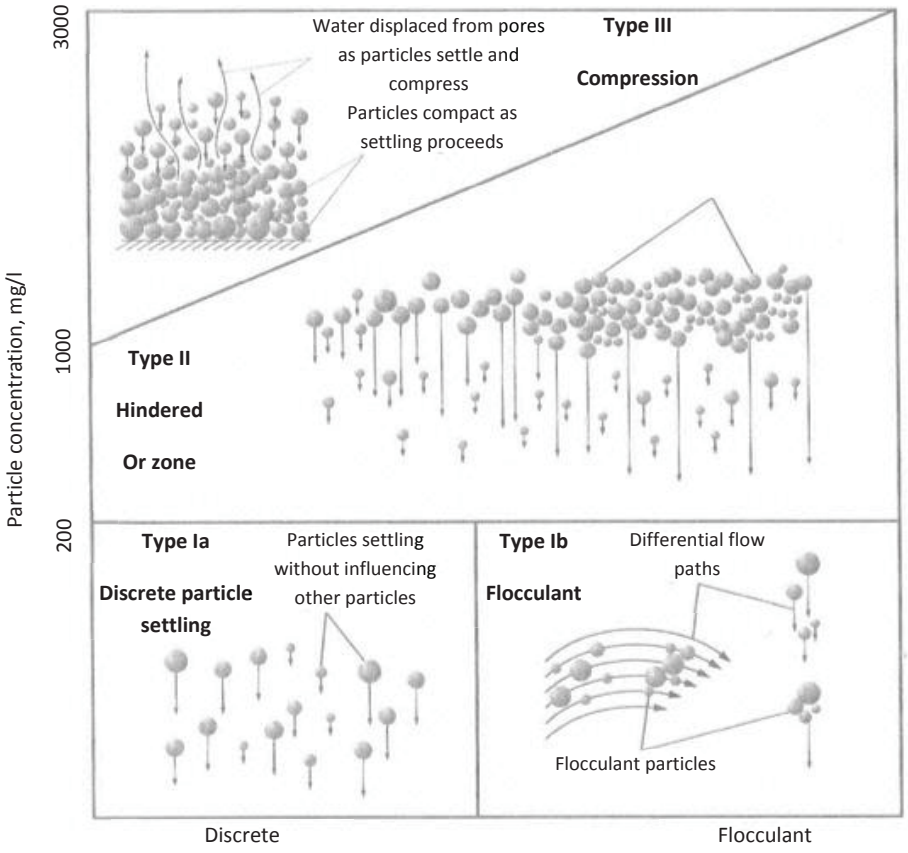

Figure 4.4. Relationship between settling type, concentration, and flocculent nature of particles redrafted from Crittenden et al. (2005).

4.4.2.1. Type I: Discrete particle settling

Discrete particle settling refers to the gravitational settling of particles in a suspension of low solids concentration (≤ ±1000 mg/l). At really low concentration (≤ ±200 mg/l) the particles have no significant interaction with neighbouring particles (Tchobanoglous et al., 2004) and the particles settle as individual entities. At these low concentrations flocculation is almost non-existent nor do the particles change in size, shape or specific gravity in time (Peavy et al., 1985). At the intermediate concentration ranges (between ±200mg/l and ±1000 mg/l) flocculation starts to play a role. Hence, in several text books (Crittenden et al., 2005; Tchobanoglous et al., 2004) this region is called flocculent settling and identified as a different settling type.

Flocculation is induced by liquid flow velocity gradients causing particles in a region of a higher velocity to collide with those in adjacent stream paths moving at slower velocities. Flocculation mainly occurs within the inlet zone of the primary sedimentation tanks where the turbulence is sufficient to create the velocity gradients. Flocculation leads to particles increasing in size, shape and mass, resulting in particles with a different settling rate. The flocculated particles settle again as discrete particles. As such within this work flocculant settling is considered to be a special case of the discrete settling and is not considered as a separate settling type. Describing the flocculation process is outside the scope of this work.

This type of settling is encountered in wastewater grit chambers, in primary sedimentation tanks, in the clarification zone of secondary clarifiers, in the clarification of certain industrial wastes (e.g. sand and gravel washings) and in clarifiers following coagulation-flocculation (Crittenden et al., 2005; Montgomery, 1985; Riffat, 2013; Tchobanoglous et al., 2004).

4.4.2.2. Type II: Hindered settling or zone settling

Hindered settling refers to gravitational settling of particles in suspensions of intermediate concentration (1000 - 3000 mg/l). Interparticle forces tend to hinder the settling of adjacent particles by decreasing the settling velocity. This type of settling is mostly observed in secondary clarifiers following biological treatment.

4.4.2.3. Type III: Compression settling

Compression settling refers to gravitational settling in highly concentrated suspensions. Due to the high concentration (> 3000 mg/l), the particles are in contact and a structure is formed and settling can occur only by compression of that structure caused by the weight of the particles. Compression settling is observed at

the bottom of secondary clarifiers following activated sludge reactors and also in solid thickeners (Riffat, 2013).

4.4.3. Primary sedimentation

Primary sedimentation is a complex process involving flocculation, gravitational settling and drag. From the four defined types of gravitational settling basically only discrete particle settling and flocculent settling occur in primary sedimentation tanks. I.e. the influent of the PSTs is rarely of sufficient particle concentration to encounter hindered settling (Montgomery, 1985; Riffat, 2013) nor compression settling.

4.4.3.1. Discrete particle settling theory

In dilute solutions, particles settle in a discrete manner due to two forces acting on the particles, i.e. the gravitational force and the drag force. The gravitational force is the result of the difference of the weight of the particle (a downward force originating from the mass of the particle) and the buoyancy force (an upward force created by the fluid displaced by the particle). The gravitational force is quantified using equation 4.6.

$$F_G = (\rho_p - \rho_w) \cdot g \cdot V_p \quad (4.6)$$

Where F_G is the gravitational force [kg.m/s²], ρ_p is the density of the particle [kg/m³], ρ_w is the density of water [kg/m³], g is the acceleration due to gravity [9.81 m/s²] and V_p is the volume of the particle [m³].

Whenever relative motion exists between a particle and a surrounding fluid, the fluid will exert a drag upon the particle. In steady flow, the drag force on the particle is calculated using equation 4.7 (Perry et al., 1997).

$$F_d = \frac{C_D \cdot A_p \cdot \rho_w \cdot v_p^2}{2} \quad (4.7)$$

Where F_d is the frictional drag force [kg.m/s²], C_D is the drag coefficient [-], A_p is the cross-sectional or project area of particles in direction of the flow [m²] and v_p is the particle settling velocity [m/s].

The drag force, opposed to the gravitational force, depends on the particle velocity. As a consequence the particle will be accelerating until both forces balance. The terminal settling velocity can then be calculated from the gravitational force and the frictional drag force for spherical particles equation 4.8.

$$v_p = \sqrt{\frac{2 \cdot g \cdot m_p \cdot (\rho_p - \rho_w)}{\rho_w \cdot \rho_p \cdot A_p \cdot C_D}} \quad (4.8)$$

Where m_p is the particle mass [kg].

Specifying the terminal velocity for spherical particles yields Newton's law (Equation 4.9).

$$v_p = \sqrt{\frac{4 \cdot g}{3 \cdot C_d} \cdot \left(\frac{\rho_p - \rho_w}{\rho_w}\right) \cdot d_p} = \sqrt{\frac{4 \cdot g}{3 \cdot C_d} \cdot \left(SG_p - 1\right) \cdot d_p} \quad (4.9)$$

Where v_p is the terminal velocity of particle [m/s], d_p is the diameter of the particle [m] and SG_p is the specific gravity of the particle [-].

The calculation of the drag coefficient depends on the flow regime surrounding the particle, i.e. whether the flow regime is laminar or turbulent. In the laminar regime (Re < 1) the drag is given by Stokes' law (Equation 4.10), which can also be written as equation 4.11. The corresponding terminal settling velocity simplifies to equation 4.12.

$$F_d = 3 \cdot \pi \cdot v_p \cdot d_p \quad (4.10)$$

$$C_D = \frac{24}{Re} \quad (4.11)$$

$$v_p = \frac{g \cdot d_p^2 \cdot (\rho_p - \rho_w)}{18 \cdot \mu} \quad (4.12)$$

In the transitional regime (1 < Re < 2000), the drag coefficient may be estimated using equation 4.13.

$$C_D = \left(\frac{24}{Re}\right) \cdot (1 + 0.14 \cdot Re^{0.70}) \quad (4.13)$$

In the turbulent regime (2000 < Re < 350000), C_D equals 0.445 (Equation 4.14). In this region the terminal velocity becomes equation 4.15.

$$C_D = 0.445 \quad (4.14)$$

$$v_t = 1.73 \cdot \sqrt{\frac{g \cdot d_p \cdot (\rho_p - \rho_w)}{\rho_w}} \quad (4.15)$$

4.4.3.2. Flocculation

Sewage contains many flocculent particles, of which the variable flocculation and settling characteristics are influenced by many factors (Christoulas et al., 1998). Particles in relatively dilute solutions may aggregate during sedimentation. As aggregation or flocculation occurs, the mass and the volume of the particle changes, and hence the settling velocity changes. The extent to which flocculation occurs depends on the opportunity for contact and the physical-chemical properties of the particles. The opportunity for contact varies with overflow rate, depth of the basin, velocity gradients in the system, concentration of particles and range of particle sizes. Population balance models (PBM) can be used to study the effect of these variables (Nopens, 2005; Nopens et al., 2015) and to interpret the results of sedimentation tests.

Two types of flocculation can be distinguished based on the particle sizes involved: (i) micro-flocculation and (ii) macro-flocculation (Tchobanoglous et al., 2004).

Micro-flocculation, significant for particles in the size range from 0.001 to about 1 µm, is the by Brownian motion induced aggregation of particles. For macro-flocculation, on the other hand, the aggregation of particles greater than 1 or 2 µm, is initiated by induced velocity gradients. Particles with a higher velocity collide with slower particles and may stick together, a larger particle is formed that depending on the porosity and hence the final floc density settles either faster or slower.

Whether or not the colliding particles aggregate depends on the physical-chemical properties of the particles and the consequent forces. Physical-chemical properties that influence aggregation are the electrical charge, presence of induced dipoles, surface roughness, hydrophobicity, ionic strength of the solution and the presence of gas bubbles. As a result of these properties several forces influence the aggregation, amongst which the electrostatic coulombic forces, the London-van der Waals dispersion force, hydrogen bonding and osmotic pressure (Grasso et al., 2002). A complete description of the different processes is considered valuable but outside of the scope of this work.

4.4.3.3. Resuspension

Resuspension or scouring is occurring in sedimentation tanks where the stored sludge bed rises to a significant level. Scouring typically occurs through vortexes that occur at too high flow velocities. Shiba and Inoue (1975) identified scouring as one of the major factors impacting the removal efficiency of primary sedimentation tanks. On the other hand Lessard and Beck (1988) and Paraskevas et al. (1993) conclude that scouring is not significant in their cases. These contradictory observations may be explained by the possible differences in operation of the sedimentation tanks. This scouring is likely to be more significant when a higher sludge bed is present in the tanks. (Tchobanoglous et al., 2004) present a critical velocity (Equation 4.16) above which scouring is likely to be important.

$$v_H = \left(\frac{8 \cdot k \cdot (SG_p - 1) \cdot g \cdot d_p}{f}\right)^{1/2} \quad (4.16)$$

Where v_H is the horizontal velocity that will just produce scour [m/s], k is a constant that depends on type of material being scoured [-], SG_p is the specific gravity of the particles [-], g is the acceleration due to gravity [9.81 m/s²], d_p is the diameter of the particles [m] and f is the Darcy-Weisbach friction factor [-]. Typical values of k are 0.04 for unigranular sand and 0.06 for more sticky, interlocking matter. The term f depends on the characteristics of the surface over which flow is taking place and is inversely proportional to the Reynolds number. Typical values of f are 0.02 and 0.03.

4.4.4. Primary sedimentation tanks

Conventional primary sedimentation tanks used in wastewater treatment are of rectangular, circular, or square configuration. In circular tanks, such as applied at the WWTP of Eindhoven, the wastewater typically enters in the centre of the basin to obtain a radial flow pattern (Figure 4.1). The inlet structure normally consists of a circular weir around the influent vertical rise pipe, which is designed to distribute the water uniformly over the entire cross section of the tank. The inlet weir provides space for energy dissipation and directs the flow downward into the bottom part of the settling tank where particles are removed (Montgomery, 1985; Riffat, 2013; Tchobanoglous et al., 2004). The bottom of the basin is sloped to form an inverted cone. The solids, which settle out, are removed by scrapers that move along the bottom of the tank, into a hopper located near the center. There, they are withdrawn by sludge pumps (Heynderickx and Defrancq, 2013; Montgomery, 1985; Tchobanoglous et al., 2004). The outlet structure normally consists of a single, V-notch weir constructed at the outside perimeter of the tank. Baffles near the outlet and surface-skimming devices are usually not provided, unless the influent water has problems with debris and flotable material (Montgomery, 1985).

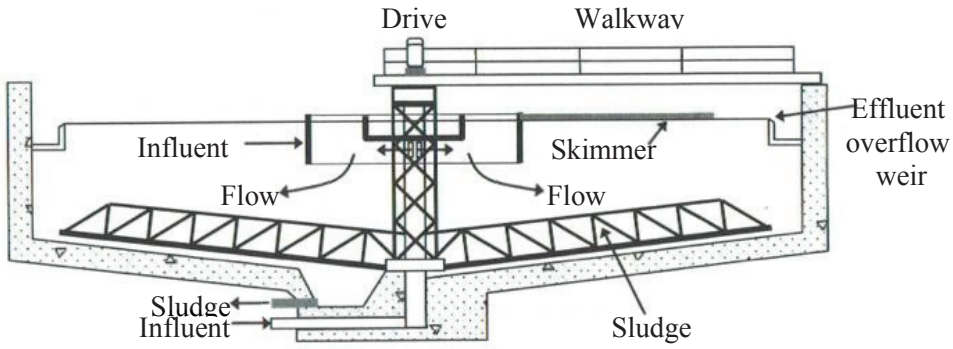

Figure 4.5. Circular sedimentation tank with central feed (Riffat, 2013).

The design of primary clarifiers is determined by the detention time, the overflow rate and the weir loading rate (Riffat, 2013). The diameter of the circular basins is normally calculated on the basis of the overflow rate (Montgomery, 1985). An ideal sedimentation tank is designed to completely remove the particles with a specified settling velocity v_o. Assuming that the particles reach the maximum settling velocity immediately, for a sedimentation tank with a constant flow field over the entire range (typical for rectangular clarifiers) the sedimentation path of the particles is more or less linear (Figure 4.6). Two forces (the gravitational force and the drag force by the fluid movement) acting on the particle cause its descent.

In the ideal horizontal tank theory (Camp and Estrada, 1953) the fluid drag force is considered horizontal and static, resulting in a quasi linear descent. Under dynamic conditions (filling of storm tanks or varying influent flow rates) the descent becomes curved (Takamatsu et al., 2009). The latter holds even more for circular primary sedimentation tanks. Given the radial pattern, even under static influent flows, the fluid velocity decreases from the inlet structures towards the outlet structures. I.e. the same flow rate passes through a larger cross sectional area. The settling zone extends from radius r_i to r_0 and the wastewater flow rate is Q. The flow paths of two particles, P_1 and P_2, are illustrated, along with their horizontal and vertical components of velocity. The fluid enters the basin in the centre of the basin (inlet zone) through the settling zone and its velocity changes according to equation 4.17 (Crittenden et al., 2005; Tchobanoglous et al., 2004).This decrease in fluid velocity results in a parabolic particle path curve (Figure 4.7).

$$v_f = \frac{Q}{2\pi(r-r_i)h_0} \tag{4.17}$$

Where v_f is the fluid velocity [m/s], Q is the flow rate [m^3/s], r is the distance measured from the centre of the basin [m], r_i is the radius of the inlet zone [m] and h_0 is the depth of the settling zone [m]

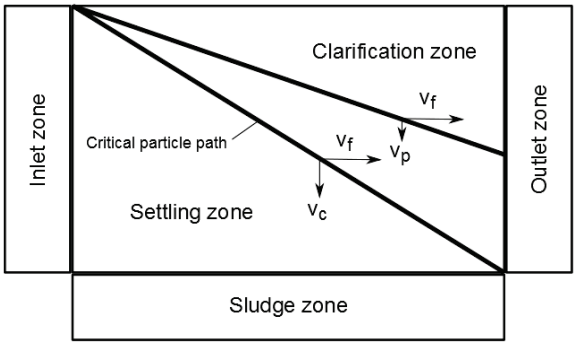

Figure 4.6. Definition sketch for the analysis of ideal discrete particle settling (Camp and Estrada, 1953) for a constant flow field over the entire range of the sedimentation tank (redrafted after Tchobanoglous et al. (2004)).

All particles with a terminal settling velocity greater than v_o will be completely removed, while particles with a lower settling velocity will be fractionally removed.

The flow path of particle 1, starts at the top of the inlet zone and enters the sludge zone just before the outlet zone. The settling velocity v_c of particle 1 and the distance it has settled are related as follows (Equation 4.18):

$$h_{p,t} = t_s \cdot v_c = \frac{\pi(r^2-r_i^2)h_0}{Q} v_c \tag{4.18}$$

Where $h_{p,t}$ is the distance from the water surface or top for particle 1 [m], t_s is the settling time [s], v_c is the critical settling velocity [m/s].

Particles with a settling velocity greater than or equal to v_c will be completely removed. The critical settling velocity and the overflow rate are related as follows (Equation 4.19):

$$v_c = \frac{h_0}{\tau} = \frac{h_0 Q}{\pi(r^2 - r_i^2)h_0} = \frac{Q}{\pi(r^2 - r_i^2)} = \frac{Q}{A} = OR \qquad (4.19)$$

Where h_0 is the depth of settling zone [m], τ is the hydraulic detention time of the basin [s], Q is the flow rate [m^3/s], r_0 is the radius of the settling zone and inlet zone [m], r_i is the radius of the inlet zone [m], A is the area of the top of the basin in the settling zone [m^2], v_c is the critical particle settling velocity [m/s], OR is the overflow rate [$m^3/m^2.s$].

Assuming the inlet zone is homogenous, i.e. the particles are uniformly distributed, particles can enter the settling zone at any height h_p. Particles with a settling velocity v_p greater than or equal to the critical settling velocity v_c will be completely removed irrespective of the starting height because they will reach the sludge zone before they could exit the basin.

Particles with a settling velocity less then v_c may also be removed but their starting position is of critical importance. Particles at the top of the basin will not be removed as they will pass through the settling zone and exit in the outlet zone. On the other hand, particles starting at height h_p and lower will be removed because they will enter the sludge zone before exiting the basin, as shown in Figure 4.7. The fraction of particles removed is given by equation 4.20 (Crittenden et al., 2005; Riffat, 2013; Tchobanoglous et al., 2004).

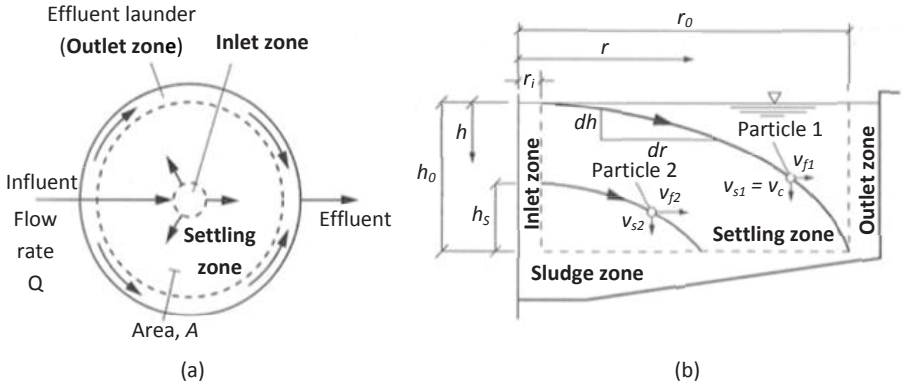

Figure 4.7. Analysis of particle settling in an ideal circular sedimentation tank: (a) plan view of circular sedimentation tank and (b) particle trajectory of discrete particles in settling zone of circular sedimentation tank (Crittenden et al., 2005).

$$X_{pr} = \frac{h_p}{h_0} = \frac{h_p/\tau}{h_0/\tau} = \frac{v_p}{OR} = \frac{v_p}{v_c} \ (v_p < v_c) \quad (4.20)$$

where X_{pr} is the fraction of particles removed [-], h_p is the height of the particle relative to the bottom of the tank at the position entering the settling zone [m] and v_p is the particle settling velocity, smaller than v_c, [m/h].

This approach of the critical particle path is an idealized approach ignoring the impact of non-ideally mixed tank reactors and particle distributions (particles size distributions (PSD), particle density distributions (PDD) and particle settling velocity distributions (PSVD)). The impact of non-ideally mixed tank reactors can be quantified more thoroughly using computational fluid dynamics (CFD). Whereas the particle distributions can be quantified using population balance models.

4.5. Primary sedimentation models in literature

4.5.1. Ideal separation

The ideal separation model or point-settler model describes the primary sedimentation in an extremely simplified way. The volume, and thus the retention time, is not taken into account at all. The particulate matter is divided according to a non-settleable fraction (Equation 4.21). The soluble fraction is divided relative according to the flow rates, i.e. the concentration of each soluble fraction is considered to be equal in both the effluent as the underflow. It is also assumed that there are no biological reactions.

$$X_{Out} = f_{ns} \cdot X_{In} \quad (4.21)$$

Where X_{Out} is the effluent suspended solids concentration [mg/l], X_{In} is the influent suspended solids concentration [mg/l] and f_{ns} is the fraction of non-settleable solids [-].

4.5.2. Silva et al. (2014)

Silva et al. (2014) developed removal efficiency curves for the process units of a wastewater treatment train of five different WWTPs based on 5-years of field data. Also primary sedimentation was considered as one of the process units and correlations between the maximum and average removal efficiency and the incoming concentration were proposed (Equation (4.22). The parameters of the proposed removal efficiency curves (Table 4.3) were estimated using linear regression (weighted least square regression).

$$E_r = \left(a - \frac{b}{C_{In}}\right) \cdot 100 \quad (4.22)$$

Where E_r is the removal efficiency [%], C_{In} is the influent concentration [mg/l] and a [-] and b [mg/l] are regression coefficients.

Table 4.3. parameters for the calculation of the removal efficiency of primary sedimentation tanks for TSS and COD.

		a	b
TSS	$E_{r,max}$	0.978	31.36
	$E_{r,avg}$	0.979	100.72
COD	$E_{r,max}$	0.895	97.57
	$E_{r,avg}$	0.953	339.77

4.5.3. Christoulas et al. (1998)

Many physical processes, such as the detailed velocity field (in its turn influenced by heat flux and wind action causing short circuiting and circulating flows), influent suspended solids concentration, particle size and density, and the density and viscosity of the fluid, influence flocculation and settling. In the absence of a practical approach, dealing with these physical processes, Christoulas et al. (1998) developed an empirical or regression model (Equation 4.23-4.26), based on the work of Tebbutt et al. (1979). In the empirical model, the impact of temperature is considered as a crucial factor. The temperature affects the settling velocities as well as the velocity gradients in the liquid which in turn affect flocculation. They concluded, based on two studies with not too much differing temperatures (15°C versus 15.9°C) where the developed regression model yielded two similar sets of values, that the influent suspended solids concentration, the surface overflow rate and temperature are the major drivers.

$$E_s = a \cdot e^{\left(-\frac{b}{S_i} - c \cdot q\right)} \quad (4.23)$$

Where E_s is the removal efficiency for suspended solids [-], S_i is the influent suspended solids concentration, q is the surface overflow rate [m/d] and a [d/m], b [g/m³] and c [d/m] are regression coefficients.

$$b = 683.6 - 21.13 \cdot T \quad (4.24)$$

$$a = 1.71 - 0.03 \cdot T \quad (4.25)$$

$$c = 0.0035 \quad (4.26)$$

Where T is the temperature [°C].

Within their study, the averaged removal efficiencies of suspended solids and organic matter revealed a good linear relationship. Using this data, a regression model was derived for the removal of organic matter, expressed as COD (Equation 4.27).

$$E_c = 0.733 \cdot E_s - 0.08 \quad (4.27)$$

Where E_c is the removal efficiency of organic matter expressed as COD [-].

4.5.4. Otterpohl and Freund (1992)

Otterphol and Freund (1992) developed a model for a primary clarifier that describes (i) dilution and buffering of influent concentrations, (ii) dynamic behaviour of flow changes (fast) and concentration changes (slow), (iii) reduction of particulate fractions of COD and nitrogen and (iv) buffering of sludge water loads added to the tank.

The removal efficiency for COD is based on an empirical equation (Equation 4.28), initially developed for BOD removal (Sierp, 1967), which links the removal to the hydraulic residence time. Otterpohl and Freund (1992) applied the curve for removal of particulate COD (Equation 4.31).

$$\eta_{COD} = 2.7 \cdot (\ln(\tau^2) + 9) \quad (4.28)$$

Where η_{COD} is the efficiency of the COD removal [%] and τ is the hydraulic retention time in the primary clarifier [h] (Equation 4.29). Note that due to the use of the natural logarithm the unit conversion of the parameters is not straightforward (Equation 4.30).

$$\tau = \frac{V}{Q_\tau} \quad (4.29)$$

Where V is the active capacity of the primary clarifier [m³] and Q_τ is the average flow for the residence time [m³/h].

$$\eta_{COD} = 2.7 \cdot \left(\ln(\tau_{nu}^2) + \left(9 + 2 \cdot \ln\left(N_{hpnu}\right)\right)\right) \quad (4.30)$$

where τ_{nu} is the hydraulic retention time in the primary clarifier in the new unit [u], u is the new unit (days, minutes, seconds…) and N_{hpnu} is the number of hours per new unit (24 hours per day, 1/60 hours per minute, 1/3600 hours per second).

$$\eta_X = \eta_{COD} \cdot \frac{COD_{Total}}{COD_{particulate}} \quad (4.31)$$

Where η_X is the efficiency of the particulate COD removal [%], COD_{Total} is the total COD [mg/l] and $COD_{particulate}$ is the particulate COD [mg/l].

In later work, Otterpohl (Otterpohl, 1995) proposed a modified version for the empirical equation to calculate η_X (Equation 4.32), which has been applied by Gernaey et al. (2014) in their work.

$$\eta_X = f_{corr} \cdot (2.88 \cdot f_X - 0.118) - (1.45 + 6.15 \cdot \ln(\tau \cdot 24 \cdot 60)) \quad (4.32)$$

Where η_X is the efficiency of the particulate COD removal [%], f_{corr} is a dimensionless correction factor [-], f_X is the mean fraction of particulate COD [-] and τ is the hydraulic retention time [d].

4.5.5. Voshel and Sak (1968)

Voshel and Sak (1968) presented a model, based on a two-month measurement campaign at the Gran Rapids Water Pollution Control Plant, showing the quality of primary effluent with and without the addition of flocculants. The model is based on a correlation (Equation 4.33), showing a directly proportional relationship between suspended solids (SS) removal and a power function of the suspended solids content and inversely proportional to a power function of the hydraulic loading. Table 4.4 shows the estimated parameter values obtained by Voshel and Sak (1968), Akça et al. (1993) and Funamizu and Takakuwa (1994).

$$R_{SS} = a \cdot \frac{W^n}{Q_{hl}^m} \qquad (4.33)$$

Where R_{SS} is the suspended solids removal [%], W is the suspended solids content of the feed [mg/l], Q_{hl} is the hydraulic loading [m³/(s.m²)] and a, n and m are regression constants.

Table 4.4. Estimated regression coefficients of SS removal for the original publication by Voshel and Sak (1968) (with and without polymer addition), by Akça et al.(1993) (without polymer addition) and by Funamizu and Takakuwa (1994) (in two parallel lanes without polymer addition).

Source		a	n	m
Voshel and Sak (1968)		1399[(1)]	0.27	0.22
Voshel and Sak (1968)	With polymer addition	517[(1)]	0.17	0.13
Akça et al. (1993)		39[(2)]	0.22	0.27
Funamizu and Takakuwa (1994)	Lane 1	0.179[(2)]	0.312	0.0265
Funamizu and Takakuwa (1994)	Lane 2	0.500[(2)]	0.290	0.0807

(1) SI unit [m³/(s.m²)]recalculated from the US customary unit [gpd/sq ft] reported in the original publication

(2) SI unit [m³/(s.m²)] recalculated from [m³/(d.m²)] as reported in the publication

4.5.6. El-Din and Smith (2002a)

El-Din and Smith (2002a) developed a model combining stochastic and transfer-function components to describe the impact of influent TSS, COD and flow on the primary clarifier effluent TSS and COD (equation 4.34 and 4.35 respectively). The data was collected during 2 measurement surveys of 1 week (June 28-July 5, 1999 and August 20-27, 1999) at a full-scale primary sedimentation tank at the Gold Bar Wastewater Treatment Plant (Edmonton, Alberta, Canada), for the model development, contained both dry weather days and rain events.

In first instance, using the Box-Jenkins methodology (Box and Jenkins, 1976), they built a mere stochastic dynamic model, which attempts to explain the variation in the output without relying on any input. In second instance, they demonstrated that

the addition of a transfer-function component improves the descriptive means and that the use of a transfer-function model by itself (no noise component) performs worse than the stochastic model on itself (no transfer-function component).

$$TSS_{Eff} = \frac{\omega_{1,0}}{1} \cdot Q_{In,t-1} + \frac{\omega_{2,0}}{1} \cdot TSS_{In,t-1} + \frac{1}{(1-\phi_1 \cdot B)} \cdot a_t \qquad (4.34)$$

Where TSS_{Eff} is the TSS effluent concentration [mg/l], t is the current time [h], $Q_{In,t-1}$ is the influent flow rate at time t minus 1 time step (hour) [m³/h], $TSS_{In,t-1}$ is the influent TSS concentration at time t minus 1 time step (hour) [g/m³], a_t is a series of uncorrelated independent ''shocks'', which are random drawings from a fixed distribution [-], B is the backshift operator [-], $\omega_{1,0}$ is the zero order term of the numerator of the first transfer function [-], $\omega_{2,0}$ is the zero order term of the numerator of the second transfer function [-] and φ_1 is the first order term of the auto-regressive operator of the stochastic model [-].

Table 4.5. Estimated parameter values for the transfer-function noise by El-Din and Smith (2002a).

Parameter	Survey 1 TSS (mg/l)	Survey 2 TSS (mg/l)	Survey 2 COD (mg/l)
$\omega_{1,0}$	0.222 (0.022)	0.173 (0.025)	-0.135 (0.046)
$\omega_{2,0}$	0.034 (0.015)	0.053 (0.024)	0.170 (0.024)
$\delta_{2,1}$	-	-	0.757 (0.036)
ϕ_1	0.716 (0.07)	0.648 (0.072)	0.648 (0.097)
ϕ_2	-	-	0.182 (0.096)

$$COD_{Eff} = \frac{\omega_{1,0}}{1} \cdot Q_{In,t-1} + \frac{\omega_{2,0}}{(1-\delta_{2,1} \cdot B)} \cdot COD_{In,t-1} + \frac{1}{(1-\phi_1 \cdot B - \phi_2 \cdot B^2)} \cdot a_t \qquad (4.35)$$

Where $COD_{In,\ t-1}$ is the influent COD concentration at time t minus 1 time step (hour) [g/m³], $\delta_{2,1}$ is the first order term of the denominator of the second transfer function [-] and φ_2 is the second order term of the auto-regressive operator of the stochastic model [-].

4.5.7. Tay (1982)

Tay (1982) presented a primary sedimentation tank model based on data collected at two full scale wastewater treatment plants at Sarnia and Windsor and at the pilot plant in Burlington. The model accounts for the hydraulics and the settling characteristics of the wastewater. The settling characteristics are specified based on the half-removal time (T_A), which is the time at which 50% of the influent suspended solids is removed. As such the removed fraction (X_r) can be described by equation 4.36.

$$X_r = \frac{S_0 - S}{S} = \frac{t_r}{T_A + t_r} \qquad (4.36)$$

Where S_0 is the suspended solids concentration in the influent to the settling tank [mg/l], S is the suspended solids concentration in the effluent of the settling tank [mg/l], t_r is the hydraulic retention time in the settling tank [min] and T_A is the half-removal time [min]

4.5.8. Tchobanoglous et al. (2004)

In most suspensions encountered in wastewater treatment, a large gradation of particle sizes will be found. To determine the efficiency of removal for a given settling time, it is necessary to consider the entire range of settling velocities present in the system. The settling velocities of the particles can be obtained by use of a settling column test.

For a given clarification rate only those particles with a velocity greater than the critical settling velocity v_c will be completely removed. The remaining particles will be removed in the ratio F_{pr}. The total fraction of particles removed for a continuous distribution is given by equation 4.37.

$$f_R = \left(1 - F_{pr}\right) + \int_0^{x_c} \frac{v_p}{v_c} dx \qquad (4.37)$$

Where v_p is the particle settling velocity [m/s], v_c is the critical settling velocity [m/s], f_R is the fraction removed [-] and $(1\text{-}F_{pr})$ is the fraction of particles with velocity v_p greater than v_c and x_c [-] is the critical concentration [mg/l].

Discretization of equation 4.37 yields equation 4.38, which can be used for a number of settling classes determined with a column settling test.

$$f_R = \frac{\sum_{i=1}^{n} \frac{v_{n,i}}{v_c} \cdot (n_i)}{\sum_{i=1}^{1} n_i} \qquad (4.38)$$

Where $v_{n,i}$ is the average velocity of particles in the i^{th} velocity range [m/s] and n_i is the number of particles in the i^{th} velocity range.

4.5.9. Takamatsu et al. (2012)

Takamatsu et al. (2009) developed a so called particle pathline model extending the ideal horizontal theory (Camp and Estrada, 1953) for storm-water detention tanks. The principal of the model is that each particle follows a typical path in the tank induced by the different forces (gravitational and drag) impacting on the particle. The applied extension considers the dynamic behaviour of the influent (both flow rate and concentrations) and the particle size distribution.

The horizontal and vertical motion of a suspended solids particle is described by equation 4.39 and (4.40 respectively.

$$\frac{dx_s}{dt} = \frac{Q_{In}(t)}{B \cdot h(t)} - \frac{x_s}{h(t)} \cdot \frac{dh}{dt} = \left(1 - \frac{x_s}{L}\right) \cdot \frac{Q_{In}(t)}{B \cdot h(t)} + \frac{x_s}{L} \cdot \frac{Q_{Out}(h)}{B \cdot h(t)} \qquad (4.39)$$

Where t is the time [s], x_s is the longitudinal location of the particle measured from the basin inlet [m], $Q_{In}(t)$ is the influent flow rate at time t [m³/s], $Q_{Out}(t)$ is the effluent flow rate at time t [m³/s], B is the width of the basin [m], L is the length of the basin [m] and h(t) is the water depth in the basin at time t [m].

$$\frac{dz_s}{dt} = v(h,t) - v_s = \frac{z_s}{h(t)} \cdot \frac{dh}{dt} - v_s \quad (4.40)$$

Where z_s is the vertical position of the particle above the bottom of the basin [m], v(h,t) is the vertical flow velocity in the basin at height h and at time t [m/s] and v_s is the particle settling velocity [m/s]. Note that the water depth and the vertical flow velocity are made time dependent and for the latter as well location dependent, as the model was developed for a tank with a variable volume (i.e. the tank is being filled during a storm event and emptied afterwards). The critical settling velocity (equation 4.41) is defined for a particle that enters the basin at the water surface and reaches the bottom at the end of the tank.

$$v_{s,c}(t_{In}) = \frac{1}{\int_{t_{In}}^{t_{Out}} \frac{d\tau}{h(\tau)}} \quad (4.41)$$

Where t_{In} is the time at which the particles enter the basin [s], t_{Out} is the time at which the particles leave the basin [s], $v_{s,c}(t_{In})$ is the critical settling velocity at time t_{In} [m/s] and τ is the detention time [s].

The overall removal ratio of suspended solids is given by equations 4.42 to 4.45.

$$F(t_{In}; v_s) = \begin{cases} \frac{v_s}{v_{s,c}(t_{In})}, v_s \leq v_{s,c}(t_{In}) \\ 1, v_s > v_{s,c}(t_{In}) \end{cases} \quad (4.42)$$

Where $F(t_{In};v_s)$ is the removal fraction of suspended solids entering the basin at time t_{In} with a settling velocity v_s [-].

$$R_{Out}(t_{In}) = \int_0^{\infty} F(t_{In}; v_s) \cdot E(v_s) \cdot dv_s$$
$$= \int_0^{v_{s,c}(t_{In})} \frac{v_s}{v_{s,c}(t_{In})} \cdot E(v_s) \cdot dv_s + \int_{v_{s,c}(t_{In})}^{\infty} E(v_s) \cdot dv_s \quad (4.43)$$

Where $R_{Out}(t_{In})$ is the removed fraction of particles entering at time t_{In} [-], $E(v_s)$ is the fraction of particles with settling velocity v_s [-]. The first integral term of the equation refers to the removal of the particles with a settling velocity smaller than the critical settling velocity and the second integral term to the particles with a larger settling velocity, which are thus completely removed. Applying Stokes' law and omitting the particle density distribution yields equation 4.44.

$$R_{Out}(t_{In}) = \int_0^{d_{p,c}(t_{In})} \frac{d_p}{d_{p,c}(t_{In})} \cdot E(d_p) \cdot dd_p + \int_{d_{p,c}(t_{In})}^{\infty} E(d_s) \cdot dd_p \quad (4.44)$$

Where $d_{p,c}(t_{In})$ is the particle diameter of particles reaching the critical settling velocity [m] and d_p is the particle diameter [m].

The overall removal ratio of suspended solids (R_{SS} [-]) is than obtained by dividing the removed fraction of particles by the total particle mass inflow.

$$R_{SS} = \frac{\int_0^{T_{In}} Q_{In}(\tau) \cdot C_{In}(\tau) \cdot R_{Out}(\tau) \cdot d\tau}{\int_0^{T_{In}} Q_{In}(\tau) \cdot C_{In}(\tau) \cdot d\tau} \quad (4.45)$$

4.5.10. Shiba and Inoue (1975)

Shiba and Inoue (1975) developed a lumped parameter model to describe the unsteady state behaviour of a primary sedimentation tank. The models points out the significant influence of the scouring on the performance of the sedimentation tank. Scouring may be caused by turbulent mixing, circulating current and short circuiting flows which interfere with the sedimentation process. The mass balance for suspended solids can be written according to equation 4.46.

$$\frac{dC}{dt} = \frac{Q_{In} \cdot C_{In}}{V} - \frac{Q_{In} + (1-k) \cdot v_p \cdot A}{V} \cdot C \quad (4.46)$$

Where Q_{In} is the influent flow rate [m³/s], C_{In} is the influent concentration of suspended solids [mg/l], k is the scouring parameter [-] (Equation 4.47), v_p is the setting velocity of suspended particles [m/s], A is the surface of the sedimentation tank [m] and C is the concentration of suspended solids in the sedimentation tank [mg/l].

$$k = 1.17 \cdot e^{\left(-\frac{8.05}{E_x}\right)} \quad (4.47)$$

Where E_x is the longitudinal turbulent diffusion coefficient [-] (Equation 4.48).

$$E_x = 3.59 \cdot e^{(58.5 \cdot F_r)} \quad (4.48)$$

Where F_r is the Froude number [-] (Equation 4.49).

$$F_r = \frac{v_{Av}}{\sqrt{g \cdot H_{Av}}} \quad (4.49)$$

Where g is the gravitational acceleration [9.81 m/s²], v_{Av} is the mean flow velocity [m/s] and H_{Av} is the mean depth of the basin [m].

4.5.11. Lessard and Beck (1988)

Lessard and Beck (1988) presented a simple lumped parameter model of primary sedimentation dynamics based on an intensive 10-day measurement campaign at the Norwich Sewage works in Eastern England. The model describes the performance of the clarifier in view of total suspended solids (TSS), volatile suspended solids (VSS), total chemical oxygen demand (COD_T), soluble chemical oxygen demand (COD_S) and ammonium nitrogen concentrations. For each of the particulate components a distinction is made between settleable and non-settleable matter. The hydraulics of the primary sedimentation tank (PST) are mimicked using a tanks-in-series (TIS) approach. Lessard and Beck (1988) proposed the use of 5 continuously stirred tank reactors (CSTR). A mass balance for the particulate settleable component over each CSTR yields equation 4.50.

$$\frac{dC_{Eff}(t)}{dt} = \frac{Q(t)\cdot\left(C_{In}(t)-C_{Eff}(t)\right)}{V} - \frac{v_s\cdot A_c\cdot C_{Eff}(t)}{V} + \frac{a_{sc}\cdot v_s\cdot A_c\cdot C_{Eff}(t)}{V} \quad (4.50)$$

Where C_{Eff} is the Effluent concentration of the component [mg/l], C_{In} is the influent concentration of the component [mg/l], Q is the settled sewage flow rate [m³/h], V is the volume of the sewage in a CSTR [m³], A_c is the cross sectional area of the clarifier [m²], v_s is the particle settling velocity [m/h], a_{sc} is a scouring parameter [-], which can be calculated according to equations 4.51 and 4.53 (Alarie et al., 1980).

$$a_{sc} = \gamma \cdot e^{\frac{-\lambda}{E_f}} \quad (4.51)$$

With E_f a function of the Froude number F_r [-].

$$F_r = \frac{v_f}{\sqrt{g\cdot h}} \quad (4.52)$$

$$E_r = \alpha \cdot e^{\frac{\beta\cdot Q}{2\cdot\pi\cdot h\cdot r\cdot\sqrt{g\cdot h}}} \quad (4.53)$$

Where α,β,γ,λ are correlation parameters [-], v_f is the fluid velocity [m/h], h is the height of the clarifier [m] and r is the radius of the clarifier [m].

For soluble components equation 4.50 reduces to equation 4.54.

$$\frac{dC_{Eff}(t)}{dt} = \frac{Q(t)\cdot\left(C_{In}(t)-C_{Eff}(t)\right)}{V} \quad (4.54)$$

In order to match the observed decrease of soluble COD (40 mg/l on average or 12% of the influent concentration) and increase of ammonium nitrogen (2 mg/l on average or 7% of the influent concentration) additional physical and biological reactions are included. Soluble COD is assumed to partly flocculate with the particulate COD and possibly undergo biodegradation. This removal of soluble COD is modelled with first-order kinetics. Ammonium nitrogen, on the other hand, is assumed to be generated by ammonification, which was modeled with zero order kinetics.

Lessard and Beck (1988) acknowledged the difference in wastewater characteristics during dry and rain weather and proposed a different set of (non-)settleable fraction and settling velocities (Table 4.6).

Table 4.6. Parameter values for dry and storm weather conditions

Name	Description	Unit	Element	Dry weather		Storm weather
				RWW[(1)]	RWW + SL[(2)]	RWW
f_s	Settleable fraction	-	SS	0.65	0.90	0.80
		-	VSS	0.65	0.90	0.80
		-	COD_X	0.50	0.85	0.60
v_s	Settling velocity	m/h	SS	1.00	10.0	2.00
		m/h	VSS	1.00	10.0	2.00
		m/h	COD_X	1.00	10.0	2.00

(1) Raw wastewater

(2) Raw wastewater mixed with sludge liquors

4.5.12. Takacs et al. (1991)

The well-known model of Takacs (Takács et al., 1991), developed for describing the settling behaviour of secondary sedimentation, considers clarification (discrete and flocculent settling) and hindered settling. As such the model could be applied on primary sedimentation by adapting the settling parameters. Coderre (1999) estimated the settling parameters of the Takacs model for the Norwich primary clarifiers (Table 4.7).

The model attempts the use of a 1-dimensional discretization scheme, dividing the height of the clarifier in a number of layers (10 values is proposed in the original publication). The settling velocity of the sludge blanket has been found to be a non-linear function of the solids concentration. The settling flux is due to gravity settling and a bulk flux (i.e. a drag force).

The calculation (Equations 4.55-4.57) of the settling velocity (v_S) depends on the concentration of particulates (Figure 4.8).

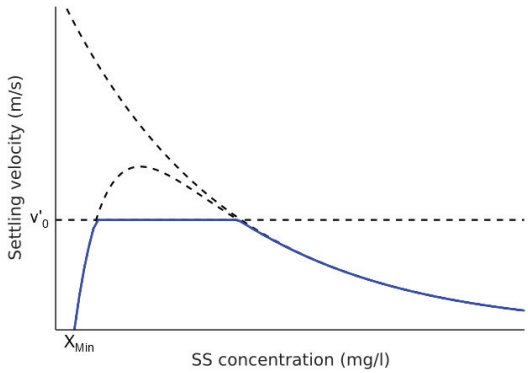

Figure 4.8. Evolution of the settling velocity in function of the concentration of suspended solids redrafted from Takacs et al. (1991).

Beneath a minimum concentration there is no gravitational settling.

$$v_s = 0; X_j < X_{Min} \quad (4.55)$$

Where v_S is the settling velocity [m/d], X_j is the suspended solids concentration in layer j [g/m³], X_{Min} is the minimum attainable suspended solids concentration below which no settling occurs [g/m³].

$$X_{Min} = f_{ns} \cdot X_{In} \quad (4.56)$$

Where f_{ns} is the non-settleable fraction [-] and X_{In} is the influent suspended solids concentration [g/m³].

Above the minimum concentration the settling velocity follows the equation of Vesilind for the hindered settling with a correction for the discrete settling (equations 4.57-4.58).

$$v_S = v_0 \cdot e^{-r_h \cdot (X_j - X_{Min})} - v_0 \cdot e^{-r_p \cdot (X_j - X_{Min})} ; X_j > X_{Min} \quad (4.57)$$

Where v_0 is the theoretical maximum settling velocity [m/d], r_h is the settling parameter characteristic of the hindered settling zone [m³/g] and r_p is the settling parameter characteristic of the low solids concentration [m³/g].

$$0 \leq v_S \leq v'_0 \quad (4.58)$$

Where v'_0 is the practical maximum settling velocity [m/d].

Table 4.7. Optimized values of Takacs model parameters for the Norwich primary clarifiers (Coderre, 1999).

Parameter	Explanation	PST	SST
v_o	Maximum theoretical settling velocity	**96 m/d**	474 m/d
v_o'	Maximum practical settling velocity	**45 m/d**	250 m/d
r_h	Settling parameter (hindered settling)	**0.00019 m³/g**	0.000576 m³/g
r_p	Settling parameter (low concentrations)	**0.0007 m³/g**	0.00286 m³/g
f_{ns}	Non-settleable fraction of suspended solids	**0.24**	0.00228

Gernaey et al. (2001b) extended the model of Takacs, applying the model parameters of Coderre et al. (1999), with the inclusion of detention time for soluble components, flocculation and ammonification.

4.5.13. Ribes et al. (2002)

Ribes et al. (2002) developed a model for a primary settler including sedimentation, compression processes and biological processes in order to be able to predict both removal efficiency as well as production of volatile fatty acids (VFA).

The sedimentation model is based on the flux theory where the total flux, which depends on the sum of the gravity settling flux and the bulk flux, is calculated over each layer of a horizontal discretisation. The gravity settling model takes into account flocculent settling, hindered settling and compression. Both flocculent settling and hindered settling are described with the double exponential function (equations 4.57 and 4.58) proposed by Takacs et al. (1991). Compression settling, on the other hand, is modelled by the compression factor concept (Equations 4.59-4.64) proposed by Härtel and Pöpel (1992).

$$\Omega = \frac{1 - B \cdot h_t^{-(1+2 \cdot F_{SVI})}}{1 - B \cdot [min(h, h_t)]^{-(1+2 \cdot F_{SVI})}} \quad (4.59)$$

Where Ω is the compression factor [-], h is the height in the settler [m] and SVI is the sludge volume index [ml/g].

$$F_{SVI} = \frac{SVI}{100 + SVI} \quad (4.60)$$

$$B = -\left(\frac{1}{F_{SVI}} + 1\right) \cdot h_c^{(1+2\cdot F_{SVI})} \quad (4.61)$$

$$h_t = min\left(2 \cdot h_c, h_f\right) \quad (4.62)$$

Where h_f is the height of the feed [m] and X_f is the feed or influent solids concentration [mg/l].

$$h_c = \left(1 - \frac{1}{X_c \cdot r_h}\right) \cdot \left(\frac{X_f \cdot h_f}{X_c}\right) \quad (4.63)$$

Where r_h is the settling parameter characteristic of the hindered settling zone [m^3/g].

$$X_c = \frac{480}{SVI} \quad (4.64)$$

The biological model is an extension of ASM2 (Henze et al., 2000) including fermentation.

4.5.14. Bachis et al. (2012)

Bachis et al. (2012) developed a phenomenological model, i.e. a grey box model, based on the work of Maruejouls et al. (2012). The model, a particle settling velocity distribution (PSVD) model, incorporates the common observation that the settling velocity distribution heavily influences the sedimentation process. The new model builds on the model developed by Lessard et al. (Lessard and Beck, 1991) and includes a number of particle classes, which cover the settling velocity distribution (Figure 4.9). Each particle class is assigned a time varying fraction of the influent TSS.

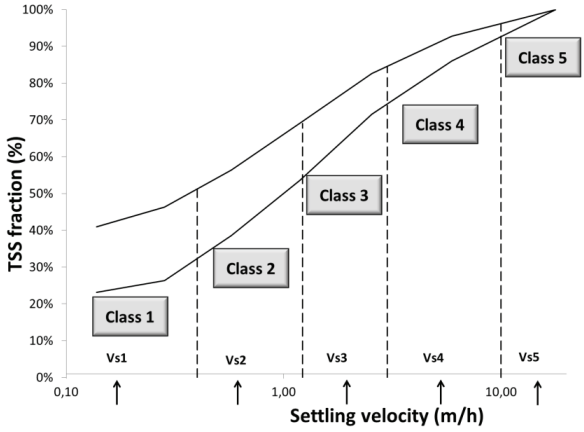

Figure 4.9. Fractionation of the ViCAs zone into 5 classes and upper and lower limits of the zone where most of the PSVD curves observed for the case study were found. Settling velocities characterising each class were calculated as the geometrical mean of the settling velocity boundaries of the class

These fractions are determined using the ViCAs (Vitesses de Chute en Assainissement) batch settling protocol developed by Chebbo and Gromaire (2009). The assignment is made by interpolating the PSVD curve between two boundary curves (continuous lines on Figure 4.9). The upper limit of this zone represents the low influent TSS concentrations, whereas the lower limit represents high influent TSS concentrations.

4.5.15. Liu and Garcia (2011)

Liu and Garcia (2011) developed a computational fluid dynamics (CFD) model for the design of large PST to be built at the Calumet Water Reclamation Plant. The model considers the rheology of the sludge (and hence its non-Newton behaviour), flocculation and hindered settling.

Assuming that the particle inertia effect and particle relative acceleration can be neglected in comparison with the fluid phase, a partially mixed two–fluid model is used to analyse the suspended solids-water mix. A k-ε turbulence model with a Bingham plastic model is used to simulate the turbulence and rheological behaviour respectively. Hindered settling is described using the double exponential settling velocity function (equation 4.57) presented by Takács et al. (1991), where the settling velocity of a single particle v0 is calculated from the drag coefficient (equations 4.65 and 4.8).

$$C_D = 1702.9 - 1270.9 \cdot Re_p - 494.14 \cdot Re_p^2 \quad (4.65)$$

Where C_D is the drag coefficient [-] and Re_p is the particle Reynolds number [-].

Different classes of particle sizes are used to characterize the particle size distribution. Flocculation is modelled (equation 4.66) according to Lyn et al. (1992), assuming that the particle sizes are smaller than the Kolmogorov length scale and that only same size particles aggregate.

$$F_{Floc}^{i} = \left(\frac{\varepsilon}{\nu}\right)^{1/2} \cdot (\beta_{i-1} \cdot \alpha_{i-1}^2 - \beta_i \cdot \alpha_i^2) \quad (4.66)$$

Where F^{i}_{Floc} is the source/sink term to shear-induced flocculation [-], α_i the single volume fraction of class i [-], β_i is a proportionality constant [-], ε is turbulence energy dissipation rate [m²/s³], ν is the kinematic viscosity [m²/s].

4.5.16. He et al. (2004)

He et al. (2004) applied a computational fluid dynamics (CFD) model for the evaluation of flow and sediment behaviour of a combined sewer overflow (CSO) retention treatment basin. Flow patterns were simulated (in 3D) first by means of a volume of fluid (VOF) model with unstructured mesh and subsequently formed a basis for simulating particle transport by the discrete phase (DP) model. This

uncoupled approach is valid for low particle concentrations (Adamsson et al., 2003). The Lagrangian particle tracking or the Euler-Lagrange approach, is applied tracking individual particle movement by calculating the balance of forces on the particle (equation 4.67). The Lagrangian particle tracking approach assumes that the suspended particles are spherical and do not interact with each other. Two particle sizes, 5 and 50 μm, with density of 2800 kg/m3 (approximating natural sand) were considered.

$$\frac{dv_p}{dt} = C_D \cdot \left(v - v_p\right) + g \cdot \frac{\rho_p - \rho_w}{\rho_p} + F_x \qquad (4.67)$$

Where t is time [s], v_p is the vertical particle velocity [m/s], C_D is the drag coefficient [-], g is the gravitational acceleration [9.81 m/s²], ρ_p is the particle density [g/m³], ρ_w is the density of water [g/m³] and F_x represent additional forces (such as Brownian force for sub-micron particles, the Saffman's lift force or lift due to shear) [N]. The first term in equation 4.67 defines the drag force whereas the second term defines the gravitational settling force.

4.6. DISCUSSION

Modelling of primary sedimentation tanks has received little attention over the past decades. Although the concept of settling is straightforward it is being impacted by a lot of different factors. Most models developed until now are data driven models, i.e. simple empirical models based on linear regression techniques or more advanced methods based on for example artificial neural networks.

Some of these empirical models rely on the correlation of the removal efficiency with one variable, usually either the incoming concentration of suspended solids (Silva et al., 2014) or the influent flow rate (expressed as hydraulic retention time or overflow rate) (Otterpohl and Freund, 1992; Smith, 1969; Tay, 1982).

However the use of regression methods with only one variable is clearly questionable. Silva et al. (2014) developed a regression model linking the removal efficiency to the influent concentration. First of all it is doubtful that this correlation exist as, for sure in the lower concentration ranges, the settling is dominated by discrete and flocculent settling, where the settling velocity depends on the characteristics of the individual particles and no or limited interaction between the different particles is present. Second, given the large scatter of removal efficiencies at these lower concentrations, but typical for (municipal) wastewater, no good fit of the model with the data can be obtained. Silva et al. (2014) gave no indication on the accuracy of the fit obtained when applying a weighted least square regression on the dataset but considering the large spread that the data

shows (Figure 4.10) it will not be very accurate. In order to circumvent this Silva et al. (2014) added a maximum removal efficiency curve to the poorly fitting average removal efficiency curve. Actually, the large spread of data (definitely at the lower concentration ranges) demonstrate that many other factors influencing the removal efficiency are not taken into account. Christoulas et al. (1998) state that only when the study is carried out with averaged data over adequately long periods, several weeks at least, the random variations are smoothed out. However, the sometimes large variations are for a major part unexplored phenomena. Instead of simply ignoring them one should, at least, try to accept and understand their impact. In addition, applying relationships derived from long term averaged data does not allow for dynamic modelling of fast flow variations (such as storm events).

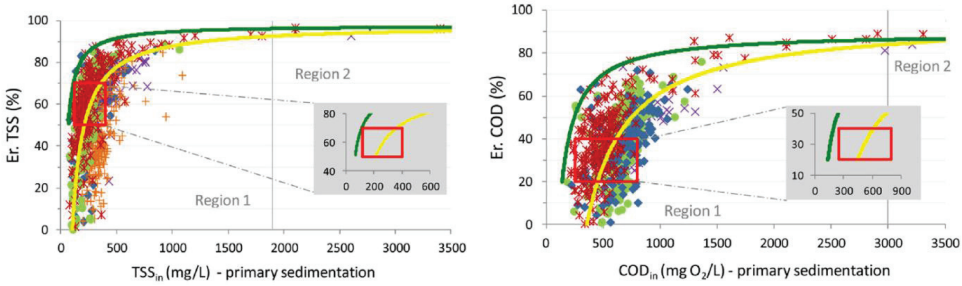

Figure 4.10. Efficiency removal curves for primary clarifiers obtained from the highly scattered field data for TSS (left) and COD (right) removal (Silva et al., 2014).

Other empirical models use a combination of both influent concentration and influent flow rate (Voshel and Sak, 1968) or hydraulic retention time (CIRIA, 1973; Escritt, 1972). Instead of using the hydraulic retention time or the overflow rate, Annesini et al. (1979) extended the empirical relation on influent concentration and flow rate with the ratio of the diameter over the height of the clarifier.

Christoulas et al. (1998) defined the temperature as an important parameter in explaining the different results given by different empirical models. The temperature impacts the density, of both the particles and the fluid, the viscosity of the fluid and the flow fields. In fact short circuiting was found to affect the flow pattern in primary clarifiers even at small temperature differences of 0.2°C (Matko et al., 1996).

El-Din and Smith (2002a, b) applied more advanced techniques to develop data driven models. They developed a combined stochastic transfer-function model as well as an Artificial Neural Network (ANN) model for describing TSS and COD removal based on influent flow rate and concentration of TSS and COD. Although a reasonable fit is obtained during the estimation (r^2 ranging from 0.73 to 0.90) the transferability of the models is questionable. For the two periods, both summer

periods on the same primary sedimentation tank, a different set of parameter values has been obtained. A similar observation can be made for the estimated parameter values of the empirical model of Voshel and Sak (1968). The parameter values estimated in different studies show a large spread (Table 4.4). This large spread is typically an indication that the model predictors are not able to fully describe the occurring processes.

In order to incorporate more theoretical knowledge about settling in the empirical observations, several phenomenological models have been developed. A first type of phenomenological models applies the particle pathline concept (Takamatsu et al., 2012; Tchobanoglous et al., 2004) in combination with a particle settling velocity. The removal efficiency is then calculated by comparing the settling velocity with the static (Tchobanoglous et al., 2004) or dynamic (Takamatsu et al., 2012) critical settling velocity, which is defined as the velocity at which a particle that enters the basin at the water surface will reach the bottom at the end of the tank.

A second type of these phenomenological models addresses the possible scouring in combination with the hydraulic behaviour of the settling tank (Lessard and Beck, 1988; Paraskevas et al., 1993; Shiba and Inoue, 1975). The models typically quantify the diurnal response of suspended and dissolved components using a tanks-in-series (TIS) model, which mimics the insufficient dispersion. The settling and scouring are modelled using empirical relations. The application of the TIS concept allows to model biological reactions in the tank which may occur depending on the length of the hydraulic retention time. However, only ammonification and removal of soluble COD through absorption or biodegradation in a simplified manner are considered (Lessard and Beck, 1988). Although a significant improvement over purely empirical models, Paraskevas et al. (1993) acknowledge the possibility to further improve the model applying particle velocity distributions (based on particle size distributions and particle density distributions).

A third type of phenomenological models applies a 1-dimensional (1D) discretization in the vertical direction to account for the dynamic and spatial variation (Coderre, 1999; Ribes et al., 2002) initially developed for secondary sedimentation tanks (Takács et al., 1991). The settling velocity is described using a relation to the local concentration (Equation 4.57). However, the application of such a relation is questionable. It may describe the hindered and compression settling reasonably well but it does not hold for discrete and flocculent settling. Mazzolani et al. (1998) also state that the use of single concentration-dependent expressions for the settling velocity of hetero disperse suspensions in sedimentation tanks appears questionable. In fact, in regions of low solid concentration an average settling velocity could lead to poor estimates of solid distribution, because

different-sized particles actually settle with different velocities. This settling velocity distributions is clearly one of the underlying reasons for the large scatter (Figure 4.10) encountered during measurement campaigns.
In addition these models only account for convective flow and gravity settling. Other phenomena such as turbulent diffusivity and dispersion are not included. The model compensates for these missing effects by applying a coarse discretization (10 layers) which introduces significant numerical dispersion (Torfs et al., 2015).
Furthermore these models typically do not include the effect of hydraulic retention times and cannot model the impact of the high ammonium load at the beginning of a storm event, when the flow rate increases but the clarifier is still filled with wastewater containing dry weather concentrations of the pollutants. However, the extension to include the propagation of the soluble components is straightforward. In addition, the model structure allows for easy integration of biological processes that can reproduce phenomena such as ammonification, hydrolysis, VFA elutration end fermentation (Ribes et al., 2002).
A fourth type of phenomenological models are particle settling velocity distribution (PSVD) models. These models are a step upwards to real population balance models (PBM), which can describe the dynamics of particle size distribution (Nopens et al., 2015). Bachis et al.(2012) applied the PSVD concept on the Lessard and Beck (1988) model. This type of models are clearly promising and more work should be investigated. However, the inclusion of biological processes may be somewhat more difficult than in the previously describe phenomenological models. The model would benefit from the integration within a rigorous discretization scheme as proposed by Bürger et al. (2011), which would increase the model reliability in varying conditions, such as storm events.
Another step forward in the inclusion of the theoretical knowledge of the systems is the use of computational fluid dynamic (CFD) models (He et al., 2004; Liu and Garcia, 2011). These models contribute largely to a better description of the flow patterns, which have a significant impact on the sedimentation performance, in the sedimentation tanks. Saul and Ellis (1992) demonstrated the very complex flow patterns within the storage tanks and that these flow patterns governed the sediment settlement, re-entrainment and transport processes in the tank. Computational Fluid dynamics models were first applied to sedimentation tank design by numerically modelling two-phase flows with the solids transport equations effectively decoupled from the flow equations. This approach was used only for primary clarifiers where solid concentrations were low and density effects could be neglected (Matko et al., 1996).
Unfortunately, the increased complexity on the hydraulic characterisation is accompanied with some incorrect modelling of the settling process. Liu and Garcia

(2011) applied the double exponential equation proposed by Takacs et al. (1991) to describe the settling behaviour. However, as mentioned above, the application of such a relation is questionable. On the other hand, He et al. (2004) applied a Lagrangian particle tracking approach assuming that the suspended particles do not interact with each other. This is an approach that is valid for the major part of the primary sedimentation tanks, certainly if the tanks are operated to avoid storage of sludge inside. Although the approach looks promising, they applied it on only 2 particle size classes, which is clearly not sufficient to describe the typical log logarithmic particle size distributions encountered in wastewater. In addition they applied densities close to that of sand which is definitely the high-end range and will not enable a good estimation of the removal of organic matter.

A promising approach is applied by Mazzolani et al. (1998) for secondary clarifiers. They describe a generalized settling model, which combines a discrete settling model (using particle size/velocity classes) with a monodisperse settling model (concentration dependent) for secondary clarifiers embedded in a CFD model. This model can be extended to primary clarifiers when applying another correlation for the discrete settling velocity, which in their case is based on activated sludge flocs. Also the parameters for the hindered settling may need recalibration as they are really sensitive to the type of sludge.

Although very interesting to gain more knowledge on systems, computational fluid dynamic (CFD) models are not compatible with the other process models applied in the whole plant model of the WWTP of Eindhoven. Furthermore CFD models require a huge amount of computational power, which restricts the use within scenario based optimizations. In addition the validation of the models is not straightforward due to the requirement for huge amounts of data (i.e. each analysis has to be performed on multiple locations). An option to circumvent the complications arising with CFD modelling, a model reduction in the form of compartmental models can be performed (Alvarado et al., 2012). Compartmental models are any kind of combination of completely mixed reactors mimicking the flow patterns in the whole reactor. Although really promising, some issues remain using compartmental models, amongst others how to account for the effect of changing flow rates, which induce changes in the flow patterns.

Other important issue in the modelling of primary sedimentation tanks is the link to the activated sludge model which is applied for the subsequent processes. Firstly, the issue arises due to the different nature of the processes driving the removal of the substances. In the modelling of sedimentation tanks the substances are fractionated in settleable and non-settleable which is governed by the particle size and density. Whereas in the consecutive activated sludge process the split up based on the ease of biodegradation, i.e. readily biodegradable, slowly biodegradable and

non-biodegradable. Secondly, the issue is created by the duality in the characterisation of the components used in the modelling of activated sludge systems. In the original activated sludge models (Henze et al., 2000), the readily biodegradable substrates are denoted as S_B and the slowly biodegradable as XC_B. The naming is confusing, as for the other components the base S refers to 'soluble' and the base X to 'particulate'. However for the biodegradable fractions, although some correlation exists between the size of the molecules and their biodegradability, the meaning of soluble and particulate does not stand. Adding to the confusion is that some wastewater characterisation methods apply physical-chemical methods (flocculation and filtering) to differentiate between readily and slowly biodegradable, as these methods are much simpler and faster in execution (Roeleveld and van Loosdrecht, 2002). Even if the application of soluble and particulate would be applied consistently, it still does not differentiate between settleable and non-settleable.

The commonly applied approach to deal with this duality is to ignore it. For the incoming flow, applying a conversion factor from particulate COD to suspended solids, the particulate activated sludge model (ASM) fractions are combined in total suspended solids (TSS). Differentiating between settleable and non-settleable is then applied within the settling models. For the outgoing flow the TSS is fractionated again in the particulate ASM fractions, assuming that after settling the TSS in the effluent or underflow constitutes of the same composition as before settling. This assumption completely ignores the differences in particles size, density and settling velocity. There is a definite need for further research on this topic. Even for highly detailed models it will always be difficult to determine a link between the settleability and the biodegradability, as the flocs do not exist of single components. This could be partially dealt with by the determination of biodegradability of sludge separated using settling techniques such as the ViCAs settling protocol (Chebbo and Gromaire, 2009).

Another issue that arises is the difference between organic and inorganic components and their settling velocities. Settling velocity is mainly driven by particle size and density. The latter and as such also the settling velocity is higher for inorganic substances than for organic substances. None of the models published so far have been dealing with this issue. However, dealing with this difference is crucial for the modelling of the subsequent (biological) processes. This difference largely influences the actual input of COD, which determines the probability and completion of several biological processes (denitrification, biological phosphorus removal and required oxygen demand for heterotrophic growth).

A proper characterisation and modelling of the primary sedimentation process is crucial for a good description of the subsequent activated sludge process. In order

to obtain this objective, measurement campaigns, as good data is essential for good models, on the primary sedimentation tanks should focus on the influent fractionation compatible for activated sludge modelling. Next to the typical activated sludge model fractions also the inorganic and organics should be segregated.

4.7. CONCLUSIONS

Despite the significant impact on the overall WWTP performance and cost effectiveness, characterisation and modelling of primary settlers has not been addressed meticulously. Most modelling efforts are based on empirical relations, which are not able to describe the high scatter present in primary sedimentation tank removal efficiency data. On the other hand a limited number of computational fluid dynamic models have been proposed, which describe the hydraulic profile carefully but unfortunately, so far, lack in describing the settling process in a coherent way. In addition these models are too complex to apply within a whole plant context.

In order to combine the primary sedimentation models with the process models in a whole plant modelling context, phenomenological models such as the model of Bachis et al. (Bachis et al., 2012) look promising as they provide sufficient detail to model the impact of particle velocity distributions. A first improvement would be to integrate this model within a rigorous discretization scheme as proposed by Bürger et al. (2011) which would increase the model reliability. A second improvement should be the differentiation between organic and inorganic matter as this is crucial for the succeeding biological treatment.

Chapter 5

Data collection for modelling of primary sedimentation tanks

"Measure what can be measured, and make measurable what cannot be measured."
Galileo Galilei

5.1. ABSTRACT

In order to evaluate the performance of the primary sedimentation tanks at the WWTP of Eindhoven data was collected in collaboration with Waterboard The Dommel and comprised routinely collected data from January 5, 2011 till June 14, 2013 as well as data from 3 measurement campaigns. One measurement campaign was organized to evaluate the possibility of reducing primary sedimentation capacity while the two other campaigns were organized to examine the impact on the whole WWTP model. Data was consequently analysed and fractionated in the activated sludge model components according to the STOWA protocol (Roeleveld and van Loosdrecht, 2002). The data collection showed a significant difference in removal efficiencies between different components (organic matter versus inorganic matter and inert COD versus biodegradable COD). From the data, correlations between the influent concentrations of particulate and total COD with the corresponding removal efficiency could be retrieved. Also some unexpected behaviour was observed, i.e. an increase in concentrations of soluble COD, NH_4, PO_4 and inorganic suspended solids.

5.2. SYMBOLS

BOD_T	Total biochemical oxygen demand (mg/l)
BOD_t	Biochemical oxygen demand after time t (mg/l)
$COD_{Eff,S}$	Effluent soluble chemical oxygen demand (mg/l)
$COD_{Inf,S}$	Influent soluble chemical oxygen demand (mg/l)
$COD_{Inf,T}$	Influent total chemical oxygen demand (mg/l)
COD_S	Filtered or soluble chemical oxygen demand (mg/l)
COD_T	Total chemical oxygen demand (mg/l)

5.3. INTRODUCTION

5.3.1.1. The primary sedimentation tanks at the WWTP of Eindhoven

At the WWTP of Eindhoven (The Netherlands), the incoming wastewater is treated in three parallel lanes with a total plant maximum hydraulic load of 26,250 m^3/h. The water enters the plant in three influent pits, which are followed by coarse screens before the water flows to the influent pumping station. In the influent pumping station the wastewater is pumped up using Archimedes screws and released over fine screens into two parallel sand traps. After the sand traps the wastewater is distributed over three parallel circular primary sedimentation tanks (Figure 5.1 and Figure 5.2), each of which are completely covered in order to avoid odour nuisance. Downstream the primary sedimentation tanks the water is mixed again before it is pumped to the biological tanks. The mixed liquor of each of the biological tanks flows over in four secondary clarifiers. An extra 8,750 m^3/h can be treated mechanically and passes a pre-settling tank or rain buffer tank before it is discharged in the river Dommel or sent to the influent pumping station when the hydraulic load again drops below 26,250 m^3/h.

Figure 5.1. Picture of the covered circular primary sedimentation tank of WWTP of Eindhoven. The outlet weirs are covered to avoid odour release.

Figure 5.2. Picture of the circular primary sedimentation tank at the WWTP of Eindhoven during maintenance. In the middle the inlet structure is clearly visible.

The capacity of the PST was originally designed for 35,000 m^3/h but a maximum flow of 20,000 m^3/h was allowed. Average removal efficiencies of the PSTs (Table 5.1) based on data from 1998 until 2000 were applied to upgrade the consecutive biological tanks. In the design for the plant wide upgrade the PSTs were kept as they were (Table 5.2), but an increased maximum flow (26,250 m^3/h) was allowed during rain events (Flameling et al., 2003). During the design an appraisal of the correlation between the removal efficiency and the hydraulic load was attempted. However, due to the large scatter in the data no obvious trend could be established (Flameling et al., 2003).

Table 5.1. Average removal efficiencies of the PSTs at the Eindhoven WWTP based on data from 1998 till 2000 (Flameling et al., 2003).

Parameter	Removal Efficiency %
COD	41.5
BOD	39.4
TSS	63
TKN	8.2
TP	15.4

Table 5.2. Dimensions of the 3 PSTs at the WWTP of Eindhoven derived from the design plans.

	Unit	1 PST	3 PSTs
Diameter	m	60	-
Side water depth	m	2.5	-
Surface area	m^2	2827	8480
Volume	m^3	9565	28695

In order to address the inherent uncertainty, a sensitivity analysis during the design phase indicated that the biological treatment does not encounter problems if the variation of the feed and the removal efficiency of the PST stays within 10% (Flameling et al., 2003).

The wastewater enters in the middle of the circular primary sedimentation tank (Figure 5.3). An inlet structure (Figure 5.2) surrounding the inlet allows for dissipation of the energy inherent to the incoming flow. The wastewater flows towards the outflow weirs, which are covered to avoid odour release, while the suspended solids settle. The settled sludge is collected with a scraper and is removed at the bottom of the tank.

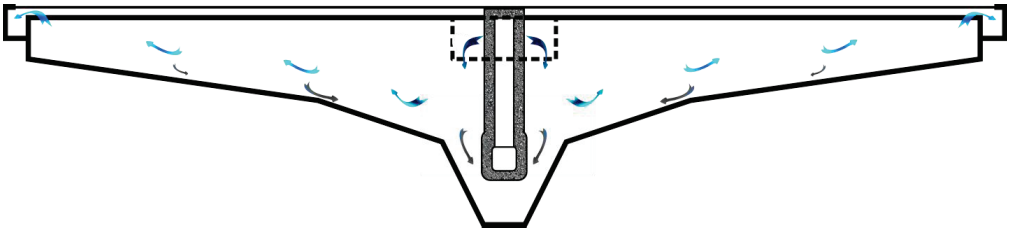

Figure 5.3. Cross sectional view of a primary sedimentation tank at the WWTP of Eindhoven.

The primary sludge is mixed together with the secondary sludge and is pumped over 7 km long pipes to the sludge dewatering installation of Mierlo. The reject water of the sludge dewatering is discharged in the sewer system and sent back to the plant through the sewer system. The impact of the reject water on the wastewater concentration is clearly visible at the wastewater treatment inlet, causing higher ammonium (NH_4) and phosphate (PO_4) loads.

5.4. MATERIAL AND METHODS

5.4.1.1. Data collection

Data collection was concerted with Waterboard The Dommel and comprised routinely collected data as well as data from measurement campaigns.

Table 5.3. Overview of the different collected data sources.

Date	Reason	Data collected
January 5, 2011 - June 14, 2013	Routine analysis	BOD_5, COD, TKN, TP, PO_4, TSS
June 24, 2013 July 23, 2013 September 9, 2013	Evaluation of reducing the capacity of the PST (including dosing of chemicals)	COD_T, COD_S, TP, PO_4, TSS
May 6, 2014	Full ASM fractionation	BOD_5, COD_T, COD_S, TSS, VSS TP, PO_4, TN, NH_4, NO_3, pH
September 2, 2014	Full ASM fractionation (repetition) and cation analysis	BOD_{10}, COD_T, COD_S, TSS, VSS TP, PO_4, TN, NH_4, NO_3, pH Ca, Mg, Na, K, Fe

5.4.1.1.1 Routine measurements 2011-2013

Waterboard the Dommel organized nearly weekly measurements to evaluate the performance of the WWTP of Eindhoven. The measurements included daily composite samples, which were analysed by an accredited lab for 5-day biochemical oxygen demand (BOD_5), chemical oxygen demand (COD), total Kjeldahl nitrogen (TKN), total phosphorus (TP), phosphate (PO_4) and total suspended solids (TSS), both sampled before and after the primary sedimentation tank. The data of the measurements performed on January 5, 2011 till June 14, 2013 were analysed for characterizing the removal efficiency of the primary sedimentation tank in view of the above listed parameters.

5.4.1.1.2 Measurement campaign with reduced PST capacity

A measurement campaign was organized by Waterboard de Dommel to evaluate the effect of reducing the capacity of the primary sedimentation by using only one PST (receiving the full hydraulic load) instead of 3 and the effect of dosing chemicals. On 3 days samples were collected. 2-hourly composite samples were collected before and after the PST. The samples were analysed by an accredited lab for total chemical oxygen demand (COD_T), filtered chemical oxygen demand (COD_S), total phosphorus (TP), phosphate (PO_4) and total suspended solids (TSS). From the data removal efficiencies, particulate phosphorus (P_{Part}), particulate COD (COD_X) and the corresponding loads were calculated. The first 2 days (June 24, 2013 and July 23, 2013) only one PST tank was in operation and no chemicals were dosed. The last day (September 9, 2013) also only one PST was in operation but coagulants were dosed to enhance the sedimentation process. For allowing comparison and calculation of the removal efficiency, the samples were synchronised using the hydraulic retention time using the sampling time for the influent at the reference

5.4.1.1.3 Measurement campaign 1 for full fractionation

In order to address the removal efficiency of the PST during dry weather conditions, a measurement campaign was organized to perform a full fractionation on the influent and effluent of the primary sedimentation tanks at the WWTP of Eindhoven. Half-hour composite samples were taken on May 6, 2014 starting from 8 a.m. onwards. The sampler after the PST was started six hours later to account for the hydraulic retention time, which is about 6 hours during dry weather flow conditions.

The samples were then transported to the lab of BIOMATH (Ghent University) in Ghent, Belgium. In the lab the samples were stored at 4°C and consequently analysed for determination of the different activated sludge model (ASM) components (Henze et al., 2000) according to the STOWA protocol (Roeleveld and

van Loosdrecht, 2002). Analyses were performed in triplicate except for BOD, of which the lab capacity did not allow this high number of analyses.
In order to compensate for the possible sudden changes in influent concentrations and the time delay within the tank, the samples were synchronised using the hydraulic retention time and using the sampling time for the influent as the reference. The hydraulic retention time was calculated based on the online flow rate measurements. Due to a rain event in the afternoon the hydraulic retention time reduced drastically and only 5 inlet-outlet sample combinations were available for the determination of the removal efficiency.

5.4.1.1.4 Measurement campaign 2 for full fractionation

In order to address the removal efficiency of the PST during dry weather conditions, a second measurement campaign was organized to perform a full fractionation on the influent and effluent of the primary sedimentation tanks at the WWTP of Eindhoven. Hourly composite samples were taken on September 2, 2014 starting from 8 a.m. onwards. The sampler after the PST was started six hours later to account for the hydraulic retention time, which is about 6 hours during dry weather flow conditions.
The samples were then transported to the lab of BIOMATH (Ghent University) in Ghent, Belgium. In the lab the samples were stored and analysed for determination of the different ASM components according to the STOWA protocol (Roeleveld and van Loosdrecht, 2002). In order to calculate the removal efficiency, the samples were synchronised using the hydraulic retention time, which was calculated based on the online flow rate measurements.
In addition to the standard measurements for the ASM fractionation also cations were measured to investigate the possibility of possible precipitation reactions occurring in the PST. The cations of Calcium (Ca), Magnesium (Mg), Sodium (Na), Potassium (K) and Iron (Fe) were analyzed by inductively coupled plasma optical emission spectrometry (ICP-OES)(International Organization for Standardization, 2011; VITO, 2012).

5.5. RESULTS AND DISCUSSION

5.5.1. Routine measurements 2011

Table 5.4 gives a descriptive statistical overview, i.e. minimum (Min), mean, maximum (Max) and standard deviation (Stdev), of the removal efficiencies for the primary sedimentation tank at the WWTP of Eindhoven from January 2011 till

June 2013. The data set consists of 142 daily composite samples, of which 114 dry weather and 28 rain weather days. A rain weather day was declared as a day for which the average flow rate was higher than 7500 m³/h. The number of rain weather days was on the low side to get a conclusive statistical analysis but are shown for completeness.

Table 5.4. Descriptive overview of the removal efficiencies for the primary sedimentation tank at the Eindhoven WWTP from January 2011 till June 2013. Analyses were performed on the entire data set as well as on dry weather and rain weather days separately. Negative values mean an increase in concentration.

		BOD_5	COD	TKN[(1)]	TP	PO_4[(2)]	TSS[(3)]
All days	Min	-38%	-26%	-38%	-18%	-20%	-10%
	Mean	29%	28%	8%	13%	43%	51%
	Stdev	15%	12%	9%	11%	16%	22%
	Max	60%	56%	27%	38%	78%	89%
Dry weather days	Min	-8%	-26%	-38%	-12%	-20%	-10%
	Mean	29%	28%	9%	14%	45%	52%
	Stdev	12%	11%	7%	10%	15%	22%
	Max	51%	56%	27%	38%	78%	89%
Rain weather days	Min	-38%	-4%	-30%	-18%	-7%	3%
	Mean	29%	31%	6%	9%	37%	51%
	Stdev	29%	16%	13%	13%	19%	19%
	Max	60%	56%	25%	30%	72%	78%

(1) One data point (with a -149% removal during dry weather) was considered to be an outlier.
(2) One data point (with a 99% removal during rain weather) was considered to be an outlier.
(3) Six data points (related to very low concentrations in the inlet which are not seen in the outlet) were considered to be an outlier.

A clear difference in average removal efficiency between the different parameters (BOD_5, COD, TKN, TP, PO_4 and TSS) can be observed. The average removal efficiency per measurement is rather constant and the difference falls within the standard deviation regardless the weather conditions. BOD_5 (29%) and TSS (52% vs 51%) removal is similar in dry as in rain weather. COD (28% vs 31%) shows a slight increase in average removal efficiency during rain weather conditions. The other measurements, TKN (9% vs 6%), TP (14% vs 9%) and PO_4 (45% vs 37%) display the expected behaviour, i.e. a (small) reduction of the removal efficiency in rain weather conditions.

PO_4, a soluble component, shows a high removal efficiency thanks to the chemical dosing regularly active during 2011. The small reduction during rain weather conditions can be contributed to the lower efficiency of the chemical reactions at low PO_4 concentration (many rain weather PO_4 concentration are between 1 and 2 mg/l opposed to an average 6 mg/l for dry weather PO_4 concentration). I.e. the efficiency decreases as the required metal to PO_4 ratio increases at low PO_4

concentrations (de Haas et al., 2000). In addition the shorter hydraulic retention time, due to the elevated flow rate, accords less time for the chemical reaction to reach completion. However, plotting the PO_4 removal efficiencies versus PO_4 influent concentration (Figure 5.4) does not show this relationship clearly. This may be attributed to the lack of automatic control for the chemical dosing.

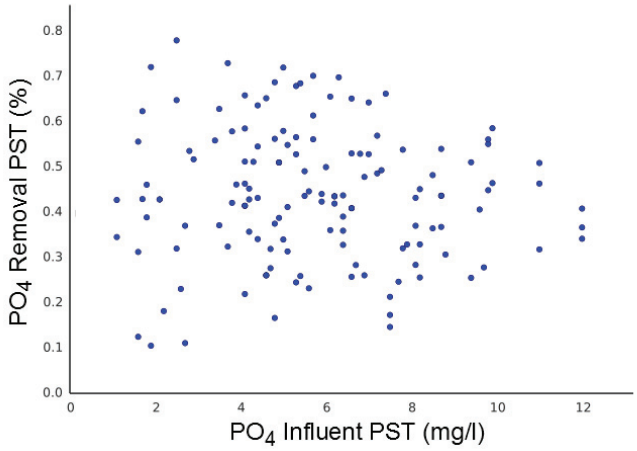

Figure 5.4. The wide spread of removal efficiencies of PO_4 from January 2011 till June 2013 shows no clear relationship with the influent PO4 concentrations.

A linear regression was applied to see if any relations between the influent and effluent concentrations, influent and effluent loads and removal efficiencies of the different measurements could be retrieved (Figure 5.5). In first instance, the obvious relations emerge from the analysis. I.e. concentrations of PO_4 and TP have a high positive correlation as PO_4 is included in TP. This is also the case for BOD_5 and COD. Furthermore there are the usual suspects, i.e. all concentrations in the influent flow are highly correlated. This is logic as all of the measurements are mere representations on the quantity of pollution. The more polluted the higher the concentrations. If the influent concentrations would not be correlated that would indicate the irregular discharge of wastewater streams with different compositions (e.g. industrial wastewater). Also the effluent concentrations are highly correlated to the influent concentration as well as to the other effluent concentrations. The same observations hold for the loads.

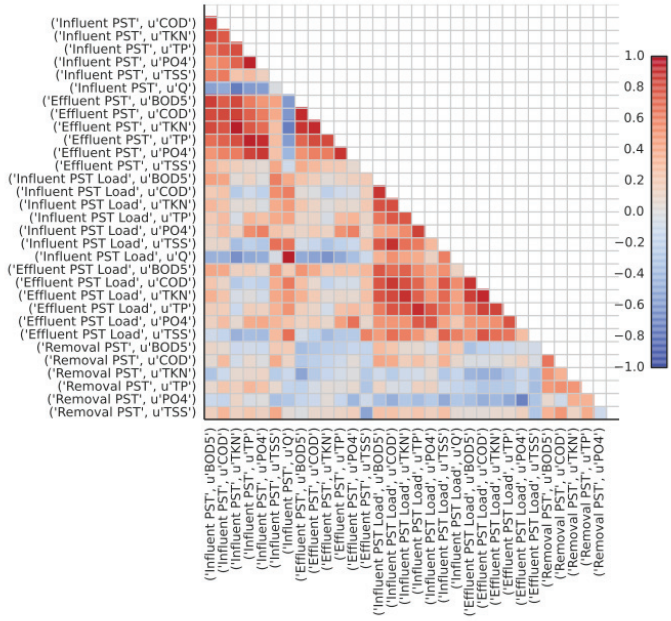

Figure 5.5. Correlations determined using linear regression for the influent, effluent and removal efficiency of the different measured variables of all analysed samples from January 2011 till June 2013. Red indicates a positive correlation and blue a negative correlation. Darker colours express a more pronounced correlation.

The flow rate is inversely correlated to the concentrations except for TSS where no correlation at all is emerging from the data. For the measurements containing soluble components, this effect is directly linked to the degree of pollution of the wastewater or dilution by the rain water. For suspended solids, sedimentation and re-suspension in the sewer system influence the concentration entering the plant. As a result, the influent TSS concentration (Figure 5.6) displays a large spread (between 22 mg/l and 500 mg/l).

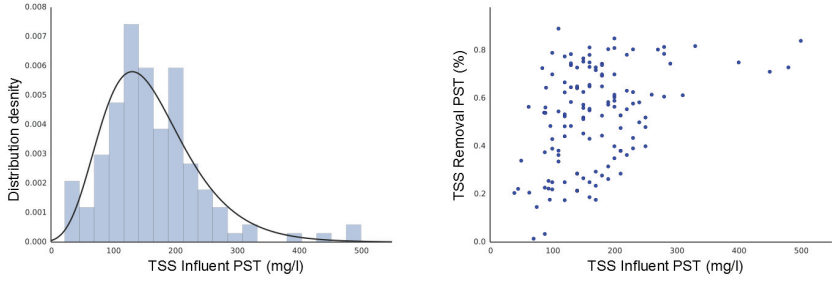

Figure 5.6. Distribution of influent TSS concentration (left) and the removal efficiency of TSS versus the influent TSS concentration for the 2011 data.

Finally, some correlations are also disclosed regarding the removal efficiency (Figure 5.5). Firstly, inverse correlations are noticed between the removal efficiency and the effluent concentration or load, i.e. logically, the higher the removal efficiency the lower the effluent concentration or load. Related to its high removal efficiency, the highest next to TSS, this inverse correlation is most pronounced for PO_4. On the other hand, for TSS this inverse correlation is totally absent. The absence of the correlation for TSS is probably inherent to the nature of TSS, which comprises a large range of different suspended solids with differing size and settling velocities.

The correlations determined for dry weather days (Figure 5.7) lead to the same conclusions as for the overall set, although less distinct. In first instance, this is mainly related to the fact that most of the sampling days (114 out of 142) were dry weather days. Secondly, the more pronounced events are observed during rain weather days. The regression analysis for rain weather days also reveal the same trends but then somewhat more pronounced (Figure 5.8).

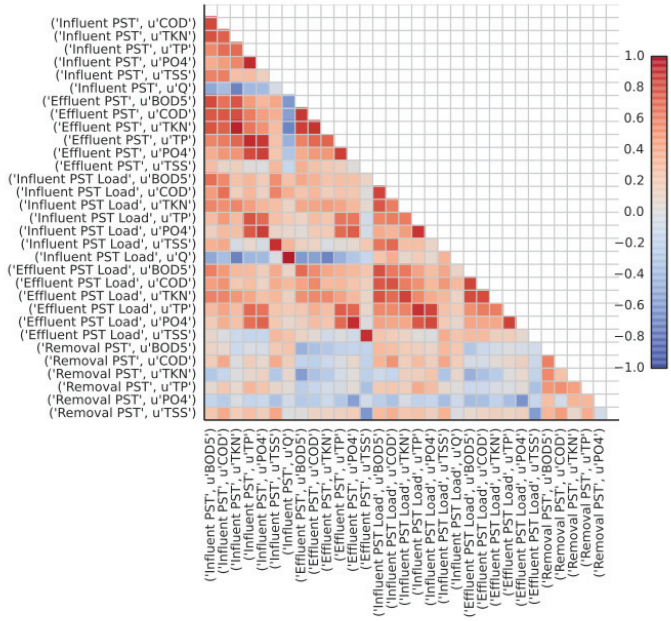

Figure 5.7. Correlations determined using linear regression for the influent, effluent and removal efficiency of the different measured variables of analysed dry weather samples from January 2011 till June 2013. Red indicates a positive correlation and blue a negative correlation. Darker colours express a more pronounced correlation.

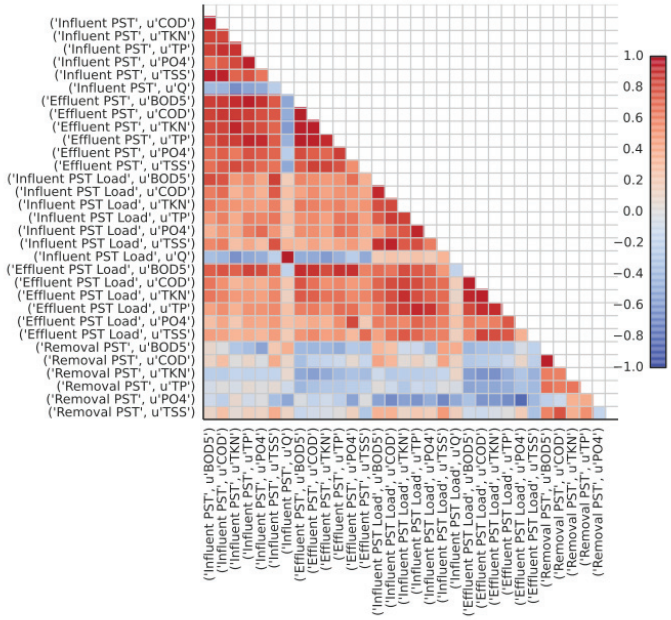

Figure 5.8. Correlations determined using linear regression for the influent, effluent and removal efficiency of the different measured variables of analysed rain weather samples from January 2011 till June 2013. Red indicates a positive correlation and blue a negative correlation. Darker colours express a more pronounced correlation.

The linear regression analysis showed a lack of correlation between influent flow rate and concentrations with the removal efficiency. This might be due to the fact that the analysis is based on daily composite samples, for which the impact of sudden changes in influent may be averaged out. The lack of correlation also entails that no empirical relations can be established based on this data set.

5.5.2. Measurement campaign with reduced PST capacity

The measurement campaign at the WWTP of Eindhoven with only one PST and without chemical dosing (Table 5.5) presented similar removal efficiencies as for the 2011 routine data (Table 5.4), i.e. TSS is removed for 50% versus 51% and COD for 34% versus 28%. This is not completely unexpected as the capacity of the primary sedimentation is mainly designed to treat peak flow, i.e. rain or storm weather, conditions. During the measurement campaign only the first day witnessed moderately elevated flow rates due to a rain event (Figure 5.9). For PO_4 and consequently TP the removal efficiencies of the data with chemical dosing are analogous with the dry weather data of 2011, i.e. PO_4 is removed with 40% versus 45% and TP with 22% versus 14%.

Table 5.5. Descriptive overview of the removal efficiencies for one operational primary sedimentation tank at the Eindhoven WWTP on June 24 and July 23 (without chemical dosing) and September 9 (with chemical dosing) in 2013. Negative values mean an increase in concentration.

		TSS	COD	COD_x	COD_s	PO_4	TP
All days	Min	-25%	17%	27%	-15%	-40%	-31%
	Mean	53%	38%	53%	7%	14%	16%
	Stdev	19%	13%	15%	8%	29%	18%
	Max	81%	65%	81%	17%	64%	40%
Without chemical dosing	Min	-25%	17%	27%	-15%	-21%	-21%
	Mean	50%	34%	47%	6%	13%	13%
	Stdev	21%	11%	13%	7%	12%	12%
	Max	77%	65%	80%	15%	31%	40%
With chemical dosing	Min	35%	25%	47%	-7%	-30%	-31%
	Mean	59%	48%	67%	10%	40%	22%
	Stdev	12%	13%	11%	8%	35%	27%
	Max	81%	65%	81%	17%	64%	39%

The data from the measurement campaign also revealed a slightly higher removal efficiency when including chemical dosing (Table 5.5). The largest difference in removal efficiency is seen for PO_4 and COD_x, respectively 27% and 20%. The PO_4 and TP data, with chemical dosing, show large standard deviations, the low ranges can be appointed to the first two points that show a remarkably lower removal efficiency (Figure 5.11). It is unclear whether these lower removal efficiencies are related to the start-up phenomena of the chemical dosing or to other factors in play. The flow rate (Figure 5.9) does not exhibit an exceptional high (nor low) value at the time instants where these low removal efficiencies occur.

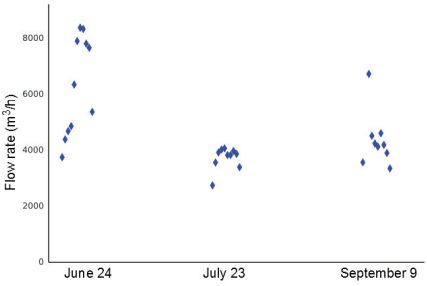

Figure 5.9. Flow rates during the measurement days at the Eindhoven WWTP on June 24 and July 23 (without chemical dosing) and September 9 (with chemical dosing) in 2013.

Figure 5.10 clearly displays the lowering of the concentrations from influent to effluent for TSS, COD and COD_x. For COD_s no apparent reduction is visible, although when applying chemical dosing the effluent concentration variation seems

to be reduced. PO_4 concentrations show a peak during the day, which is probably due to the effect of the sludge treatment effluent of Mierlo. The effect of the chemical dosing is unmistakably noticed in the PO_4 concentrations. Although less evident, also in the COD_x concentration the effect is visible.

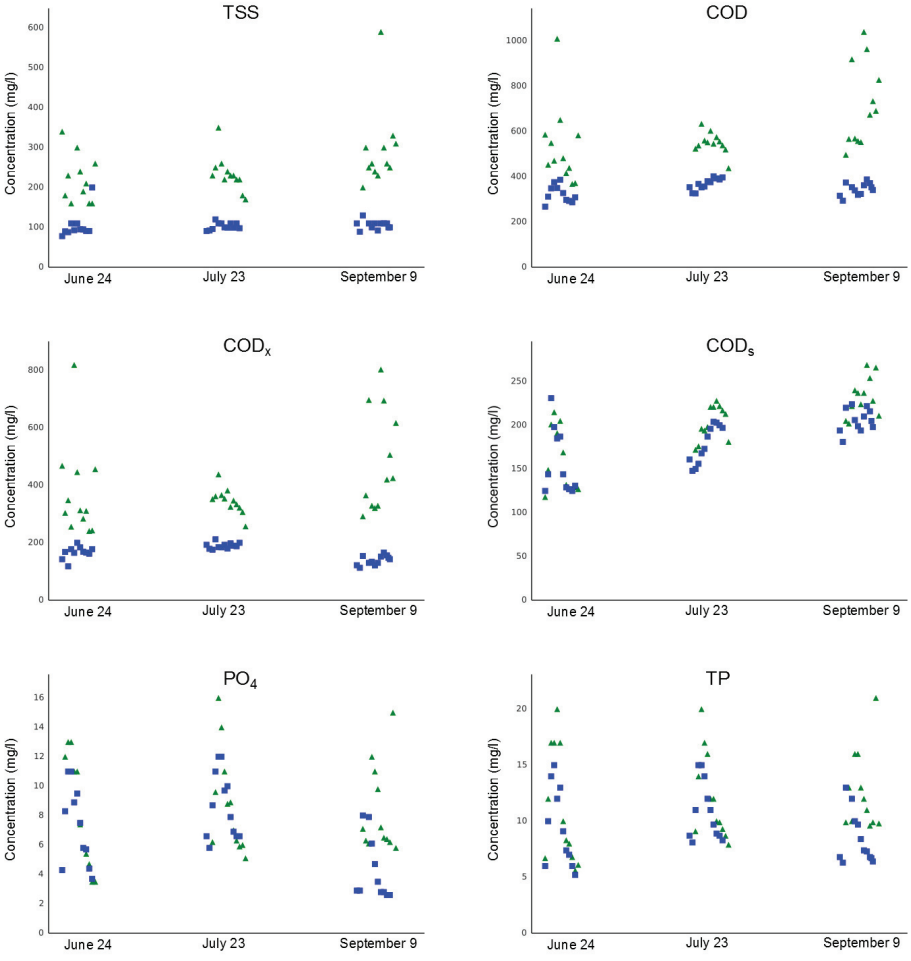

Figure 5.10. Influent (green triangles) en effluent concentrations (blue squares) for TSS, COD, COD_x, COD_s, PO_4 and TP for one operational primary sedimentation tank at the Eindhoven WWTP on June 24 and July 23 (without chemical dosing) and September 9 (with chemical dosing) in 2013. Time for the effluent concentrations has been synchronised to enable comparison with the influent concentrations.

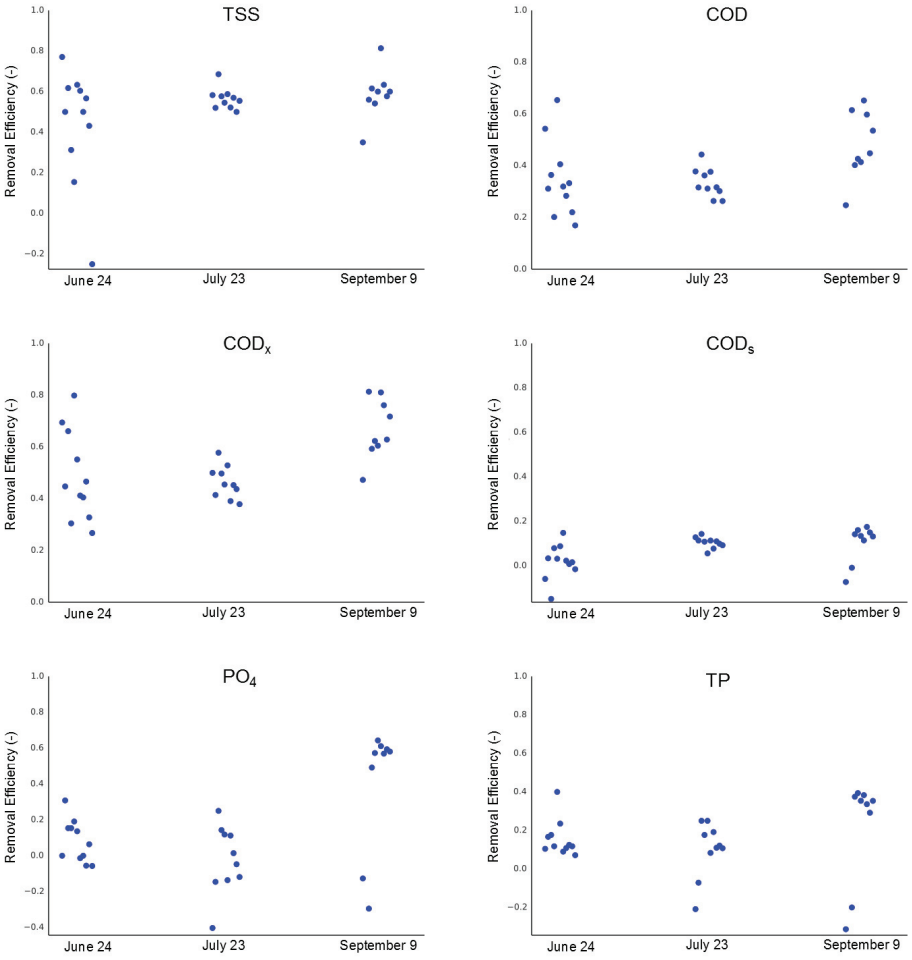

Figure 5.11. Removal efficiencies for TSS, COD, COD_x, COD_s, PO_4 and TP for one operational primary sedimentation tank at the Eindhoven WWTP on June 24 and July 23 (without chemical dosing) and September 9 (with chemical dosing) in 2013.

A linear regression was applied to see if any relations between the influent and effluent concentrations, influent and effluent loads and removal efficiencies of the different measurements could be established (Figure 5.12). First observation is that the only correlation with regard to flow rate are the loads, which are calculated by multiplying with the flow rate, hence the obvious correlation. But neither the effluent concentrations nor the removal efficiencies display any relation with the flow rate.

Again the self-evident relations between PO_4 and TP as well as COD_x and COD appear in the analysis. Also a high correlation is found between the effluent and

influent concentration of COD_s, demonstrating the limited removal (as it is a soluble component) in the PST. In contrast with the routine measurements, the inverse correlation between the removal efficiency of TSS and the corresponding effluent concentration stands out. The fact that the correlation is seen now is contributed to the higher measuring frequency, i.e. 2-hourly versus daily composite samples.

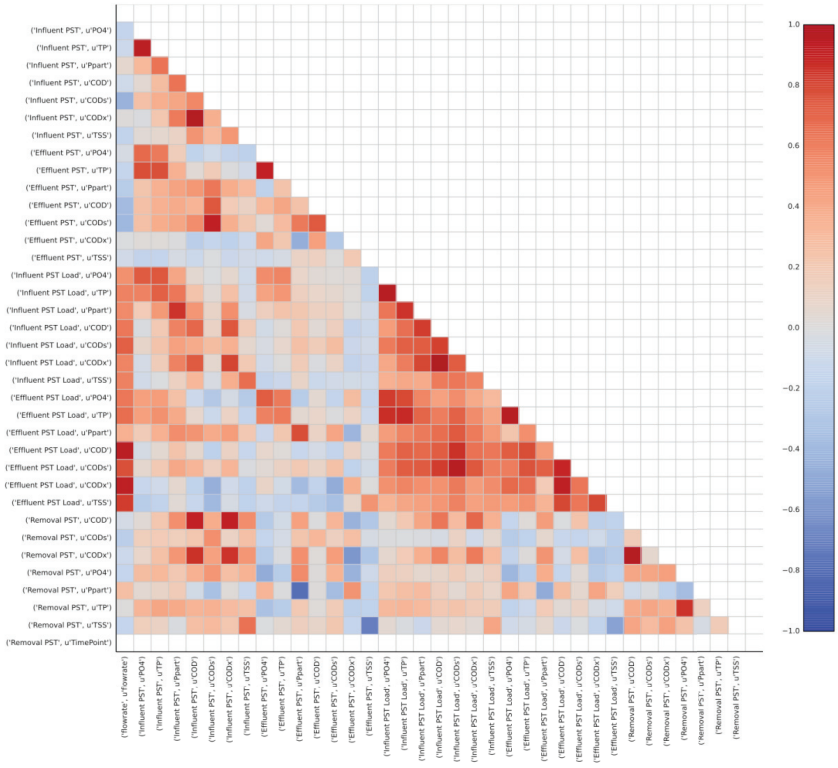

Figure 5.12. Correlations determined using linear regression for the influent, effluent and removal efficiency of TSS, COD, COD_x, COD_s, PO_4 and TP for the measurement campaign with only one operational primary sedimentation tank at the Eindhoven WWTP on June 24 and July 23 (without chemical dosing) and September 9 (with chemical dosing) in 2013. Red indicates a positive correlation and blue a negative correlation. Darker colours express a more pronounced correlation.

Interestingly we also see a correlation between the influent concentration of both COD (Figure 5.13 and Table 5.6) and COD_x (Figure 5.14 and Table 5.6) and the corresponding removal efficiency. This observation opens the possibility of finding empirical relations between these influent concentrations and their removal efficiency, in case sufficiently high frequency data is available. The correlation between TSS influent concentration and its removal efficiency is also present but not as pronounced (Figure 5.15 and Table 5.6).

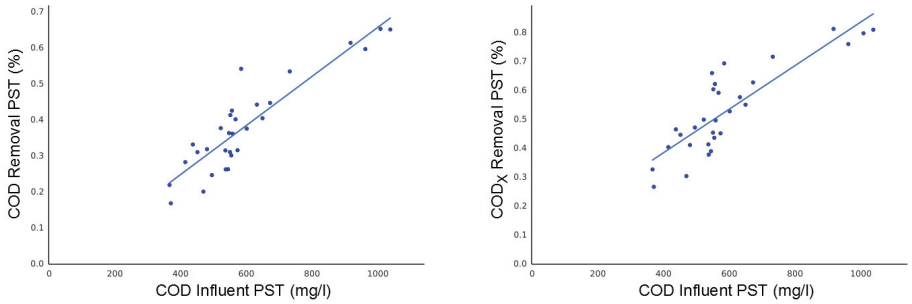

Figure 5.13. Linear regression for the high correlations of the influent concentration of COD with the removal efficiency of COD (left) and the removal efficiency of COD_x (right). Correlation coefficients are listed in Table 5.6.

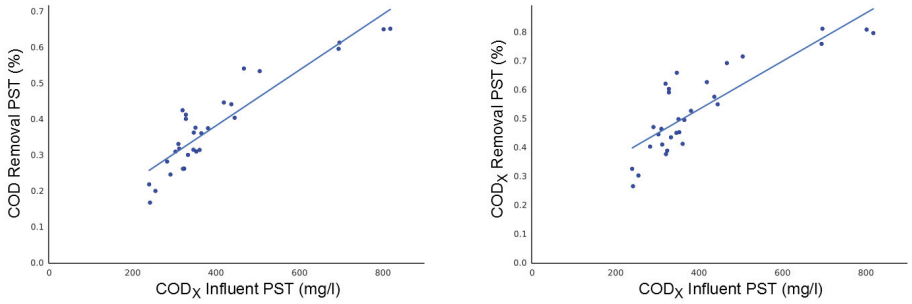

Figure 5.14. Linear regression for the high correlations of the influent concentration of COD_x with the removal efficiency of COD (left) and the removal efficiency of COD_x (right). Correlation coefficients are listed in Table 5.6.

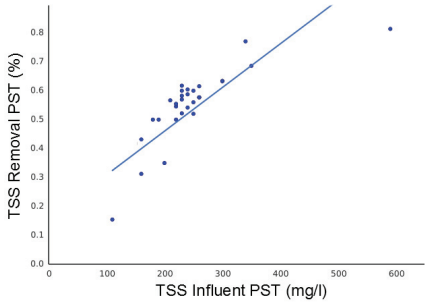

Figure 5.15. Linear regression for the modest correlation of the influent concentration of TSS with the removal efficiency of TSS. Correlation coefficients are listed in Table 5.6.

Table 5.6. The linear regression coefficients (Y=Intercept+Gradient*X) for the high correlations encountered in the data set.

Y	X	Gradient	Intercept	R^2
Influent COD	Removal COD	6.8e-4	-2.4e-2	0.82
Influent COD	Removal CODx	7.5e-4	8.3e-2	0.74
Influent CODx	Removal COD	7.8e-4	7.2e-2	0.84
Influent CODx	Removal CODx	8.3e-4	2.0e-1	0.72
Influent TSS	Removal TSS	1.5e-3	1.6e-1	0.42

5.5.3. Measurement campaign 1 for full fractionation

The analysed data of this measurement campaign was used for the fractionation of the influent into ASM fractions (Roeleveld and van Loosdrecht, 2002). Some of the fractionation calculations resulted in negative ASM fractions. The negative results arose from the BOD_T and COD_s analyses and accordingly a number of the analysis results were omitted and replaced by estimated values. The choice to omit certain values was based on the calculation of the COD over BOD_T and COD_S over COD ratios, which were subsequently compared with typical values (Rieger et al., 2012). The values out of range were replaced by applying the average (without outliers) COD over BOD_T and COD_S over COD ratios determined for this measurement campaign. TSS and VSS data were discarded as the analysis results were considered to be erroneous. Flow rates during the day were rather constant until a storm event in the afternoon drastically reduced the hydraulic retention time, which reduced the number of samples available to calculate the actual removal efficiency. The removal efficiency of COD_X reaches 37%. As expected, steered by the removal of the particulates, COD_T and BOD_T effluent concentrations are clearly lower than the influent concentrations (Figure 5.16), exhibiting a removal of about 20% (Table 5.7). TP and TN display negative removal efficiencies, driven by the PO_4 and NH_4 removal efficiencies respectively. Concentrations of the soluble components (COD_S, NH_4 and PO_4) at the effluent are slightly higher than at the influent. The increase is 13% on average for both COD_s and NH_4 and about 40 % for PO_4 (Table 5.7 and Figure 5.17). A possible explanation for this is the imperfect mixing in the tank, which hinders the synchronisation of influent and effluent samples. The increase of NH_4 could also be contributed to ammonification, which is the hydrolysis of organic nitrogen into NH_4. In contrast to the other soluble components NO_3 is being removed with 25% on average. Although the NO_3 concentrations are really low (smaller than 1 mg/l), this behaviour could indicate the presence of biological reactions. Finally, the pH shows a marginal increase, which might be an indication of biological reactions as well (or it may simply be introduced by imperfect mixing in the tank).

Table 5.7. Descriptive overview of the removal efficiencies for COD_T, COD_s, BOD_T, PO_4, TP , TN, NH_4, and pH for normal operation of the primary sedimentation tanks at the Eindhoven WWTP on May 6, 2014. Negative values mean an increase in concentration.

	COD_T	COD_s	COD_x	BOD_T	PO_4	TP	TN	NH_4	NO_3	pH
Min	12%	-25%	28%	3%	-55%	-39%	-17%	-21%	8%	-1%
Mean	20%	-16%	37%	18%	-42%	-26%	-6%	-13%	25%	2%
Stdev	7%	9%	8%	11%	15%	14%	13%	8%	26%	3%
Max	29%	-4%	46%	31%	-20%	-5%	12%	-1%	70%	5%

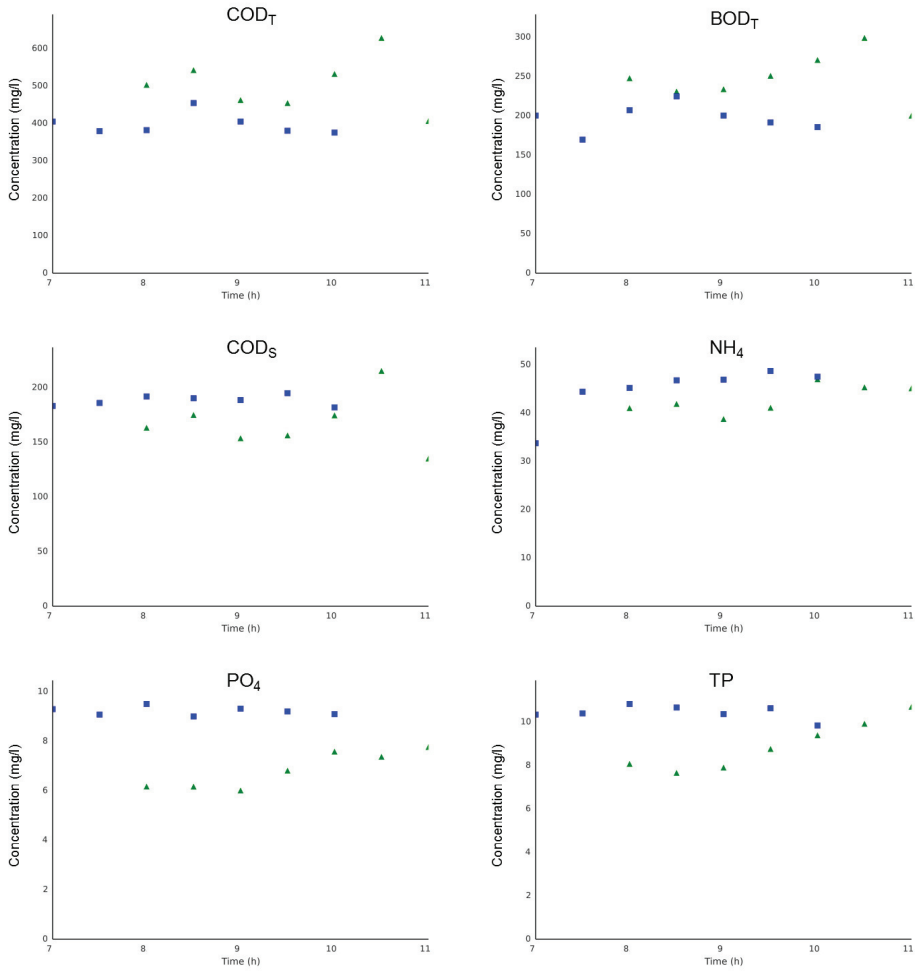

Figure 5.16. Influent (green triangles) and effluent concentrations (blue squares) for COD_T, BOD_T, COD_s, NH_4, PO_4 and TP for normal operation of the primary sedimentation tanks at the Eindhoven WWTP on May 6, 2014. Time for the effluent concentrations has been synchronised to enable comparison with the influent concentrations.

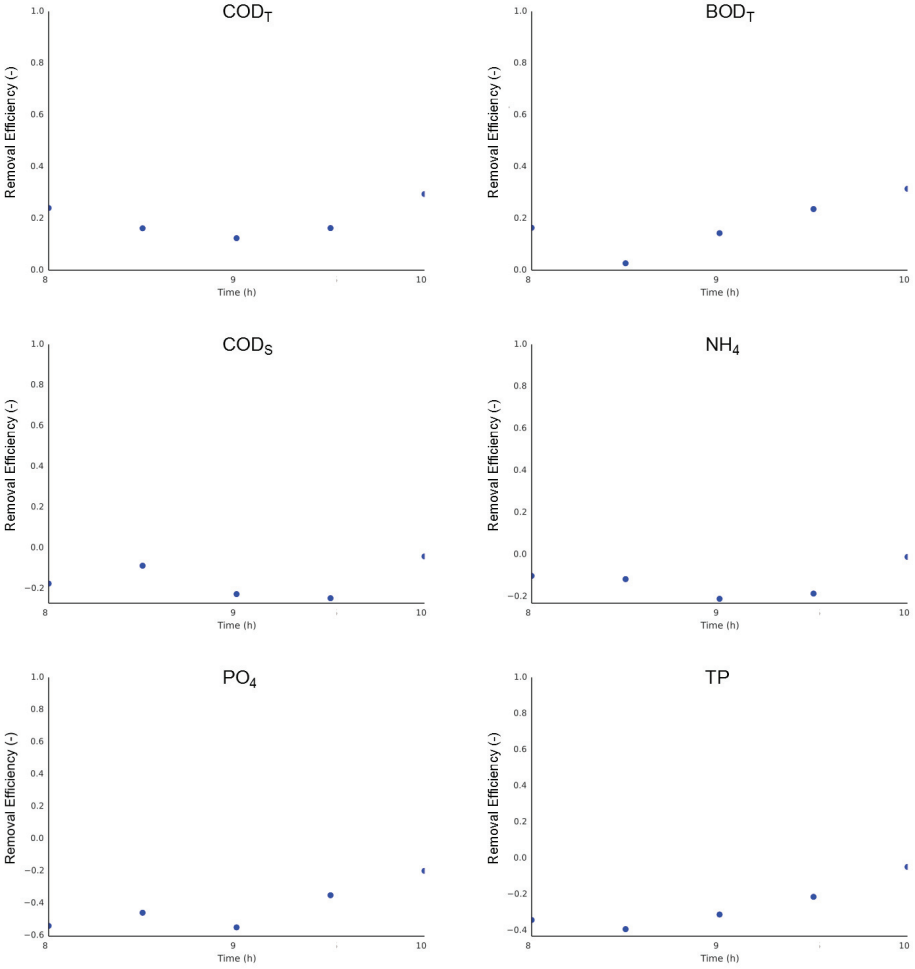

Figure 5.17. Removal efficiencies for COD_T, BOD_T, COD_s, NH_4, PO_4 and TP for normal operation of the primary sedimentation tanks at the Eindhoven WWTP on May 6, 2014. Time for the effluent concentrations has been synchronised to enable comparison with the influent concentrations.

The effluent concentrations of both X_U and XC_B are lower than the corresponding influent concentrations (Figure 5.18). But the trends which the fractions are exhibiting are different (Figure 5.19). The removal efficiency of X_U fluctuates from about 40% down to nearly 0% (Table 5.8). XC_B on the other hand has higher removal efficiencies (a mean of 50% versus 23% for X_U) and varies between 19% and 67%. This is an important finding in view of the modelling of the subsequent activated sludge system. However, it also has to be placed into context as the fractions exhibit a certain interdependence, i.e. X_U is calculated (Equation 3.15) as

the difference of the particulate COD and XC_B (assuming the concentration of heterotrophs to be negligible).

Table 5.8. Descriptive overview of the removal efficiencies for the carbonaceous ASM fractions S_B, S_U, XC_B and X_U for normal operation of the primary sedimentation tanks at the Eindhoven WWTP on May 6, 2014. Negative values mean an increase in concentration.

	S_U	S_B	X_U	XC_B
Min	0%	-29%	3%	19%
Mean	0%	-18%	23%	50%
Stdev	0%	11%	15%	19%
Max	0%	-5%	39%	67%

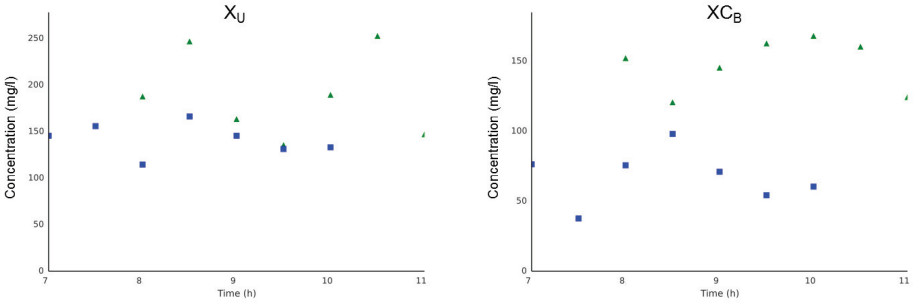

Figure 5.18. Calculated influent (green triangles) and effluent concentrations (blue squares) for the ASM fractions X_U and XC_B for normal operation of the primary sedimentation tanks at the Eindhoven WWTP on May 6, 2014. Time for the effluent concentrations has been synchronised to enable comparison with the influent concentrations.

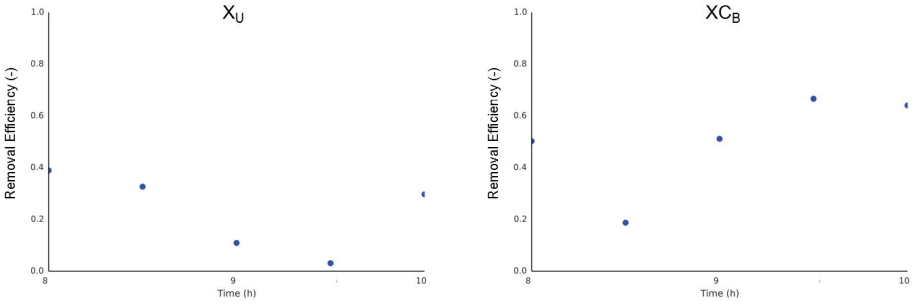

Figure 5.19. Removal efficiencies for the ASM fractions X_U and XC_B for normal operation of the primary sedimentation tanks at the Eindhoven WWTP on May 6, 2014.

Influent and effluent concentrations of S_U are equal, and as such is the removal efficiency 0%. The reason for the equal influent and effluent concentrations is the calculation method. S_U is calculated as a percentage of the soluble COD

concentration in the effluent of the activated sludge plant (Roeleveld and van Loosdrecht, 2002), which is the same for both influent and effluent of the PST.
Due to the limited number of points no correlation analysis was performed. Nonetheless, the measurement campaign revealed an important difference in the removal of the different ASM fractions. The difference may be, in part, depending on the calculation method. However it is likely that it is also inherent to the different nature of the ASM fractions. The inert particulate COD (X_U) seemed to exert smaller removal efficiencies than the slowly biodegradable COD (XC_B), however due to the limited number of analysis, further analysis is required. Therefore, a second measurement campaign was set up.

5.5.4. Measurement campaign 2 for full fractionation

Also for this campaign the analysed data was used for the fractionation in ASM fractions (Roeleveld and van Loosdrecht, 2002). Due to the limited capacity of the lab, the BOD_{10} took several weeks to be completed, which gave cause for doubting the results. The ratios COD over BOD_{10} gave very high values, out of the range to be accepted plausible in wastewater (compared to the ratios given in Rieger et al. (2012)), indicating that biodegradation during storage of the samples may have occurred. Applying the BOD_{10} values in the fractionation resulted in negative values for the biodegradable ASM fractions. As such it was decided to replace the BOD_{10} values in the calculations by the average COD over BOD_T determined in the measuring campaign of May 6, 2014.
Logically, COD_x and VSS gave similar results for the removal efficiency (Table 5.9) and also TSS showed a clear removal. The lower removal of TSS compared to VSS is related to the surprising increase of ISS. A plausible explanation for the increase in ISS could be the formation of PO_4 and NH_4 salts. This possible explanation corresponds to the removal of PO_4 and NH_4 (Table 5.10), which seems to be occurring when higher influent concentrations, attributed to the sludge treatment reject water from Mierlo, are noticed (Figure 5.20). On September 2 a typical day pattern is noticed, with an increase in the influent of NH_4 and PO_4 concentration of respectively 15 mg/l and 8 mg/l. On the other hand, the effluent concentration remains rather constant, suggesting substantial removal.

Table 5.9. Descriptive overview of the removal efficiencies for COD_T, COD_s, COD_x, TSS, ISS and VSS for normal operation of the primary sedimentation tanks at the Eindhoven WWTP on September 2, 2014. Negative values mean an increase in concentration.

	COD_T	COD_s	COD_x	TSS	ISS	VSS
Min	22%	-27%	32%	5%	-23%	25%
Mean	34%	3%	46%	17%	-7%	42%
Stdev	7%	13%	8%	6%	8%	12%
Max	44%	16%	58%	28%	2%	64%

Table 5.10. Descriptive overview of the removal efficiencies for PO_4, TP, TN, NH_4, NO_3 and pH for normal operation of the primary sedimentation tanks at the Eindhoven WWTP on September 2, 2014. Negative values mean an increase in concentration.

	PO_4	TP	TN	NH_4	NO_3	pH
Min	-38%	-51%	3%	-4%	-1%	-3%
Mean	8%	11%	14%	9%	24%	0%
Stdev	23%	21%	9%	8%	10%	2%
Max	37%	32%	37%	20%	36%	3%

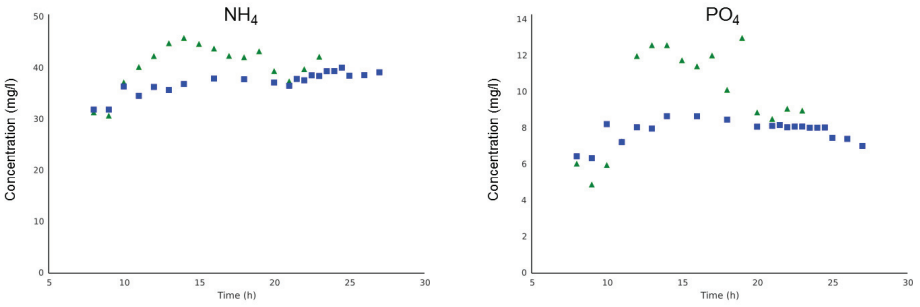

Figure 5.20. Influent (green triangles) and effluent concentrations (blue squares) for NH_4 (left) and PO_4 (right) for normal operation of the primary sedimentation tanks at the Eindhoven WWTP on September 2, 2014. Time for the effluent concentrations has been synchronised to enable comparison with the influent concentrations.

On September 2, an increase in influent concentration of the monovalent cation K and the di-valent cations Ca and Mg, although not as expressive, is coinciding with the trend for PO_4 and NH_4 (Figure 5.21). The other cations (Na and Fe) do not express a similar trend. Ca shows the greater removal efficiency (4%) versus 1% for both Na and Mg (Table 5.11). K shows a small average increase but removal efficiency is varying considerably. This variation in removal efficiency is even huge for Fe, with a surprisingly large average increase in concentration.

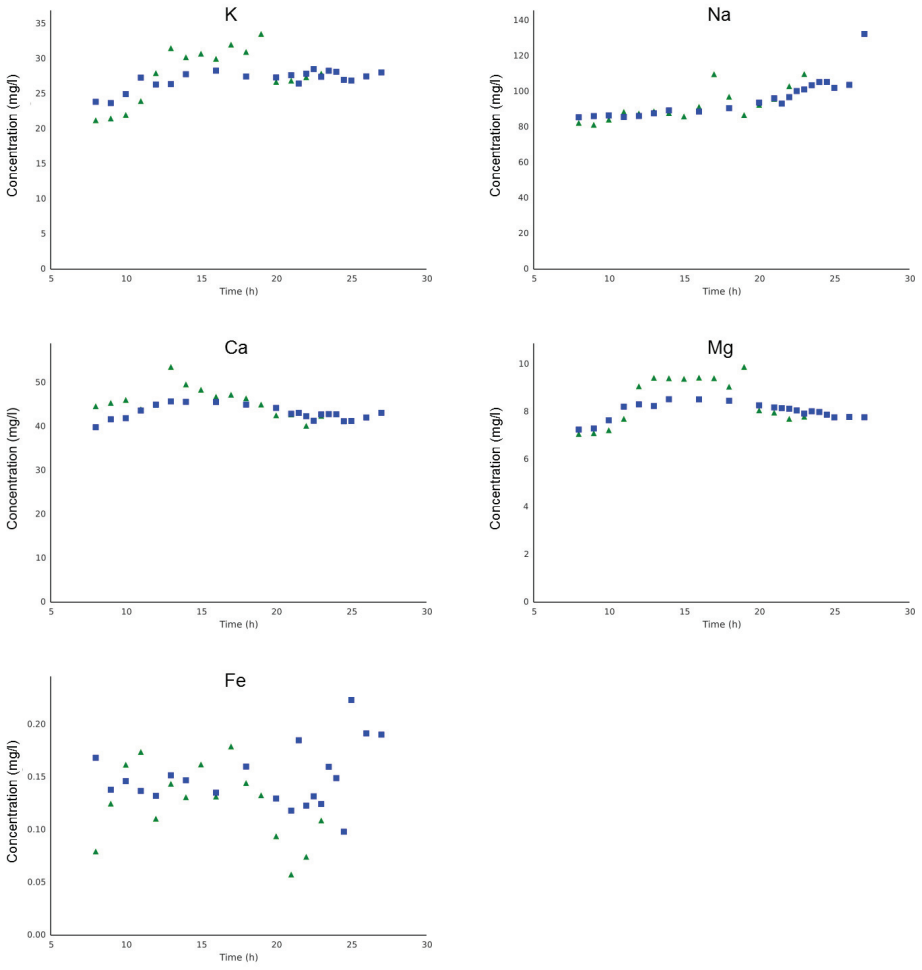

Figure 5.21. Influent (green triangles) and effluent concentrations (blue squares) for K, Na, Ca, Mg and Fe for normal operation of the primary sedimentation tanks at the Eindhoven WWTP on September 2, 2014. Time for the effluent concentrations has been corrected to enable comparison with the influent concentrations.

Table 5.11. Descriptive overview of the removal efficiencies for the cations K, Na, Ca, Mg and Fe for normal operation of the primary sedimentation tanks at the Eindhoven WWTP on September 2, 2014. Negative values mean an increase in concentration.

	K	Na	Ca	Mg	Fe
Min	-14%	-6%	-5%	-7%	-112%
Mean	-1%	1%	4%	1%	-28%
Stdev	10%	4%	6%	7%	41%
Max	16%	8%	15%	13%	21%

Due to the fractionation method applied, the removal of S_U is 0% (Table 5.12). The S_B fraction, a soluble component, displays as expected only a marginal average removal (3%). However it shows a large standard deviation. It is not clear whether this is caused by the fractionation method itself or if there is some flocculation occurring, after which the S_B is removed together with the particulate fractions. The flocculation could be enhanced by, in case of an overdose, the polymers used at the sludge treatment of Mierlo.

Table 5.12. Descriptive overview of the removal efficiencies for the carbonaceous ASM fractions S_B, S_U, XC_B and X_U for normal operation of the primary sedimentation tanks at the Eindhoven WWTP on September 2, 2014. Negative values mean an increase in concentration.

	S_U	S_B	X_U	XC_B
Min	0%	-45%	29%	34%
Mean	0%	3%	42%	48%
Stdev	0%	20%	7%	9%
Max	0%	21%	53%	66%

The removal of X_U is lower than the removal of XC_B (Table 5.12 and Figure 5.23). The removal efficiency of XC_B reaches nearly the same value (48% versus 50%) as for the measurement campaign in May (Table 5.8), though with a significantly lower standard deviation (9% versus 19%). The removal efficiency of X_U proves to be significantly larger in this measurement campaign compared to the previous one (42% versus 23%). The higher efficiency corresponds to the higher removal efficiency noticed for COD_X (46% versus 37%). This higher removal efficiency of COD_X is completely attributed to the higher removal of X_U. This observation is considered not to be largely influenced by the fact that the BOD_{10} measurements were replaced using a ratio to the total COD. From the measurement campaign in May it can be deduced that COD_T and BOD have nearly the same removal efficiency (20% versus 18%) and as such the estimation of BOD does not significantly influence the fractionation. A final observation from the data is that the overall effect of the removal is that for both fractions the effluent concentrations fluctuations are buffered (Figure 5.22).

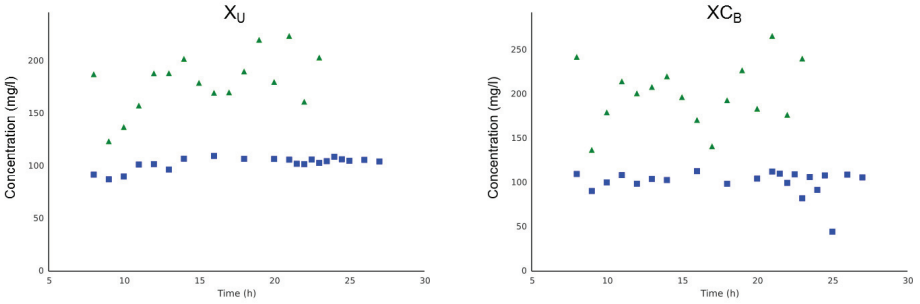

Figure 5.22. Calculated influent (green triangles) and effluent concentrations (blue squares) for the ASM fractions X_U and XC_B for normal operation of the primary sedimentation tanks at the Eindhoven WWTP on September 2, 2014. Time for the effluent concentrations has been corrected to enable comparison with the influent concentrations.

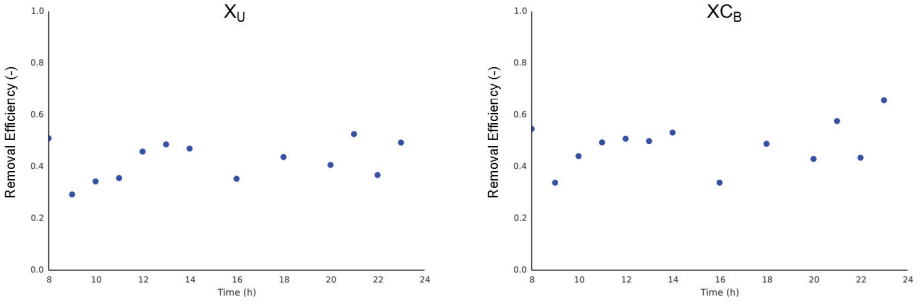

Figure 5.23. Removal efficiencies for the ASM fractions X_U and XC_B for normal operation of the primary sedimentation tanks at the Eindhoven WWTP on September 2, 2014.

5.5.5. Overall discussion

The data collection demonstrated that the primary sedimentation is a complex process. In all measurement data sets a difference in removal efficiency between the different particulate components was encountered. First, there is the difference between volatile suspended solids and the inorganic suspended solids. The VSS constitutes primarily of the organic matter largely contributing to the biodegradable COD. As such incorporating a single TSS removal mechanism in models will compromise the modelling of the subsequent activated sludge process as the incoming COD will not be correctly quantified. In addition the difference between the different measurement campaigns does not allow for a simplifying approach. On the other hand, the measurement campaign in September 2013 shows a high

(53%) but equal removal efficiency for both TSS and COD_x and thus consequently for VSS and ISS. However, during the measurement campaign in September 2014, the ISS solids increase whereas the VSS decreased. Applying the TSS removal efficiency, which is in the middle, for both would severely overestimate the VSS and consequently the COD entering the activated sludge tanks. As a consequence denitrification would be over predicted.

Secondly, the measurement campaigns also demonstrated a difference in the removal of the different particulate ASM fractions, i.e. X_U exhibits a lower removal efficiency that XC_B. Again this implies the need to incorporate this in view of the modelling of the activated sludge process. However, this inclusion is not trivial because the ASM fractions are not at all linked to the settling characteristics of the respective components. In addition, the characterisation of ASM components is not (yet) a trivial exercise as it largely depends on respirometric tests (either BOD or short term respirometry), which are sometimes more of an art than science.

Third, the data shows the time dependent behaviour of the removal efficiencies in the PSTs and the need for dynamic modelling including a dynamic characterisation of the influent. Even during dry weather on an hourly basis the removal efficiencies of the different components change. This change may be driven by dynamic influent characteristics such as the influence of industrial discharges or recycles from the off-site sludge treatment. On the other hand, the dynamics in influent composition between dry weather and rain weather do not seem to impact the removal efficiencies. However, care must be taken as the comparison has been made only by means of daily averages, which may overlook short events as the first flush effect. In any case, a thorough characterisation of the influent wastewater is desirable as it may also identify other phenomena, such as precipitation or biological processes, that impact the removal efficiency.

Fourth, no correlations are found between the removal efficiencies and the flow rate. This conclusion may be disputable for rain weather conditions as only a few data points were available. This observation, however, shows that empirical models depending on the flow rate are not appropriate for the modelling of the primary sedimentation tanks at the WWTP of Eindhoven, at least not during dry weather conditions. Interestingly, when applying higher frequency sampling, we also see a correlation between the influent concentration of both COD, COD_x and TSS and the corresponding removal efficiency. The correlation with TSS, however is less obvious. These observations open the possibility of applying empirical models between these influent concentrations and their removal efficiency.

5.6. CONCLUSIONS

The data collection showed a significant difference in removal efficiencies between different components (organic matter versus inorganic matter and inert COD versus biodegradable COD), which needs to be addressed in view of whole plant modelling. These results indicate that also the removal of organic matter shows variability.

Only a few correlations arose from the data, i.e. the impact of influent concentrations of particulate and total COD on the corresponding removal efficiency. Some unexpected behaviour was observed as well. First a moderate increase in CODs and NH_4 is revealed during the measurement campaign in May 2014 and a considerable increase of PO_4 concentration as well. In contrast, NO_3 is being removed. During the measurement campaign in September 2014 an unexpected increase in ISS (while VSS was decreasing) was disclosed. The data also highlights the need for further data collection and research.

The routinely collected data for 2011-2013 shows no important difference between dry and wet weather days and the measurement campaign in September 2013 for evaluating the possibility of a reduced volume also does not show a large difference with the full capacity. Indicating, that for dry weather the capacity of 1 clarifier is sufficient.

Chapter 6

Modelling of primary sedimentation and its impact on the whole WWTP of Eindhoven

"All truths are easy to understand once they are discovered; the point is to discover them."
Galileo Galilei

6.1. ABSTRACT

A model based approach was taken in view of the evaluation of the performance of the primary sedimentation tanks and their impact on the performance of the whole wastewater treatment plant of Eindhoven. Four different approaches were taken to explain different observations made during the data collection at the treatment plant. In first instance the increase of ammonium and phosphate and the decrease of nitrate observed during the measuring campaign on May 6, 2014, was explained using a modified version of ASM2d. The increase and decrease of the nutrients could be explained by the presence of both ordinary heterotrophic and phosphate accumulating organisms in the wastewater. In second instance, the unexpected increase of inorganic suspended solids noticed during the measurement campaign on September 2, 2014, was partially clarified applying a physical-chemical model in the modelling software PHREEQC, which demonstrated the formation of the precipitate hydroxylapatite and a consequent removal of phosphate. In third instance the applicability of a new phenomenological model, developed by implementing a particle settling velocity distribution model in a mathematical rigid model structure, was evaluated. Finally the impact of the sedimentation process on the whole WWTP of Eindhoven was modelled and implemented in the modelling software WEST (mikebyDHI). It was proven that the primary sedimentation tanks definitely affect the denitrification but may also affect the nitrification. For this

reason, the integration of sufficiently detailed primary sedimentation models is essential to model the performance of a whole WWTP. An important contribution to obtain a better description is the separate modelling of the particulate inorganic and organic fractions. In addition, modelling processes influencing the performance of the sedimentation tanks results in a better understanding of the observed phenomena.

6.2. ABBREVIATIONS AND SYMBOLS

C_{ISS}	Concentration of inorganic suspended solids (g/l)
C_{TSS}	Concentration of total suspended solids (g/l)
C_{VSS}	Concentration of volatile suspended solids (g/l)
Q	Flow rate (m³/h)
Q_{actual}	Actual flow rate that the pump delivers (m³/h)

6.3. INTRODUCTION

The modelling of the primary sedimentation tanks of the WWTP of Eindhoven received more attention in view of the WWTP evaluation with respect to wet weather behaviour. In first instance the primary sedimentation tank model was upgraded from a mere ideal separation model to a model taking into account the effect of the hydraulic retention time on the removal efficiency (Tay, 1982). In addition, the model of the secondary sedimentation tank was upgraded from the Takacs model (Takács et al., 1991) to the Bürger-Diehl model which has a more sound mathematical structure allowing improved prediction of the sludge blanket height and underflow concentration during wet weather (Bürger et al., 2012).
It was considered essential to have a model that could predict the impact of high flow rates on the removal efficiency of the primary sedimentation tank, but the model first needs to be able to describe the sedimentation process during dry weather. However, despite the model adaptations on the primary and secondary sedimentation tank, the simulation results, which were excellent for ammonium, still diverged significantly from the measurement data for nitrate. In an attempt to reduce this divergence, the model of the primary sedimentation tank was extended to account for different removal efficiencies for the different suspended fractions, based on repeated measurements, during the year 2011, performed on the primary sedimentation tanks (See Chapter 10). This resulted in a higher chemical oxygen

demand (COD) concentration entering the activated sludge tanks as such improving the nitrate removal predictions considerably.

The modelling of the primary sedimentation tanks at the WWTP of Eindhoven is applied within the framework of modelling the whole plant and even beyond the plant boundaries in the modelling of the whole integrated urban water systems, i.e. including sewers, river and WWTP (Benedetti et al., 2013; Langeveld et al., 2013a). In order to deal with this context of whole plant modelling, the models need to consider compliance. For primary sedimentation tank models, this compliance involves the description of the removal of the different activated sludge model (ASM) fractions (Henze et al., 2000). This evolution of the ASM fractions over the primary sedimentation tank, however, is not a trivial effort as the ASM fractionation does not contain any information about the settling ability of the different components.

This chapter intends to shed light on how the modelling of the primary sedimentation tank influences the modelling of the whole plant and how the modelling of the primary sedimentation tanks is applied to increase the understanding of certain phenomena observed during the data collection.

Four different approaches were implemented to explain different observations made during the data collection at the treatment plant (Chapter 5). First, a modified version of ASM2d implemented in a single completely mixed tank reactor mimicking the hydraulic retention time in the PST was evaluated to describe the increase of ammonium and phosphate and the decrease of nitrate observed during the measuring campaign on May 6, 2014. Second, a physical-chemical model in the modelling software PHREEQC modelling the formation of precipitates was applied to shed light on the unexpected increase of inorganic suspended solids and a concurrent removal of phosphate noticed during the measurement campaign on September 2, 2014. Third, a new phenomenological model in a mathematical rigid model structure was evaluated. Fourth, the impact of the sedimentation process on the whole WWTP of Eindhoven was modelled using an empirical model describing the difference in removal for inorganic suspended solids (ISS) and volatile suspended solids (VSS).

6.4. MATERIALS AND METHODS

6.4.1. Modelling biological reactions in the primary sedimentation tank

In order to find a plausible explanation for the change in the soluble components, i.e. the removal of NO_3 and the increase of NH_4 and PO_4, biological reactions occurring in the primary sedimentation tank were modelled. A continuous stirred tank reactor model (CSTR) including an extended version of the ASM2d model (Henze et al., 2000) was implemented in WEST (mikebyDHI). The CSTR did not include any settling model, which is clearly an oversimplification but the objective of the model is merely to show the possibility and to steer further investigation.
The ASM2d extension, which is the same as the bio-kinetic model applied in the whole plant model of the WWTP of Eindhoven, has two major modifications. The first modification is the adaptation to make the lysis of biomass dependent on the environmental factors, i.e. anaerobic, anoxic or aerobic conditions (Gernaey and Jørgensen, 2004). The second extension is the inclusion of a particulate inorganic fraction (Wentzel et al., 2002), which was necessary for the calculation of the removal efficiencies of the primary sedimentation tanks.
The model was fed with the fractionated data from the measurement campaign on May 6, 2014. This data was selected because the change in nitrate, ammonium and phosphate concentration was significant. The influent fractionation as applied did neglect the concentration of heterotrophic biomass, which was assumed to be zero. However, the heterotrophic biomass concentration in wastewater has been shown to contribute up to 25% of the raw wastewater COD (Sperandio et al., 2001). In order to study the effect of this contribution on the nutrient concentrations, the influent fraction was varied. The percentage (0-25%) of the heterotrophic biomass was subtracted from both the X_U and XC_B fractions equally, resulting in an unchanged COD_x. The same procedure was also repeated for the phosphate accumulating organisms (PAO) to contribute to 10% of the COD_x.

6.4.2. Physical-chemical modelling of precipitation

In order to investigate the precipitation of NH_4 and PO_4 salts in the primary sedimentation tanks, contributing to an increase in ISS, PHREEQC (Parkhurst and Appelo, 2013) was applied to model the possibility of the formation of different precipitates under the concentrations encountered in the wastewater. The minteq v4 database was applied for equilibrium precipitation modelling, acknowledging that

the primary purpose for the database are geochemical applications. This implies that some crystals, although thermodynamically stable, would not precipitate under WWTP conditions for kinetic reasons. Taking this into account the predicted precipitates are subsequently scanned whether they would occur in practice (Wadley and Buckley, 1997). Because they were not in the database, ammonium struvite and potassium struvite were added based on Ronteltap et al. (2007). Finally, calcium phosphate, iron phosphate, calcite and iron hydroxide were allowed to precipitate.

The cation concentrations (K, Na, Ca, Mg, Fe) measured during the measurement campaign of September 2, 2014, were complemented with assumptions for a number of anions (as no measurements were available). The concentration of chlorides (90 mg/l) was determined based on infrequent measurements. Sulphides were calculated assuming that all the sulphates in the effluent of the WWTP plant reside from the sulphides, i.e. one mole of sulphide for each mole of sulphate. Because of the high importance of carbonates in the formation of different precipitates, the concentration of carbonate was varied within an acceptable range (from 3 up to 6 mmol/l) and the results were checked for differences.

6.4.3. Modelling of the sedimentation process in primary sedimentation tanks

6.4.3.1. A modification of the model of Tay (1982)

The model of Tay was extended to reflect the difference in removal efficiency between COD (containing only organic fractions) and TSS (containing both inorganic and organic fractions). This difference can be explained by the difference in settling velocity, which is driven by the density difference, between the particulate organic and inorganic fractions. The model was implemented in WEST (mikebyDHI) and integrated within the whole plant model of the WWTP of Eindhoven.

The settling characteristics are specified based on the half-removal time (T_A), which is the time at which 50% of the influent suspended solids is removed.

$$X_r = \frac{S_0 - S}{S} = \frac{t_r}{T_A + t_r} \quad (6.1)$$

Where S_0 is the suspended solids concentration in the influent to the settling tank [mg/l], S is the suspended solids concentration in the effluent of the settling tank [mg/l], t_r is the hydraulic retention time in the settling tank [d] and T_A is the half-removal time [d].

The model contains two new parameters determining the removal efficiency of the particulate organic fractions (or particulate COD) and the particulate inorganic

fraction. These parameters are then used to calculate the new non-settleable fractions (f_{ns}) and the half-removal times (T_A).

$$f_{ns,XCOD} = \frac{(1-ER_{XCOD})}{f_{Out,DW}} \quad (6.2)$$

Where $f_{ns,XCOD}$ is the non-settleable fraction for the particulate COD [-], ER_{XCOD} is the removal efficiency for the particulate COD [-] and $f_{Out,DW}$ is the fraction of the incoming flow rate going to the effluent [-].

$$f_{ns,XIg} = \frac{(1-ER_{XIg})}{f_{Out,DW}} \quad (6.3)$$

Where $f_{ns,XIg}$ is the non-settleable fraction for the particulate inorganic fraction [-] and ER_{XIg} is the removal efficiency for the particulate COD [-].

$$T_{A,XCOD} = \frac{V_{Clar}}{Q_{In,DW}} * \frac{f_{ns,XCOD}}{(1-f_{ns,XCOD})} \quad (6.4)$$

Where $T_{A,XCOD}$ the half-removal times for the particulate COD [d], V_{Clar} is the volume of the primary sedimentation tank [m³] and $Q_{In,DW}$ is the average incoming flow rate during dry weather conditions [m³/d].

$$\boldsymbol{T_{A,XIg} = \frac{V_{Clar}}{Q_{In,DW}} * \frac{f_{ns,XIg}}{(1-f_{ns,XIg})}} \quad (6.5)$$

Where $T_{A,XIg}$ the half-removal times for the particulate inorganic fraction [d], V_{Clar} is the volume of the primary sedimentation tank [m³] and $Q_{In,DW}$ is the average incoming flow rate during dry weather conditions [m³/d].

6.4.3.2. A discrete settling model with multiple settling velocity classes for organics and inorganics

As a first attempt to come to a more rigorous discrete settling model the particle settling velocity distribution (PSVD) concept applied by Bachis et al. (2012) was embedded in the rigorous discretization scheme proposed by Bürger et al. (2011), previously applied for modelling secondary settling tanks. In contrast to secondary settling only discrete settling is considered and the hindered settling and compression settling are assumed to be non-existent and as a consequence omitted. Although hindered settling and compression settling are neglected at this stage, the model structure allows for easy reintegration, as such paving the way to a 'unified' sedimentation tank model.

The settling velocity depends solely on the particle size and density, for which different particle classes have been implemented to mimic the according distributions. Two sets of particle classes, one for ISS and one for VSS, are introduced to reflect the difference in removal efficiency between COD and TSS. The model was implemented in WEST (mikebyDHI) providing flexibility to choose the number of particle classes for both ISS and VSS.

The number of particles (expressed as concentration) for each of the particle classes are determined as a fraction of the total ISS (Equation 6) or VSS (Equation 7).

$$C_{ISS,i} = f_{ISS,i} \cdot C_{ISS} \quad (6.6)$$

Where $C_{ISS,i}$ is the concentration of inorganic particles in the i^{th} ISS particle class [mg/l], $f_{ISS,i}$ is the fraction of the total ISS concentration of inorganic particles pertaining to the i^{th} ISS particle class [mg/l] and C_{ISS} is the concentration of ISS [mg/l].

$$C_{VSS,i} = f_{VSS,i} \cdot C_{VSS} \quad (6.7)$$

Where $C_{VSS,i}$ is the concentration of organic particles in the i^{th} VSS particle class [mg/l], $f_{VSS,i}$ is the fraction of the total VSS concentration of organic particles pertaining to the i^{th} VSS particle class [mg/l] and C_{VSS} is the concentration of VSS [mg/l].

The model as proposed by Bürger et al. (2011), is based on the conservation of mass, which can be cast into the following one-dimensional (1D) partial differential equation (PDE) of nonlinear convection–diffusion type for the solids concentration as a function of depth z and time t (Equation 6.8). Discretization of the mathematical model is developed according to Bürger et al. (2011).

$$\frac{\partial C_i}{\partial t} + \frac{\partial}{\partial z} F(C_i, z, t) = \frac{\partial}{\partial z}\left(\{d_{disp}(z, Q_{In}(t)\}\frac{\partial C_i}{\partial z}\right) + \frac{Q_{In}(t)C_{i,In}(t)}{A}\delta(z) \quad (6.8)$$

Where C_i is the concentration of solids (either organic or inorganic) pertaining to the i^{th} particle class [mg/l], $C_{i,In}$ is the influent concentration of solids pertaining to the i^{th} particle class [mg/l], d_{disp} is the dispersion function as defined in Bürger et al. (2011) [m²/d] and Q_{In} is the influent flow rate and A is the surface area of the tank. The second term on the left-hand side models discrete settling combined with the bulk flux (Equation 6.9). The first term on the right side describes dispersion and the second term is a singular source term for the influent.

$$F(C_i, z, t) = \begin{cases} -Q_{out}(t)\cdot\frac{C_i}{A} & for\ z<-H \\ -Q_{out}(t)\cdot\frac{C_i}{A}+f_{bd}(C_i, v_{s,i}) & for\ -H\leq z<0 \\ Q_{Under}(t)\cdot\frac{C_i}{A}+f_{bd}(C_i, v_{s,i}) & for\ 0<z\leq \\ Q_{Under}(t)\cdot\frac{C_i}{A} & for\ z>B \end{cases} \quad (6.9)$$

Where Q_{Out} is the effluent flow rate [m³/d], Q_{Under} is the underflow rate [m³/d], H is the height of the tank above the feed point [m], B is the depth of the tank below the feed point [m], f_{bd} is the batch flux density function for discrete settling, and $v_{s,i}$ is the average settling velocity of i^{th} particle class [m/d].

In analogy to the Kynch batch flux density for hindered settling (Kynch, 1952) a batch flux density for discrete settling (f_{bd}) is defined (Equation 6.10), which depends on the concentration of a particle class and the settling velocity of a certain particle class. The settling velocity of the particle class depends only on the particle size and density and not on the concentration.

$$f_{bd}(C_i, v_{s,i}) = C \cdot v_{ds}(d_{p,i}, \rho_{p,i}) \quad (6.10)$$

Where v_{ds} is the discrete settling velocity [m/d], $d_{p,i}$ is the average particle diameter for the i^{th} particle class [m] and $\rho_{p,i}$ is the average particle density for the i^{th} particle class [g/m³].

6.5. RESULTS AND DISCUSSION

6.5.1. Modeling biological reactions in the primary sedimentation tank

The PST model, which only applies the biological reactions appearing in the tank, applying the ASM fractionation as it was determined, did not result in any change for nitrate, ammonium nor phosphate concentration (Table 6.1). However, when a percentage of the particulate COD was contributed to heterotrophic biomass, a removal of nitrate and a small increase in ammonium and phosphate concentrations are observed. Already when the heterotrophs take up 5% of the particulate COD the effluent nitrate concentration drops by 88%, which is more than what is observed from the data. With a further increasing percentage of heterotrophs the NH_4 concentrations and PO_4 concentrations enlarge from 1% increase to respectively 4% and 7% increase.

Table 6.1. The simulated removal efficiencies for NO3, NH4 and PO4 compared to the measured data for the primary sedimentation tanks during the measuring campaign on May 6, 2014.

Source	Fraction of X_{OHO}	Fraction of X_{PAO}	NO_3	NH_4	PO_4
Simulation	0%	0%	0%	0%	0%
Simulation	5%	0%	88%	-1%[2]	-1%[2]
Simulation	10%	0%	94%	-1%[2]	-3%[2]
Simulation	15%	0%	96%	-2%[2]	-4%[2]
Simulation	20%	0%	97%	-3%[2]	-6%[2]
Simulation	25%	0%	97%	-4%[2]	-7%[2]
Simulation	0%	10%	97%	0%	-36%[2]
Measured data	ND[1]	ND[1]	25%	-13%[2]	-42%[2]

[1] Not determined.

[2] Negative values indicate an increase instead of a removal.

For small concentrations of heterotrophs, which are likely to occur (Sperandio et al., 2001) in the wastewater, the model already overestimates the denitrification. This might be contributed to the use of default parameter values, which are describing conditions and biomass composition typical for activated sludge, that are

too high for the biological growth in the primary sedimentation tanks. On the other hand, fermentation results in an increasing amount of NH_4 and PO_4. Again, without proper data for calibration, the model is applied using default values, typical for activated sludge processes, which apparently underestimates the increase of the components.
An interesting result for the PO_4 concentrations pops up when contributing 10% of the COD_x to phosphate accumulating organisms instead of to ordinary heterotrophs (Table 6.1). The PO_4 concentration after the primary sedimentation tank is 36% higher than before, which is almost equal to the observed increase during the measurement campaign (42%). Although PAOs have not been reported in influent wastewater and usually are considered to be negligible, it is not impossible that they are present in the sewer system of Eindhoven (Schilperoort, 2011). Firstly there is the reject water from the sludge treatment of Mierlo, where centrifugation is applied to dewater the sludge of the WWTP of Eindhoven for which enhanced biological phosphorus removal has been recognized to occur. Considering that the sludge treatment does not contain anaerobic digestion nor any other destructive treatment, the reject water may still contain PAOs in combination with high NH_4 and PO_4 concentrations. Secondly the sewer system exists of both pressure mains and free flow sections, which means that alternating aerobic and anaerobic conditions are likely to exist. The combination of alternating conditions and high PO_4 concentrations are favourable for the present PAOs.
The model can be further improved by extending the model structure applying a tanks-in-series model or a settling model and by a thorough calibration, but this falls outside the scope of this work, which was only demonstrating plausible mechanisms that explain the observations. Even though the model is susceptible for improvement, the model demonstrates a plausible explanation for the observed change in NO_3, NH_4 and PO_4 data collected during the measurement campaign on May 6, 2014, at the WWTP of Eindhoven. The main conclusion is that in some circumstances modelling biological reactions in the primary sedimentation tanks is advisable. In the case of a significant sludge blanket, these biological reactions could be extended to include also anaerobic processes and fermentation (Ribes et al., 2002).

6.5.1.1. Physical-chemical modelling of precipitation

One of the observations made during the measurement campaign on September 2, 2014, is the increase of ISS over the primary sedimentation tanks. One of the plausible mechanism could be the formation of inorganic PO_4 and NH_4 salts. Kempton et al. (1987) mentioned the clear association of metals with non-volatile suspended solids, supporting the hypotheses for the dependency of the removal on

precipitation. In addition the resulting insoluble discrete particles, having a small size, often will not settle independently, requiring flocculation for their removal (Stephenson and Lester, 1987). Because of this behaviour, a large part of the precipitated metal salts may remain in the wastewater leaving the primary sedimentation tank, contributing to the augmentation of ISS.

In order to check for possible precipitates a modelling study in PHREEQC was conducted. Table 6.2 lists the precipitates with a positive saturation index, which indicates oversaturation and the possibility that they might precipitate. Changing carbonate concentration does not alter the list. Out of the list with oversaturated precipitates goethite, hematite and hydroxylapatite are likely to occur in wastewater (Wadley and Buckley, 1997). The iron metals listed are crystals likely to develop from $Fe(OH)_3$ with time. Hydroxylapatite is the only phosphate salt that is predicted to form. Hydroxylapatite is a colourless to pale coloured salt (Anthony et al., 2009) and could be responsible for the scaling that was observed on the UV-VIS analyser that was tested for online monitoring of the wastewater composition after the primary sedimentation tanks (PST).

Table 6.2. The modelling results of PHREEQC with regard to precipitation in the primary sedimentation tanks of the WWTP of Eindhoven.

Name	SI[1]	Formula
Fe(OH)2.7Cl.3	3.71	$Fe(OH)_{2.7}Cl_{0.3}$
Goethite	2.78	FeOOH
Hematite	7.91	Fe_2O_3
Hydroxylapatite	6.13	$Ca_5(PO_4)_3OH$
Lepidocrocite	2.27	FeOOH
Maghemite	0.89	Fe_2O_3
Magnetite	6.64	Fe_3O_4

[1] Saturation index.

From the composition of hydroxylapatite the possible removal of PO_4 can be deduced, i.e. for 5 moles of Ca removed, 3 moles of PO_4 will be removed. In the measurement campaign 4.6 mg PO_4/l is removed at the time when the maximum PO_4 concentration (12.6 mg/l) occurs. At the same time the maximum concentration of Ca (53.6 mg Ca/l) occurs, of which 7.8 mg/l is removed. This 7.8 mg Ca/l corresponds stoichiometricaly (for hydroxylapatite) with 11.1 mg PO_4/l, which is about double as the measured removal (4.6 mg PO_4/l) but still smaller than the total available (12.6 mg/l). This would correspond with a production of 20 mg/l hydroxylapatite, which does not entirely cover the increase of ISS observed (28 mg/l). For a removal of 4.6 mg PO_4/l about 2.7 mg Ca/l would be removed forming about 8.1 mg/l hydroxylapatite. The removed amounts of Ca and PO_4 and the formed amount of hydroxylapatite does not correspond entirely with the observed values but give an indication of what might be happening and gives direction to future investigation.

6.5.1.2. Modelling the settling Process in primary sedimentation tanks

6.5.1.3. A modification of the model of Tay (1982)

Unfortunately, due to various reasons, none of the data sets includes all the necessary information , i.e. removal efficiencies of COD_x and ISS, for the model calibration. It was decided to evaluate the model performance for the data of the measurement campaign of May 6, 2014. The necessary parameters were evaluated based on correlations retrieved from the other collected data sets.

The removal efficiencies of COD_x and ISS were calculated from the TSS data in the dataset of the routine measurements of 2011-2013 (Table 5.4). First, in order to calculate the COD_x removal efficiency, COD_x concentrations were estimated using a ratio COD_x over TSS ($F_{CODX,TSS}$) estimated from the data collected during the measurement campaign to evaluate the performance of primary sedimentation under reduced capacity. The obtained values for $F_{CODX,TSS}$ are 1.72 for the influent and 1.62 for the effluent of the primary sedimentation tanks. These values correspond very well to the 1.69 deduced by Hauduc et al. (2009). Second, in order to derive the ISS removal efficiency, concentrations were estimated using a ratio ISS over TSS ($F_{ISS,TSS}$) estimated from the data collected during the measurement campaign on September 2, 2014. The derived values for $F_{ISS,TSS}$ are 0.51 for the influent and 0.62 for the effluent of the primary sedimentation tanks. These values do not correspond at all to the value 0.26 (1- $F_{VSS,TSS}$) reported by Rieger et al. (2012). This may be due to the formation of precipitates as explained above. The average removal efficiencies obtained from this exercise are 54% for COD_x and 40% for ISS (Table 5.4).

Table 6.3. Overview of the removal efficiencies derived for COD_x and ISS of the primary sedimentation tank at the Eindhoven WWTP from January 2011 till June 2013.

		COD_x[(1)]	ISS[(1)]
All days	Min	-3%	-35%
	Mean	54%	40%
	Stdev	20%	27%
	Max	90%	87%

Simulations were performed using the data from the measurement campaign of May 6, 2014. A first simulation run (ST1) was executed using the values (ER_{XCOD}=0.51 and ER_{XIg}=0.85) determined for simulations of a 2008 dataset (See Chapter 10). A second simulation run (ST2) was executed using the values (ER_{XCOD}=0.54 and ER_{XIg}=0.40) determined from the 2011 and 2013 data. A third simulation run was executed using the removal efficiency of COD_x (ER_{XCOD}=0.37) determined from the May 6 (2014) measurement campaign and the removal efficiency of ISS estimated from a best fit for effluent TSS (ER_{XIg}=0.40).

The first simulation (ST1) underestimates both the effluent concentrations of COD_x and TSS (Table 6.4), indicating a too high removal efficiency. Also the second simulation (ST2) underestimates the effluent concentrations, although a better approximation is obtained for the effluent TSS concentration. Finally the third simulation (ST3) obtained a better approximation for the effluent concentrations. These observations show the difficulty of the model parameter values to be extrapolated outside the period for which the parameters are estimated. This is due to both the changing influent wastewater composition (e.g. the effect of the reject water from the sludge treatment in Mierlo) as well as to the operational strategy (e.g. the dosing of chemicals). As this poses a fundamental limitation on its applicability for predictive modelling, it is essential to account for the boundary conditions causing these differences.

Table 6.4. Overview of the simulation results of the modified model of Tay (1982) with the different parameter combinations for the removal of COD_x and ISS.

		COD_x				TSS			
		ST1	ST2	ST3	Meas.	ST1	ST2	ST3	Meas.
Min	mg/l	0	0	0	**186**	0	0	0	**334**
Mean	mg/l	177	166	230	**209**	183	329	377	**377**
Stdev	mg/l	16	15	21	**28**	16.6	30	35	**50**
Max	mg/l	213	199	277	**264**	220	395	455	**476**

6.5.1.4. Discrete settling model with multiple settling velocity classes for organics and inorganics

The model was set up as a first attempt to come to a more rigorous discrete settling model. The goal of the exercise is to demonstrate the concept rather than a thorough calibration and no further steps have been undertaken to obtain a good calibration. A rather coarse discretization of 20 layers was chosen and simulations were run with both 5 (LN5) and 20 (LN20.1 and LN20.2) particle classes. As a typical distribution for wastewater particles (Delgado Diaz et al., 2012), a log normal distribution was chosen to apportion the particles to the different classes (Table 6.5). A first simulation run (B5) was performed using 5 particle classes and the particle settling velocities and particle class fractions as determined by Bachis et al. (2014). As no information was available about the VSS and ISS, the same fractions and velocities were taken for both.

All simulations were executed using dynamic influent based on the full ASM fractionation data from the measurement campaign of May 6, 2014. Both the influent concentration of particulate COD (about 20%) and the influent flow rate (about 5%) vary over the simulated period.

Table 6.5. Particle fractions and discrete particle settling velocities for the discrete settling model with organic and inorganic PSVD classes.

	B5		LN5		LN20	
	Fraction	$v_{ds,TSS}$	Fraction	$v_{ds,VSS}$	Fraction	$v_{ds,VSS}$
	-	m/d	-	m/d	-	m/d
Class 1	0.06	320.64	0.125	11.42	0.000	17.98
Class 2	0.145	131.52	0.403	6.42	0.001	12.98
Class 3	0.175	45.84	0.279	3.92	0.010	10.48
Class 4	0.205	16.80	0.135	2.25	0.032	8.81
Class 5	0.415	1.44	0.058	1.00	0.059	7.56
Class 6	-				0.083	6.56
Class 7	-	-	-	-	0.097	5.73
Class 8	-	-	-	-	0.102	5.02
Class 9	-	-	-	-	0.100	4.39
Class 10	-	-	-	-	0.092	3.83
Class 11	-	-	-	-	0.082	3.33
Class 12	-	-	-	-	0.071	2.88
Class 13	-	-	-	-	0.060	2.46
Class 14	-	-	-	-	0.050	2.08
Class 15	-	-	-	-	0.042	1.72
Class 16	-	-	-	-	0.034	1.39
Class 17	-	-	-	-	0.028	1.08
Class 18	-	-	-	-	0.023	0.79
Class 19	-	-	-	-	0.018	0.51
Class 20	-	-	-	-	0.015	0.25

The simulation run (B5), with the particle classes and settling velocities as suggested by Bachis et al. (2014), shows (Table 6.6) an important underestimation of the average effluent concentrations of both COD_x (120 mg/l versus 209 mg/l) and TSS (202 mg/l versus 377 mg/l). Furthermore, the effluent concentrations of the suspended solids show much less variation than in the measurements. The high settling velocities might have this flattening effect on the suspended solids concentrations. However, simulations with lower settling velocities do show nearly the same flattening effect.

In an attempt to improve the estimation of the effluent concentrations, the model with the 5 particle classes, is simulated (LN5) with a log normal distribution for the particle fractions and lower settling velocities (Table 6.5). The simulation results (Table 6.6) improved for both COD_x (151 mg/l versus 120 mg/l) and TSS (255 mg/l versus 202 mg/l). It may be noted that there is a rather large difference in settling velocities applied in the LN5 simulation compared to the original values of Bachis et al. (2014). Further attempts would definitely result in an even better fit but it would be advisable to base these attempts on additional measurements.

Table 6.6. Overview of the simulation results of the discrete settling model with organic and inorganic PSVD classes with the different parameter combinatons for COD_x and TSS.

		COD_x					TSS				
		B5	LN5	LN20.1	LN20.2	Meas.	B5	LN5	LN20.1	LN20.2	Meas.
Min	mg/l	119	150	193	193	**186**	201	253	235	326	**334**
Mean	mg/l	120	151	194	194	**209**	202	255	237	328	**377**
Stdev	mg/l	0.2	0.5	0.6	0.6	**28**	0.3	0.9	0.9	1	**50**
Max	mg/l	120	152	195	195	**264**	202	256	238	330	**476**

In order to determine how sensitive the simulation results are with regard to the number of particle classes applied, a simulation was executed using 20 particle classes. In first instance, assuming that the higher density of the inorganic particles cause a higher settling velocity, a simulation (LN20.1) was ran with higher settling velocities for ISS than for VSS. The settling velocity applied for VSS are in the same range as for simulation LN5 and the ones of ISS are taken as the double (Table 6.5). The model seems to predict the average effluent concentration of COD_x (Table 6.6) quite well (194 mg/l versus 209 mg/l). The prediction of TSS however is even worse than with B5 (237 mg/l versus 377 mg/l). The increased settling velocity for the ISS apparently created this divergence and a new simulation run was executed with the same settling velocity again for both ISS and VSS (LN20.2). This improved the prediction of the average effluent TSS concentration (328 mg/l versus 377 mg/l) considerably (Table 6.6). The lower settling velocity for ISS may be attributed to the fact that the main contributor to the ISS concentration are precipitates, which will be rather small in size (Stephenson and Lester, 1987). Due to this higher amount of smaller particles the settling velocity distribution will be lower than expected only on the basis of the density difference.

Also for the last simulation run (LN20.2) the effluent concentration of COD_x seems to be flattened and does not follow the trend in the measured data at all (Figure 6.1). On the other hand, the soluble COD (COD_s) shows some dynamics but does not follow the trend of the data neither. In contrast with the COD_x, the effluent concentration of XC_B follows the trend of the data reasonably well (Figure 6.2). The dynamic trend of X_U does not follow the data at all but shows more or less the inverse pattern of XC_B. This inverse pattern is logical as the sum of X_U and XC_B makes up the major part of COD_x, which is fairly constant in the effluent model predictions (Figure 6.1).

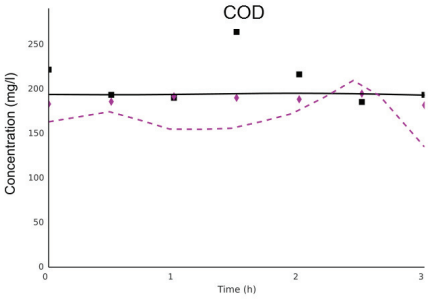

Figure 6.1. Comparison of the measured data versus the simulation results of the discrete settling model with organic and inorganic PSVD classes for COD_S (purple diamonds versus purple dotted line) and COD_x (black squares versus black solid line).

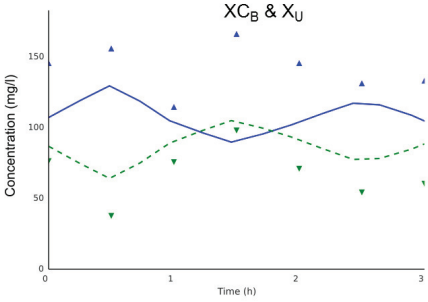

Figure 6.2. Comparison of the measured data versus the simulation results of the discrete settling model with organic and inorganic PSVD classes for XC_B (green downward triangles versus green dotted line) and X_U (blue triangles versus blue solid line).

Table 6.7 lists the concentrations of both ISS and VSS in the influent, effluent and underflow of the primary sedimentation tank for the different simulation runs as explained above. Here as well the flattening effect is clearly visible (standard deviations in the outgoing flows are less or equal to 1). This effect needs more investigation when applying the model do other data sets. The effect of different settling velocities for ISS is demonstrated in the results of LN20.1 and LN20.2. The simulations with the higher settling velocities for ISS (LN20.1) show a significantly lower effluent concentration of ISS (91 mg/l versus 182) and consequently a higher concentration in the underflow (2868 mg/l versus 1854 mg/l).

The measurement of particle size distributions (PSD) during settling tests is getting more and more attention. These PSDs give useful information for the validation of the model as they can be compared with the model output. The difference in the particle classes per layer (bottom is layer 22 and top is layer 3) for VSS (Figure 6.3,

left) and ISS (Figure 6.3, right) can be clearly seen. Moreover, for both VSS and ISS the shift from more slow settling particles (high numbers) at the top (layer 3) towards more fast settling particles (low numbers) at the bottom (layer 22) can be deduced as well.

Table 6.7. Overview of the simulation results of the discrete settling model with organic and inorganic PSVD classes for ISS and VSS.

			In		Out		Under	
			ISS	VSS	ISS	VSS	ISS	VSS
B5	Min	mg/l	254	204	112	89	2632	2109
	Mean	mg/l	320	256	112	90	2634	2110
	Stdev	mg/l	30	24	0.2	0.1	1	0.8
	Max	mg/l	387	310	112	90	2635	2111
LN5	Min	mg/l	254	204	141	113	2310	1851
	Mean	mg/l	320	256	141	113	2310	1851
	Stdev	mg/l	29	23	0.5	0.4	0.05	0.04
	Max	mg/l	387	310	142	114	2310	1851
LN20.1	Min	mg/l	254	204	90	145	2868	1485
	Mean	mg/l	320	256	91	146	2868	1485
	Stdev	mg/l	29	24	0.4	0.45	0.1	0.02
	Max	mg/l	387	310	91	147	2868	1485
LN20.2	Min	mg/l	254	204	181	145	1854	1485
	Mean	mg/l	320	256	182	146	1854	1485
	Stdev	mg/l	29	24	0.6	0.4	0.03	0.02
	Max	mg/l	387	310	183	147	1854	1485

Modelling the particle velocity distributions gives an added value in the modelling of the primary sedimentation tanks. The model seems to be able to deal with the observations made for COD and TSS during the measurement campaign and is expected to give good predictions after a thorough calibration. One of the points of attention in this calibration is the impact of the combination of the particle size distribution and the particle density distribution on the particle velocity distribution. A possible method to measure this is the application of a discontinuous linear gradient of Percoll solutions with different densities to segregate the different density praticles (Dammel and Schroeder, 1991) after which a particle size distribution could be measured. A second point of attention, is the lack of variation in the dynamics as it is not clear yet whether this is a calibration issue or a model structure issue.

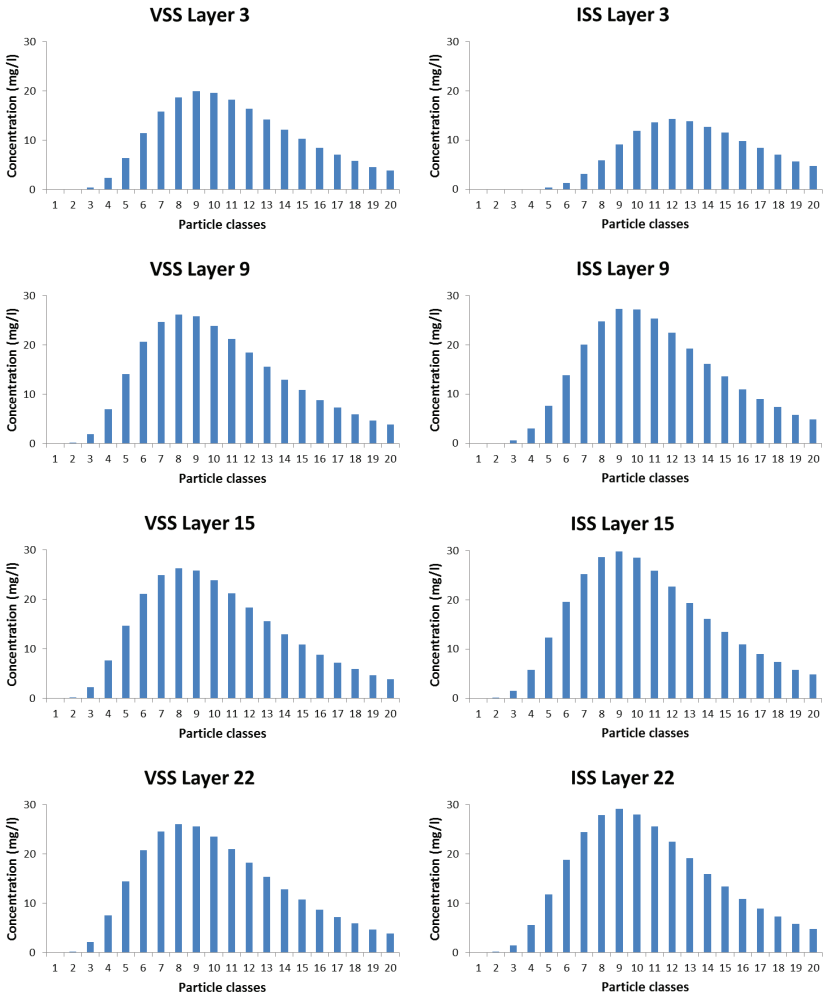

Figure 6.3. Shows the PSD in layers 3 (top), 9, 15 and 22 (bottom) for both VSS and ISS for simulation run LN20.1. Class 1 are the fast settling particles while class 20 are the slowest settling particles.

In addition, implementing the model in the rigorous structure of Bürger et al. (2011), is a step closer to a unified sedimentation tank model (for both primary and secondary settling tanks together). The discretization in the different layers allows for future integration of biological and chemical kinetic reactions. Furthermore, the model could be easily extended to include the dilution effect and the plug flow behaviour observed during storm events.

6.5.2. Modelling the impact of the primary sedimentation tanks on the activated sludge process

In order to analyse the impact of the modelling of primary sedimentation tanks on the modelling of the subsequent processes several primary sedimentation tank models were integrated in the whole plant model of the WWTP of Eindhoven (Table 6.8). The WWTP model version EHV10 fed with data for the operational controls (aeration, sludge wastage and internal recycles), implemented in WEST (mikebyDHI), was used to evaluate the impact on NO_3, NH_4 and TSS. As this is still the most complete and validated data set available for the modelling of the WWTP of Eindhoven, the simulations were run with data collected from the 23rd of December 2008 till the 11th of January 2009, of which 15 days are selected for the simulations.

In first instance the impact of applying the removal efficiencies for the different ASM fractions was evaluated. A model simply calculating the effluent concentrations based on the calculated removal efficiency (Equation 6.11) was implemented in WEST (mikebyDHI) and simulated using the removal efficiency determined from the measurement campaign on the 5th of May 2014 (RE5) and the 2nd of September 2014 (RE9) at the WWTP of Eindhoven.

$$C_{Out,i} = C_{In,i} \cdot ER_i \quad (6.11)$$

Where $C_{Out,i}$ is the PST effluent concentration for the i^{th} ASM component [mg/l], $C_{In,i}$ is the PST influent concentration for the i^{th} ASM component [mg/l] and $ER_{Out,i}$ is the PST removal efficiency for the i^{th} ASM component [-]

In second instance an ideal settling model was applied with the fraction of non-settleable solids determined (Equation 6.12) from the 2011-2013 routine data (ID53). Afterwards this fraction was increased to obtain a better fit for the nitrate concentrations (ID70).

$$f_{ns} = \frac{1-ER}{f_{Out,av}} = \frac{Q_{In,av}}{Q_{Out,av}} \cdot (1 - ER) \quad (6.12)$$

In third instance the modification of the model of Tay (1982) was used, as it was deemed essential to have a model that could predict the impact of high flow rates. The parameter sets ST1, ST2 and ST3 as described above are used in the evaluation.

Table 6.8. Overview of different parameter combinations for the different primary sedimentation tank models evaluated for their impact on the subsequent activated sludge models.

Name	Description	Parameters	
RE5	Calculates the effluent concentrations from the average removal efficiencies for all ASM fractions	The removal efficiencies as calculated from the measurement campaign on May 6, 2014	Table 5.6 Table 5.7
RE9	Calculates the effluent concentrations from the average removal efficiencies for all ASM fractions	The removal efficiencies as calculated from the measurement campaign on September 2, 2014	Table 5.8 Table 5.9 Table 5.11
ID53	Ideal separation model	Non-settleable fraction determined from the 2011-2013 routine data	f_{ns}=0.53
ID70	Ideal separation model	Non-settleable fraction determined based on expert judgment	f_{ns}=0.70
ST1	Modification of the model of Tay (1982)	Removal efficiencies determined for simulations of the 2008 dataset	ER_{XCOD}=0.51 ER_{XIg}=0.85
ST2	Modification of the model of Tay (1982)	Removal efficiencies determined from the 2011-2013 routine data	ER_{XCOD}=0.54 ER_{XIg}=0.40
ST3	Modification of the model of Tay (1982)	Removal efficiencies determined from the measurement campaign on May 6, 2014	ER_{XCOD}=0.37 ER_{XIg}=0.40

Figure 6.4 shows the variation in predicted NO3 concentrations in both the anoxic middle ring (left) as in the aerobic outer ring (right). The worst simulations show an over prediction of more than 5 mg/l. In first instance the removal efficiencies for each ASM fraction separately was implemented and evaluated. The simulations based on the removal efficiencies determined from the measurement campaign in May 2014 (RE9) yields the best results for NO_3 (Figure 6.5, upper left and right). The results of the simulations with the removal efficiencies calculated from the data of the measurement campaign in September 2014 shows a slight under estimation for NO_3 (Figure 6.5, upper left and right). However, both simulation runs significantly over predict TSS concentrations in the activated sludge tanks (Figure 6.5, lower right). Ammonium concentrations are still very well predicted by the RE9 simulation (Figure 6.5, lower right). On the other hand, the simulation results RE5, are completely off. The increase of 13% of NH_4 concentration over the PST, as observed in the measurement campaign is too high for the nitrification capacity provided. The provided nitrification capacity depends on the supplied airflow rate, which is automatically controlled at the plant. However, in the model version of the WWTP of Eindhoven, used here, the operational controls are decoupled from the biological model, i.e. aeration, sludge wastage and internal recycle flow rates are read from input files. These input files are based on the detailed information extracted from the SCADA system at the WWTP. Without this decoupling the aeration controller would simply have reacted increasingly until the concentrations were at the desired values, i.e. the control set point, and the

divergence would not have been visible. Therefore, it is important for process understanding that controllers are uncoupled as much as possible in the simulation. These results indicate that the removal efficiency in a whole, but especially for the different ASM components, is not transferable as such and care needs to be taken when applying the results on other periods than the one of the data collection. In addition, modelling the increase of ammonium in the PST requires a more detail implementation of biological reactions, which will balance the increased ammonium concentration with the other ASM components.

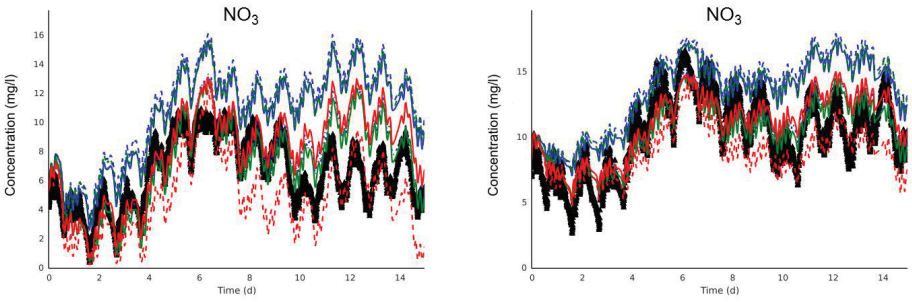

Figure 6.4. An overview of the impact of the primary sedimentation models and the parameter values on the prediction of nitrate in the anoxic middle ring (left) and aerobic outer ring (right) in comparison with the measured data (black dots) of the WWTP of Eindhoven. RE5 (red solid line), RE9 (red dashed line), ID53 (green dashed line), ID70 (green solid line), ST1 (blue solid line), ST2 (blue dashed line) and ST3 (blue dash-dot line).

When simulating with the ideal separation model, applying the non-settleable fraction (f_{ns}=0.53) determined from the 2011-2013 routine data (ID53) the nitrate concentrations are reasonably well predicted in the first week. However in the second week an over prediction in both the middle and outer ring is noticed (Figure 6.6, upper left and right). The too high prediction might be induced by the divergence observed in the TSS data in the activated sludge tanks (Figure 6.6, lower right). The too low TSS concentrations do not provide sufficient capacity anymore for denitrification. For the simulation run (ID70) with the on expert basis estimated non-settleable fraction (f_{ns} = 0.70), which is considerably higher than the calculated fraction, both the TSS and the NO_3 concentrations reproduce the measured data. These observations show again the need for caution when transferring the results from a measurement campaign to other periods.

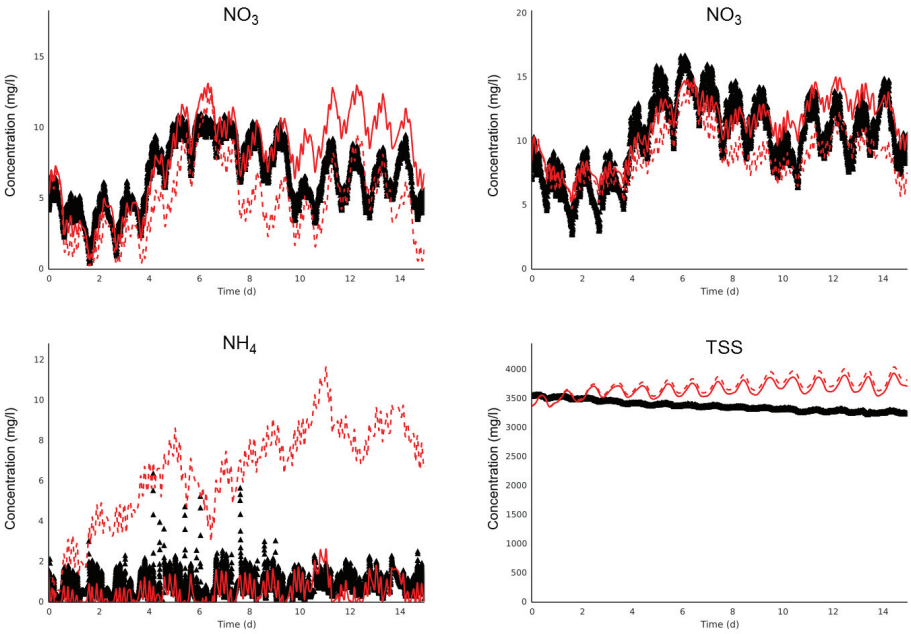

Figure 6.5. An overview of the impact of the primary sedimentation model based on the average removal efficiencies for all the ASM fractions and the parameter values on the prediction of nitrate in the anoxic middle ring (upper left), nitrate in the aerobic outer ring (upper right), ammonium in the aerobic outer ring (lower left) and TSS in the aerobic outer ring (lower right) in comparison with the measured data (black dots) of the WWTP of Eindhoven. RE5 (red solid line) and RE9 (red dashed line).

The modified model of Tay gives the best results for NO_3 for the parameters used in simulation run ST3 (Figure 6.7, upper left and right). These parameters determined based on the measurement campaign of May 2014 even outperform the model parameters estimated especially for the 2008 data (ST1). However, the simulation results for TSS (Figure 6.7, lower right) divert considerably. One of the possible effects already noticed within the 15 day period is the too high predictions of ammonium during peak loads (Figure 6.7, lower left).

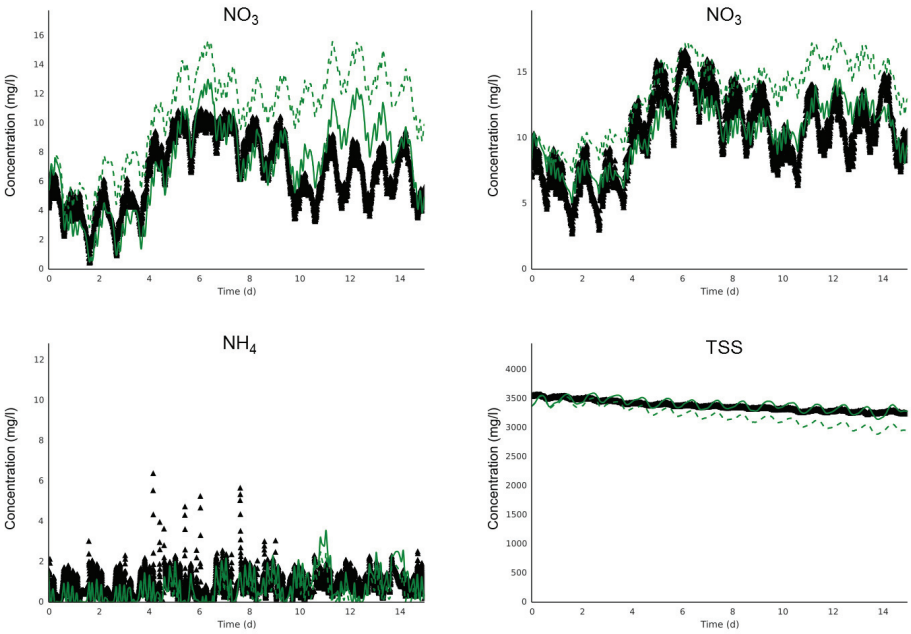

Figure 6.6. An overview of the impact of an ideal separation model based and the parameter values on the prediction of nitrate in the anoxic middle ring (upper left), nitrate in the aerobic outer ring (upper right), ammonium in the aerobic outer ring (lower left) and TSS in the aerobic outer ring (lower right) in comparison with the measured data (black dots) of the WWTP of Eindhoven. ID53 (green dashed line) and ID70 (green solid line).

The application of the different primary sedimentation tank models demonstrates its considerable impact on the modelling of the subsequent processes. Denitrification is clearly influenced which can be ascertained by the large spread in NO_3 concentrations in the simulation results (Figure 6.4). But also the nitrification can be impacted, even more so for systems on the edge of their nitrification capacity, which is not the case for the WWTP of Eindhoven during dry weather conditions but may occur during storm events.

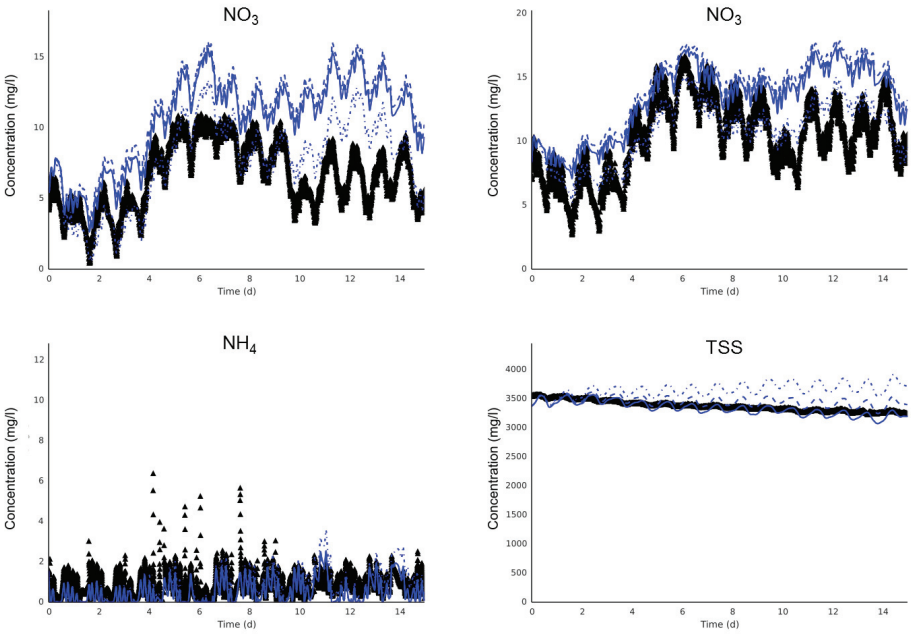

Figure 6.7. An overview of the impact of the modified model of Tay (1982) and the parameter values on the prediction of nitrate in the anoxic middle ring (upper left), nitrate in the aerobic outer ring (upper right), ammonium in the aerobic outer ring (lower left) and TSS in the aerobic outer ring (lower right) in comparison with the measured data (black dots) of the WWTP of Eindhoven. ST1 (blue solid line), ST2 (blue dashed line) and ST3 (blue dash-dot line).

6.6. CONCLUSIONS

The integration of sufficiently detailed primary sedimentation tank models is crucial in view of whole plant modelling. The primary sedimentation tanks definitely affect the denitrification but also the nitrification. The modelling results obtained show that transferring the parameter values outside of the measurement campaign is not trivial, which is certainly caused by the many factors affecting the sedimentation process.

Investing in modelling more details of processes influencing the performance of the sedimentation tanks results in a better understanding of the observed phenomena. In this manner, the bio-kinetic model was able to describe the increase of ammonium and also the incidentally occurring increase of phosphate concentration over the primary sedimentation tank. On the other hand, the physical-chemical model was able to describe the formation of the precipitate hydroxylapatite in the

primary sedimentation tank and the consequent removal of PO_4 and the corresponding increase of inorganic suspended solids measured at the outlet.
Finally, a first attempt to come to a more rigorous discrete settling model was taken by the incorporation of a particle settling velocity distribution model in the structured model proposed by Bürger et al. (2011). Actually, this model may be a step in the direction of a unified sedimentation tank model as hindered settling and compression settling have previously been implemented in this model structure, which should simplify further integration, at least with regard to model implementation.
The application of primary sedimentation models is still not straightforward and more research is needed. The models applied so far do not fully describe the dynamics encountered in the tanks and transferability of the model parameters is an issue of concern. In addition, the integration of the modelling of the different processes influencing the sedimentation should be facilitated. Amongst the processes influencing the sedimentation are hydraulic behaviour (plug flow and dilution effects), flocculation and biological and chemical reactions.

PART IV

Aeration and consumption of energy

Chapter 7

Modelling of the aeration system at the WWTP of Eindhoven

"Do what you can, with what you have, where you are."
Theodore Roosevelt

7.1. ABSTRACT

At wastewater treatment plants (WWTPs), the aerobic conversion processes in the bioreactor are driven by the presence of dissolved oxygen. Within these conversion processes, the oxygen transfer is a rate limiting step and as well the largest energy consumer. Even though the high importance, WWTP models often lack detail on the aeration part. An extensive measurement campaign with off-gas tests was performed at the WWTP of Eindhoven to provide more information on the performance and behaviour of the aeration system. A high spatial and temporal variability in the oxygen transfer efficiency was observed. Applying this gathered system knowledge in the aeration model resulted in an improved fit of the dissolved oxygen concentrations. Moreover, an important consequence of this was that ammonium predictions could be improved by resetting the ammonium half-saturation coefficient for autotrophs to its default value. This again proves the importance of balancing sub-models with respect to the need for model calibration as well as model predictive power.

Part of this chapter was published as:
Y. Amerlinck, G. Bellandi, A. Amaral, S. Weijers I. Nopens, 2015, Detailed off-gas measurements for improved modelling of the aeration performance at the WWTP of Eindhoven: 2nd New Developments in IT & Water Conference.

Y. Amerlinck, G. Bellandi, A. Amaral, S. Weijers I. Nopens, 2015, Detailed off-gas measurements for improved modelling of the aeration performance at the WWTP of Eindhoven: Water Science and Technology (submitted).

7.2. ABBREVIATIONS AND SYMBOLS

a	Diffuser specific area (m²)
A	Surface of the gas-liquid interface (m²)
a_{spec}	Interfacial area (m²)
AOTR	Actual oxygen transfer rate (m/d)
A_{VH}	Empirical constant of the Van't Hoff equation (-)
B_{VH}	Empirical constant of the Van't Hoff equation (-)
c	Concentration of the component (mol/m³)
C	Dissolved oxygen concentration (g/m³)
$c_{L,G}$	Concentration in the gas film at the liquid-gas interface (mol/m³)
c_s*	Saturation concentration in the liquid (mol/l)
C_s	Saturation concentration in process water (g/m³)
$C_{S,CW}$	Saturation concentration in clean water (g/m³)
$C^*_{\infty 20}$	Oxygen saturation concentration at 20°C and 1 atm (g/m³)
C^*_{S20}	Oxygen saturation concentration at 20°C (g/m³)
C^*_{ST}	Oxygen saturation concentration at process water temperature (g/m³)
D	Diffusion coefficient (m²/s)
D_G	Diffusion coefficient in the gas phase (m²/s)
D_L	Diffusion coefficient in the liquid phase (m²/s)
F	Fouling factor (-)
g	Gravitational acceleration (m/s²)
J	Flux going through the gas-liquid interface (mol/(m².s))
k_G	Gas film mass transfer resistance coefficient (m/s)
k_H	Henry coefficient for the component (l.atm/mol)
k_L	Liquid film mass transfer resistance coefficient (m/s)
k_La	Gas transfer coefficient (1/s) or oxygen transfer coefficient (1/d)
k_La_{CW}	Oxygen transfer coefficient in clean water (1/d)

$k_La_{CW,20}$	Oxygen transfer coefficient in clean water 20°C and 1 atm with a dissolved oxygen concentration of 0 mg/l (1/d)
$k_{L,G}$	Mass transfer resistance coefficient (m/s)
$MR_{o/i}$	Molar ratio of oxygen to inerts in the inlet (-)
$MR_{og/i}$	Molar ratio of oxygen to inerts in the off-gas (-)
N_d	Total number of diffusers (-)
p_a	Atmospheric pressure (atm)
p_0	Atmospheric pressure (Pa)
$p_{G,L}$	Pressure in the gas film at the gas-liquid interface (atm)
Q_{air}	Airflow rate (m^3/s)
$Q_{N,air}$	Normalized airflow rate (s^{-1})
T_K	Temperature (K)
T	Temperature (°C)
$t_{b,Av}$	Mean bubble residence time (s)
V	Volume of the liquid phase (m^3)
Y	Mole fraction of oxygen in gas phase (-)
Y_{og}	Mole fraction of oxygen in off-gas (-)
Y_r	Mole fraction of oxygen in the inlet (-)
$Y_{CO2,og}$	Mole fraction of CO_2 in off-gas (-)
$Y_{CO2,r}$	Mole fraction of CO_2 in the inlet (-)
x	Position (m)
z	Actual depth (m)
Z	Diffuser submergence depth (m)
z_d	Aerator submergence depth (m)
z_G	Thickness of the gas film (m)
z_L	Thickness of the liquid film (m)
α	k_La correction factor (-)
β	Oxygen saturation concentration correction factor (-)
θ	Temperature correction factor (-)
ρ	Density of water (g/m^3)
τ	Temperature oxygen saturation concentration correction factor (-)
χ	Correlation factor (Rosso et al., 2005) (-)
Ω	Oxygen saturation concentration pressure correction factor (-)

7.3. INTRODUCTION

At wastewater treatment plants (WWTPs), the conversion processes in the bioreactor are driven by the presence of an electron acceptor, i.e. dissolved oxygen in the case of aerobic processes (e.g. aerobic heterotrophic growth and nitrification). Within these conversion processes, the gas-liquid oxygen transfer has been reported as a rate limiting step (Garcia-Ochoa and Gomez, 2009). In addition, aeration is the largest energy consumer at WWTPs (Devisscher et al., 2006; Zahreddine et al., 2010). Hence, a good description is vital in the cost-effective optimization of the aerobic, biokinetic processes.

Another important aspect is that aeration and the corresponding gas transfers have an indirect impact on conversion processes (either biological or chemical). Removing (through liquid-gas transfer) or adding (through gas-liquid transfer) one of the products of a certain chemical process can shift that process in one or the other direction. E.g. CO_2 stripping can influence pH (Kim et al., 2003; Kim et al., 2004) or processes, such as crystallization in air stripping equipment (Segev et al., 2011).
From a modelling perspective a good description of the gas-liquid and liquid-gas transfer is vital. Benedetti et al. (2008) performed a global sensitivity analysis on biochemical, design and operational parameters with the benchmark simulation model n° 2 (Jeppsson et al., 2007; Nopens et al., 2010) and showed that Kla (for oxygen) is the second most sensitive parameter in the model. In a modelling study comparing different model choices on a full scale wastewater treatment plant, Maere et al. (2008) and Cierkens et al. (2012) show that a good estimation of the aeration flow rate (and hence the oxygen input), leads to excellent prediction of oxygen consumption and concentrations in the activated sludge process. Further modelling work on improving the aeration model has led to even better prediction of the oxygen consumption and concentrations, consequently, improving the ammonium removal, which omits the need for unnecessary calibration of the biokinetic model (personal communication, Cierkens).

To date, WWTP models consist of highly detailed biokinetic models (Barker and Dold, 1997; Henze et al., 2000) but often lack detail of other critical processes such as aeration. This chapter is addressing (1) the need for higher detail in modelling of the aeration process hereby using off-gas measurements for more detailed insight in the process and (2) calibration of the model. Based on a measurement campaign the applied aeration model, which is a combination of several models available in

literature, is calibrated. The effect of this improved calibration on the overall model calibration is shown.

7.4. THEORETICAL BACKGROUND AND MODELLING OF AERATION IN WWTPs

The most used concept for aeration in WWTP modelling is the two-film theory (Whitman, 1962), which is based on the assumption that when two phases contact, a thin stagnant layer exists on each side of the phase boundary (Figure 7.1). The mass transfer is described by steady-state diffusion only, which satisfies Fick´s first law of diffusion (Equation 7.1).

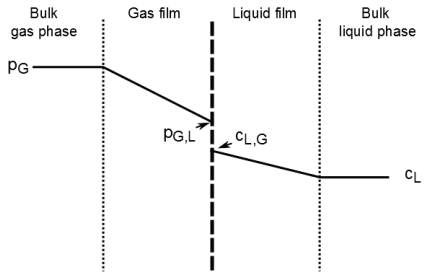

Figure 7.1. Visual representation of the two film theory of Whitman (1962).

$$J = -D \cdot \frac{dc}{dx} \quad (7.1)$$

Where J is the flux going through the gas-liquid interface [mol/(m².s)], D is the diffusion coefficient [m²/s], c is the concentration of the component [mol/m³] and x is the position [m].

The steady state solution for equation 7.1 is given by equation 7.2.

$$J = -\frac{D_G}{z_G} \cdot \frac{1}{R \cdot T}\left(p_G - p_{G,L}\right) = -\frac{D_L}{z_L} \cdot \left(c_{L,G} - c_L\right) \quad (7.2)$$

Where D_G is the diffusion coefficient in the gas phase [m²/s], z_G is the thickness of the gas film [m], p_G is the pressure in the gas phase [atm], $p_{G,L}$ is the pressure in the gas film at the gas-liquid interface [atm], D_L is the diffusion coefficient in the liquid phase [m²/s], z_L is the thickness of the liquid film [m], c_L is the concentration in the liquid phase [mol/m³], $c_{L,G}$ is the concentration in the gas film at the liquid-gas interface [mol/m³], R is the universal gas constant [8.205736 m³.atm/(K.mol)] and T is the temperature of the gas [K].

If there are no chemical reactions at the interface $p_{G,L}$ and $c_{L,G}$ are related by Henry's law.

$$c_{L,G} = k_H \cdot p_{G,L} \quad (7.3)$$

Where k_H is the Henry coefficient for the component [l.atm/mol].

The Henry coefficient strongly depends on temperature and salt concentrations. The temperature dependence can be described empirically according to the Van 't Hoff equation (Equation 7.4) (Tchobanoglous et al., 2004; Wang et al., 2007).

$$\log_{10} k_H = \frac{-A_{VH}}{T_K} + B_{VH} \quad (7.4)$$

Where A_{VH} and B_{VH} are the Van't Hoff empirical constants and T_K is the temperature [K]. Wang et al. (2007) report values for A_{VH} and B_{VH} for different gases (for oxygen A_{VH}=595.27 and B_{VH}=6.644).

Also for the influence of salt, many correlations exist either in tabulated form (Tchobanoglous et al., 2004) or as empirical correlations (Benson and Krause Jr, 1984; Garcia and Gordon, 1992; Weiss, 1970), but this level of detail is beyond the scope of this work.

The effect of the two films can be combined in a parameter $k_{L,G}$. The driving force is assumed to be proportional to the concentration difference between the bulk values in liquid and gaseous phases, expressed in compatible units.

$$\frac{1}{k_{L,G}} = \frac{1}{k_L} + \frac{1}{k_G \cdot k_H} \quad (7.5)$$

Where k_L (Equation 7.6) is the resistance to mass transfer in the liquid film [m/s] and k_G (Equation 7.7) is the resistance to mass transfer in the gas film [m/s].

$$k_L = \frac{D_L}{z_L} \quad (7.6)$$

$$k_G = \frac{D_G}{z_G} \quad (7.7)$$

Due to the rather low solubility, oxygen diffuses very slowly through the liquid film but quickly through the gas film. As a consequence, the liquid at the interface is rapidly saturated and the need for considering the gas film resistance can be omitted. Following this reasoning equation 7.5 can be reduced to equation 7.8.

$$\frac{1}{k_{L,G}} = \frac{1}{k_L} \quad (7.8)$$

The most important limitation of the two-film theory is the assumption for steady state. To overcome this limitation, other theories such as the surface renewal theory, have been proposed (Danckwerts, 1951; Higbie, 1935), for which the boundary layers are not assumed to be stagnant but continuously renewed, hence the name. Higbie (1935) proposed a solution (Equation 7.10) for Fick's second law of diffusion (equation 7.9). Combining equations 7.2, 7.6, 7.8 and 7.10 results in a possible manner to calculate resistance to mass transfer in the liquid film (Equation 7.11). Later, Danckwerts (1951) introduced a factor to describe stochastic

behaviour of turbulent movement. The factor represents the distribution of the fraction of fluid elements that remain at the phase interface for a certain time.

$$J = -D \cdot \frac{\partial^2 c}{\partial z^2} \tag{7.9}$$

$$J = 2 \cdot \sqrt{\frac{D_L}{\pi \cdot t_{b,Av}}} \cdot (c_L - k_H \cdot p_G) \tag{7.10}$$

Where $t_{b,Av}$ is the mean bubble residence time [s].

$$k_L = 2 \cdot \sqrt{\frac{D_L}{\pi \cdot t_{b,Av}}} \tag{7.11}$$

The total change in concentration over time due to aeration can now be described with equation 7.12. Taking into account that the saturation concentration can be quantified as in equation 7.13, when the liquid phase is in equilibrium with the gas phase and that k_La, which is typically used in WWTP modelling to quantify the amount of aeration, is defined by equation 7.14.

$$\frac{dc_L}{dt} = k_L a \cdot (c_s^* - c_L) \tag{7.12}$$

Where c_s* (Equation 7.13) is the saturation concentration in the liquid [mol/l] and k_La (Equation 7.14) is the gas transfer coefficient [1/s]. The first factor in equation 7.12 defines the rate at which the transfer occurs. The second factor on the other hand defines the driving force for the transfer.

$$c_s^* = k_H \cdot p_G \tag{7.13}$$

$$k_L a = k_L \cdot \frac{A}{V} \tag{7.14}$$

Where A is the surface of the gas-liquid interface [m²] and V is the volume of the liquid phase [m³].

In first instance there are correlations that link the k_La to the airflow rate (Gillot and Héduit, 2000) or the gas flow velocity (Dold and Fairlamb, 2001; Gillot et al., 2005; Gillot and Heduit, 2008; Rosso et al., 2005).

In second instance, the consideration that environmental factors or contamination (salt concentrations, surfactants) have an impact on the gas transfer, is considered. The environmental factors may influence the driving force (i.e. caused by changes in the saturation concentration), the resistance factors (i.e. in the liquid phase k_L or in the gas phase k_G) or the interfacial area a. The impact on the saturation concentrations is usually lumped in a β-factor (Equation 7.16). The impact on the resistance factors and the interfacial area is usually quantified by the α-factor (Equation 7.15), i.e. the ratio of process water to clean water mass transfer coefficients. This α-factor lumps together several conditions having an impact on the gas-liquid transfer (Stenstrom and Gilbert, 1981).

$$\alpha = \frac{k_L a_W}{k_L a_{CW}} \quad (7.15)$$

Where k_La is the oxygen transfer coefficient in the process water [1/d], k_La_{CW} is the oxygen transfer coefficient in clean water [1/d].

$$\beta = \frac{C_S}{C_{S,CW}} \quad (7.16)$$

Where C_S is the saturation concentration in the process water [g/m³], $C_{S,CW}$ is the saturation concentration in clean water [g/m³].

The corrections to apply for the calculation of the actual transfer rates can be described with the formula as proposed for oxygen by the US EPA (1989).

$$AOTR = \alpha \cdot F \cdot k_L a_{CW,20} \cdot (\beta \cdot \tau \cdot \Omega \cdot C^*_{\infty 20} - C) \cdot \theta^{T-20} \cdot V \quad (7.17)$$

Where AOTR is the actual oxygen transfer rate [g/d], $k_La_{CW,20}$ is the oxygen transfer coefficient in clean water at 20°C and 1 atm with a dissolved oxygen concentration of 0 mg/l [1/d], α is the ratio of process water k_La over clean water k_La [-], F is a fouling factor defined as the ratio of the aeration system performance after use to new aeration system performance [-], β is the ratio of process water oxygen saturation concentration to clean water oxygen saturation concentration [-], τ is the ratio of oxygen saturation concentration at actual temperature to oxygen saturation concentration at 20°C [-], Ω is the oxygen saturation concentration pressure correction factor [-], $C^*_{\infty 20}$ is the oxygen saturation concentration at 20°C and 1 atm [g/m³], C is the actual mixed liquor dissolved oxygen concentration [g/m³], θ is the temperature correction coefficient, T is the mixed liquor temperature [°C] and V is the volume of the reactor [m³].

Several attempts have been made to predict α-factors, assigning its observed variation to either surfactant concentrations (Rosso and Stenstrom, 2006), mixed liquor suspended solids concentration (Germain et al., 2007; Racault et al., 2011), sludge age (Gillot and Heduit, 2008; Henkel et al., 2011; Rosso et al., 2005) and viscosity (Fabiyi and Novak, 2008). Most of the observed correlations have in common that the studied factors affect the shape of the bubbles and the gas flow at the interface. Also the physical properties of the liquid together with its flowing regime can influence the k_La as coalescence or breakage can vary the bubble sizes and thus the available area for gas transfer (*a* coefficient). Viscosity in particular was observed to affect the shape of a bubble plume and thus increasing the probability that a bubble will collide with a neighbouring one (Ratkovich et al., 2013).

The β factor is the correction for the process water oxygen saturation concentration. The factor is governed by the same corrections as the Henry coefficient, by which the saturation concentration is determined in combination with the mole fraction of oxygen in the gas phase.

The theta factor, also known as geometric temperature correction coefficient, is used to relate mass transfer coefficients to a standard temperature (Equation 7.17). Because of lack of a proper appraisement, a value of 1.024 should be used unless differently specified and strongly supported by consultants and manufacturers. Moreover, it is also recommended to limit the temperature correction for deviations smaller than 10°C, although it is well known that corrections over a wider range are often needed (Stenstrom and Gilbert, 1981).

Ω is the oxygen saturation concentration pressure correction factor, which depends on the height of the water column. In submerged aeration, oxygen transfer occurs throughout the tank volume and saturation concentration varies with depth (Equation 7.18) caused by the progressive decreases in both hydrostatic pressure and the oxygen mole fraction as the bubbles move upward (Stenstrom et al., 2006).

$$C^*_{\infty,20} = \frac{\int_0^{z_d} k_H \cdot Y \cdot (p_a + \rho \cdot z) \cdot dz}{z_d} \quad (7.18)$$

Where z is the actual depth [m], z_d is the aerator submergence depth, assumed to be equal to liquid height above the aerator h [m], p_a is the atmospheric pressure [atm], Y is the mole fraction of oxygen in gas phase [0.2095, -] and ρ is the density of water [g/m³].

For submerged aerators placed at the bottom of the tank equation 7.19 is derived for the pressure correction factor.

$$\Omega = \frac{p_0 + \rho \cdot g \cdot h}{p_0} \quad (7.19)$$

Where p_0 is the atmospheric pressure [Pa], g is the gravitational acceleration [9.81 m/s²].

7.5. MATERIALS AND METHODS

7.5.1. Submerged aeration diffusers

A number of solutions exist to provide the necessary oxygen to an activated sludge system. Surface aerators increase the contact area at the gas-liquid interface by agitation of the water surface, shearing the liquid into small droplets under very turbulent conditions. Although these devices have easier maintenance (primarily in terms of accessibility), submerged aeration systems are currently the most widely used technology due to their higher efficiency and, hence, lower energy requirements.

In submerged systems, oxygen is brought into solution by bubbling air or pure oxygen into the liquid through nozzles or porous material placed at the tank

bottom. These devices are called diffusers and can be divided in two classes, coarse bubble and fine bubble diffusers, depending on the size of the generated bubbles. Coarse bubble systems generally have orifices larger than 6 mm and release bubbles up to 50 mm in diameter, whereas a bubble is considered fine when having a diameter less than 5 mm (WEF, 2009a). Rising coarse bubbles are classified as high-flow regime interfaces due to their high interfacial velocity at the gas-liquid interface, while fine bubbles present lower interfacial velocity and are therefore grouped as low-flow regime interfaces (Rosso and Stenstrom, 2006; Wagner et al., 2002). This is of particular importance for the renewal of the oxygen concentration in the gas phase at the interfacial layer.

7.5.2. Aeration system at the WWTP of Eindhoven

The aeration is provided by plate aerators in two separate aeration packages: a so-called summer package, which provides the aeration under normal dry weather conditions, and a so-called winter package, which provides aeration when the first package is not sufficient, mainly under rain weather conditions and cold temperatures. The summer package comprises 504 plate aerators, totalling a surface of 1063 m², whereas the winter package comprises 84 plate aerators totalling a surface of 177 m². The plate aerators are evenly distributed over the aeration zones and have a submergence depth of 6.9 meters.
The airflow of the summer package is continuous and controlled by an ammonium (NH_4)-dissolved oxygen (DO) cascade feedback controller. This in contrast with the winter package, which is only turned on in case the capacity of the summer package proves not to be sufficient (mainly during storm events) and is running on full capacity when active. Ammonium is measured online using the AMTAX sc sensor from Hach Lange (LXV421.99.03001), which has a measurement error of 3% of the measured value plus 0.05 mg/l. Dissolved oxygen is measured online using the LDO online sc sensor from Hack Lange (LXV416.99.20001), which has a measurement error 0.1 mg/l in the measurement range (0-5 mg/l) required for the activated sludge tanks at the WWTP of Eindhoven.

7.5.3. Modelling of aeration

The WWTP was modelled using WEST (mikebyDHI). Cierkens et al. (2012) implemented a new model for the calculation of the oxygen transfer based on the work of Rosso et al. (2005). Within this model the alpha factor (ratio between clean water and process water) and standard oxygen transfer efficiency (SOTE) are calculated based on a correlation with the sludge retention time (SRT) and the

airflow rate (equations 7.20-7.23). The link between alpha factor and SRT is an indirect link and can be explained by the link of the SRT with parameters influencing (e.g. suspended solids concentration and degradation of surfactants) the alpha factor.

$$\chi = \frac{SRT}{Q_{air}} \quad (7.20)$$

$$Q_{N,air} = \frac{Q_{air}}{a_{spec} \cdot N_d \cdot Z} \quad (7.21)$$

$$\alpha = 0.172 \cdot log\chi - 0.131 \quad (7.22)$$

$$\alpha SOTE = 5.717 \cdot log\chi - 6.815 \quad (7.23)$$

where Q_{air} is the airflow rate [m^3/s], a_{spec} is the diffuser specific area [m^2], N_d is the total number of diffusers [-], Z is the diffuser submergence depth [m] and $Q_{N,air}$ is the resulting normalized airflow rate [s^{-1}].

7.5.4. Off-gas measurements

In order to evaluate the parameters of this correlation, off-gas measurements were performed according to the official protocol for process water testing described by the Oxygen Transfer Standards Subcommittee from the American Society of Civil Engineers (1997). In the month of August 2012, three locations at the outer ring of the aeration tank of lane II (Figure 7.2), namely the beginning, the middle and the end of the summer package, were monitored during an extensive measurement campaign.

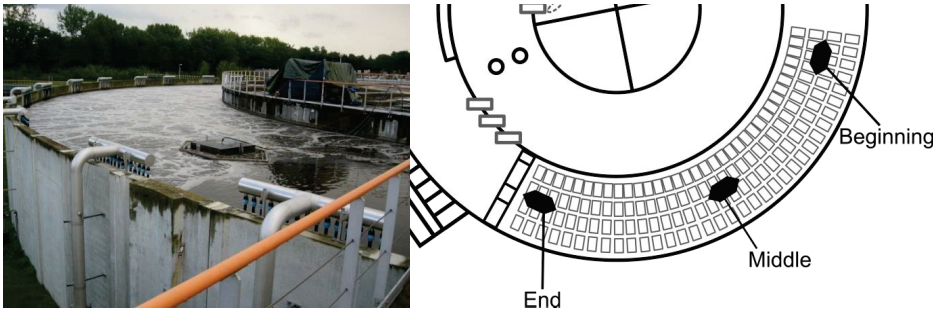

Figure 7.2. Picture of the aeration hood placed at the beginning of the summer package (s.p.) of the aeration tank of line II (left) and schematic view of the three hood locations (right).

The off-gas equipment was composed of a reinforced polyethylene hood floating on the wastewater surface (1.5 x 1.5 x 0.3 m, LxWxH). The hood was connected to an off-gas analyser through a flexible hose of 40 mm in diameter. The total flow rate of off-gas was not measured as the aeration is assumed to be evenly distributed

over the aeration zones. In the off-gas analyser (Figure 7.3), a vacuum pump diverges a small fraction of the off-gas from the main hose to a desiccator unit in order to remove water vapour. The spilled airflow is then circulated inside a zirconium oxide fuel cell (AMI Model 65, Advanced Micro Instruments, USA) to measure oxygen partial pressure. Ambient air was sampled by means of a three-way valve at the start and end of each experiment as reference for the efficiency evaluation.

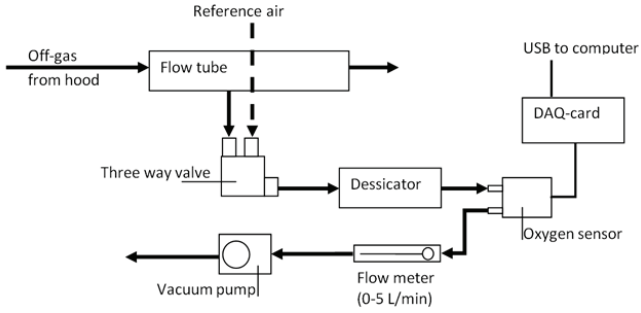

Figure 7.3. A schematic overview of the off-gas analyser.

When the humidity is stripped out of the gas stream, only the knowledge of the CO_2 content is necessary in order to calculate the actual mass fraction of oxygen (Redmon et al., 1983). With this purpose, the CO_2 content of both the ambient air and the off-gas stream was measured with a photo-acoustic infrared gas analyser (X-Stream, Emerson). Knowing the CO_2 content of the gas stream, the partial pressure of oxygen and its ratio with inerts were calculated using equations 7.24 and 7.25.

$$MR_{o/i} = \frac{Y_r}{1-Y_r-Y_{CO_2 r}} \quad (7.24)$$

$$MR_{og/i} = \frac{Y_{og}}{1-Y_{og}-Y_{CO_2 og}} \quad (7.25)$$

where $MR_{o/i}$ and $MR_{og/i}$ represent the molar ratio of oxygen to inerts (i.e. gases that do not have a net absorption nor desorption) in the inlet and off-gas respectively [-]. Y_r [-] and Y_{og} [-] are the mole fractions of oxygen in the inlet and off-gas, while $Y_{CO_2 r}$ [-] and $Y_{CO_2 og}$ [-] are the mole fractions of CO_2. Finally, oxygen transfer efficiency (OTE) can be calculated with Equation 7.26 considering the dynamic CO_2 content in the off-gas.

$$OTE = \frac{MR_{o/i}-MR_{og/i}}{MR_{o/i}} \quad (7.26)$$

Typically, for clean water applications, results are reported as standard oxygen transfer efficiency (SOTE, %), referring to zero DO, zero salinity, 20°C and 1 atm. In order to correct for process water conditions, the alpha factor is used and results are normally shown as αSOTE (Equation 7.27).

$$\alpha SOTE = OTE \cdot \frac{C^*_{S20}}{(\beta \cdot C^*_{ST} - \mathrm{C})} \cdot \theta^{(20-T)} \quad (7.27)$$

Where C is the actual oxygen concentration [mg/l] and T the actual temperature [°C]. This method allows to standardize results of OTE calculating the oxygen saturation concentration in clean water at 20°C (C^*_{S20}) and the saturation concentration for clean water at 44% of the diffuser submergence depth in process temperature conditions (C^*_{ST}).

The floating hood was equipped with an LDO probe (Hach-Lange), with an measurement error of 0.05 mg/l below 1 mg/l and 0.01 mg/l below 5 mg/l, and DO data were acquired in order to correct for variable DO gradients during the oxygen transfer process and relate the efficiency results to standard conditions with Equation 4. Data of DO and oxygen content in the off-gas were acquired with a data acquisition card (DAQ-card USB-6341, National Instruments, USA) using a graphical user interface developed in LabView (National Instruments, USA). Adjustments for CO_2 content in the off-gas were performed in a post processing step when both the data from the off-gas analyser and the X-Stream were available.

7.6. RESULTS AND DISCUSSION

The main findings of the campaign were the observation of a high variation in the αSOTE (Figure 7.4), a significant increase in αSOTE (Figure 7.5) from the beginning towards the end of the summer package (following the flow direction) and the relatively high efficiency of this system as compared to other similar applications (10-20% deduced from (Gillot and Heduit, 2008)). This increase in αSOTE over the locations, assuming that the entire aeration package distributes the airflow homogeneously, may be attributed to the gradual contaminant oxidation occurring (Rosso and Stenstrom, 2006a). The high variation in αSOTE looks inversely correlated with the airflow rate, when the flow rate is gradually changing. Fast changes in airflow rate, however, seem to make αSOTE follow the trend of the airflow rate. This effect, i.e. increasing airflow rate combined with increasing αSOTE, makes the change made by the controller more pronounced than what the controller expects and as such creates oscillations when the controller tries to correct for the too strong manipulation. Further investigation is needed to disclose the mechanisms related to this behaviour.

The manner of calculating the saturation concentration may influence the results of αSOTE. In particular the pressure correction and the applied effective saturation depth vary depending on the source, either 50% (Tchobanoglous et al., 2004), 22-

44% (US EPA, 1989) or 33% (Gillot et al., 2005) of the total submergence depth. The application of 33% of the total submergence depth would result in slightly higher αSOTE values and as such lead to the same conclusion as the applied 44%.

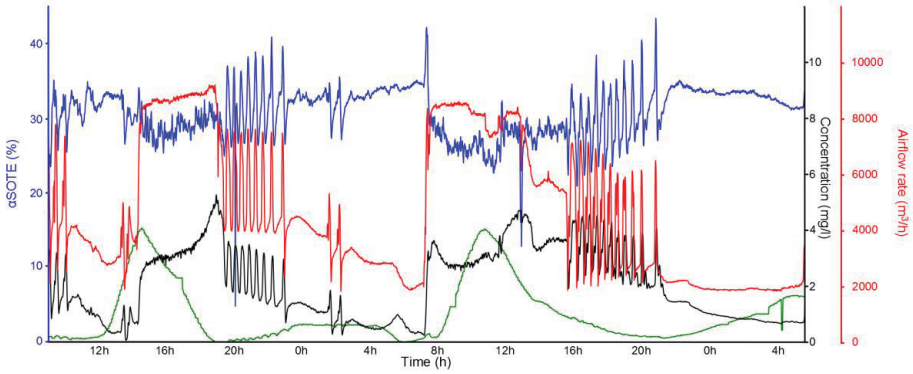

Figure 7.4. The high variation in αSOTE (blue line), DO (black line), NH_4 (green line) dynamics and airflow rate (red line) measured continuously at the end of the summer package during the last two days of the measurement campaign.

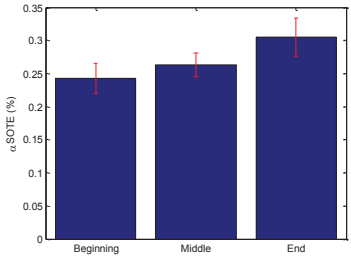

Figure 7.5. Increasing average values and the variation of αSOTE at the three locations monitored with the hood.

The data collected during the off-gas measurements were compared with the modelling results in order to evaluate the prediction performances of the aeration model (Figure 7.6). The modelling results for DO are 4 to 6% lower than the ones measured in the middle of the summer package (which previously was assumed to be representative for the entire aeration package). When applying the measured αSOTE directly as model input instead of the correlation described above, DO predictions improve (red line versus black line) compared to the DO values from the SCADA logs (green line) and DO measurements at the hood location (blue line) (Figure 7.6, left). This improvement reveals the need to update the correlation specific for the WWTP of Eindhoven.

On a side note, but worthy to mention, is the difference in oxygen concentration between the SCADA system and the hood measurements. The difference amounts

up to 0.5 mg/l and is due to mixing patterns. It emphasises the importance of, one, have a good location for the sensor measurements and, two, for an appropriate hydraulic mixing model (Rehman et al., 2015).

As expected, the NH_4 was even further depleted (red line) as compared to the previous simulations and therefore more distant from the measured NH_4 (green line) (Figure 7.6, right). These observations may lead to consider a re-evaluation of the model parameters linked to NH_4 depletion, in particular the ammonium half-saturation coefficient for autotrophs ($K_{NH,ANO}$), which was previously fixed (0.05 mg/l) to match the SCADA measurements. Resetting the half-saturation coefficient to its default value (1.0 mg/l) improves the model predictions for ammonium (black line) considerably (Figure 7.6, right). This shows again the importance of sufficient model complexity of sub-models which otherwise forces the modeller to calibrate biokinetic parameters.

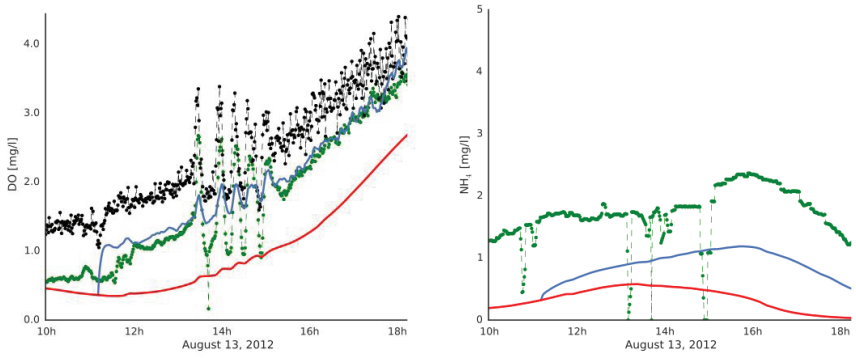

Figure 7.6. Left – The improved DO predictions for the model using αSOTE directly as model input (New DO prediction – blue line) versus the model using the correlation with SRT and airflow rate (Old DO prediction - red line) compared to the DO values from the SCADA logs (green dots) and DO measurements at the hood location (black dots). Right - The model using αSOTE directly as model input shows improved NH_4 predictions for the model where the half-saturation constant for NH_4 was reset to the default value (New NH_4 prediction – blue line) versus the model using the adapted value (Old NH_4 prediction - red line) compared to the NH_4 values from the SCADA logs (green dots).

The aeration model applied is certainly an improvement over state of the art aeration models applied in WWTP models and provided good simulation results for the WWTP of Eindhoven. However, the new measurement campaign shed light on the real evolution of the α-factors in the aerated tanks and it was demonstrated that applying this real α-factors improves the simulation results. This observation proves the need for a recalibration of the aeration model. Moreover, ammonium predictions could be improved by resetting the ammonium half-saturation coefficient for autotrophs to its default value.

However, the model could still be improved as it shows some features that are doubtful. The α-factor is linked to the sludge age (SRT). This approach is questionable as the SRT is a global WWTP characteristic and aeration (oxygen transfer and the α factor) is a local parameter influenced by local physics. Actually the US EPA (1989) mentions the change over the length of the aeration tank.
The apparent correlation between SRT and the α factor can be explained by the link of SRT with some of the influential factors. First, SRT is directly linked to the mixed liquor suspended solids concentrations (MLSS) concentration, which is considered of having an impact on the oxygen transfer, and also to the sludge composition and morphology. The combination of sludge concentration, composition and morphology can be related to changes in viscosity which are known to influence the gas-liquid transfer (Fabiyi and Novak, 2008; Ratkovich et al., 2013). In addition, the floc volume is one of the drivers for changing α factors mentioned by Henkel et al (2011). The SRT is also linked to the amount of biodegradation of e.g. surface active agents, although that should only be really differing with very low SRTs. The surface active agents however are known to impact oxygen transfer (Rosso and Stenstrom, 2006). Finally, the need for the recalibration, in this study, also shows that the SRT is not the only predictor for the variations in the α factor.
Many of the factors (surfactants, viscosity, floc volume) mentioned above, have an impact on the formation and shape of the air bubbles. As such another suggested future improvement in the modelling of the aeration process would be the evaluation of the drivers and the impact of bubble coalescence. In this evaluation, bubble column tests in combination with modelling frameworks such as population balance models (Nopens et al., 2015) will have a definite added value.

7.7. CONCLUSIONS

The aeration model applied is certainly an improvement over state of the art aeration models applied in WWTP models. An extensive measurement campaign with off-gas tests was performed at the WWTP of Eindhoven. A high variability was observed in the oxygen transfer efficiency. Applying this gathered system knowledge in the aeration model and after adaptation of the ammonium half-saturation coefficient for autotrophs, the model proved, based on the airflow rates, to give good predictions for the oxygen and consequently ammonium concentrations at the WWTP of Eindhoven. As such, it was shown that the effect of applying the correct α-factors omits the need for calibration of the bio-kinetic

model. This again proves the importance of balancing sub-models which is preferred over parameter calibration with respect to model predictive power.

Chapter 8

Realistic dynamic blower energy consumption models for wastewater applications

"Sometimes the questions are complicated and the answers are simple."
Dr. Seuss

8.1. ABSTRACT

At wastewater treatment plants (WWTPs) aeration is the largest energy consumer. This high energy consumption requires an accurate assessment in view of plant optimization. Despite the ever increasing detail in process models, models for energy consumption still lack detail to enable a global optimization of WWTPs. A new dynamic model for a more accurate prediction of aeration energy costs in activated sludge systems, equipped with submerged air distributing diffusers (producing coarse or fine bubbles) connected via piping to blowers, has been developed and demonstrated. The current chapter addresses the model structure, its calibration and application to the WWTP of Mekolalde (Spain). The new model proved to give an accurate prediction of the real energy consumption by the blowers and captures the trends better than the constant average power consumption models currently being used. This enhanced prediction of energy peak demand, which dominates the price setting of energy, illustrates that the dynamic model is preferably used in multi-criteria optimization exercises for minimizing the energy consumption.

Part of this chapter was presented as a poster at the IWA Specialised conference: Activated Sludge: 100 years and counting in Essen (Germany).

Amerlinck, Y., W. De Keyser, G. Urchegui, T. Maere, and I. Nopens, 2014, Realistic dynamic blower energy consumption models for activated sludge systems: IWA Specialised conference: Activated Sludge: 100 years and counting.

Part of this chapter was published as:
Amerlinck, Y., W. De Keyser, G. Urchegui, and I. Nopens, A realistic dynamic blower energy consumption model for waste water applications: Appl Energy (submitted).

8.2. SYMBOLS

A_{PL}, B_{PL}, C_{PL}	Parameters of the power law (-)
A_{QL}, B_{QL}, C_{QL}	Parameters of the quadratic law (-)
d	Air line inside diameter (mm)
f_{Diff}	Linear pressure loss factor (m H_2O.($Nm^3.h^{-1}.m^{-2}$)$^{-1}$)
$f_{fouling}$	Fouling factor (-)
$f_{fouling,max}$	Maximum fouling factor (-)
FP	Fraction of the power consumption at full load (-)
FPL	Friction power loss at actual operating conditions (kW)
H_0	Cut-off head (m H_2O)
H_w	Height of water above the diffusers (m)
L	Air line length (m)
L_{equiv}	Equivalent pipe length (m)
K_v	valve-specific flow factor (Nm^3/h)
N	Relative blower speed (-)
$N_{desired}$	Desired relative blower speed (-)
P_{blower}	Blower outlet pressure (kPa)
p_{in}	Inlet pressure (kPa)
p_m	Mean system pressure (kPa)
p_{out}	Pressure at the blower outlet (kPa)
p_{std}	Atmospheric at sea level (kPa)
P	Power draw (kW)
P_{actual}	Actual power draw (kW)
PV_a	Saturated vapour pressure of water (kPa)
Q_1, Δp_1	Flow rate – pressure combination on the blower curve (Nm^3/h, kPa)
Q_2, Δp_2	Flow rate – pressure combination on the blower curve (Nm^3/h, kPa)
Q_3, Δp_3	Flow rate – pressure combination on the blower curve (Nm^3/h, kPa)
Q_{Air}	Airflow rate (Nm^3/h)

$Q_{Air,actual}$	Actual airflow rate (Nm^3/h)
$Q_{Air,desired}$	Desired airflow rate (Nm^3/h)
$Q_{Air,in,N}$	Normalized volumetric air flow rate (Nm^3/h)
Q_{BEP}	Airflow rate at which the best efficiency is reached (Nm^3/h)
Q_{design}	Design airflow rate (Nm^3/h)
Q_{max}	Maximum airflow rate (Nm^3/h)
Q_0	Blower's theoretical airflow rate at full speed and $p_{out} = p_{in}$ (Nm^3/s)
RH	Relative humidity (-)
t	Time (d)
$t_{last\ cleaning}$	last cleaning time (d)
T_{in}	Air temperature at the blower inlet (K)
Z	Altitude above sea level (m)
η_m	Mechanical efficiency (-)
η_{max}	Maximum efficiency (-)
η_{min}	Minimum efficiency (-)
η_p	Electrical efficiency (-)
η_p	Pneumatic efficiency (-)
η_v	Volumetric efficiency (-)
η_{VFD}	VFD efficiency (-)
η_t	"wire-to-air" efficiency or total efficiency (-)
$\eta_{throttling}$	Efficiency for outlet throttling control (-)
ρ_{air}	Relative specific gravity of air ($kg.m^{-3}$)
ρ_w	density of the water ($kg.m^{-3}$)
Δp_{design}	Design pressure difference (kPa)
Δp_{DWP}	Diffuser dynamic wet pressure (kPa)
Δp_{line}	Pressure losses in the air line (kPa)
Δp_{max}	Maximum pressure (kPa)
Δp_{system}	Total pressure loss in the system (kPa)
Δp_w	Water head above the diffuser (kPa)
$\Delta t_{cleaning}$	Periods in between consecutive cleaning (kPa)
μ	Mean of the distribution of the EE (-)
μ^*	Mean of the distribution of absolute values of the EE (-)
σ	Standard deviation of the distribution of the EE (-)

8.3. INTRODUCTION

One of the main challenges for the optimization of wastewater treatment plants (WWTPs), today, is the proper evaluation of all important performance indicators such as effluent quality (including priority pollutants), energy consumption and greenhouse gas emissions. At WWTPs aeration is the largest energy consumer (Ast et al., 2008; Devisscher et al., 2006; Fenu et al., 2010; Tchobanoglous et al., 2004; Zahreddine et al., 2010) and as such aeration energy consumption is an essential factor to be considered in the optimization of WWTPs.

Key factors that influence WWTP aeration cost are the type of aeration blower employed, the aeration system configuration (e.g. diffuser types, water head and piping characteristics) and the control strategy implemented on the aeration system. The blowers employed in fine bubble diffuser aeration systems are compressors operating at low relative pressures and can be classified into two broader classes, i.e. centrifugal and positive displacement (PD) types (Henze, 2008). To date, three main control strategies are implemented to enable "turn-up" or "turn-down" capacity to these aeration blowers, namely variable Inlet Guide Vane (IGV) control, Outlet Throttling (OT) control and Variable Frequency Drive (VFD) control.

Despite the increasing level of detail in wastewater treatment process models, oversimplified energy consumption models (i.e. constant "average" power consumption) are still being used in design and optimization exercises (Copp, 2002; Gernaey et al., 2006; Martín de la Vega et al., 2013; Rosso and Stenstrom, 2005; Wambecq et al., 2013). As these models have the interesting potential to be used in multi-criteria optimization exercises (e.g. optimizing effluent quality, greenhouse gas emissions and operational costs simultaneously (Flores-Alsina et al., 2014)), they may lead to poor predictions and their use in optimization could lead to suboptimal operation.

Although the design, selection and control of blowers and pumps are very similar, significant differences and complexities are introduced to aeration blower applications due to the compressibility of air. Characteristics such as air density, relative humidity, altitude and temperature influence the required airflow to the system and therefore also the energy requirement of the blower.

A new dynamic model for a more accurate prediction of aeration energy costs in activated sludge systems, equipped with submerged air distributing diffusers (producing coarse or fine bubbles) connected via piping to blowers, has been developed to overcome this imbalance in the coupled sub-models. The objective of the proposed model is to allow for dynamically simulating the power consumed by

an aeration system in function of (a) the physical characteristics of the aeration system (i.e. blowers, piping, diffusers), (b) the water height in the aerated tanks and (c) the volumetric air flow rate imposed by a control system. The remainder of the chapter will illustrate the dynamic model, its calibration and application to the WWTP of Mekolalde (Spain). Finally, a comparison is made with the currently frequently used average power consumption models and the preferable use in optimisation efforts for energy minimisation is explained.

8.4. MATERIALS AND METHODS

8.4.1. Centrifugal and positive displacement blowers

Similar to pumps, aeration blowers are classified into two main categories: i) centrifugal blowers and ii) Positive Displacement (PD) blowers. Centrifugal blowers, sometimes referred to as dynamic type blowers, have the air intake along the axis of rotation at the impeller centre and continuously discharge air radially. This rotational action increases the kinetic energy within the air stream, thereby increasing the pressure over the system (Henze, 2008). Centrifugal blowers are economical for applications in all scales of WWTPs but comparatively more so for large scale installations. Single-stage centrifugal blowers can be used for cases where only a limited pressure increase is required, whereas multi-stage centrifugal blowers are needed in situations where high pressure increases are required. However, operating at excessively high flows can cause surge that could result in blower damage or destruction.

Positive displacement (PD) blowers utilise a different approach compared to that of centrifugal blowers by virtually moving “batches” of air from the blower inlet to the oulet instead of converting the kinetic energy of the air stream to pressure, as is the case for centrifugal blowers (Henze, 2008). The result is that PD blowers have the capacity to operate against higher ouput pressures than centrifugal blowers for the same air flow rates (Henze, 2008) and can be applied in cases where the aeration system has a high pressure requirement. However, the efficiencies of PD blowers are lower than those of centrifugal blowers, specifically at high air flow rates. In addition, there is a significant difference between the characteristic blower curves of centrifugal and PD blowers and this needs to be accounted for in the models.

The energy consumption for blowers, similar to that of pumps, is a function of air flow rate, efficiencies and discharge pressure. However, the compressibility of air needs to be considered for blowers and this introduces significant differences

between the characteristics of aeration systems compared to the characteristics influencing the water and sludge pumps (WEF, 2009b). The aeration blower process can be described as an adiabatic compression process (Tchobanoglous et al., 2004; WEF, 2009b), which can be defined as a thermodynamic process where no heat is transferred to or from its surroundings. Technically this is valid for aeration systems where heat loss to the environment is negligible, e.g. well insulated systems, where temperature changes in the system are the net result of a change in pressure.

Each blower delivers a certain flow rate (Q_{Air}), decreasing as function of the pressure. This relation is described by the blower characteristic curve (Figure 8.1), which is as well as the blower efficiency usually provided by the manufacturer. The total pressure or head delivered by the blower shows a monotonic decreasing trend with increasing flow rate, whereas the blower efficiency (Figure 8.1) shows an optimum with varying flow rate. This optimum is more explicit for centrifugal blowers then for PD blowers. This optimum of the blower efficiency curve is called the Best Efficiency Point (BEP), although the term usually refers to the flow rate at which the best efficiency is reached (Q_{BEP}).

While in operation, a blower experiences a certain pressure, which is both of static and dynamic nature, caused by the system. This varying pressure caused by the system is expressed by the system curve (Figure 8.1). The most important factors influencing the system curve are (i) the pressure losses in the air line due to friction caused by the piping and in-line equipment, (ii) the diffuser dynamic wet pressure (DWP) and (iii) the water head above the diffuser.

The system curve and the blower curve intersect in one point only, i.e. the duty point or operating point (OP), expressing the only possible flow rate and pressure in that particular system with that particular blower configuration and blower settings (e.g. speed) (Figure 8.1). The operating point also coincides with a certain efficiency and power consumption. For a well-designed system this operating point should be as close as possible to the Best Efficiency Point.

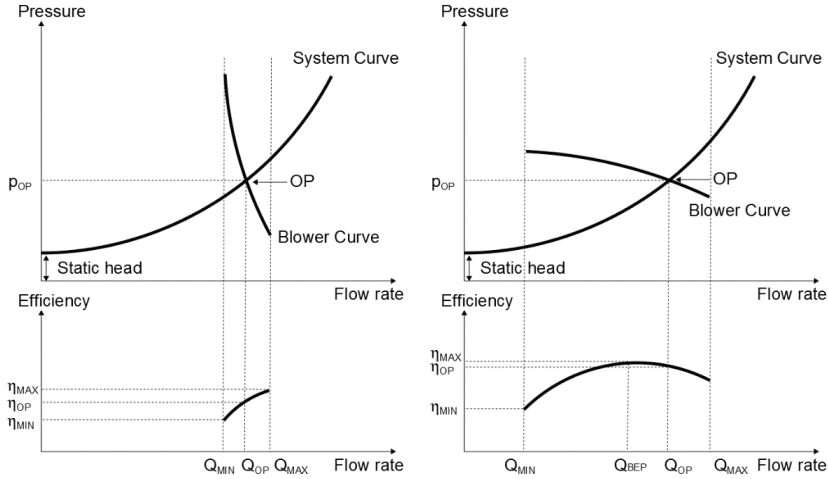

Figure 8.1. Schematic representation of the operating point (OP) or the intersection of the blower curve and the system curve and the corresponding efficiency curve for a positive displacement blower (left) and for a centrifugal blower (right).

The efficiency of centrifugal aeration blowers can have a significant impact on the energy requirement for these units during operation and is dependent on the blower type, design, air conditions and control strategies (BEE, 2006). Blower efficiency is the ratio of the output total energy (including both kinetic energy and energy related to the pressure build-up) contained in the airflow stream over the electrical energy input at the wire supply point. The overall energy efficiency of a centrifugal aeration blower (η_t) considers the pneumatic efficiency (η_p), the volumetric efficiency (η_v) (air tightness of the airline), the electrical efficiency (η_e) (including losses incurred from the controller and transformers) and the mechanical efficiency (η_m) (including losses incurred from the motor, bearings and shaft).

8.4.2. Control strategies

Control strategies can be designed to ensure process stability or for the optimization of the overall plant including energy consumption. However, changing or controlling the operating point, in order to meet operational requirements, can only be established by modifying either the system curve (e.g. by using valves) or the blower curve (e.g. by changing the speed). However, in doing so, the energy requirement of a specific aeration system is changed and should be accounted for in the overall evaluation.

Three control strategies are commonly implemented for aeration blowers: a) Variable Frequency Drive (VFD) control, b) variable Inlet Guide Vane (IGV)

control and c) outlet throttling (with either an in-line valve or a blow-off valve). The selection of the control strategy is based on the blower type. VFD control can be applied to both centrifugal and PD blowers. Actually, VFD control is the only realistic control strategy to be implemented for PD blowers. IGV control, on the other hand, is only implemented for centrifugal blowers. With regard to outlet throttling both the blow-off valve and the in-line throttling valve are commonly used as a control strategy under operating conditions. A blow-off valve or vane is mostly used (i) at the start-up of large centrifugal blowers in order to reach steady state conditions, and (ii) as a security measure to prevent damage due to too high pressures in the aeration system.

A Variable Frequency Drive (VFD) controls the frequency of the alternating current (AC) supplied to the blower drive motor, thereby adjusting the blower electric motor rotational speed (Henze, 2008). This adjustment in the motor speed results in a shift of the blower curve. This shifted blower curve forces the operating point to move along the system curve and results in a new airflow rate versus pressure combination (Figure 8.2). Additionally, the change in motor rotational speed also alters the efficiency.

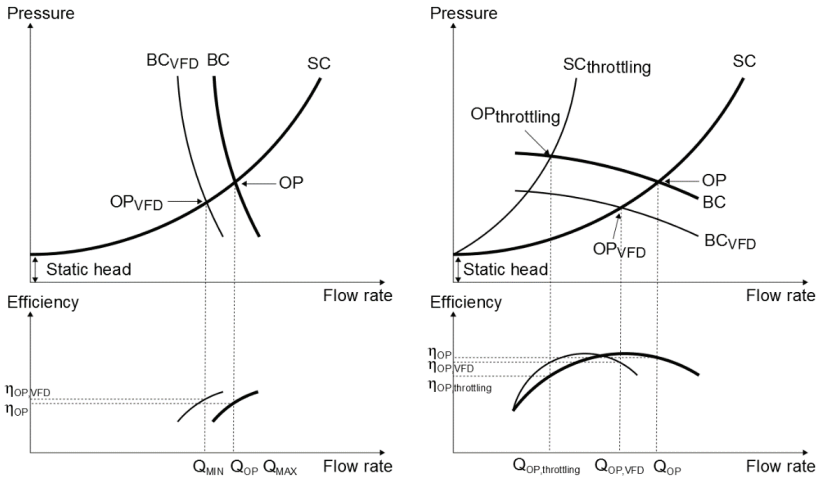

Figure 8.2. Schematic representation of different control strategies for PD blowers (left) and centrifugal blowers (right). VFD control shifts both the blower curve (BC towards BC_{VFD}) and the efficiency curve, resulting in a new operating point (OP_{VFD}) and efficiency (η_{VFD}). Outlet throttling (only applied to centrifugal blowers) shifts the system curve, resulting in a new operating point ($OP_{throttling}$) and efficiency ($\eta_{throttling}$).

Variable IGV control is commonly applied as a control strategy to centrifugal blowers. The design of IGV control is founded on rotatable guide vanes fitted at the inlet section, before the impeller, of a centrifugal blower. These guide vanes are commonly straight-blades with low aerodynamic resistance that can adjust within a

90^o angle as it is fitted in the inlet air flow path (Xiao *et al.*, 2006). In practice, the capacity of most IGV-controlled blowers can only be turned down to about 60% to 80% of the maximum capacity. On adjustment of the guide vanes angle, the operating point of the aeration system is shifted due to a change in the blower curve (Boyce, 2002).

Single stage, lower speed centrifugal blowers can be controlled with outlet throttling using an in-line valve similar to throttling on centrifugal pumps. The characteristic of the system curve is based on a control valve being fully open (in system design) thus any change in the setting of the control valve will result in an increase in pressure and a change in the system curve, similar to the case of centrifugal pumps. As these control strategies are much less commonly utilized in aeration systems they will not be addressed in the remainder of the chapter.

8.4.3. Mathematical model

In this section, the generic dynamic models that were developed for both uncontrolled and controlled aeration systems are explained. In contrast to textbook knowledge and blower manufacturer data (that are often intended for selecting a blower for a certain application), these models can be used to dynamically calculate the energy consumption of a certain motor-blower combination, hereby accounting for the required flow rate as well as the control actions. The basic assumption is always that the dynamic blower model input is the desired flow rate ($Q_{Air,desired}$), as demanded by the controller, and that the dynamic model outputs are the actual flow rate ($Q_{Air,actual}$) and actual power draw (P_{actual}), given certain blower and system characteristics, which need to be specified by the user. These system characteristics can be parameters that are fixed during the simulation (e.g. the blower curve at full speed, piping layout, etc.) or dynamic model inputs that vary in time (e.g. the water level in the aerated tank, air temperature, etc.). Note that most equations for variable speed blowers can also be written in terms of the relative blower speed (N) as the independent variable. This allows transforming the model in a way that desired speed is the input signal ($N_{desired}$) rather than $Q_{Air,desired}$. This approach links better to reality, where the WWTP's automatic control system instructs the actuators to run at a certain percentage of their maximum capacity. However, in an integrated water quality modelling context, it is common to use the blower flow rate as the controlled variable.

Key issues to be considered when modelling the energy consumption of aeration systems are: (1) energy requirement for compression, (2) inlet conditions of the air, (3) system characteristic curve, (4) blower characteristic curve, (5) blower efficiency and (6) the type of process control strategy employed.

8.4.4. The mathematical model for the energy requirement for compression

The blower energy consumption, in the case of centrifugal blowers for both fine and coarse bubble diffuser aeration systems, can be estimated using the expression for power requirement P [kW] for adiabatic compression (Tchobanoglous *et al.,* 2003). However, considering the significant impact of the dynamics in the inlet air on the energy requirements, a modified form proposed by WEF (2009b) is used (Equation 8.1).

$$P = (9.816 \cdot 10^{-4}) \cdot \left[\frac{Q_{Air,in,N} \cdot p_{in}}{\eta_t} \cdot \left[\left(\frac{p_{out}}{p_{in}}\right)^{n} - 1\right]\right] \quad (8.1)$$

where $Q_{Air,in,N}$ is the normalized volumetric air flow rate [$Nm^3.h^{-1}$] and n is a dimensionless constant for air (0.285) [-]. The number 9.816 x 10^{-4} lumps constants related to air characteristics (a.o. the universal gas constant R and the number of moles per volume of air*)* and those related to the use of $Q_{Air,in,N}$ instead of the air mass flow rate.

In case PD blowers are used, the power consumption can be calculated as in equation 8.2 (inspired by WEF (2009b)):

$$P = N \cdot Q_0 \cdot (p_{out} - p_{in}) + FPL \quad (8.2)$$

with N the relative rotational speed [-], Q_0 the blower's theoretical flow rate at full speed and $p_{out} = p_{in}$ [$Nm^3.s^{-1}$] and FPL the friction power loss at actual operating conditions [kW]. The latter is to be received from the manufacturer, but is typically around 5% of the power consumption at full load (maximum pressure Δp_{max} [kPa]) at that speed N. This means that if FPL would not be available, an acceptable default value could be calculated as in equation 8.3 and 8.4:

$$FPL = FP \cdot (N \cdot Q_0 \cdot \Delta p_{max} + FPL) \quad (8.3)$$

$$FPL = \frac{FP}{1-FP} \cdot N \cdot Q_0 \cdot \Delta p_{max} \quad (8.4)$$

With FP the fraction of the power consumption at full load (0.05 corresponds to 5%).

Data and calculations related to compressible fluids are always expressed in terms of so-called 'standard conditions' to keep everything transparent. The data of the actual input signal (real desired air flow rate Q_{in}) needs to be transformed into a normalized desired air flow rate $Q_{Air,in,N}$ (Equation 8.5). The definition of standard conditions varies a lot, depending on the application, the country, etc. , but 101.325 kPa, 293 K and 50% relative humidity (RH) are common in Europe (International Organization for Standardization, 2002).

$$Q_{Air,in,N} = Q_{Air,in} \cdot \left[\left(\frac{101.3}{p_{in} - (RH \cdot PV_a)}\right) \cdot \left(\frac{T_{in}}{273}\right)\right]^{-1} \quad (8.5)$$

where RH is the relative humidity [-], PV_a is the saturated vapour pressure of water at the actual temperature [kPa], T_{in} is the air temperature at the blower inlet [K], p_{in} is the inlet pressure [kPa], which can be approximated to consider altitude using equation 8.6 (The Engineering Toolbox, 2005).

$$p_{in} = p_{std}\left(1 - Z \cdot 2.26 \times 10^{-5}\right)^{5.2559} \quad (8.6)$$

where p_{std} is 101.325 kPa and Z is the altitude above sea level [m].

8.4.5. The mathematical model for the system curve

The flow rate produced by the blower and the corresponding power consumption can be calculated based on the descriptions of the blower curve and the system curve. The latter is calculated based on the pressure developed in the system. The pressure develops due to (i) the pressure losses in the air line caused by friction in the piping and in-line equipment (Δp_{line}), (ii) the diffuser dynamic wet pressure (Δp_{DWP}) and (iii) the water head above the diffuser (Δp_w). The total pressure loss in the system (Δp_{system}) is calculated as the sum of the three pressure losses (Equation 8.7).

$$\Delta p_{system} = \Delta p_{line} + \Delta p_{DWP} + \Delta p_w \quad (8.7)$$

First, pressure or head losses occur within the air pipe lines as a result of pipe line friction losses, bends, fittings and other in-line equipment. Tchobanoglous et al. (2004) quantify the pressure losses based on a modified form of the Darcy-Weisbach equation. Alternatively, WEF (2009b) describes the pressure loss in the air line using an empirical formula for air flow in clean steel pipes (Equation 8.8)

$$\Delta p_{line} = \left(4 \cdot 10^7 \cdot \frac{Q_{Air,in,N}^{1.85}}{d^5 \cdot p_m} \cdot \frac{T_{in}}{273.15} \cdot \frac{L}{100}\right) + \left(\left(\frac{Q_{Air,in,N}}{4.78 \cdot K_v}\right)^2 \cdot \frac{\rho_{air} \cdot T_{in}}{p_{out}}\right) \quad (8.8)$$

where T_{in} is the air temperature [K], L is the air line length [m], d is the air line inside diameter [mm], $Q_{Air,in,N}$ is the normalized air flow rate [$Nm^3.h^{-1}$], K_v is the valve-specific flow factor [$Nm^3.h^{-1}$], ρ_{air} is the relative specific gravity of air [-], p_{out} is the pressure at the blower outlet (= the pipe inlet) [kPa] and p_m is the mean system pressure [kPa]. The latter can be calculated iteratively according to equation 8.9.

$$p_m = p_{out} - \frac{\Delta p_{line}}{2} \quad (8.9)$$

Friction losses due to fittings are included in this equation via the equivalent pipe length method (Equation 8.10).

$$L = L_{pipe} + L_{fittings} = L_{pipe} + \sum L_{equiv} \quad (8.10)$$

with L_{equiv} the equivalent pipe length [m] of a fitting (Table 8.1).

Table 8.1. Equivalent pipe lengths (as function of the diameter *d*) (adopted from WEF (2009b)).

Fitting	Equivalent pipe length [m]
90° elbow	30d
45° elbow	16d
T straight through	20d
T through side	60d
Transition	20d
Open butterfly valve	20d

Second, the diffuser dynamic wet pressure loss (Δp_{DWP}) is the pressure loss over the fine bubble diffuser membrane, disk or plate during operation under submerged conditions (US EPA, 1989). The variation of DWP with air flow rate (Figure 8.3) is product-specific. Most manufacturers provide this variation in tabulated form (usually two points only). Considering the limited amount of information available a linear approach is adopted (First term equation 8.11).

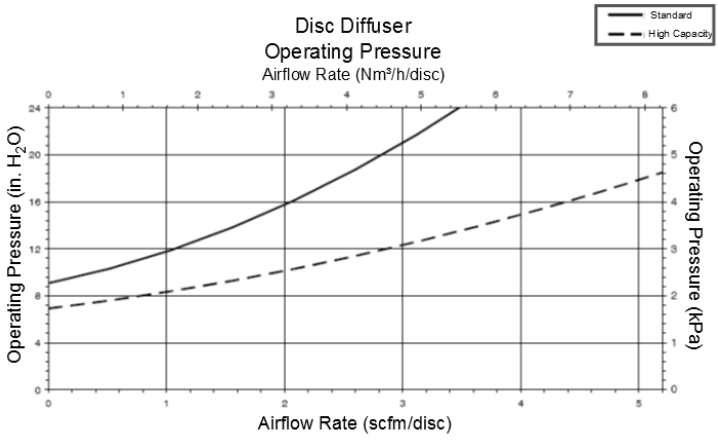

Figure 8.3. An example of manufacturer data on head loss in function of normalized air flow rate for two types of fine bubble disk diffusers. Note that not all the units are SI units.

Figure 8.4 demonstrates the increase of the pressure drop over the diffuser due to membrane fouling (Rosso et al., 2008), which is another factor affecting the DWP. After cleaning, the pressure drop, and consequently the power consumption, returns to approximately its original level.

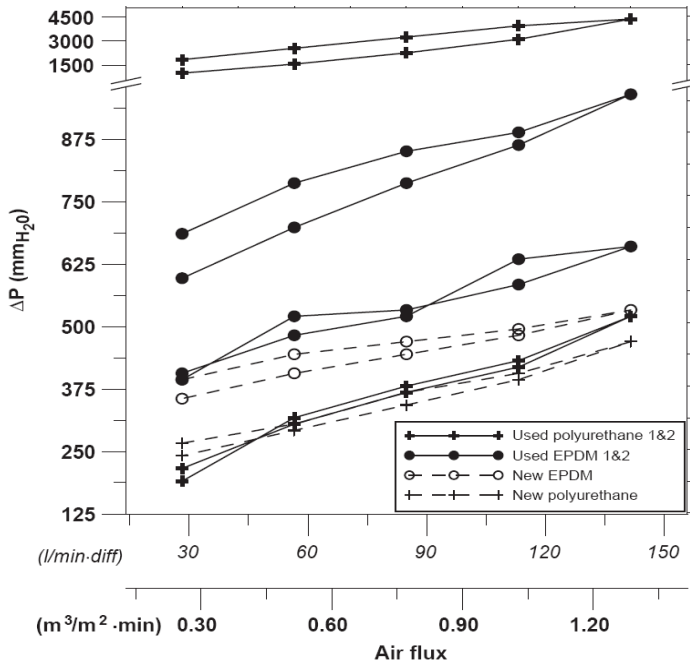

Figure 8.4. Head loss in new and used fine bubble diffuser membranes in function of the air flow rate (Rosso et al., 2008).

Dynamic wet pressure loss (Δp_{DWP}) is calculated according to equation 8.11, derived from Rosso et al. (2008).

$$\Delta p_{DWP} = \left(f_{Diff} \cdot Q_{Air,in,N} + H_0\right) \cdot f_{fouling} \cdot \frac{\rho_w \cdot g}{1000} \qquad (8.11)$$

where $Q_{Air,in,N}$ [$Nm^3.h^{-1}$] is the normalized air flow rate, f_{Diff} is the linear pressure loss factor [m $H_2O.(Nm^3.h^{-1}.m^{-2})^{-1}$], H_0 is the cut-off head [m H_2O] , ρ_w is the density of the water [$kg.m^{-3}$] and $f_{fouling}$ is a fouling factor [-]. The latter is function of time (Equation 8.12) and increases linearly from 1 to $f_{fouling,max}$ [-] over a period of $\Delta t_{cleaning}$ [d] (the cleaning interval):

$$f_{fouling} = 1 + \left(f_{fouling,\max} - 1\right) \cdot \frac{t - t_{last\ cleaning}}{\Delta t_{cleaning}} \qquad (8.12)$$

with t the current time [d] and $t_{last\ cleaning}$ the last cleaning time [d].

Third, the head loss due the the submersion of the diffusers (Equation 8.13) or water head is commonly the most significant contributor to the total system pressure in aeration systems.

$$\Delta p_w = \frac{\rho_w \cdot g \cdot H_w}{1000} \qquad (8.13)$$

where Δp_w is the pressure loss due to the water head [kPa] and H_w the (variable) water height above the diffuser [m].

8.4.6. The mathematical model for the blower curve

The characteristic curve for (single stage) centrifugal blowers (Figure 8.1, right) can be approximated quantitatively using a power law (Equation 8.14), analogous to the approach used to describe the characteristic curve of centrifugal pumps.

$$p_{blower} = p_{out} = p_{in} + \Delta p_{system} = A_{PL} - B_{PL} \cdot Q_{Air,in,N}^{C_{PL}} \quad (8.14)$$

where the coefficients A_{PL}, B_{PL} and C_{PL} (Equations 8.15-8.17) can be determined in function of three given (Q,p) combinations (Figure 8.5, left).

$$A_{PL} = p_1 \quad (8.15)$$

$$B_{PL} = (p_1 - p_3) \cdot exp\left(\frac{ln(Q_3) \cdot ln\left(\frac{p_1 - p_3}{p_1 - p_2}\right)}{\ln\left({}^{Q_2}/_{Q_3}\right)}\right) \quad (8.16)$$

$$C_{PL} = -\left(\frac{ln\left(\frac{p_1 - p_3}{p_1 - p_2}\right)}{\ln\left({}^{Q_2}/_{Q_3}\right)}\right) \quad (8.17)$$

Note that p_{out}, p_{in}, p_1, p_2 and p_3 are used here as absolute pressures, whereas in most manufacturer data sheets only the differential pressure over the blower (Δp_{out}, Δp_1, Δp_2 and Δp_3) is considered.

Following the pragmatic approach for pumps described in Walski *et al.* (2004), this method constructs a blower curve expressing the pressure (p) as a continuous function of the flow rate ($Q_{Air,in,N}$). Point 1 ($0,p_1$) should be the cut-off pressure at zero flow, point 2 (Q_2,p_2) is to be selected in the real operating window of the blower (probably around the Best Efficiency Point (BEP)), and point 3 (Q_3,p_3) is to be selected at a larger air flow rate. In a situation where no blower curve is available, a default blower curve can be constructed (Figure 8.5, right) based on the selection of a single desired operating point (Q_2,p_2), near a design operating point or BEP. The curve is then completed based on the following two assumptions. First, the projected maximum pressure at zero air flow (Δp_1) is 1.45 times Δp_2 and second, the projected maximum blower flow, at zero pressure loss (i.e. $p_3 = p_{in}$ or $\Delta p_3 = 0$), is 1.5 times Q_2.

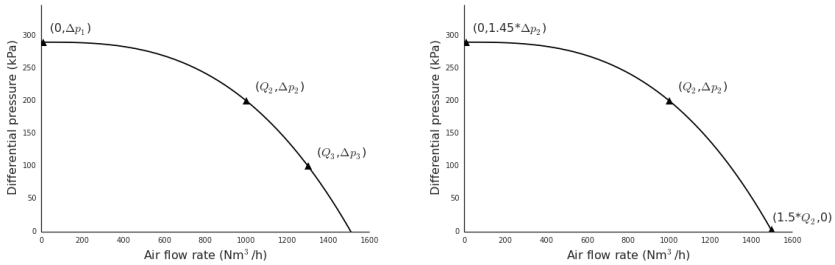

Figure 8.5. Centrifugal blower curves constructed following the power-law (Equation 8.14), based on either three (left) or one (right) flow-pressure combination(s)

For positive displacement blowers the variation of output pressure in function of flow rate is mainly limited by the blower speed, modifying this speed is generally used to control PD blowers. For this reason, manufacturers generally provide the characteristics of their PD blowers as plots in function of rotational speed instead of flow rate. However, to be consistent with the approach used for centrifugal pumps, a characteristic curve expressing the pressure in function of flow rate is used to model the PD blower curves (Figure 8.6).

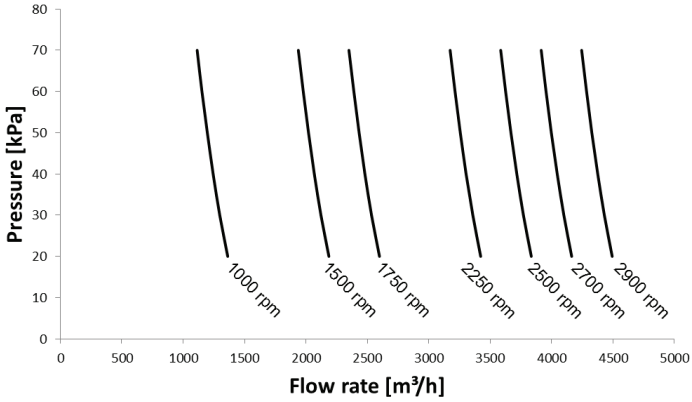

Figure 8.6. The change in differential pressure vs. flow rate characteristic of a positive displacement blower (Mapner SEM.40TR) for seven different motor rotational speeds.

For PD blowers, the relation pressure vs. air flow rate is quantified using a quadratic function (Equation 8.18). The quadratic function is deemed to be superior to a linear function, which would not be able to describe the (slight) curvature.

$$p_{out} = A_{QL} \cdot Q^2 + B_{QL} \cdot Q + C_{QL} \tag{8.18}$$

where the coefficients A, B and C (Equations 8.19-8.21) can be determined in function of three given (Q,p) combinations (Figure 8.7, left).

$$A = \frac{p_1(Q_2 - Q_3) + p_2(Q_3 - Q_1) + p_3(Q_1 - Q_2)}{Q_1^2(Q_2 - Q_3) + Q_2^2(Q_3 - Q_1) + Q_3^2(Q_1 - Q_2)} \tag{8.19}$$

$$B = \frac{p_1\left(Q_3^2 - Q_2^2\right) + p_2\left(Q_1^2 - Q_3^2\right) + p_3\left(Q_2^2 - Q_1^2\right)}{Q_1^2(Q_2 - Q_3) + Q_2^2(Q_3 - Q_1) + Q_3^2(Q_1 - Q_2)} \tag{8.20}$$

$$C = \frac{p_1\left(Q_2^2 Q_3 - Q_3^2 Q_2\right) + p_2\left(Q_3^2 Q_1 - Q_1^2 Q_3\right) + p_3\left(Q_1^2 Q_2 - Q_2^2 Q_1\right)}{Q_1^2(Q_2 - Q_3) + Q_2^2(Q_3 - Q_1) + Q_3^2(Q_1 - Q_2)} \tag{8.21}$$

Equation 8.18 actually describes a parabolic shape, so two solutions are possible: one p_{out} corresponds to two different values for Q. Obviously a boundary check is necessary and only the left half of the parabolic function should be used, i.e. for $Q \leq Q_{max}$.

The latter can be found from the first derivative (Equation 8.23) of equation 8.22.

$$p_{out} = A_{QL} \cdot Q_{max}^2 + B_{QL} \cdot Q_{max} + C_{QL} \quad (8.22)$$

$$\dot{p}_{out} = 2 \cdot A_{QL} \cdot Q_{max} + B_{QL} = 0 \Leftrightarrow Q_{max} = -\frac{B_{QL}}{2 \cdot A_{QL}} \quad (8.23)$$

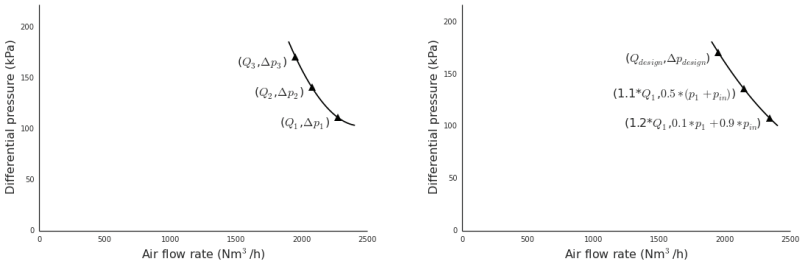

Figure 8.7. PD blower curve constructed following the quadratic function (Equation 8.18), based on either three (left) or one (right) flow-pressure combination(s).

In case no characteristic curves of the blower are available, one flow-pressure combination (Q_{design},Δp_{design}) can be used as (Q_1,Δp_1), assuming Δp_{design} to be the maximum pressure to operate against at full speed. The remaining two points are then calculated with equations 8.24-8.27.

$$p_2 = p_{in} + 0.5 \cdot \Delta p_1 = p_{in} + 0.5 \cdot (p_1 - p_{in}) = 0.5 \cdot (p_1 + p_{in}) \quad (8.24)$$

$$p_3 = p_{in} + 0.1 \cdot \Delta p_1 = p_{in} + 0.1 \cdot (p_1 - p_{in}) = 0.1 \cdot p_1 + 0.9 \cdot p_{in} \quad (8.25)$$

$$Q_2 = 1.1 \cdot Q_1 \quad (8.26)$$

$$Q_3 = 1.2 \cdot Q_1 \quad (8.27)$$

8.4.7. The mathematical model for the blower efficiency (η_t)

Determining the actual value for each of the efficiency factors is complex and case specific. In some cases, manufacturers supply overall efficiency factors. The efficiency of centrifugal blowers (Figure 8.1) typically follows a parabolic trend in function of the flow rate (BEE, 2006; Liptak, 2005). This parabolic trend can be quantified in a similar way as was proposed for centrifugal pumps (Equation 8.28).

$$\eta_t = -\left(\frac{\Delta_\eta}{Q_{BEP}^2}\right) \cdot \left(Q_{Air,in,N}\right)^2 + \left(\frac{2 \cdot \Delta_\eta}{Q_{BEP}}\right) \cdot \left(Q_{Air,in,N}\right) + \eta_{min} \quad (8.28)$$

with η_{max} and η_{min} the maximum and minimum efficiency [-] respectively, Δ_η the difference between the maximum and miniumum efficiency, Q_{BEP} the BEP flow rate and $Q_{Air,in,N}$ the normalized flow rate.

$$\Delta_\eta = \eta_{max} - \eta_{min} \quad (8.29)$$

The efficiency of PD blowers differs from that of centrifugal blowers because they operate in a completely different manner. In the calculation of the power consumption for PD blowers (Equation 8.2) the term FPL, i.e. the friction power

loss at actual operating conditions, was introduced to quantify the efficiency loss induced by the rotary parts causing shear on the inside casing of the blower. This shear depends on the rotation speed and the blower characteristics (Equations 8.3 and 8.4).

The blower efficiency of centrifugal blowers normally transcends that of PD blowers (Henze, 2008). For PD blowers efficiency ranges from 50 to 60% are observed and from 72 to 80% for single stage centrifugal blowers with Inlet Guide Vane (IGV) control (Figure 8.8).

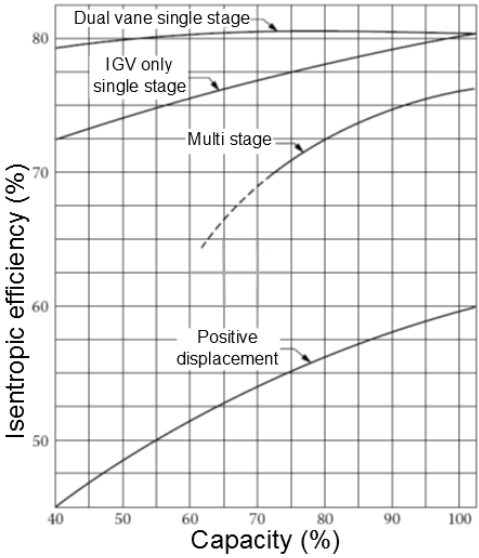

Figure 8.8. The isentropic efficiencies of four blower types in function of turn-down capacity (Lipták, 2006)

8.4.8. Mathematical modelling of control strategies for aeration blowers

8.4.8.1. VFD control

VFD control modifies the rotational speed of the blower and the blower curve shifts accordingly. The relative blower speed N is incorporated in the generic blower curves (Equation 8.30), both for centrifugal and positive displacement, by using the affinity laws (Equations 8.31-8.33).

$$p_{out} = N^2 \cdot A - B \cdot N^{2-C} \cdot Q_{Air,in,N}^{C} \quad (8.30)$$

$$\frac{N_1}{N_2} = \frac{Q_1}{Q_2} \tag{8.31}$$

$$\frac{N_1}{N_2} = \sqrt{\frac{H_1}{H_2}} \tag{8.32}$$

$$\frac{N_1}{N_2} = \sqrt[3]{\frac{P_1}{P_2}} \tag{8.33}$$

Since the exponent 2-C, in equation 8.30, is not an integer, an iterative or interpolation method is needed to solve for N. By filling in the desired $Q_{air,in,N}$ and several values for N in equation 8.30, the corresponding pressures can be calculated. Next, a linear interpolation yields the N that allows for obtaining the p_{out} that corresponds to $Q_{Air,in,N}$ via the system curve.

At a fixed rotational speed, a centrifugal blower's efficiency shows a parabolic behaviour in function of the air flow rate (Figure 8.1, right). However, when a VFD control reduces the speed, this parabolic curve is squeezed towards the origin of the plot (Figure 8.9). This squeezing effect is quantified by introducing the relative blower speed N_i into equation 8.28 (Equation 8.34).

$$\eta_t = -\left(\frac{\Delta_\eta}{Q_{BEP}^2}\right)\cdot\left(\frac{Q_{Air,in,N}}{N}\right)^2 + \left(\frac{2\cdot\Delta_\eta}{Q_{BEP}}\right)\cdot\left(\frac{Q_{Air,in,N}}{N}\right) + \eta_{min} \tag{8.34}$$

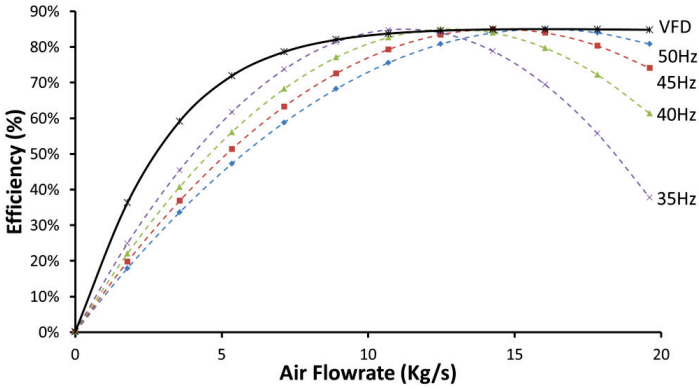

Figure 8.9. Centrifugal blower efficiencies at different impeller speeds (dashed lines) and the efficiency trajectory followed under Variable Frequency Drive (VFD) control (bold line) for a specific system curve

The incorporation of the relative blower speed N [-] in the generic blower curve (Equation 8.18) for positive displacement blowers results in equation 8.35.

$$p_{out} = A\left(Q + Q_0(1-N)\right)^2 + B\left(Q + Q_0(1-N)\right) + C \tag{8.35}$$

with

$$Q_0 = \frac{-B - \sqrt{B^2 - 4A(C - p_{in})}}{2A} \tag{8.36}$$

where Q_0 [m^3h^{-1}] is the flow rate the blower would produce at full speed (N=1) when $p_{out} = p_{in}$.
For PD blowers, the calculation of the efficiency is based on the friction power loss at actual operating conditions (Equations 8.2-8.4) and already include the rotational speed.

8.4.8.2. IGV control

As variable IGV control is mainly applied as a control strategy to centrifugal blowers only this application will be dealt with in this chapter. Determining the efficiency (η_t) for IGV control is different and probably more complex than for VFD control. Unfortunately no quantitative information on IGV controlled blowers' efficiency was found in literature. Due to the lack of a formula describing the efficiency distribution when using IGV control, a preliminary workaround was developed based on the expected curve for energy requirement.
In the first step the vane setting needs to be determined as an opening fraction. This is achieved by modifying Equation 8.14, the equation that describes the blower characteristic curve, into equation 8.37.

$$f_{IGV} = \frac{Q_{Air,in,N}}{k} \cdot \left(\frac{B}{A - p_{out,IGV}}\right)^{1/C} \qquad (8.37)$$

where f_{IGV} [-] is the guide vane opening fraction (1 = 100% open), k is an experimental scaling factor, $Q_{Air,in,N}$ the operating flow rate (determined using the system curve), $p_{out,IGV}$ the outlet pressure (determined using the system curve) and the variables A, B and C can be determined as described for the derivation of a centrifugal blower curve using equations 8.15-8.17.
In a next step the generic efficiency curve presented in equation 8.28 needs to be modified to incorporate the guide vane setting into the generic efficiency formula. The resulting equation 8.38 can be used to determine the efficiency for IGV control.

$$\eta_t = \left(-\Delta_\eta \cdot f_{IGV} \cdot \alpha\right) \cdot \left(\frac{Q_{Air,in,N}}{\beta \cdot f_{IGV} \cdot Q_{BEP}}\right)^2 + \left(\left(2 \cdot \Delta_\eta \cdot f_{IGV} \cdot \alpha\right) \cdot \left(\frac{Q_{Air,in,N}}{\beta \cdot f_{IGV} \cdot Q_{BEP}}\right)\right) + \eta_{min} \qquad (8.38)$$

with α and β experimental scaling factors.

8.5. RESULTS AND DISCUSSION

The model was implemented in the WEST (mikebyDHI) and applied for the aeration system at the Mekolalde WWTP located in Bergara (Guipúzcoa, Spain). The model is validated in two steps. In first instance the model is compared to manufacturer data and in second instance a measurement campaign is organized.

The Mekolalde WWTP (originally designed to treat wastewater of 40,000 PE) has two primary sedimentation tanks (3 m height and 24 m diameter) followed by three waterlines, of which at the time of the measurement campaign only one was in operation. Each waterline consists of a Modified Ludzack-Ettinger process (one denitrification tank of 722 m^3 and 3 nitrification tanks of each 561 m^3). Two secondary clarifiers (3 m height and 24 m diameter) separate the sludge from the treated water. The secondary sludge is then further thickened in a dissolved air flotation unit (2 m height and 6 m diameter) and mixed with the primary sludge coming from a thickener (3 m height and 8 m diameter). The sludge is finally further treated in an anaerobic digester (1600 m^3).

The aeration in the nitrification tanks is provided by five positive displacement blowers of 110 kW each (PD blower Mapner SEM.40TR, Figure 8.10). Three of them are frequency-controlled, the others are on/off controlled (with a soft starter). During the measurement campaign the blowers were manually configured so that one blower provides air to one water line. The air is dispersed through 595 diffusers (SSI^{TM} Fine Bubble Diffusers AFD270 9" discs) for each of the three lines (1785 discs in total).

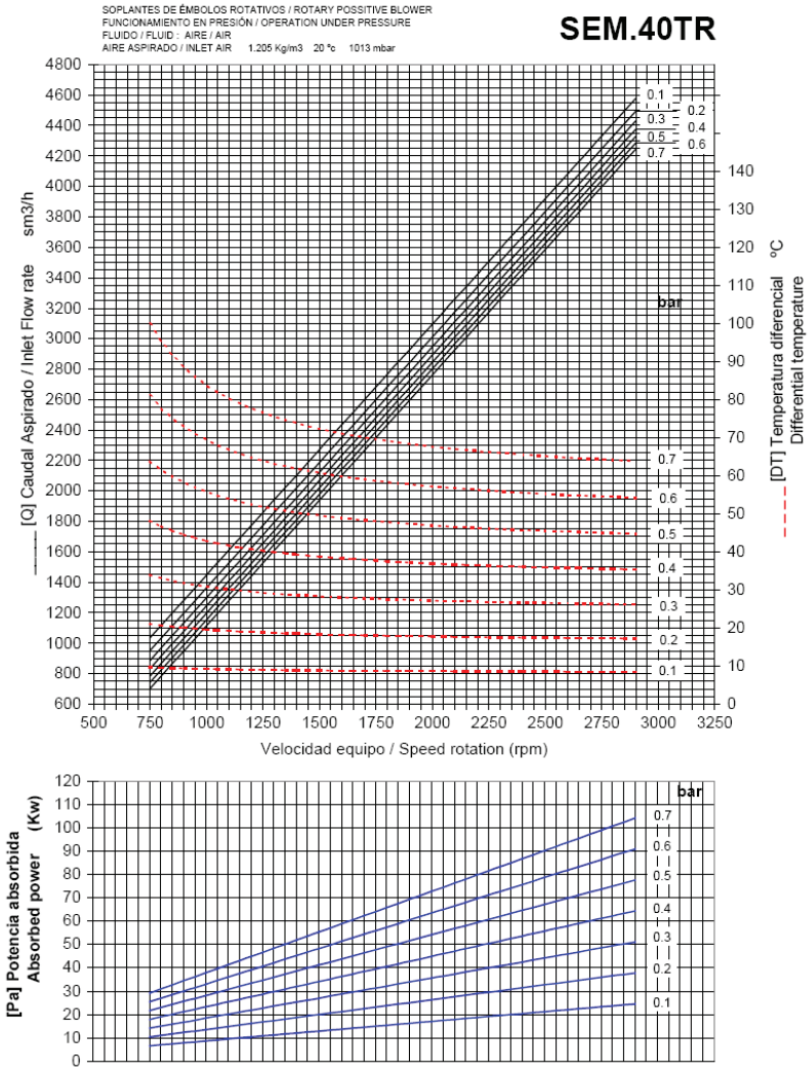

Figure 8.10. Technical data sheet for positive displacement blower SEM.40TR (Mapner 2007)

8.5.1. Comparison to manufacturer data

From the manufacturer's technical info sheet (Figure 8.10), three flow rate – pressure (Q,p) combinations were derived (at 2900 rpm, assumed to correspond with N = 1) and used as input to the PD blower model: (4250 Nm³/h, 70 kPa), (4375 Nm³/h, 40 kPa) and (4575 Nm³/h, 10 kPa). The water height in the aerated tank was supposed to be constant at 5.7 m above the diffuser surface and the input signal (desired air flow rate during one day) varied between 1615 and 4500 Nm³/h

with an average of 2765 Nm³/h. The aeration system consisted of 100 m pipe (diameter 0.25 m), 45 m equivalent pipe length for fittings, and a diffuser surface area of 73.23 m². The motor efficiency was put at 100% to enable comparison of simulated power consumption with the manufacturer data (the bottom graph in Figure 8.10 shows the power absorbed at the motor-blower coupling). Other parameters were left at their default values.

Simulations show a nearly constant system pressure, i.e. the impact of the varying flow rate (influencing Δp_{DWP} and Δp_{line}) is small compared to the static head of the liquid Δp_w. Additionally, the simulation results show an excellent match between the predicted air flow rates and the manufacturer data (Table 8.2). The simulated power consumption, on the other hand, shows a systematic underestimation compared to the manufacturer-supplied power consumption data. The presumed cause is an underestimation of the friction power loss. By adjusting the FP in Equation 8.4 from 5 to 12%, the predictions improve significantly.

Table 8.2. Comparison between simulation results and manufacturer data for Δp = 60 kPa

Relative speed N [-]	Air flow rate [Nm³/h]		Power consumption [kW]	
	Simulation	Manufacturer	Simulation min-max	Manufacturer
1.00 (2900 rpm)	4290	4290	84-91.3	91
0.69 (2000 rpm)	2840	2800	57-62	64
0.51 (1500 rpm)	1981	1980	42-46	48

8.5.2. Comparison to real plant data

In the next step the model was confronted with real plant data. The diffuser area was calculated based on the number of diffusers (595) and their active surface area per diffuser (380.9 cm²). Also the altitude, pipe diameter, pipe length and minor losses equivalent were derived from the system. The flow rates for the definition of the blower curve (Q_1, Q_2 and Q_3) were derived from the manufacturer data.

The parameters to be estimated during the calibration were selected on expert knowledge. For fitting the power consumption the following parameters were estimated using a constrained simplex optimization algorithm (Nelder and Mead, 1965a): cut-off head, motor efficiency and friction power losses. Moreover, the uncertainty bounds on the estimated parameters are determined using the inverse of the Fisher Information Matrix FIM (Donckels, 2009). After calibration (cut-off head=160±12mm H_2O, motor efficiency 0.80±0.03 and friction power losses=0.36±0.02) the model proved to give an accurate prediction of the real energy consumption by the blowers (Figure 8.16). The root of the sum of squared errors totaled 1.103 (versus 12.830 with the parameters derived in the comparison with the manufacturer data).

8.5.3. Comprehensive calibration

In order to further improve the trust in the model calibration a more comprehensive procedure was followed. First, a sensitivity analysis was performed for the parameter selection (i.e. a ranking of the parameters according to their sensitivity) followed by an automatic parameter estimation and calculation of the uncertainty bounds.

A local sensitivity (De Pauw and Vanrolleghem, 2006), global sensitivity analysis using Monte Carlo simulation followed by a linear regression on the results (Saltelli et al., 2008) and a global screening method based on Elementary Effects (Campolongo et al., 2007; Morris, 1991; Saltelli et al., 2008) were conducted.

The local sensitivity on the power consumption was calculated using the parameter values obtained after the first calibration and a perturbation factor (PF) of 1e-6. A forward sensitivity (i.e. PF*parameter value is added to the original parameter value), a backward sensitivity (i.e. PF*parameter value is subtracted from the original parameter value) and a central sensitivity (the average of the forward and backward sensitivities) were calculated. The relative forward, backward and central sensitivities lead to the same ranking. From the ranking determined with the relative sensitivity function (Figure 8.11), the order of parameters with a significant sensitivity is Q_2, Q_1, Q_3, Δp_2, Δp_1, η_m, ρ_w,FP,Δp_3. The local sensitivity shows the importance of the parameters determining the blower curve on the final power consumption.

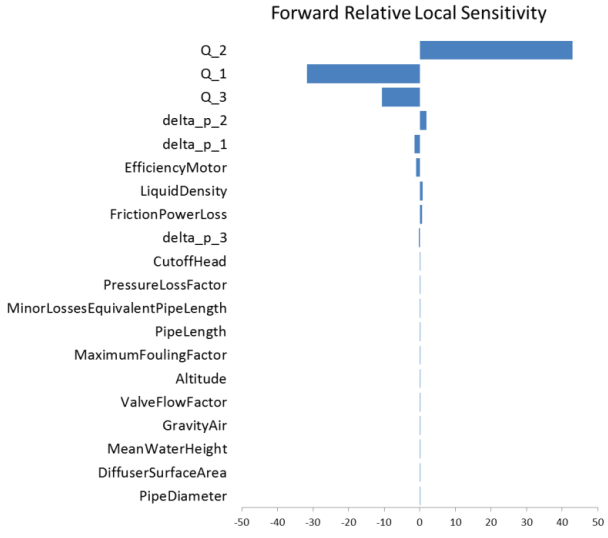

Figure 8.11. Tornado plot showing the differences for ranking in the parameters based on the forward relative local sensitivity.

Next, a global sensitivity analysis was set up to determine the sensitivities on the power consumption in the whole parameter space. Table 8.3 lists the parameter ranges as deemed acceptable and realistic for the system at hand. For the ranges, normal distributions are assumed for parameters on which a priori knowledge is available, i.e. measurements, manufacturer data or literature values. A uniform distribution is imposed if no a priori knowledge is available. The parameter ranges were applied for the Monte Carlo simulation and regression coefficients (Linear correlation coefficient (LCC), Normalized regression coefficient (NRC), Ordinary regression coefficient (ORC), Partial correlation coefficient (PCC), semi-partial correlation coefficient (SPC), standardized regression coefficient (SRC), Variance inflation factor (VIF), t-statistics of the linear correlation coefficient (tLCC), t-statistics of the partial correlation coefficient (tPCC), t-statistics of the semi-partial correlation coefficient (tSPC) and t-statistics of the standardized regression coefficient (tSRC)) were calculated, each of which give the same ranking in case the assumptions for the (linear) regressions are valid.

Table 8.3. Ranges applied in the global sensitivity analysis and parameter estimations for the different model parameters.

Name	Min	Max	Distribution	Mean	Stdev	Unit
Altitude	0.00	3400.00	Normal	155	7.5	m
Cut-off Head	0.00	250.00	Normal	160	20	mm H2O
Diffuser Surface Area	0.00	143.00	Normal	67.99065	16.004675	m2
Efficiency Motor	0.50	1.00	Uniform	0.8	N.A.	-
Friction Power Loss	0.00	1.00	Uniform	0.36	N.A.	-
Specific gravity of Air	0.70	1.30	Normal	1.1	0.05	-
Liquid Density	900.00	1100.	Normal	1000	12.5	kg/m3
Mean Water Height	4.56	6.84	Normal	5.7	0.1425	m
Minor losses	0.00	90.00	Uniform	45	N.A.	m
Pipe Diameter	0.00	0.50	Normal	0.25	0.025	m
Piper Length	0.00	100.00	Normal	40	5	m
Pressure Loss Factor	0.00	4.00	Uniform	0.5	N.A.	mm H2O/(m3/h/m2)
Q_1	4143.75	4356.25	Normal	4250	10.625	m3/h
Q_2	4265.63	4484.38	Normal	4375	10.9375	m3/h
Q_3	4460.63	4689.38	Normal	4575	11.4375	m3/h
Valve Flow Factor	0.00	50000	Uniform	12500	N.A.	m3/h
delta p_1	65.00	75.00	Normal	70	1.25	kPa
delta p_2	35.00	45.00	Normal	40	1.25	kPa
delta p_3	5.00	15.00	Normal	10	1.25	kPa

Unfortunately the ranking obtained for each of the regressions coefficients differed in a small to larger extent (Table 8.4). For most of the regression coefficients, motor efficiency and friction power loss were quantified as the by far most sensitive parameters. However, some of the regression coefficients identify either

the blower curve specific flow rates (Q_1, Q_2 and Q_3) or the pipe diameter as the most sensitive parameters. The different ranking may be induced by the nonlinear or absence of linear behaviour of the objective function in regard to the model parameters.

Table 8.4. Varying ranking based on the different regression coefficients of the sensitivity output from the Monte Carlo simulation (dark green cells imply a high sensitivity).

	LCC	NRC	ORC	PCC	SPC	SRC	VIF	tLCC	tPCC	tSPC	tSRC
Altitude	0.026	0.079	0.518	0.007	0.009	0.009	1.012	0.813	0.208	0.286	-1.274
Cut-off Head	0.046	0.339	2.165	0.028	0.038	0.039	1.023	1.411	0.859	1.180	0.719
Diffuser Surface Area	-0.038	-0.143	-2.145	-0.014	-0.019	-0.019	1.023	-1.156	-0.421	-0.579	2.962
Efficiency Motor	-0.205	-1.001	-1277.964	-0.181	-0.250	-0.252	1.021	-6.437	-5.604	-7.944	-1.454
Friction Power Loss	0.880	0.885	2160.105	0.544	0.881	0.890	1.022	56.980	19.754	57.262	-19.334
Gravity Air	0.020	2.291	2335.183	0.015	0.020	0.021	1.020	0.628	0.459	0.630	68.156
Liquid Density	0.015	0.762	0.776	0.025	0.035	0.035	1.016	0.453	0.775	1.065	1.583
Mean Water Height	-0.008	0.391	69.939	0.009	0.012	0.012	1.010	-0.256	0.279	0.383	2.675
Minor Losses	-0.008	0.022	0.494	0.006	0.009	0.009	1.024	-0.259	0.194	0.266	0.962
Pipe Diameter	-0.095	-0.619	-2520.925	-0.017	-0.023	-0.023	1.029	-2.952	-0.505	-0.693	0.669
Pipe Length	0.022	-0.231	-5.899	-0.001	-0.001	-0.001	1.010	0.663	-0.023	-0.031	-1.742
Pressure Loss Factor	0.053	-0.005	-10.728	-0.004	-0.006	-0.006	1.036	1.619	-0.124	-0.170	-0.079
Q1	-0.072	-6.577	-1.577	-0.021	-0.029	-0.029	1.024	-2.237	-0.640	-0.879	-0.428
Q2	0.038	6.734	1.569	0.020	0.028	0.028	1.018	1.177	0.618	0.849	-2.209
Q3	0.054	5.914	1.318	0.017	0.023	0.023	1.018	1.677	0.507	0.696	2.133
Valve Flow Factor	-0.021	0.018	0.001	0.003	0.004	0.004	1.021	-0.656	0.084	0.115	1.748
delta p1	0.003	-0.070	-1.015	-0.001	-0.002	-0.002	1.010	0.088	-0.039	-0.054	0.289
delta p2	-0.014	0.379	9.658	0.013	0.017	0.018	1.024	-0.443	0.392	0.538	-0.135
delta p3	0.022	0.089	9.092	0.012	0.016	0.016	1.021	0.687	0.362	0.497	1.352

Figure 8.12 shows the simulated variation in the mean power consumption for the different parameter combinations generated within the random sampling of the Monte Carlo simulation. Only a clear (but non-linear) evolution is observed for the mean in relation to the friction power loss. Values for motor efficiency within the acceptable range (from 50% efficiency up to almost 1) correspond to mean power consumption values over the entire range. However there seems to develop a pareto front at the lower end allowing for lower power consumption with higher efficiency but limiting the power consumption with lower efficiency. The valve flow factor does not display any correlation to the mean power consumption and neither do the other investigated parameters.

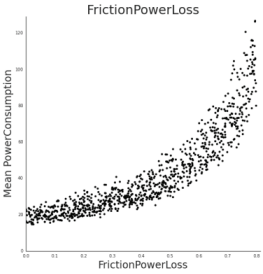

a

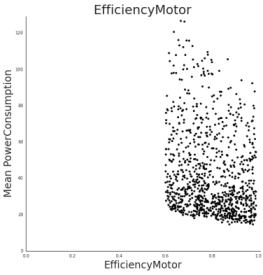

b

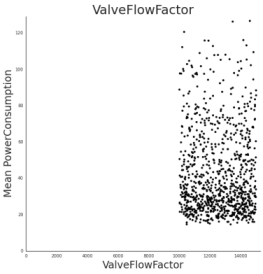

c

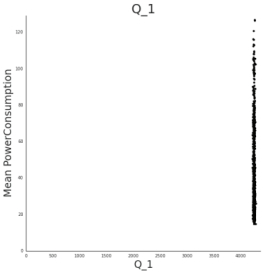

d

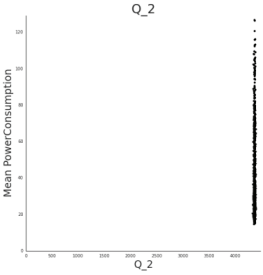

e

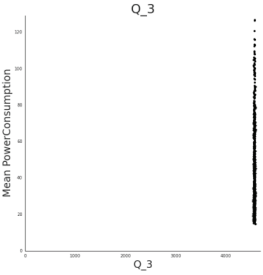

f

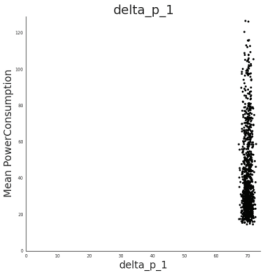

g

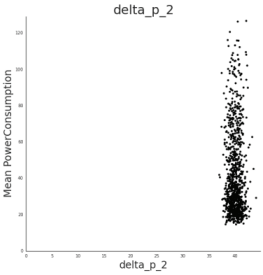

h

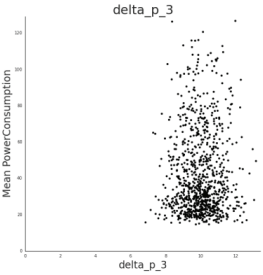

i

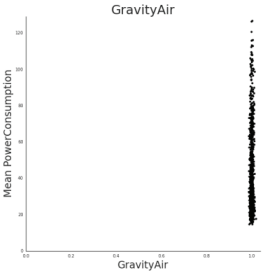

j

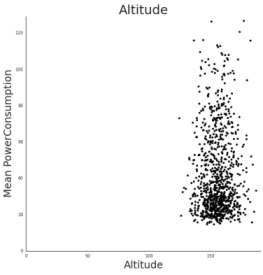

k

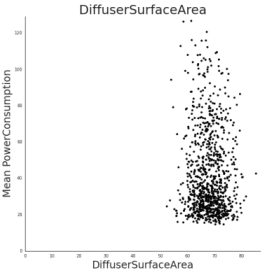

l

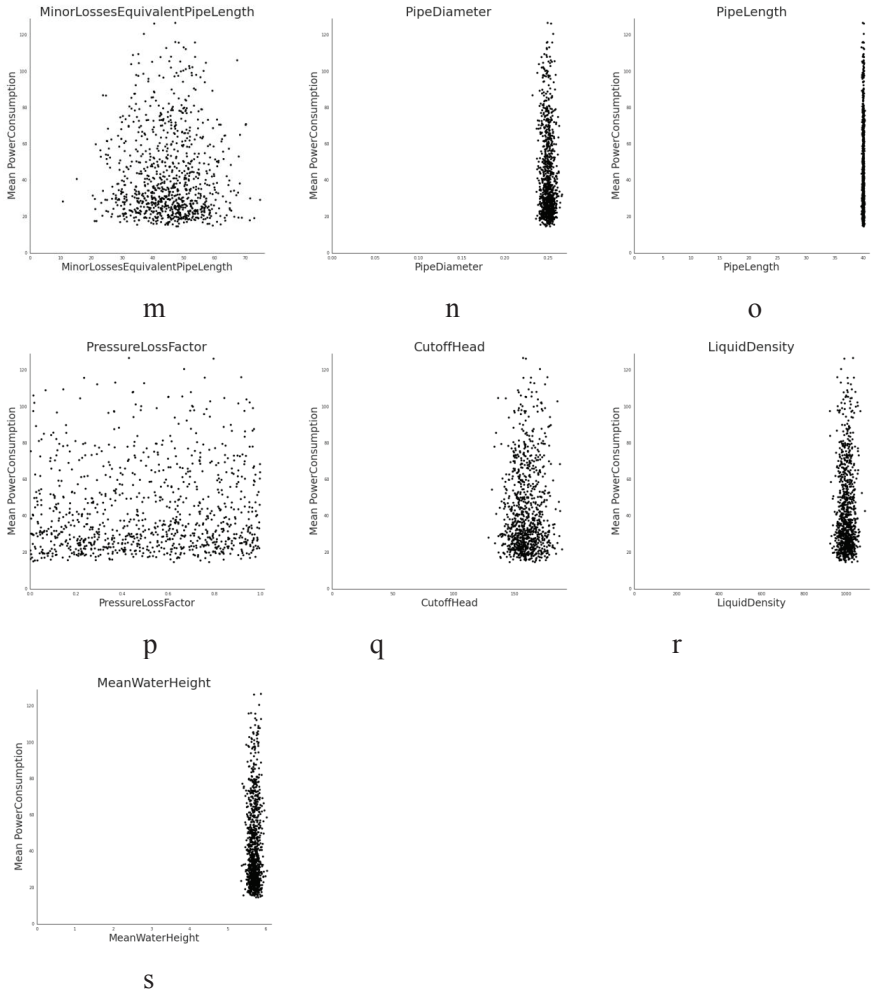

Figure 8.12. Dotty plots showing the lack of linear behaviour of the mean of the simulated power consumption for the different parameter values generated within the Monte Carlo simulation. (a) Friction power loss, (b) motor efficiency, (c) valve flow factor, (d) Q_1, (e) Q_2, (f) Q_3, (g) Δp_1, (h) Δp_2, (i) Δp_3, (j) gravity, (k) Altitude, (l) diffuser surface area, (m) minor losses equivalent pipe length, (n) pipe diameter, (o) pipe length, (p) pressure loss factor, (q) cut-off head, (r) liquid density and (s) mean water height.

Finally, the global screening method based on Elementary Effects (EE) proposed by Morris et al. (1991) was applied. The screening was conducted with 20 intervals and 60 optimized runs. The mean μ and the standard deviation σ of the distribution of the elementary effects and also on the mean of the distribution of the absolute values of the EE, μ^* were calculated to allow for ranking and evaluation of the results (Campolongo et al., 2007). For the three evaluation criteria the friction power loss and the pipe diameter are the most sensitive parameters in regard to the

power consumption. Small differences occur in the ranking for the less sensitive parameters. In this work μ* is considered as the main driver for the ranking as it prevents that EE with different signs cancel each other (Van Hoey et al., 2014). The most sensitive parameter, according to the ranking in regard to both the mean of the simulation results and the mean difference of the simulation results with the measured data, proved to be the friction power loss (FP) followed by the pipe diameter, Δp_3, η_m, Q_3, Q_2, Δp_1, diffuser surface area, Q_1 and Δp_2 (Figure 8.14).

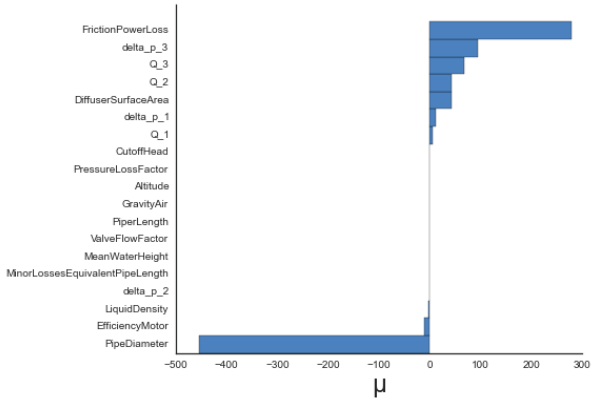

Figure 8.13. The ranking of the parameters according to the mean (μ) for the distribution of the EE in the applied global screening method.

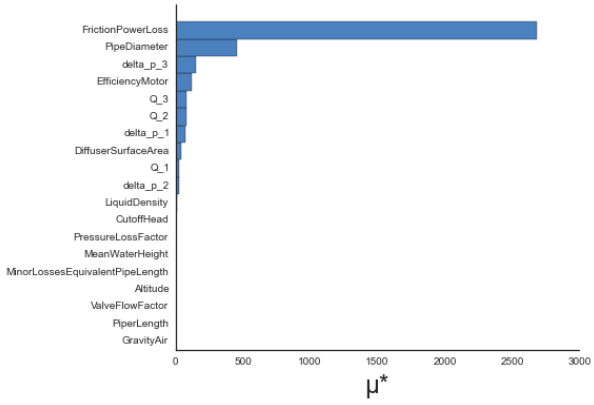

Figure 8.14. the ranking of the parameters according to the mean (μ*) for the distribution of the absolute values of the EE in the applied global screening method.

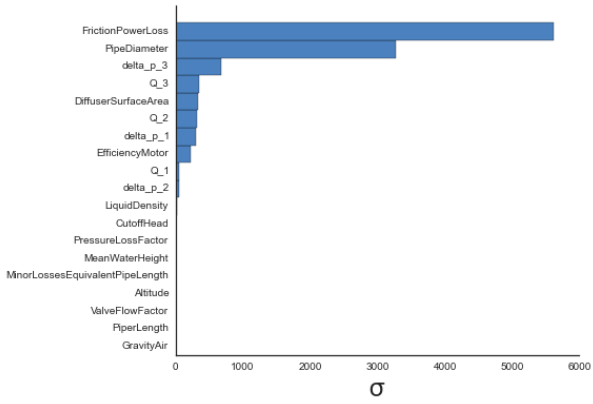

Figure 8.15. the ranking of the parameters according to the standard deviation (σ) for the distribution of the EE in the applied global screening method.

The ranking obtained was then used in an automatic parameter estimation experiment (estimating the 4 most sensitive parameters) using a constrained simplex optimization algorithm (Nelder and Mead, 1965a). The estimated parameters differed significantly from the parameter estimation based on the local sensitivity analysis, FP=9.64E-2±5E-5, d=2.8521E-1±9E-5 and Δp_3=4377.5217±6E-4 η_m=5.502E-1±3E-4. The root of the sum of squared errors proved to be slightly better (1.064 versus 1.103) pointing towards an even better fit (Figure 8.16). In addition, the uncertainty bounds on the parameter estimates improved drastically.

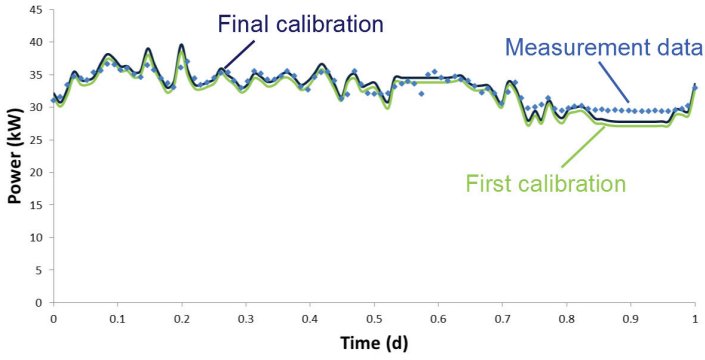

Figure 8.16. The final calibrated dynamic model (dark blue line) shows an even better fit, including the trends, to the measurement data (blue dots) then the first calibration attempt (green line).

8.5.4. Comparison to other models

Comparison is made with constant average power consumption (a fixed ratio power consumption over flow rate) models (Figure 8.18). The cumulative power consumption shows an exceptional fit to the measured data (Figure 8.17). On the other hand the model with the constant best fit average power consumption ratio performs excellent as well in regard to the cumulative power consumption. The model by Rosso and Stenstrom (2005) underpredicts the cumulative measured power consumption considerably.

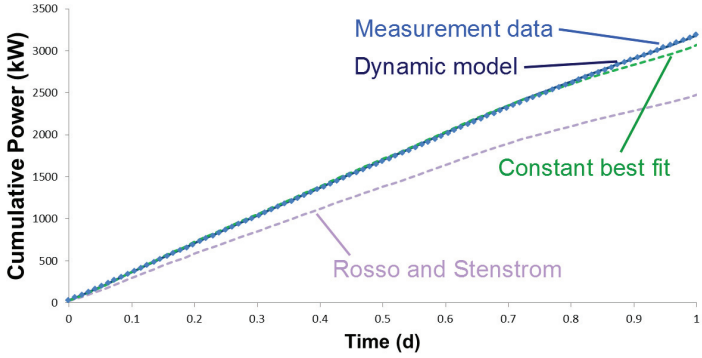

Figure 8.17. The exceptional fit of the cumulative power consumption for the dynamic model (dark blue line) to the measurement data (blue dots), outperforms the models with constant average power consumption ratios, although the model with the best fit for the average of the data (green dashed line) gives also a good fit. The model by Rosso and Stenstrom (2005) (purple dashed line) under predicts the measured cumulative power consumption.

Inspecting the dynamic data, the new detailed dynamic model shows a significantly better fit to the data than the constant average power consumption models. The root of the sum of squared errors for the new detailed dynamic model, the constant average power consumption model based on the parameters determined by Rosso and Stenstrom (2005) and best fit model constant average power consumption model are respectively 1.064, 7.694 and 3.469. Also the sum of squared errors SSE reveals the same improvement (112 versus 5742 and 1167). The mean of the constant average power consumption model based on the parameters determined by Rosso and Stenstrom (2005) reveals a consistent under prediction (a mean of 25.5 kW opposed to 32.9 kW for the measured data) explaining the high SSE. This result indicates that the model result should not be transferred blindly from one case to another. The best fit constant average power consumption model clearly performs better on the mean value (a mean of 31.7 kW opposed to 32.9 kW for the measured data). But the new detailed dynamic model outperforms both of them (a mean of 32.2 kW opposed to 32.9 kW for the measured data). The main difference,

however, is in the variance occurring in the model output. The average consumption models over predict the variance considerably (a standard deviation of 4.3 kW and 5.3 kW opposed to 2.3 kW for the measured data) and as such the peak energy demand. On the other hand, the new detailed dynamic model approaches the measured data variance closely (a standard deviation of 2.9 kW opposed to 2.3 kW for the measured data).

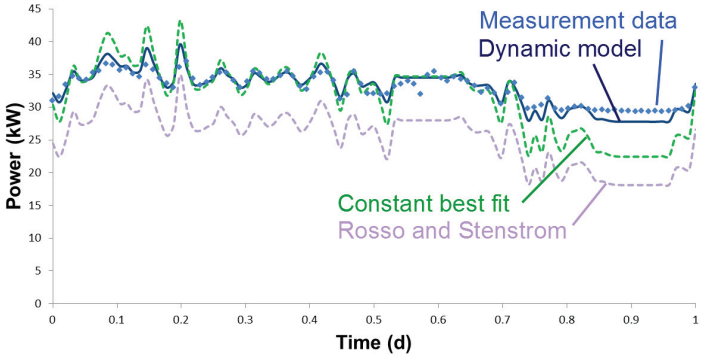

Figure 8.18. The dynamic model (dark blue line), describes the measurement data (blue dots) and its trends significantly better than the models with constant average power consumption ratios. Both the model by Rosso and Stenstrom (2005) (purple dashed line) and the model with the best fit for the average of the data (green dashed line) show larger variations.

In view of a global optimization study for WWTPs, including many different parameters as effluent quality, energy consumption and greenhouse gas emissions, the newly developed and rigorously calibrated model adds another dimension. I.e. the model restores the balance by adding dynamics in the calculation of the energy consumption, which have a smoothening effect compared with the flow rate data. This dynamic calculations, which are worked out in a high detail for the influent characteristics and in the biokinetic model, allow now for a more accurate estimation of the peak energy demand. This peak energy demand is crucial as determines the energy price setting.

Furthermore the study demonstrated that care has to be taken when transferring results from another study and a proper evaluation of the background should be performed. I.e. the type of blowers and the system characteristics (height of the water level, type of diffusers, etc.) influence highly the obtained results.

8.6. CONCLUSIONS

A new dynamic model for a more accurate prediction of aeration energy costs in activated sludge systems, equipped with submerged air distributing diffusers (producing coarse or fine bubbles) connected via piping to blowers, has been developed and demonstrated. The new model proved to give an accurate prediction of the real energy consumption by the blowers and captures the trends better than the constant average power consumption models currently being used. In addition it is demonstrated that transferring model parameters from one installation to the other introduces a large risk in incorrectly predicting the power consumption.
The results clearly illustrate, also because the cost of energy depends on peak demand values, that the dynamic model is preferably used in multi-criteria optimization exercises for minimizing the energy consumption.

8.7. ACKNOWLEDGEMENTS

The authors would like thank the financial support received from the EU FP7-SME-2008-1 program (project ADD CONTROL 232302) as well all project partners (http://www.addcontrol-fp7.eu/). They would also like to thank Waterboard the Dommel for the data on the energy consumption of their pump.

Chapter 9

Detailed dynamic pumping energy models for optimization and control of wastewater applications

"If I have seen further it is by standing on the shoulders of Giants."
Isaac Newton

9.1. ABSTRACT

Despite the increasing level of detail in wastewater treatment process models, oversimplified energy consumption models (i.e. constant "average" power consumption) are being used in optimization exercises. A new dynamic model for a more accurate prediction of pumping costs in wastewater treatment has been developed to overcome this unbalance in the coupled sub-models. The model is calibrated using two case studies. The first case study concerns the centrifugal influent pumps (Nijhuis RW1-400.525A) of the municipal WWTP of Eindhoven (the Netherlands), governed by Waterboard the Dommel. For the second case study, a centrifugal pump (Flygt, type NT3153.181) of the intermediate pumping station (pumping primary treated wastewater) of the Mekolalde WWTP located in Bergara (Guipúzcoa, Spain), a model extension was necessary in order to allow a better description of the pump curve, making the model more generic. Both cases showed good agreement between the model predictions and the measured data of energy consumption. The model is also more accurate compared to approaches to quantify energy consumption thus far. This paves the way towards 'global' process optimisation and new, improved control strategies for energy reduction at WWTPs.

Part of this chapter was published as:
De Keyser, W., Y. Amerlinck, G. Urchegui, T. Harding, T. Maere, and I. Nopens, 2014, Detailed dynamic pumping energy models for optimization and control of wastewater applications: Journal of Water and Climate Change, v. 5, p. 299-314.

9.2. SYMBOLS

A_{pl}, B_{pl}, C_{pl}	Factors of the power law describing the pump curve (-)
A_{qp}, B_{qp}, C_{qp}	Factors of the quadratic polynomial describing the pump curve (-)
A_{sa},B_{sa},C_{sa},D_{sa},E_{sa},F_{sa},G_{sa}	Coefficients of the sixth order approximation of the pump curve (-)
$CorrF$	Correction factor for a varying impeller pump speed (-)
C_{TSS}	Concentration of total suspended solids (g/l)
d_i	Internal pipe diameter for the different segments (m)
$d_{discharge}$	Internal pipe diameters of the discharge outlet (m)
$d_{suction}$	Internal pipe diameters of the suction inlet (m)
f	Darcy friction factor (-)
f_i	Darcy friction factor for the different segments (-)
g	Gravitational acceleration (m/s²)
H	Head (m)
H_1	Pump head for the first selected point on the pump curve (preferably at the intercept) (m)
H_2	Pump head for the second selected point on the pump curve (m)
H_3	Pump head for the third selected point on the pump curve (m)
$H_{discharge}$	Water levels at the discharge well (m)
H_{OP}	Head at normal operating point (m)
H_p	Pump head (m)
$H_{p,min}$	Minimum efficiency
$H_{p,max}$	Maximum efficiency
H_{ref}	Reference pump head or design head (m)
H_s	System head (m)
H_{stat}	Static head loss or static pumping head (m)
$H_{suction}$	Water levels at the suction well (m)
$H_{throttling}$	Head at the new operating point with a partially closed throttling valve (m)
H_{VFD}	Head at the new operating point with speed reduced by VFD control (m)
k	Flow consistency index (-)
K_f	Friction loss coefficient due to pipes and fittings ($s^2\ m^{-5}$)
K_v	Velocity head loss coefficient ($s^2\ m^{-5}$)

L	Pipe length (m)
M	Relative motor load (-)
n	Flow behaviour index (-)
N	Relative pump speed (-)
$N_{desired}$	Desired pump speed (-)
N_{min}	Minimal pump speed (-)
N_{max}	Maximal pump speed (-)
N_{ref}	Impeller speed at the reference pump head (-)
P	Shaft power or pumping power (kW)
P_{actual}	Actual power draw (kW)
$P_{nom,N}$	Nominal motor power for a certain pump speed (kW)
P_{nom}	Nominal motor power (kW)
Q	Flow rate (m³/h)
Q_2	Flow rate for the second selected point on the pump curve (m³/h)
Q_3	Flow rate for the third selected point on the pump curve (m³/h)
Q_{actual}	Actual flow rate that the pump delivers (m³/h)
Q_{BEP}	Flow rate at which best efficiency is reached (m³/h)
$Q_{controlled}$	Flow rate at the new operating point with either the partially closed throttling valve or speed reduced by VFD (m³/h)
$Q_{desired}$	Desired flow rate (m³/h)
Q_{min}	Minimal possible flow rate that the pump can deliver (m³/h)
Q_{max}	Maximal possible flow rate that the pump can deliver (m³/h)
Q_{OP}	Flow rate at the normal operation point (m³/h)
Re	Reynolds number (-)
SG	Fluid's specific gravity (-)
$z_{discharge}$	Vertical elevation of the discharge point (m)
$z_{suction}$	Vertical elevation of the suction point (m)
ε	Roughness height (m)
η_m	Motor efficiency (-)
η_p	Pump efficiency (-)
$\eta_{p,min}$	Minimum pump efficiency (-)
$\eta_{p,max}$	Maximum pump efficiency (-)
$\eta_{p,OP}$	Pump efficiency at the normal operating point (-)

$\eta_{p,throttling}$	Pump efficiency at the new operating point with a partially closed throttling valve (-)
$\eta_{p,VFD}$	Pump efficiency at the new operating point with speed reduced by VFD control (-)
η_t	"wire-to-water" efficiency or total efficiency (-)
η_{VFD}	VFD efficiency (-)
$\eta_{VFD,min}$	Minimal VFD efficiency (-)
$\eta_{VFD,max}$	Maximal efficiency (-)
μ	Dynamic viscosity (Pa.s)
ρ	Density (kg/m³)
ρ_{ss}	Density of the suspended solids (kg/m³)
ρ_{water}	Density of water (kg/m³)

9.3. INTRODUCTION

Pumping systems account for nearly 20% of the world's energy usage and the more efficiently they are operated, the greater the cost savings to the owner (Davidson and Benson, 2003). For water utilities, pumping is the prime user of power, typically 90% to 95% of the total energy purchases are used by pumping plants (Bunn, 2007). On wastewater treatment plants (WWTPs) pumping is the second largest energy consumer – aeration being the largest (Ast et al., 2008; Devisscher et al., 2006; Fenu et al., 2010; Tchobanoglous et al., 2004; Zahreddine et al., 2010).
Observations from practice learn that many pumps are working far from their optimal efficiency point due to over-dimensioning in the design phase of treatment plants or due to configurational changes during the plant's service life. This implies that there is a large energy savings potential in optimizing the employed pumping infrastructure and its automation and control system.
Water use tends to peak in the same diurnal profile as energy demand thereby increasing the need for pumping during peak energy periods and consequently increasing the need for less efficient electricity generators/sources to enter the market to supply energy. Shifting energy use from peak to off peak therefore can significantly reduce the greenhouse gas foot print and result in cost savings achieved by purchasing cheaper energy (Bunn, 2007).
Mathematical models could help in this optimization exercise by testing different scenarios without harming the real system. However, models with a sufficient level of detail are required to come to the right answers.

Automatic control represents a promising technology whose adoption in full-scale plants can contribute to further improve current effluent quality, process robustness and operational cost. Plant-wide control, considering the interactions between different unit-processes, is increasingly replacing the traditional perspective of local control. Designing a successful controller requires detailed know-how about the entire system: (1) the process to be controlled and its response to control actions; (2) the instrumentation and actuators; and (3) the automation and control system. Lack of specific tools for supporting the design and validation of practical control solutions is a bottleneck to achieve the consolidation of automatic control in the water industry. Within the FP7 SME EU Project ADD CONTROL such a framework has been developed (Maiza et al., 2011).

Today, more and more studies are reported where energy consumption is being calculated in combination with process models. However, despite the relatively high level of detail in the process models, very simplified energy consumption models are being used, i.e. mostly a fixed averaged energy consumption/cost regardless of the delivered pumping flow rate as illustrated in Table 9.1 (Amerlinck et al., 2009; Copp, 2002; Devisscher et al., 2006; Gernaey et al., 2014; Maere et al., 2011). However, as these models have the interesting potential to be used in multi-criteria optimization exercises (e.g. optimizing effluent quality, greenhouse gas emissions and operational costs simultaneously(Flores-Alsina et al., 2014)), they may lead to poor predictions and their use in optimization could lead to suboptimal operation.

The assumption of the energy consumption being constant over the entire range of flow rates that the pump delivers is a very rough approximation and could give rise to misleading cost calculations if the pump is operating constantly at higher or lower power consumption. As a general rule, operation of pumps at flows less than approximately 25 to 30 percent of the best efficiency point is undesirable. Also the motor efficiency deteriorates significantly if loading is reduced to 25 percent or lower (Henderson and Reardon, 2004). A variable frequency drive (VFD) controlling a pump motor that usually runs less than full speed can substantially reduce energy consumption over a motor running at constant speed for the same period of time (Monteith et al., 2007).

Table 9.1. Fixed energy consumption cost values reported in the literature.

Reference	Pumped flows	Pumping energy (kWh/m³)
BSM1 (Copp, 2002)	All	0.040
BSM2 (Gernaey et al., 2006)	Mixed liquor recycle - Secondary sludge recycle - Secondary sludge to thickener - Primary sludge to digester - Thickened secondary sludge to digester - Dewatering liquid to primary clarifier	0.004 - 0.008 - 0.050 - 0.075 - 0.060 - 0.004
Combined algae production with WWTP (Beal et al., 2012)	Pumping wastewater – Pumping Primary sludge – Pumping secondary sludge	0.037 (133 J/l) – 0.0089 (32.2 J/l) – 0.013 (48.3 J/l)
Engineered wetlands (Austin and Nivala, 2009)	Recycle pumps	$\frac{\rho \cdot g \cdot H_{stat}}{\eta_p \cdot \eta_m}$
MAgIC (Devisscher et al., 2006)	All	$\frac{\rho \cdot g \cdot H_{stat}}{\eta_t}$
WWTP of Ostend (Amerlinck et al., 2009)	Empirical relationship for Archimedes screws	4.2+1.79879e-4x24xH_{stat}
MBR (Maere et al., 2011)	Activated sludge pumps - permeate and backwashing pumps	0.0075 – 0.075
Seawater desalination (Monteith et al., 2007)	desalination	2

In this chapter, dynamic models for centrifugal AC motor driven pumps (Figure 9.1), which are widely used in WWTPs to pump influent, mixed liquor, return sludge and effluent, are developed and calibrated. The aim is to obtain a more accurate calculation of dynamic pumping energy with an easy-to-use model that is compatible with currently used activated sludge models. It is shown that modelling power consumption dynamically yields a significantly more accurate prediction of energy consumption compared to the commonly used static approaches.

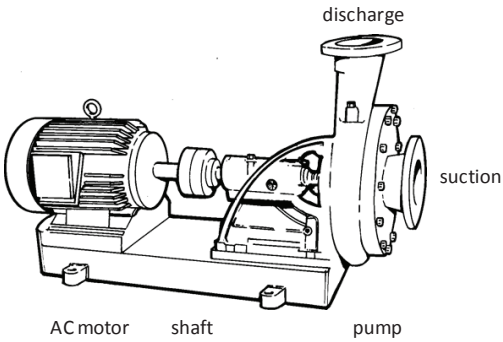

Figure 9.1. Schematic drawing of an AC motor driving a centrifugal pump.

9.4. MATERIAL AND METHODS

9.4.1. Pump curve and system curve

Each pump delivers a certain flow rate (Q), decreasing as function of the pressure (or "head", H) at its discharge flange. This pump characteristic curve is provided by pump manufacturers and typically also shows pump efficiency (η_p) and required shaft power (P). The latter is the mechanical power that needs to be delivered by the pump motor. Note that this pump characteristic curve is only valid for a single pump with a single-sized impeller operating at a single speed. The total head delivered by the pump shows a monotonic decreasing trend with increasing flow rate, whereas the pump efficiency shows a clear optimum with varying flow rate (Figure 9.2). This optimum of the pump efficiency curve is called the Best Efficiency Point (BEP), although the term usually refers to the flow rate at which the best efficiency is reached (Q_{BEP}).

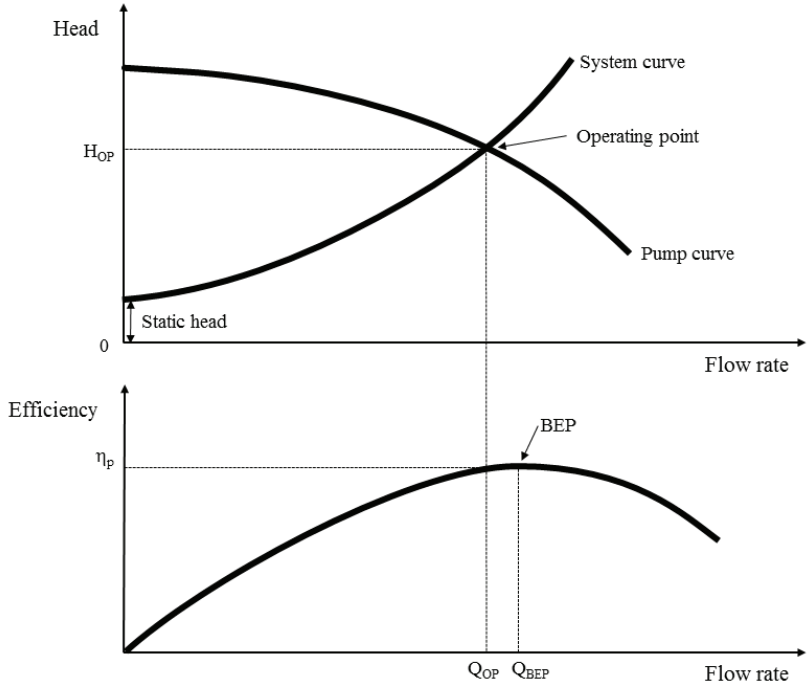

Figure 9.2. Schematic representation of pump curve, system curve and efficiency curve.

While in operation, a pump experiences a combination of static head (actual lift between suction and discharge point) and dynamic head (friction head losses due to

water flow through the piping system including valves and fittings). The total head, i.e. the sum of the static head and the dynamic head, in the system in relation to the delivered flow rate is described by the system curve. There is only one intersection of the system curve with the pump curve, i.e. the duty point or operating point, expressing the only possible flow rate and pressure in that particular system with that particular pump configuration and pump settings (e.g. speed) (Figure 9.2, top). The operating point coincides with a certain efficiency and power consumption. For a well-designed system this operating point should be as close as possible to the Best Efficiency Point (BEP).

9.4.2. Controlling pumps

However, the desired flow rates and, hence, power consumption are usually not constant. Two methods are commonly applied in practice to control the flow rate: (1) a throttling valve downstream the pump (steepening the system curve) or (2) modifying the rotational speed of the pump impeller (moving up or down the pump curve) through Variable Frequency Drives. The first (and oldest) method is to install a throttling valve downstream of the pump. Adjusting the position of the control valve results in more friction (dynamic system head) and consequently in a changed system curve. The operating point hereby shifts *along the pump curve* (Figure 9.3, top) but no change in the efficiency curve is introduced. The second method is often promoted in the framework of reducing energy consumption and is based on modifying the rotational speed of the pump impeller, thereby repositioning the pump curve. The operating point now shifts *along the system curve* (Figure 9.3, top). Variable speed pumping can be implemented by a transmission device (placing a gearbox in between the motor and the pump shaft), or by altering the motor speed. The latter could energetically be very efficient (in comparison to throttling) and is mostly achieved by applying Variable Frequency Drives (VFD). These electronic devices modify the frequency and voltage that are supplied to the pump motor. Since the speed of an AC induction motor depends on (the number of phases and) the frequency of the supplied current, it is possible to change motor (and thus pump) rotational speed without adding unnecessary system head.

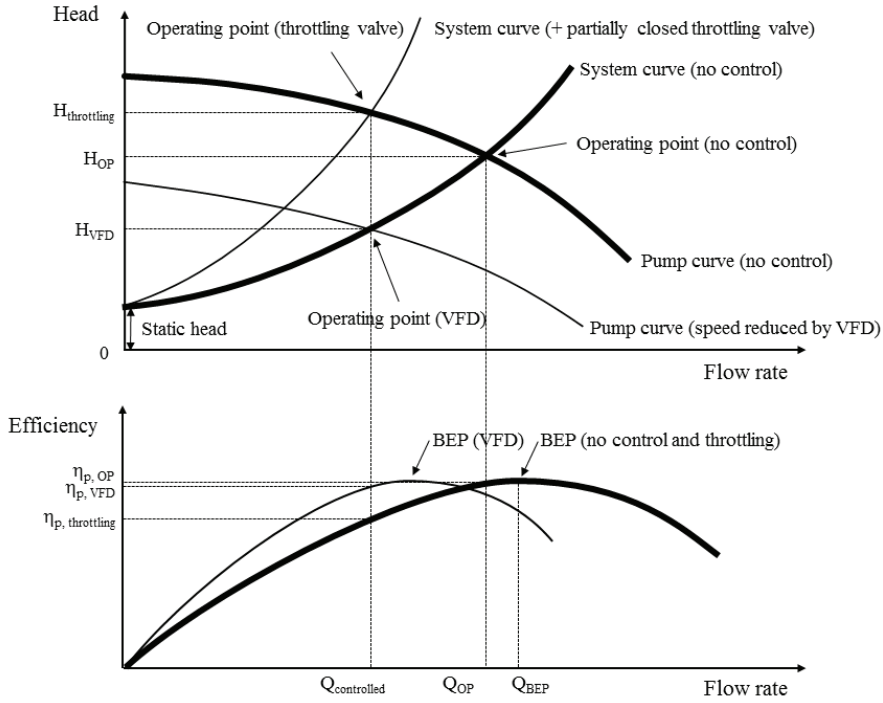

Figure 9.3. Schematic representation of pump curve, system curve and efficiency curve and the influence of throttling valve control and VFD control.

The necessary pumping power (P) is proportional to the head (H) and flow rate (Q), and inversely proportional to the total "wire-to-water" efficiency (η_t). The latter is the product of the pump efficiency (η_p), the motor efficiency (η_m) and – if applicable – the VFD efficiency (η_{VFD}). Note that the pump efficiency curve is horizontally squeezed or stretched in function of the pump speed (Figure 9.3, bottom). This is the key to higher efficiencies at reduced flow rates in comparison to throttling, where the pump efficiency is read from the original efficiency curve and thus is lower. The motor's efficiency clearly deteriorates at low motor loadings, whereas it is more or less constant at its half to full rated load (Figure 9.4). Rooks and Wallace (2003), Walski (2003) and the US Department of Energy (2008) report the well-known fact that VFD efficiencies have significantly improved the last decade, usually to being above 90%, but the losses are still significant and should be accounted for.

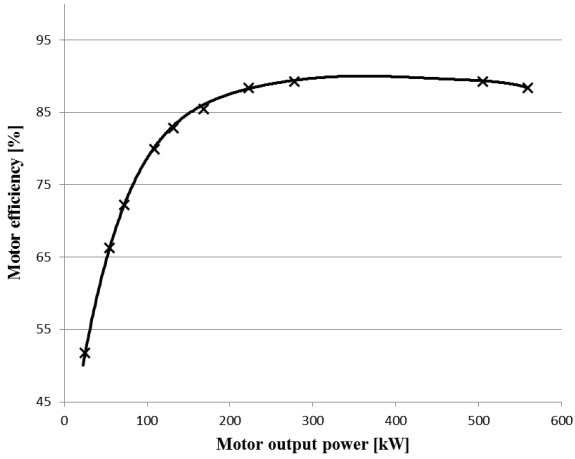

Figure 9.4. Efficiency characteristic of an electric motor redrafted from Ulanicki et al. (2008).

9.4.3. Mathematical model

In this section, the generic dynamic models that were developed for both throttled and VFD controlled pump systems are introduced. In contrast to textbook knowledge and pump manufacturer data (that are often intended for selecting a pump for a certain application), these models can be used to dynamically calculate the energy consumption of a certain motor-pump combination, hereby accounting for the required flow rate as well as the VFD or throttling valve actions. The basic assumption is always that the dynamic pump model input is the desired flow rate ($Q_{desired}$), as demanded by the controller, and that the dynamic model outputs are the actual flow rate (Q_{actual}) and actual power draw (P_{actual}), given certain pump and system characteristics that need to be specified by the user. These system characteristics can be parameters that are fixed during the simulation (e.g. the pump curve at full speed, piping layout, etc.) or dynamic model inputs that vary in time (e.g. the water level in suction and discharge tanks, water temperature, etc.). Note that most equations for variable speed pumps can also be written in terms of the relative pump speed (N) as the independent variable. This allows transforming the model in a way that desired speed is the input signal ($N_{desired}$) rather than $Q_{desired}$. This approach links better to reality, where the WWTP's automatic control system instructs the actuators to run at a certain percentage of their maximum capacity. However, in an integrated water quality modelling context, it is common to use the pumped flow rate as the controlled variable. This flexibility was included in the model.

9.4.4. The mathematical model for the system curve

The pumped flow rate and the power consumption can be calculated based on the descriptions of the system curve and the pump curve. The system curve is calculated based on the head developed in the system, H_s [m] and is composed out of four components, i.e. elevation, friction, a velocity gradient and a pressure difference. It was chosen to ignore the pressure difference because the majority of cases exist of open suction and discharge tanks at atmospheric pressure. Taking this into account, the developed head can be written as a function of the flow rate Q [m^3h^{-1}] as:

$$H_S = H_{stat} + \left(K_f + K_v\right) \cdot Q^2 \quad (9.1)$$

where H_{stat} is the static head loss, K_v the velocity head loss coefficient and, K_f the friction loss coefficient due to pipes and fittings which are respectively defined as:

$$H_{Static} = \left(H_{discharge} + z_{discharge}\right) - \left(H_{suction} + z_{suction}\right) \quad (9.2)$$

where $H_{discharge}$ [m] and $H_{suction}$ [m] are the water levels at the discharge and suction well respectively and $z_{discharge}$ [m] and $z_{suction}$ [m] the vertical elevation of the discharge and suction point from a reference point.

$$K_v = \frac{1}{2 \cdot g} \cdot \left(\frac{4}{\pi}\right)^2 \cdot \left(\frac{1}{d_{discharge}^4} - \frac{1}{d_{suction}^4}\right) \quad (9.3)$$

where g is the gravitational acceleration (9.81 [m/s²]), $d_{discharge}$ [m] and $d_{suction}$ [m] are the internal pipe diameters of the discharge outlet and suction inlet.

$$K_f = \sum_i \left(\frac{1}{2 \cdot g} \cdot \left(\frac{4}{\pi \cdot d_i^2}\right)^2 \cdot f_i \cdot \frac{L_i}{d_i}\right) \quad (9.4)$$

where L_i is the pipe length [m], d_i the internal pipe diameter for the different segments (pipes, elbows and fittings) [m], and f_i the friction factor for the different segments [-]. Equation 9.4 is a deduction of the well-known Darcy-Weisbach equation. Several methods, either implicit or explicit in nature, exist for solving for the Darcy-Weisbach friction factor. For laminar flow regimes, i.e. for Re smaller or equal to 2400, the friction factor f can be estimated by Equation 9.5.

$$f = \frac{64}{Re} \quad (9.5)$$

where Re is the Reynolds number [-] calculated as in Equation 9.6.

$$Re = \frac{\rho \cdot \left(\frac{4 \cdot Q}{3600 \cdot \pi \cdot d^2}\right) \cdot d}{\mu} = \frac{\rho \cdot Q}{900 \cdot \mu \cdot d \cdot \pi} \quad (9.6)$$

where ρ is the fluid's density [kg/m³] and μ the dynamic viscosity [Pa s].

Note that the fluid's behaviour in WWTPs is here considered Newtonian for the water and mixed liquor suspended solids lines. For turbulent flows, i.e. Re larger than 2400, contrary to laminar flows the distinction between Newtonian and non-Newtonian is important. As general rule one can say that mixed liquor suspended

solids flows with total suspended solids (TSS) concentrations in the lower ranges exert Newtonian behaviour and thickened sludge, with TSS in the higher ranges, exert non-Newtonian behaviour (Liu and Garcia, 2011). For turbulent flows showing Newtonian behaviour, the Swamee-Jain equation (Equation 9.7) can be used.

$$f = 0.25 \cdot \left(\log_{10}\left(\frac{\varepsilon}{3.7 \cdot d} + \frac{5.74}{Re^{0.9}}\right)\right) \quad (9.7)$$

where ε is the Roughness height (m).

Following the approach described by (Maere et al., 2009), Equations 9.8 to 9.12 are proposed to describe the friction phenomena in the case of turbulent flows for fluids showing non-Newtonian behaviour (the single quote ‘ in the variable names indicates that the variables are specifically calculated for non-Newtonian fluids):

$$f' = 0.3168 \cdot n^{0.675} \cdot Re'^{-0.2} \quad (9.8)$$

where *f'* is the Darcy-Weisbach friction factor for non-Newtonian fluids, *n* is the flow behaviour index (-) and *Re'* is the Reynolds number (-) calculated similar to Equation 9.6, but using the bulk apparent viscosity (η_b) instead of the dynamic viscosity (μ) and ρ is the fluid's density [kg/m³], which can be calculated according to Equation 9.9.

$$\rho = C_{TSS} + \left(1 - \frac{C_{TSS}}{\rho_{ss}}\right) \quad (9.9)$$

where ρ_{ss} is the density of the suspended solids [kg/m³], C_{TSS} is the concentration of total suspended solids (g/l) and ρ_{water} is the density of water [kg/m³].

The apparent viscosity of a non-Newtonian fluid is not constant and when considering that sludge can be described by the Ostwald - de Waele law for fluids with pseudo-plastic behaviour (Ratkovich et al., 2013), one can calculate the apparent viscosity of sludge in the bulk region μ' of a full-flowing circular pipe with Equation 9.10.

$$\mu' = k \cdot \left(\frac{3 \cdot n + 1}{4 \cdot n}\right)^n \cdot \left(\frac{8}{d} \cdot \left(\frac{4 \cdot Q}{3600 \cdot \pi \cdot d^2}\right)\right)^n \quad (9.10)$$

where *k* is the flow consistency index (-) and *n* is the flow behaviour index (-). Rosenberger et al. (2002) proposed the following models to determine *k* and *n* of sludge as function of TSS, which should be used with care when calibrated (Ratkovich et al., 2013).

$$k = 0.001 \cdot e^{(2 \cdot TSS^{0.41})} \quad (9.11)$$

$$n = 1 - 0.23 \cdot TSS^{0.37} \quad (9.12)$$

Friction in elbows and pipe fittings is taken into account by calculating the equivalent pipe lengths (Table 8.1) and considering these as terms in the summation in Equation 9.2.

9.4.5. The mathematical model for the pump curve

A simplified mathematical model for the pump curve is proposed, following the pragmatic approach described in Walski et al. (2004) and Rossman (2000), expressing the pump curve as a power law (Equation 13) connecting three points (combinations of flow rate Q and head H) of the actual pump curve.

$$H_p = A_{pl} - B_{pl} \cdot Q^{C_{pl}} \tag{9.13}$$

The three points can be chosen randomly but it is advised to choose the first one as intercept with the Y axis, i.e. flow rate equal to zero, as this allows for an analytical solution for A_{pl}, B_{pl} and C_{pl} from Equation 13. For the three points $(0,H_1)$, (Q_2,H_2) and (Q_3,H_3) the analytical solution is given by Equations 14 to 16.

$$\mathrm{A_{pl}} = \mathrm{H_1} \tag{9.14}$$

$$\mathrm{B_{pl}} = (\mathrm{H_1} - \mathrm{H_3}) \cdot \mathrm{e}^{(-\mathrm{C_{pl}} \cdot \ln(\mathrm{Q_3}))} \tag{9.15}$$

$$\mathrm{C_{pl}} = -\ln\left(\frac{\mathrm{H_1}-\mathrm{H_3}}{\mathrm{H_1}-\mathrm{H_2}}\right) \cdot \left(\ln\left(\frac{\mathrm{Q_2}}{\mathrm{Q_3}}\right)\right)^{-1} \tag{9.16}$$

In case a complete pump curve is not available, it is advised to use a design operating point as (Q_2,H_2) and to estimate H_1 as 1.33 H_2, Q_3 as $2Q_2$ and H_3 as zero (Rossman, 2000).

The effect of frequency converters on the pump curve can be quantified by introducing the relative pump speed N [-] and combining Equation 13 with the affinity laws (Equations 17 to 19) resulting in Equation 20.

$$\frac{N_1}{N_2} = \frac{Q_1}{Q_2} \tag{9.17}$$

$$\frac{N_1}{N_2} = \sqrt{\frac{H_1}{H_2}} \tag{9.18}$$

$$\frac{N_1}{N_2} = \sqrt[3]{\frac{P_1}{P_2}} \tag{9.19}$$

$$H_p = N^2 \cdot A_{pl} - B_{pl} \cdot N^{2-C_{pl}} \cdot Q^{C_{pl}} \tag{9.20}$$

9.4.6. The mathematical model for the "wire-to-water" efficiency

As described in Ulanicki et al. (2008), the overall "wire-to-water" efficiency (η_t) is the product of the pump efficiency (η_p, modelled as a parabolic function of the flow rate Q and the relative pump impeller speed), the motor efficiency (η_m, modelled as an exponential function of the relative motor load) and, if applicable, the VFD efficiency (η_{VFD}, modelled as a 4th order function of the relative pump impeller speed).

The pump efficiency η_p is pump-specific and follows a parabolic trajectory as function of the flow rate and the relative pump impeller speed N. After evaluation of several pump curves, a parabolic function (Equation 21) is proposed in this work to describe the change in overall efficiency for a generic pump operating at its nominal speed.

$$\eta_p = -\left(\eta_{p,max} - \eta_{p,min}\right) \cdot \frac{\left(\frac{Q}{N}\right)^2}{Q_{BEP}{}^2} + 2 \cdot \left(\eta_{p,max} - \eta_{p,min}\right) \cdot \frac{\left(\frac{Q}{N}\right)}{Q_{BEP}} + \eta_{p,min} \qquad (9.21)$$

with $\eta_{p,max}$ the maximum efficiency [-], $\eta_{p,min}$ the minimum efficiency [-], Q_{BEP} the flow rate corresponding to the maximum efficiency [m³/h], N the actual impeller speed [-] and Q the actual flow rate [m³/h]. The minimum efficiency ($\eta_{p,min}$), is determined as the intercept of the parabolic efficiency curve on the vertical axis. In most cases, the latter will be zero. In cases where no specific pump efficiency curve is available, values between 0.75 and 0.90 can reasonably be taken as a default value for $\eta_{p,max}$ and the design flow rate can be used as an estimation of Q_{BEP}.

In many applications, motor efficiency is assumed to be constant at about 90%. However, this strongly depends on the motor load (Figure 9.4). Bernier and Bourret (1999) used an exponential function (Equation 22) to approximate η_m as function of the relative motor load M:

$$\eta_m = \eta_{m,max} \cdot \left(1 - e^{-0.0904 \cdot M}\right) \qquad (9.22)$$

A common value for $\eta_{m,max}$ is 0.9 to 0.95 [-]. The relative motor load can be calculated according to Equation 23, deduced from (Ulanicki et al., 2008).

$$M = \frac{P}{P_{nom,N}} = \frac{SG \cdot g \cdot Q \cdot H}{3600 \cdot \eta_p \cdot \left(P_{nom} \cdot N^3\right)} \qquad (9.23)$$

with P_{nom} the nominal motor power [kW], SG the fluid's specific gravity (i.e. the density of the fluid over the density of water) [-] and Q [m³/h] and H [m] are defined by the pump's operating point. Since in practice motors are slightly over dimensioned, a default value of 0.75 can be used for M in generic or hypothetical cases where no specific P_{nom} value is known.

Although most manufacturers only specify the VFD's full-load efficiency, it is clear from Rooks and Wallace (2003), Walski (2003) and US Department of Energy (2008) that η_{VFD} strongly depends on the relative load (or speed) and size. To cover this range of variation, an empirical fourth order function in relation to the pump speed is proposed here.

$$\eta_{VFD} = \frac{N^4 - {N_{min}}^4}{{N_{max}}^4 - {N_{min}}^4} \left(\eta_{VFD,max} - \eta_{VFD,min}\right) + \eta_{VFD,min} \qquad (9.24)$$

with N_{min} and N_{max} respectively the minimal (taken at N=0.5) [-] and maximal pump speed (taken at N=1) [-] and $\eta_{VFD,min}$ and $\eta_{VFD,max}$ respectively the minimal [-] and maximal VFD efficiencies [-].

This function approximates the curves reported in Rooks and Wallace (2003), Walski (2003) and US Department of Energy (2008) well for $\eta_{VFD,max}$ = 0.95 and

$\eta_{VFD,min}$ = 0.87. Extrapolation below relative loads less than N=0.5 is not recommended, but neither needed since in practice pumps are usually not run at speeds less than 50 to 60% of their nominal speed.

9.4.7. The mathematical model for the actual dynamic power consumption

The actual dynamic power consumption can now be calculated according to Equation 25 (Coulson et al., 1999):

$$P(t) = \frac{\rho \cdot g \cdot Q_{out}(t) \cdot H(t)}{3600 \cdot \eta_p(t) \cdot \eta_m(t) \cdot \eta_{VFD}(t)} \quad (9.25)$$

Integrating this over a time period with dynamic flows allows a better comparison of the proposed model compared to assuming a constant power consumption across the entire flow rate range.

When using the proposed model in a plant wide modelling context, the model will be fed (i.e. model input) with a desired flow rate $Q_{desired}$ [m³/h] (calculated by the plant's control algorithm). The flow rate that the pump actually delivers (Q_{actual}) will normally be equal to $Q_{desired}$, unless it is outside the operating window of the pump. The maximum possible flow rate that the pump can deliver (Q_{max}) is determined as the intersection of the system curve with a fully opened throttling valve and the pump curve for the maximum value of N in case of VFD control. The minimal possible flow rate (Q_{min}) is obtained similarly as Q_{max}, now using the minimum value for N instead of the maximum value.

9.4.8. Case studies

The model was implemented in the WEST (mikebyDHI) and evaluated for two independent case studies. The case studies were selected based on the availability of detailed measurements of the energy consumption, which is not a common measurement at a WWTP.

The first case study concerns the centrifugal influent pumps (Nijhuis RW1-400.525A) of the municipal WWTP of Eindhoven (the Netherlands), governed by Waterboard the Dommel. As the pump had been modified, a new pump curve was composed based on measurements at the plant. The following parameter values were derived from this newly composed pump curve: $\eta_{p,max}$ = 0.875, $\eta_{p,min}$ = 0, H_1 = 16.7 m, H_2 = 12.5 m, H_3 = 7.0 m, Q_2 = Q_{BEP} = 1500 m³/h, Q_3 = 2000 m³/h. The pump is driven by a three phase eight pole induction motor (Schorch DA7315M-DB71P-Z) with P_{nom} = 75 kW and $\eta_{m,max}$ = 0.937. The motor is fed by a recently installed VFD (Emotron FDU48-146 54CE) with $\eta_{VFD,max}$ = 0.98, N_{min} set at 0.68, receiving the desired frequency (≤ 50 Hz) from a PID controller. The latter controls

the water level in the intake tank at a fixed level set point. The piping system configuration (Figure 9.5) consists of a steel suction line with an inlet, a long sweep 90° elbow (∅ 0.85 m), 1.20 m horizontal pipe (∅ 0.85 m), and a reducer (from ∅ 0.85 to 0.40 m), whereas the steel discharge pipe consists of 7.60 m vertical pipe (∅ 0.40 m), 2.10 m horizontal pipe (∅ 0.40 m), two long sweep 90° elbows (∅ 0.40 m) and an outlet. The total lift (i.e. static head) is normally about 7.00 m but is calculated dynamically from the discharge level and the measured water level in the intake tank. Another dynamic model input is the desired flow rate Q_{desired}, which is in fact the actual output flow rate measured in reality and logged in the WWTP's SCADA system with a one-minute resolution. Assumptions were made for the pipe roughness ε = 1.50E-4 m (value for commercial steel and wrought-iron (Coulson et al., 1999)), the fluid's density ρ = 1000 kg/m³ and the dynamic viscosity μ = 0.0012 Pa.s (the fluid's behavior was assumed Newtonian).

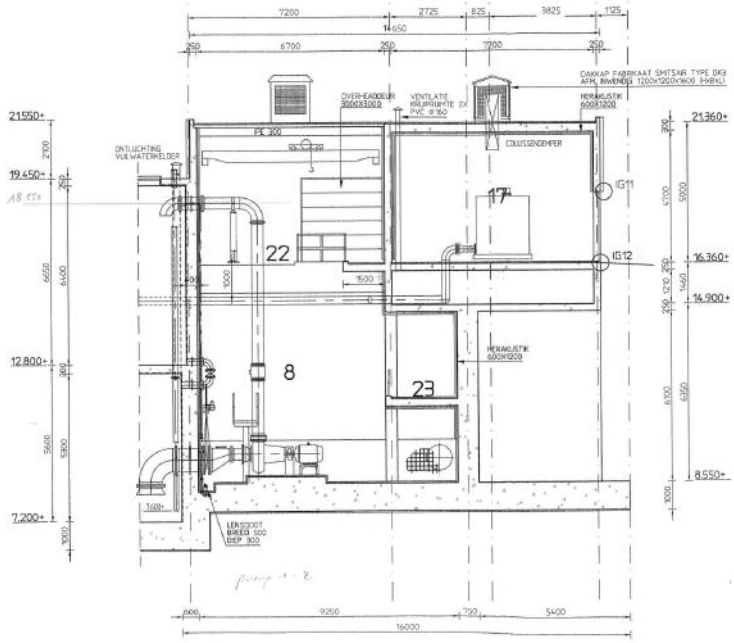

Figure 9.5. Schematic overview of the influent pumping system at the WWTP of Eindhoven.

The second case study deals with a pump (Flygt, type NT3153.181) of the intermediate pumping station (pumping primary treated wastewater) of the Mekolalde WWTP (originally designed to treat wastewater of 40,000 PE) located in Bergara (Guipúzcoa, Spain). The pump has a blade diameter of 186 mm and is powered by a 9 kW motor (for technical data see Table 9.2). Figure 9.11 shows the manufacturer's pump curve. The pump well has 4 pumps but due to the reduced capacity of the plant only one pump is in operation at a time. Each pump has an

individual discharge pipe of 250 mm diameter and 6 m length, with two elbows, these individual pipes discharge in a common pipe of 500 mm diameter and 6.6 m length. The water level in the intake tank is controlled to keep the elevation between intake water level and discharge water level constant at 3.97 m.

Table 9.2. Technical data of the intermediate pump of the WWTP of Mekolalde.

Technical data		
Cos Phi Engine	0.72	-
Efficiency Engine (Fully charged) η_{max}	85.5	%
Power Engine	9	kW
Nominal current	21	A
Nominal speed	955	rpm

9.5. RESULTS AND DISCUSSION

9.5.1. Case study 1

Figure 9.6 shows the two model inputs (static head H_{stat} and required flow rate $Q_{desired}$) and the simulated operating head H for the Nijhuis pump (case 1). In normal condition the static head is around 7.5 m. A rise in the water level (i.e. caused by a rain event), which can be seen by the decreasing static head, causes the PID controller in the WWTP's control system to increase the desired flow rate. The static head decreases with an increase in the water level because the static head is calculated as the difference between the discharge level (fixed) and the level (variable). The correlation between the total head and the flow rate can also be deduced from Figure 9.6.

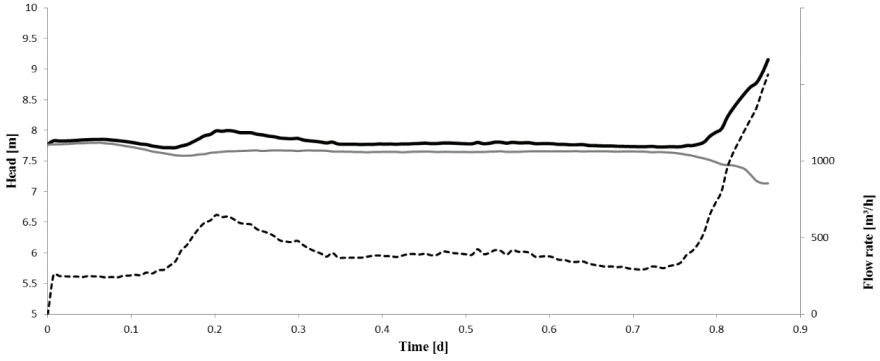

Figure 9.6. Model inputs, static head (grey full line, left axis) and incoming flow rate (dashed line, right axis) and the simulated operating head (black full line, left axis).

Figure 9.7 compares the dynamically modelled power consumption with actual data. Figure 9.7 (left) shows the real (as logged in the SCADA system) and modelled power consumption as function of the actual flow rate. The power

consumption is predicted perfectly for low flow rates whereas some deviations occur at higher flow rates. Figure 9.7 (right) shows the scatter plot of the modelled power consumption and the real power consumption. Data points on the bisector indicate a perfect prediction. The modelled power consumption, using the newly developed dynamic model, yields a reliable prediction of dynamic power consumption, especially within the frequently operated range of the pump. A slight overestimation is seen for elevated flow rates (e.g. during rain events).

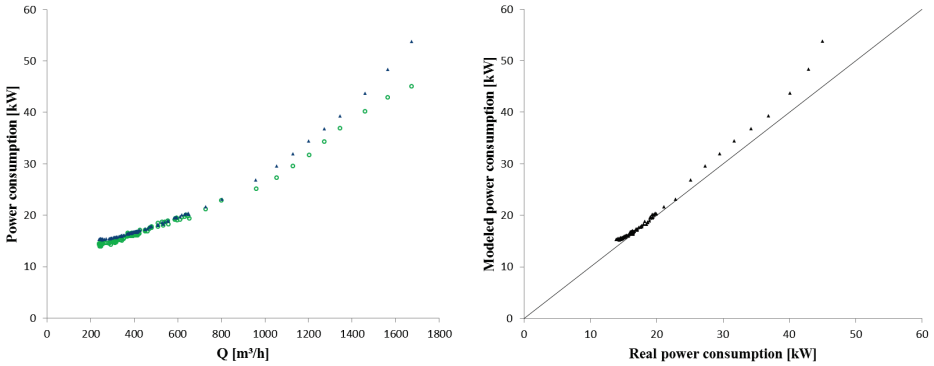

Figure 9.7. Comparison between the real (green circle symbols) and modelled power consumption (blue triangular symbols) as function of the pumped flow rate (left) and the scatter plot of the real and modelled power consumption (right).

To further illustrate the improvement of the dynamic power prediction by the newly proposed model, the dynamic model was compared to power consumption models using a constant weighing of the flow rate (a value (0.04 kWh/m³) used in BSM1 by Copp (2002), a value (0.008 kWh/m³) used for the secondary sludge recycle of BSM2 by (Gernaey et al., 2006) and a value (0.04 kWh/m³) calculated from the manufacturer data). Figure 9.8 (left) shows flow rate and the modelled energy consumption according the two different modelling approaches. This reveals clearly that a constant factor results in high power consumption predictions when the pump is operated close to the best efficiency point (1500 m³/h), whereas the dynamic model correctly captures the higher pump efficiency in that region, demonstrating the importance of accounting for this in a dynamic way. When applying a factor that was not computed specifically for the studied pump system (pumped liquid, static pumping head…) and that is not dynamic, one can end up with large deviations in the predictions. This is demonstrated here when incorrectly applying the factor of the secondary sludge recycle of BSM2, although this factor has been calculated in detail taking into account length of pipes, roughness, etc for a specific plant, however, different from the one under study here. Figure 9.8 (right) shows the cumulative energy consumption for the different modelling approaches. The difference between the dynamic model, which gives an excellent

description of the measured energy consumption, and the constant factor over 1.5 days, for 1 pump, already mounts up to 46% (about 400 kWh) for the factor introduced by Copp (2002) and 17% (about 150 kWh) for the factor based on the manufacturer data. The main contribution in the variations is imposed by the pump efficiency (Figure 9.9). In this context it should be noted that the factors introduced in the BSM models were only intended to bring some more realism in the calculations but are there used for comparison, not for absolute energy predictions. Hence, they can be used in such frameworks. The addition of dynamics could however also provide further realism for benchmarking.

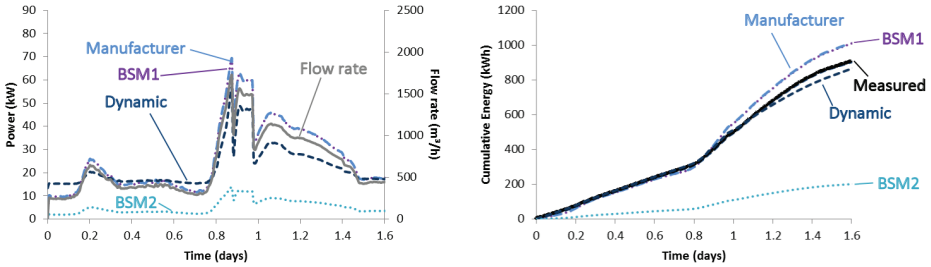

Figure 9.8. Comparison between the dynamic model and constant factor models (constant weighing factor BSM1 (Copp, 2002), constant weighing factor manufacturer, constant weighing factor BSM2 (Gernaey et al., 2006)) for the pumping energy consumption and their correlation with the pumped flow rate (left). Comparison of the dynamic model and constant factor models with the measured data of the cumulative energy consumption (right).

In the overall 'wire-to-water' efficiency (Figure 9.9), a similar, but not identical, trend can be seen as in the flow rate dynamics. The overall 'wire-to-water' efficiency reaches its maximum close to the Q_{BEP} (1500 m³/h). The variations in pump and overall 'wire-to-water' efficiency are identical and indicate that the variation is mainly due to the pump efficiency and not due to the VFD and motor efficiency.

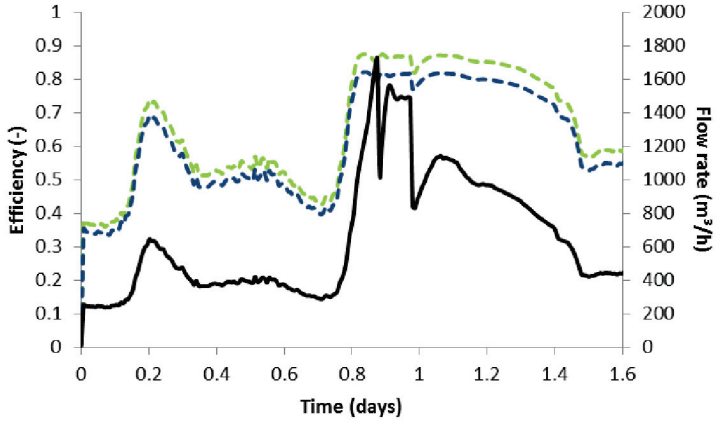

Figure 9.9. Dynamic pump efficiency as function of time. Pumped flow rate (black line - right axis), pump efficiency dynamic model (green dashed - left axis) and overall 'wire-to-water' efficiency dynamic model (dark blue dashed - left axis).

9.5.2. Case study 2

For the second case study, the power consumption based on the dynamic model described above (Equations 1 to 25) was found inadequate to describe the dynamics in the observed power consumption (Figure 9.10). The reason was found to reside in the quite different pumping curve shape of the studied pump that could not be accurately captured by the model. In a certain working range of the pump, the model as described earlier is a good approximation, but the head could not be captured for lower flow rates (Figure 9.11). This results in large deviations from the proposed curve, especially when the pump is not operated close to its best efficiency point (BEP), as was the case here (observed pumping rates were in general between 150 to 300 m³/h while the BEP was around 450 m³/h).

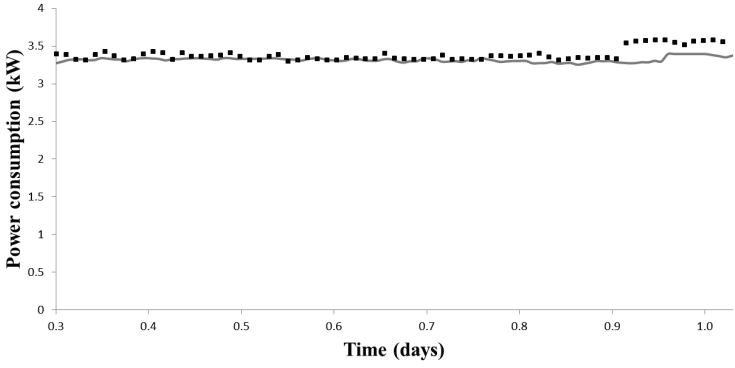

Figure 9.10. Results of the simulation for power consumption for case study 2 using the initial model valid for the WWTP of Eindhoven. Data (black dots), model prediction (grey line).

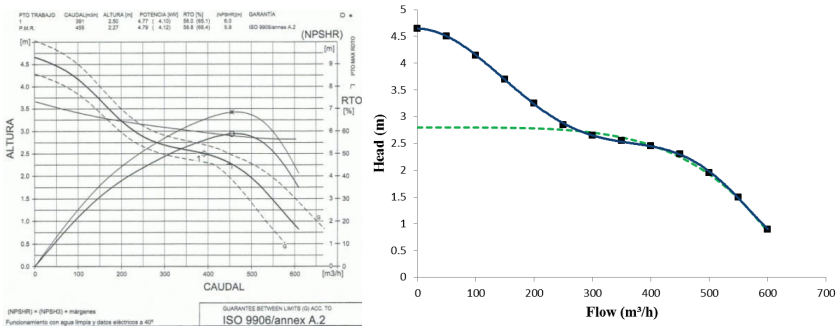

Figure 9.11. Manufacturer pump curve (left). Model fit (right), data (black dots), 6th order polynomial approximation (blue line) and model results according to Equation 13 (green dashed line).

To overcome this problem, a 6th order polynomial, which can be fitted to the available pump specification sheet data (this is also applicable for the first case study), is proposed (Equation 26):

$$H = A \cdot Q^6 + B \cdot Q^5 + C \cdot Q^4 + D \cdot Q^3 + E \cdot Q^2 + F \cdot Q + G + CorrF \quad (9.26)$$

with A to G the different order coefficients of the polynomial and $CorrF$ the correction factor for a varying impeller pump speed (Equation 27), which is calculated based on the affinity laws (Equations 17 to 19).

$$CorrF = H_{Ref} \cdot \left(\frac{N^2}{N_{Ref}{}^2} - 1 \right) \quad (9.27)$$

with H_{ref} a reference pump head or design head (as provided by the manufacturer), N_{ref} the corresponding impeller speed and N the actual impeller speed.

On a side note, when dealing with other viscosities than that of water the pump curve may change. The change of the pump curve due to viscosity may be related to the pressure losses inside the pump (Vieira et al., 2015). As such an extension of the model might be required when applying the model for pumping sludge (e.g. from the underflow of the clarifier).

The dynamic pump model received input for the measured elevation (in the pump well) and the frequency (N). The model needs calibration because of the changed conditions, i.e. different composition of the (waste)water and differences in the pump compared to the manufacturer data (e.g. wear and modifications). In the calibration procedure a step by step procedure was used. First, the flow rate was calibrated and afterwards the power consumption. For each of the steps a scenario analysis was performed to find the best matching parameters. For fitting the flow rate the following parameters were altered: friction of inline equipment, H_{ref} and minor losses equivalent pipe length. The values for the dynamic viscosity of water and pipe roughness were not changed as they only had a minor impact on the result. The value for dynamic viscosity of water is derived from a physical property table for water with a temperature of 15°C (Tchobanoglous et al., 2004). Table 9.3

summarizes the final values for the different parameters, whereas Figure 9.12 shows the best fit obtained for flow rate (grey line).

Table 9.3. Parameter values obtained for the fit of the flow rate.

Parameter name	Estimated value	Default/Calculated value	Unit
Dynamic Viscosity of water (15°C)	0.001139	0.001139	Pa.s
Friction Inline Equipment	**0.05**	0	m
H_{ref}	**1.5**	2.5	M
Minor Losses Equivalent Pipe Length	32.5	32.5	m
Pipe roughness	0.00015	0.00015	m

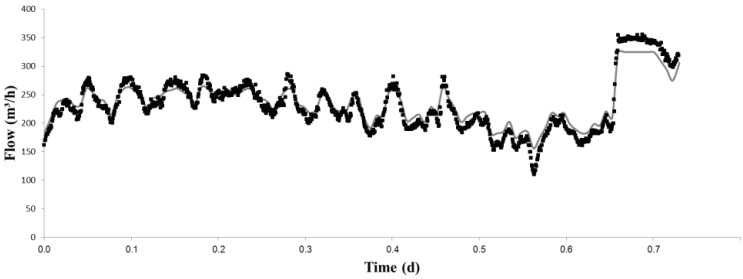

Figure 9.12. Time series of pump flow rate. Data (black dots), model prediction (grey line).

In the second step the power consumption was fitted to the measured data. For the estimation the following parameters were altered: efficiency of the motor, maximum pump efficiency, half efficiency of the VFD, maximum efficiency of the VFD and the best efficiency pumping flow rate (Q_{BEP}). In this second step, the maximum pump efficiency and Q_{BEP} were first estimated using a solver (GRG Nonlinear) minimizing the sum of squared errors between the prediction (given by equation 22) and the data from the pump manufacturer (Figure 9.13). Subsequently, the other parameters were calibrated on a trial and error basis after a scenario analysis based screening. After the whole calibration procedure a good fit was obtained (the sum of squared errors was reduced from more than 10 to 0.045). Figure 9.14 shows the simulation results after calibration. The estimated parameters are summarized in Table 9.4.

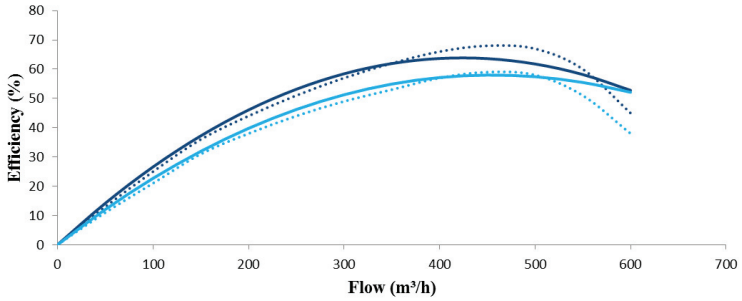

Figure 9.13. Best fit from the parameter estimation of the maximum pump efficiency and Q_{BEP} between model (full line) and manufacturer data (dotted line) for the high (dark blue) and low (light blue) pump efficiency.

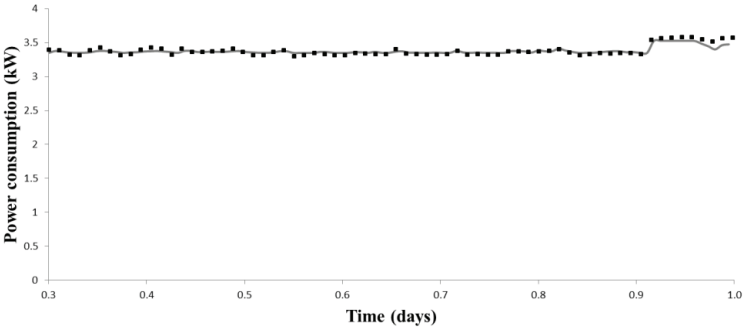

Figure 9.14. Dynamic power consumption of the pump. Measurement data (black dots) and model predictions for the best fit (grey line).

Table 9.4. Parameter values obtained for the fit of the power consumption.

Parameter name	Estimated value	Default/Calculated value	Unit
η_m	0.9	0.9	-
$\eta_{p,min}$	0	0	-
$\eta_{p,max}$	**0.88**	0.648	-
$\eta_{VFD,min}$	**0.94**	0.89	-
$\eta_{VFD,max}$	**0.96**	0.95	-
Q_{BEP}	**425**	455	m³/h

After calibration the model yielded an excellent description of the dynamic power consumption (Figure 9.14). It is noteworthy that the dynamic model is able to predict the smoothening seen in the dynamic power consumption, despite the dynamics in the flow rate. This is established by the dynamic change in efficiency captured by the dynamic model. The latter cannot be achieved with a fixed power consumption as clearly illustrated in Figure 9.15. This is an important point of attention in the context of WWTP management when negotiating for a reduction on

electricity tariff based on shaving the maximum power peaks. The latter indeed requires a good description of pump dynamics.

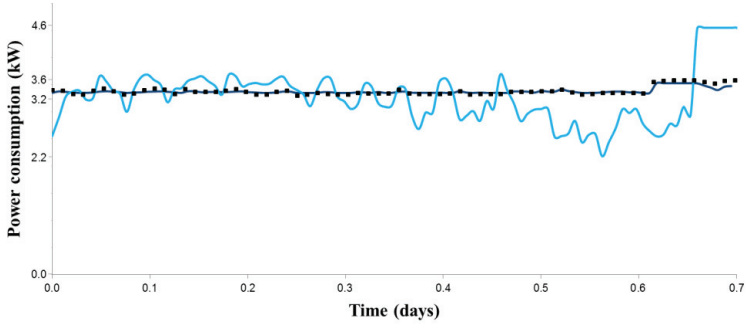

Figure 9.15. Power consumption of the pump at Mekolalde. Data (black dots), dynamic power consumption model (dark blue line) and fixed power consumption model (light blue line).

A point of attention is the large deviation between the maximum pump efficiency provided by the manufacturer and the final estimated value. This could be due to the followed parameter estimation procedure, which splits the estimation of parameters related to the flow rate and the parameters related to the power consumption in two parts. An advantage of this approach is that the objective function is not overly complicated (including multiple false optima). A disadvantage is that a bias in the estimation of the flow rate related parameters may cause a bias in the estimation of the parameters related to power consumption. This disadvantage could be eliminated by applying a rigorous global sensitivity analysis followed by a automatic parameter estimation.

9.5.3. General discussion

Setting up a dynamic pump model using the approach described above is quite time consuming. However, application of the modelling approach to more pumps in the near future will provide more knowledge and maybe indicate certain trends. This can shed light on the necessity of a certain level of detail. Model reduction might be possible if certain parameters seem to have limited sensitivity revealed from a global sensitivity analysis. However, this was beyond the scope of this study. Data-driven models are another possible approach. E.g. for the first case study (Figure 9.7) a data driven approach could be used but would result in a model that is only valid for this pump (as it is trained using this particular data set). The idea of this study was to set up a generic mechanistic model (at least as much as possible) that has a much broader application range, also for cases where no power consumption data is available (this is not a standard measurement and also time consuming to set up).

There is a large energy savings potential in optimizing pumping infrastructure and its automation and control system as observations from practice learn that many pumps are working far from their optimal efficiency point. The opportunity to obtain the largest impact on the energy saving potential presents itself during the design phase, where smart combinations of pumping groups may allow pumps to nearly all the time operate close to their BEP. The newly developed dynamic model can help in assessing the best optimal configuration of a pumping station. For example in case study 1, The overall 'wire-to-water' efficiency (Figure 9.9) reaches its maximum close to the Q_{BEP} (1500 m³/h), however the delivered flow rate is most of the time around 500 m³/h and only during rare high flow conditions (storm events) the BEP is reached. A pump group of two pumps, one of which has its BEP around 500 m³/h and one with a higher BEP might be a better solution.
In summary, different modelling approaches have their merits depending on the modelling objective. But foremost, users should be aware of the potential and limitations of different approaches. Simpler models will typically either sacrifice accuracy or generality.
The availability of this new, more accurate and dynamic, model for predicting pumping energy consumption will lead to improved management of the pumps resulting in the reduction of energy consumption and as such in reduction of greenhouse gas emissions, contributing to climate change mitigation. The proposed calibrated model allows for more accurate testing of strategies such as shifting energy use from peak to off-peak, which can significantly reduce the greenhouse gas foot print (Bunn, 2007). Furthermore, the possibility to link the proposed model with existing treatment process models provides opportunities to reduce the energy consumption on the level of the whole treatment plant without the risk of violating the imposed discharge limits. The model is more accurate than currently existing models used for energy quantification of pumps at WWTPs.

9.6. CONCLUSIONS

The newly developed dynamic model is demonstrated for two case studies and yields accurate predictions of the dynamically evolving power consumption opposed to the frequently applied fixed power consumption models. For the fixed power consumption models, large over predictions (17% based on manufacturer data and 46% for a constant energy consumption model) were found for cumulative energy consumption after 1.5 days for case study 1. In case study 2, the model

needed some extension as well as significant calibration, but this results in an even more generic model.
In the future, the model can even become more generic when more cases are tested. This should lead to proposed sets of default values for certain pump types as well as a calibration protocol. A global sensitivity analysis, for determining the parameters deserving special attention and the parameters that can be, possibly, left out by model reduction, is an important step in this calibration protocol and the way to a more generic model.
The availability of this new, more accurate and dynamic, model for predicting pumping energy consumption will lead to improved management of the pumps resulting in the reduction of energy consumption and as such in reduction of greenhouse gas emissions and, hence, climate change mitigation.
As the model is foreseen to be used in developing control strategies (linked with biological process models), the model also needs further testing on longer time series.

9.7. ACKNOWLEDGEMENTS

The authors would like thank the financial support received from the EU FP7-SME-2008-1 program (project ADD CONTROL 232302) as well all project partners (http://www.addcontrol-fp7.eu/). They would also like to thank Waterboard the Dommel for the data on the energy consumption of their pump.

PART V

Simulation methodology

Chapter 10

A practical and sound calibration procedure

"Your assumptions are your windows on the world. Scrub them off every once in a while, or the light won't come in."
Isaac Asimov

10.1. ABSTRACT

Mathematical modelling is state of the art practice in optimization of wastewater treatment plants. Notwithstanding this increased popularity, many questions remain regarding the fine tuning or calibration of the models. A calibration methodology focusing on a better description of the different sub-processes rather than force-fitting bio-kinetic parameters was further extended and improved. This chapter sheds light on the application of this calibration procedure for the wastewater treatment plant of Eindhoven and highlights the many similarities but also a few differences with the GMP Unified Protocol. Improving the model description of the aeration model and the primary sedimentation model improved the simulation results of respectively ammonium NH_4 and nitrate NO_3 concentrations. Following this model calibration procedure increased the understanding of the plant behaviour and the confidence in the simulation results in view of scenario analyses for plant optimization.

Part of this chapter was published as:
Amerlinck, Y., K. Cierkens, T. Flameling, S. Weijers, and I. Nopens, 2014a, A practical and sound calibration procedure applied to the WWTP of Eindhoven: IWA World Water Congress & Exhibition.

10.2. SYMBOLS

$K_{NH,ANO}$	Ammonium half saturation coefficient for autotrophic biomass

10.3. INTRODUCTION

Waterboard De Dommel (Boxtel, The Netherlands) has been using models of their wastewater treatment plants (WWTPs) since the early 1990s. Since 2007, a model of the WWTP of Eindhoven (The Netherlands) is under continuous development (See section 2.4). During the course of time models have continuously been improved through a repeating learning cycle using gained system knowledge and to be able to address more difficult model objectives (Sin et al., 2008).
Over the years several modelling and simulation methodologies, of which a thorough review is given in MOP31 (WEF, 2013), have been postulated. One of these protocols, developed at BIOMATH (Vanrolleghem et al., 2003), focuses on calibration and validation of the biokinetic and settler models. More recent, based on a survey and in-depth discussion with several modelling experts, Rieger et al. (2012) proposed a simulation protocol (the GMP Unified Protocol), with the intention to provide a framework to allow for rigorously applying modelling and simulation without limiting the development of improvements. Five major project steps were identified and explained, i.e. (i) Project definition, (ii) Data collection and reconciliation, (iii) Plant model set-up, (iv) calibration and (v) result interpretation.
This chapter presents the practical and sound calibration procedure applied to the WWTP of Eindhoven and the similarities and differences with the GMP Unified Protocol.

10.4. MATERIAL AND METHODS

Over the years several versions of a process model of the WWTP of Eindhoven have been set up and calibrated using WEST (mikebyDHI).
The calibration procedure corresponds largely to the GMP Unified Protocol, but focuses on a better description of the different sub-processes and not putting all calibration efforts in force-fitting biokinetic parameters. An iterative procedure is

proposed where during every iteration the quality of the modelling results is improved. For well-defined biokinetic models (such as for C/N removal) deviations between simulation and experimental results are corrected by improving the model structures of the sub-processes rather than "compensating" adjustment of certain biokinetic model parameters, however safeguarding to not further over-parameterise the model. The overall aim is to identify structural uncertainties of the applied models as it is believed that the largest uncertainties are located in the description of influent, hydraulics, gas-liquid mass transfers and other physical processes such as primary and secondary settling. In fact, the biokinetic parameters are only to be changed when the default parameter set is considered not to be adequate.

The applied model calibration procedure consists of the following five major steps: (i) project definition, (ii) data collection and reconciliation, (iii) plant model set-up, (iv) calibration and validation and (v) simulation and result interpretation (Figure 10.1). These will be briefly discussed.

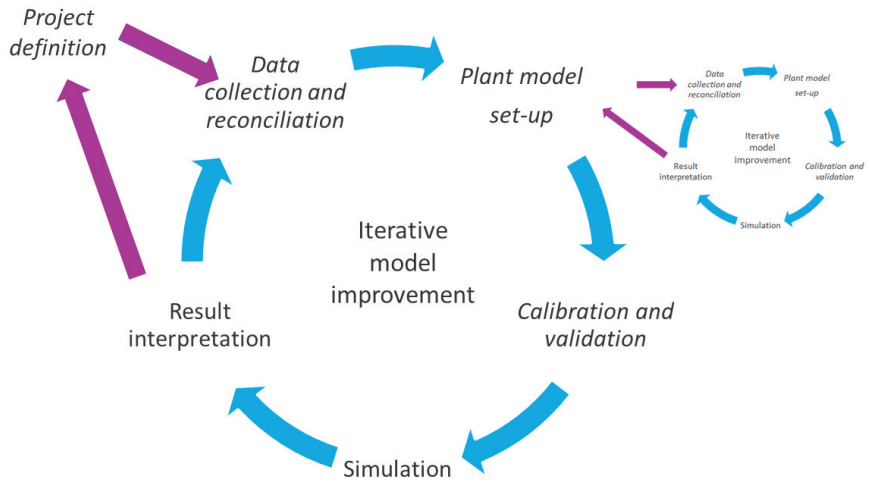

Figure 10.1. The proposed iterative model calibration procedure.

10.4.1. Procedure

10.4.1.1. Project definition

In a start-up meeting the objectives and the necessary steps of the project are discussed and defined. The objective of this project is the optimization of the WWTP of Eindhoven in order to improve the water quality in the Dommel River to which it discharges its effluent in view of meeting the requirements of the European Union Water Framework Directive, in particular looking at DO

depletion, ammonia peaks and seasonal average nutrient concentration levels (Weijers et al., 2012).

10.4.1.2. Data collection and reconciliation

The data used for the calibration is a combination of online measurements, lab analysis, measurement campaigns (both organized for the purpose of operations optimization as well as for modelling purposes) and book keeping data (such as excess sludge transports to the sludge treatment plant). Using high-frequency data has increased the accuracy of the simulation results significantly (Cierkens et al., 2012) but has also put an even larger burden on data validation.

10.4.1.3. Plant model set-up

The plant model is set up based on the available design guides, plans, schemes, P&IDs and discussions with the plant staff. The biokinetic model and the model of the control logics are calibrated separately, as such avoiding bias in the calibration of either. For the calibration of the biokinetic model, the control logics are decoupled, i.e. operational data (e.g. airflow rates) logged at the wastewater treatment plant is used instead and for the calibration of the control logics the logged sensor data (e.g. oxygen and ammonium) is used as input to the control algorithms.

10.4.1.4. Calibration and validation

The calibration of the model of the Eindhoven WWTP has been a combination of expert judgment (to determine which parameters to change and which values to take) and mathematical methods (i.e. sensitivity analysis and automated parameter estimation). The overall aim during the calibration exercise was not to change biokinetic parameters values, for these changes are assumed to be mostly the result of model structure inadequacies, i.e. the largest uncertainties are located in the description of influent, hydraulics, gas-liquid mass transfers and other physical processes such as primary and secondary settling. During the calibration a step-wise approach has been used repeatedly. When new models were integrated they were individually calibrated (where possible) first on lab tests (e.g. settling tests), subsequently on full scale data of the unit process under study (e.g. the chemical phosphorus removal model) and finally integrated with the pre-existing plant model.

After calibration the result is validated on short term simulations, i.e. investigated whether the model with the calibrated or estimated parameters also predicts the data of another period, preferably with slightly different conditions (e.g. different sludge age or another season).

10.4.1.5. Simulation and result interpretation

As a last step of the calibration cycle, the simulation results are thoroughly discussed with the wastewater technologists at the Waterboard and the outcomes are checked against the assumptions taken in the model. Additional calculations are performed for assisting the discussion, such as mass balances and a colour based analysis tool (See Chapter 11).

10.4.2. Flow of action according the new calibration protocol

When starting a new modelling project with the newly proposed methodology, the cyclic calibration procedure is performed a first time. This first calibration, comparable to a calibration level 1 according to WERF classification (Melcer, 2003), is based on available data sets, default values, assumptions and engineering experience. The choice of the sub-models and their corresponding complexity is based on expert judgement taking into account the goals set forth in the project definition. As the final step in the calibration procedure the simulation results are interpreted and a decision is taken whether it is required or not to run a second iteration of the calibration cycle.

In order to take this decision, discrepancies in the validation and anomalies in the simulation results of different scenarios are thoroughly evaluated to determine their source. The source can be either an artefact of the parameter estimation or a more profound model structure issue. In the proposed calibration procedure, it is suggested to evaluate in first instance whether the differences are caused by a model structure issue and the possible lack of detail in the description of the different sub-models. The evaluation, of which sub-models to change, starts from the fundamentals of the processes impacting the incorrectly predicted variables and looks at the different driving forces. Studying the fundamentals can be supported by mass balances and the simulation of several hypotheses.

In a second or later iteration of the procedure additional data is required to improve either the parameter estimation or the implementation, calibration and validation of more detailed sub-models. At the end of each iteration the simulation results are appraised again. Important during this appraisal, is to consider also the uncertainty in the model outcome, as it determines whether the model quality is considered to be adequate to meet the objectives set in the project definition. This uncertainty can be addressed by a thorough discussion with the water technologists but also by applying numerical techniques such as Monte-Carlo based techniques (Belia et al., 2009) or ensemble modelling (Bates and Granger, 1969). Addressing the uncertainty has as objective to move from total ignorance towards quantifiable or scenario uncertainty as such supporting the decision making process.

10.5. RESULTS AND DISCUSSION

10.5.1. Iteration for the improvement of ammonium prediction

In order to improve the predictions of ammonium removal a new model for the calculation of the oxygen transfer (from airflow rates), based on the work of Rosso et al. (2005), was implemented (Cierkens et al., 2012) (See Chapter 8). In combination with feeding the measurement data of the air flow rate to the model, as such decoupling the controller model from the biokinetic model, and high frequency data for the influent characterization, dissolved oxygen and ammonium concentrations could be predicted with high accuracy (Figure 10.2). Despite the good fit, some of the peaks in ammonium concentration are not predicted by the model. The prediction of these peaks can probably be improved by taking into account the mixing behaviour in the model structure (Rehman et al., 2014). Within this model version, although debateable, the ammonium half saturation coefficient for autotrophic biomass ($K_{NH,ANO}$), which is the only biokinetic model parameter that was adjusted, was lowered compared to the default parameter value.

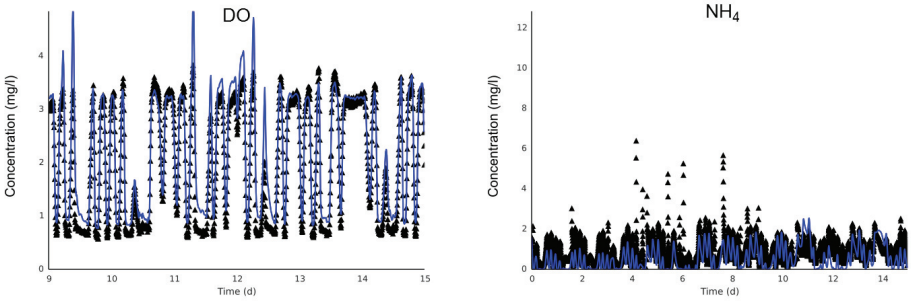

Figure 10.2. Model fit for dissolved oxygen (left) and ammonium (right) after the adaptations to the aeration model and the model input. Lines indicate simulation results, triangles the online measurement data.

10.5.2. Iteration for the improvement of nitrate prediction

After the previous model improvement, more attention was given to the wet weather behaviour. Hereto the primary sedimentation tank (PST) model was upgraded to a model taking into account the effect of the hydraulic retention time on the removal efficiency (Tay, 1982). The model of the secondary sedimentation tank was upgraded from the Takacs model (Takács et al., 1991) to the Bürger-Diehl model which has a more sound mathematical structure allowing improved

prediction of the sludge blanket height and underflow concentration during wet weather (Bürger et al., 2012).
Despite the model adaptations on the aeration model and for the wet weather behaviour, the simulation results for nitrate still diverged significantly from the measurement data. In an attempt to reduce this divergence, the model of the primary sedimentation tank was extended to account for different removal efficiencies for the different suspended fractions, based on repeated measurements, during the year 2011, performed on the PSTs (Chapter 7). This resulted in a higher chemical oxygen demand (COD) concentration entering the activated sludge tanks as such improving the nitrate removal predictions considerably (Figure 10.3).

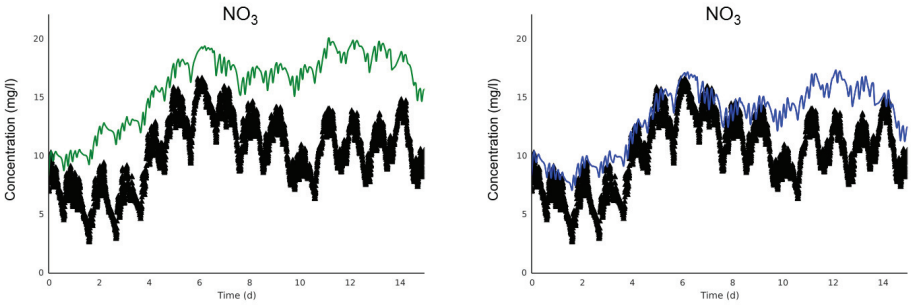

Figure 10.3. Improvement of nitrate model predictions with the adapted primary sedimentation tank model (right) compared to the results before the adaptations (left). Lines show the simulation results, triangles the online measurement data.

10.6. CONCLUSIONS

The calibration procedure applied to the WWTP of Eindhoven had major similarities to the GMP Unified Protocol. Main differences were the decoupling of the controller logics from the biokinetic model and the emphasis on slightly increasing the complexity of the sub-models rather than force-fitting the biokinetic parameters. This is done in view of maintaining the predictive quality of the model under varying process conditions.
Improving the level of detail in the different sub-models is decided based on possible discrepancies in the simulation results and the requirement for parameter calibration and the subsequent evaluation of their cause. Acceptance of the model complexity depends on the appraisal of the inherent uncertainty.
After improving the model for the aeration the simulation results match very well for DO and NH_4. The adaptation to the primary sedimentation model resulted in an improved fit for the simulation results of NO_3. However, the prediction of NO_3

should be further improved and the work on the modelling of the primary sedimentation tank (See Chapter 6) is a first step in this direction.
Other options to improve the balance in the complexity of the sub-models are the application and calibration of an improved secondary settler model, a better description of the hydraulics (applying compartmental models) and a further exploration of the dynamics in the aeration process (impact on α and β-factors).

Chapter 11

Application of a colour-based system analysis tool at the WWTP of Eindhoven

"To invent, you need a good imagination and a pile of junk."
Thomas A. Edison

11.1. ABSTRACT

Model-based analysis and optimization of wastewater treatment plants usually consists of numerous simulations and large data sets generated. Finding specific information in these data sets is not always a trivial task especially when this information is hidden in intermediate algebraic variables that are not easily accessible or not defined as such in the model. An extremely simple yet effective colour-based evaluation method is proposed for system analysis, e.g. for bottleneck identification. The tool proved very useful in evaluating large amounts of data and in taking certain decisions. Including the tool in simulation platforms makes activated sludge model analysis more efficient and provides transparency for both experienced and inexperienced modellers.

Part of this chapter was published as:
Amerlinck, Y., K. Cierkens, and I. Nopens, 2015, Application of a colour-based system analysis tool at the WWTP of Eindhoven: 2nd New Developments in IT & Water Conference.

11.2. SYMBOLS

$C(S_{Alk})$	Concentration of alkalinity (mg/l)

$C(S_{O2})$	Concentration of oxygen (mg/l)
$C(S_{NHx})$	Concentration of ammonium (mg/l)
$C(S_{PO4})$	Concentration of phosphate (mg/l)
$C(X_{ANO})$	Concentration of autotrophic nitrifying organisms (mg/l)
ρ_{ANO}	Process rate of autotrophic growth (g/d)
μ_{ANO}	growth rate of autotrophs (d^{-1})

11.3. INTRODUCTION

Present-day wastewater treatment plant (WWTP) optimization is largely based on model based analysis. However, this analysis usually results in the execution of a large number of simulations and the generation of large simulation data sets. Trying to find explanations why one scenario (unexpectedly) performs better than the other or even trying to determine which scenario is the better one requires "number crunching". Visual inspection of time series contains the risk of overlooking things, whereas summarizing time series into single numbers (average, minimum, maximum, etc.) results in significant loss of information. Simple colour-based evaluation methods might be a third approach to facilitate the data evaluation. In addition, the description of process rates or kinetics has become increasingly complex and typically multiple switching functions are joined to yield the overall process rate. Although of profound importance, these switching functions are somewhat "hidden" and often not explicitly available as output variable, meaning that intermediate calculation results are not directly accessible for the modeller. Detailed analysis of these switching functions can, however, provide useful insight.
The goal of this chapter is to demonstrate the proposed system analysis tool based on two illustrative examples at the WWTP of Eindhoven. The first example addresses the evolution of enhanced biological phosphorus removal (EBPR), nitrification and denitrification activity in scenarios with reduced phosphate concentration in the inlet (induced by the possible application of dissolved air flotation (DAF)). The second example highlights the usefulness of the method for evaluating the implementation of a control strategy for dosing a carbon source to stimulate denitrification.

11.4. MATERIAL AND METHODS

A method is proposed for the analysis of kinetic expressions that consist of a product of switching functions. These switching functions, e.g. Monod functions (Monod, 1942), are used to describe the effect of a limiting factor on a particular biological process or to (de)activate a process when a factor is exceeding a threshold. Typically, several switching functions are joined together and finally result in having a process run in the range between its maximal rate and zero. As an illustrative example, the process rate limitation of autotrophic growth is shown here. In the ASM2d model (Henze et al., 2000) the growth rate of autotrophs (Equation 11.1) contains switching functions for oxygen (S_{O2}), ammonium (S_{NHx}), phosphate (S_{PO4}) and alkalinity (S_{Alk}).

$$\boldsymbol{\rho_{ANO} = \mu_{ANO} \cdot \frac{C(S_{O_2})}{C(S_{O_2})+K_{O,ANO}} \cdot \frac{C(S_{NH_x})}{C(S_{NH_x})+K_{NH,ANO}} \cdot \frac{C(S_{PO_4})}{C(S_{PO_4})+K_P} \cdot \frac{C(S_{Alk})}{C(S_{Alk})+K_{Alk,ANO}} \cdot C(X_{ANO})} \quad (11.1)$$

Where ρ_{ANO} is the process rate of autotrophic growth [g/d], μ_{ANO} is the growth rate of autotrophs [d^{-1}], $C(X_{ANO})$ is the concentration of autotrophic nitrifying organisms [mg/l], $C(S_{O2})$ is the oxygen concentration [mg/l], $C(S_{NHx})$ is the ammonium concentration [mg/l], $C(S_{PO4})$ is the phosphate concentration [mg/l], $C(S_{Alk})$ is the alkalinity concentration [mg/l], $K_{O,ANO}$ is the half saturation concentration for oxygen [mg/l], $K_{NH,ANO}$ is the half saturation concentration for ammonium [mg/l], $K_{PO,ANO}$ is the half saturation concentration for phosphate [mg/l] and $K_{Alk,ANO}$ is the half saturation concentration for alkalinity [mg/l].

However, when a rate drops, it is not always obvious from the simulation which switching function is actually the limiting factor due to their joined nature and the fact that they are not separately calculated as algebraic states or output variables. Hence, these switching functions contain valuable "hidden" information on the activity of the process. Using colour coding for all distinctive switching functions allows for a fast inspection of the impact of all switching functions on the overall process rate and to detect which factor is limiting the process performance. Conceptually, this colour coding is applied by linking the actual substrate concentration through the calculation of the switching function and mapping the value, which lays between 0 and 1 (or 100%), on a colour map (Figure 11.1).

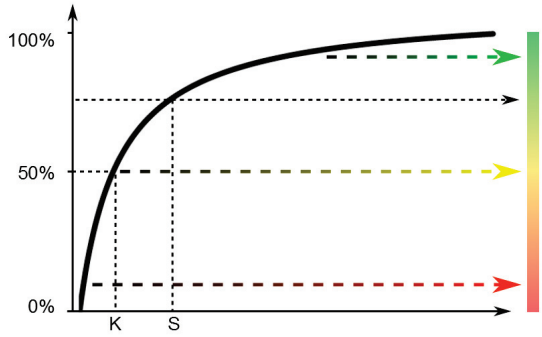

Figure 11.1. The application of the color coding for a monod swithching function. K is the substrate half saturation coefficient for the particular monod function and S is the actual substrate concentration.

The method is demonstrated using the WWTP model of Eindhoven. Over the years, several gradually more complex versions of a process model of the plant have been set up and calibrated using WEST (mikebyDHI). The model that served as the basis for the model based evaluation in the current study was thoroughly calibrated for describing carbon and nitrogen removal under dry weather flow (See Chapter 12). Prior to the scenario analysis a calibration with special focus on phosphorus removal was performed. This calibration, a calibration level 1 according to WERF classification (Melcer, 2003), was based on default values, assumptions and engineering experience. For further processing mass balances, calculation of the sludge phosphorus content and effluent phosphate concentration ranges were compared with the practical experience of the plant staff and data available from measurement campaigns.

In order to deal with DO depletion, ammonia peaks during peak events while maintaining seasonal average nutrient concentration levels (Weijers et al., 2012), the potential of replacing the primary sedimentation tanks (PST) by dissolved air flotation (DAF) units was investigated. The DAF units proved successful in getting a higher performance in removing particles, and consequently chemical oxygen demand (COD), compared to the conventional primary sedimentation tanks. But in conjunction with the higher COD removal also a higher removal of phosphorus (both particulate organic phosphorus and soluble ortho-phosphate) is observed. The impact of this reduced inflow of phosphorus on the subsequent biological treatment needed to be investigated before a final decision could be taken.

In order to guarantee the seasonal average nutrient concentration levels for nitrate, the dosing of carbon in the first zone (DT01) of denitrification tank (Figure 11.2) as a control measure was investigated. Also the location of the nitrate sensor, steering the dosage, is used as degree of freedom to optimize the control. The first location

for the sensor analysed is at the end of the denitrification tank (zone DT02) and the second location is at the end of the aerobic tank (BT06).

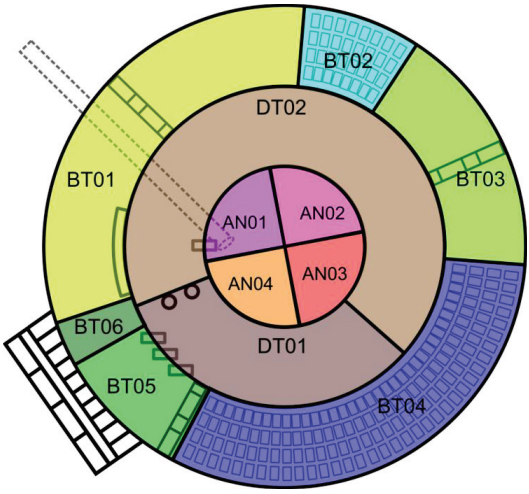

Figure 11.2. The circular modified UCT configuration of the activated sludge tanks at the WWTP of Eindhoven and the mapping of tanks in series used in the model.

11.5. RESULTS AND DISCUSSION

For the first illustrative example, one of the dynamic simulations of a scenario with reduced phosphate concentration in the inlet of the biological treatment (Figure 11.2), resulting from the application of a DAF, showed an unexpected but significant increase in ammonium concentration while dissolved oxygen levels and the amount of nitrifiers seemed sufficiently high.

At some points in time phosphate was rather low but it could not be deduced directly from the dynamic simulation results that this was causing the decrease in nitrification activity. In contrast, the proposed method gave a clear view on this aspect. Table 11.1 shows the individual effect of the distinct Monod switching functions (row 1-4) and the overall autotrophic growth rate as a fraction of the maximum growth rate (row 5, being the product of rows 1-4), for the different reaction zones, averaged over the entire simulation period. Colours evolve from green, indicating a high value (no limitation) over orange to red, indicating a low value (severe limitation).

From Table 11.1 it can be clearly seen that phosphate is not limiting in the anaerobic (AN01 through AN04) and anoxic zones (DT01 and DT02). The limiting factor in these zones is obviously the lack of dissolved oxygen. However, in the aerobic zones (BT01 through BT06) a relation can be seen between the limitation

in the autotrophic growth rate and the Monod switching function for phosphate. I.e. while the Monod switching functions for alkalinity, ammonium and oxygen are high (and thus not limiting), the Monod switching function for phosphate and as a consequence also the overall autotrophic growth rate is low.

Table 11.1. Dissolved oxygen limitation (in the anaerobic and anoxic zones) and phosphate limitation (in the aerobic zones) of the overall autotrophic growth visualized through the impact of the different Monod terms for the different sections of the activated sludge tank, averaged over the entire simulation period, using a colour-based system analysis tool.

AVERAGE	AN01	AN02	AN03	AN04	DT01	DT02	BT01	BT02	BT03	BT04	BT05	BT06
Monod S_ALK	0.93	0.93	0.92	0.92	0.93	0.93	0.93	0.93	0.93	0.93	0.93	0.93
Monod S_NH	1.00	1.00	1.00	1.00	1.00	1.00	0.99	0.99	0.99	0.99	0.98	0.98
Monod S_O	0.06	0.00	0.00	0.00	0.02	0.06	0.77	0.75	0.70	0.88	0.88	0.85
Monod S_PO	0.98	0.99	0.99	0.99	0.80	0.76	0.36	0.29	0.28	0.29	0.29	0.29
Overall	0.05	0.00	0.00	0.00	0.01	0.01	0.21	0.13	0.10	0.21	0.20	0.19

Table 11.2. shows the dynamic behaviour of the same autotrophic growth rate (as a fraction of the maximum growth rate; similar as row 5 of Table 11.1 but dynamic instead of averaged). Table 11.3 on the other hand shows only the Monod term for phosphate as nutrient for growth (similar as row 4 of Table 11.1 but dynamic). Also from Table 11.2 and Table 11.3 this relation, between the autotrophic growth rate and the Monod switching function for phosphate, can be deduced. I.e. when the Monod term for phosphate reaches higher percentages (green colour) the growth of autotrophs increases (yellow to green colours). The switching functions for oxygen (S_{O2}), ammonium (S_{NHx}) and alkalinity (S_{Alk}) remain high and do not show the same trend (results not shown), although they lower the activity of the nitrification process slightly.

Table 11.2. Recovery over time of the growth rate of autotrophs for the different sections of the activated sludge tank shown using a colour-based evaluation method.

Time	AN01	AN02	AN03	AN04	DT01	DT02	BT01	BT02	BT03	BT04	BT05	BT06
11.962	0.05	0.00	0.00	0.00	0.00	0.01	0.28	0.16	0.11	0.12	0.12	0.13
11.965	0.05	0.00	0.00	0.00	0.00	0.01	0.29	0.17	0.12	0.14	0.14	0.14
11.969	0.05	0.00	0.00	0.00	0.00	0.01	0.31	0.19	0.13	0.15	0.15	0.16
11.972	0.05	0.00	0.00	0.00	0.00	0.01	0.32	0.21	0.15	0.17	0.17	0.18
11.976	0.05	0.00	0.00	0.00	0.00	0.01	0.34	0.23	0.17	0.20	0.20	0.21
11.979	0.05	0.00	0.00	0.00	0.00	0.01	0.36	0.26	0.20	0.24	0.24	0.25
11.983	0.05	0.00	0.00	0.00	0.00	0.01	0.38	0.29	0.23	0.29	0.30	0.30
11.986	0.05	0.00	0.00	0.00	0.00	0.01	0.41	0.33	0.27	0.36	0.36	0.37
11.990	0.05	0.00	0.00	0.00	0.00	0.01	0.44	0.37	0.30	0.43	0.43	0.43
11.993	0.05	0.00	0.00	0.00	0.00	0.01	0.47	0.40	0.32	0.49	0.49	0.49
11.997	0.05	0.00	0.00	0.00	0.00	0.01	0.49	0.42	0.32	0.53	0.53	0.53
12.000	0.05	0.00	0.00	0.00	0.00	0.01	0.50	0.43	0.31	0.57	0.57	0.56
12.004	0.05	0.00	0.00	0.00	0.00	0.00	0.51	0.43	0.29	0.60	0.60	0.59
12.007	0.05	0.00	0.00	0.00	0.00	0.00	0.52	0.44	0.28	0.62	0.62	0.61
12.011	0.05	0.00	0.00	0.00	0.00	0.00	0.53	0.44	0.27	0.64	0.64	0.62
12.014	0.05	0.00	0.00	0.00	0.00	0.00	0.54	0.45	0.27	0.66	0.65	0.64
12.018	0.05	0.00	0.00	0.00	0.00	0.00	0.55	0.46	0.27	0.67	0.67	0.65
12.021	0.05	0.00	0.00	0.00	0.00	0.00	0.56	0.46	0.28	0.68	0.68	0.66
12.024	0.05	0.00	0.00	0.00	0.00	0.00	0.57	0.47	0.28	0.69	0.69	0.67
12.028	0.05	0.00	0.00	0.00	0.00	0.00	0.58	0.48	0.29	0.70	0.70	0.68

Table 11.3. Recovery of the phosphate limitation over time shown through the impact of the Monod term of phosphate for the different sections of the activated sludge tank using a colour-based evaluation method.

Time	AN01	AN02	AN03	AN04	DT01	DT02	BT01	BT02	BT03	BT04	BT05	BT06
11.962	0.99	0.99	0.99	0.99	0.96	0.95	0.36	0.21	0.15	0.15	0.15	0.15
11.965	0.99	0.99	0.99	0.99	0.96	0.95	0.37	0.23	0.17	0.16	0.16	0.17
11.969	0.99	0.99	0.99	0.99	0.96	0.95	0.39	0.25	0.19	0.18	0.18	0.19
11.972	0.99	0.99	0.99	0.99	0.96	0.95	0.41	0.28	0.21	0.21	0.21	0.21
11.976	0.99	0.99	0.99	0.99	0.96	0.95	0.44	0.31	0.24	0.24	0.24	0.25
11.979	0.99	0.99	0.99	0.99	0.95	0.95	0.47	0.35	0.29	0.29	0.29	0.30
11.983	0.99	0.99	0.99	0.99	0.95	0.95	0.50	0.40	0.35	0.35	0.35	0.37
11.986	0.99	0.99	0.99	0.99	0.95	0.95	0.55	0.47	0.42	0.43	0.44	0.45
11.990	0.99	0.99	0.99	0.99	0.95	0.95	0.59	0.53	0.49	0.51	0.52	0.53
11.993	0.99	0.99	0.99	0.99	0.95	0.95	0.64	0.59	0.57	0.59	0.59	0.60
11.997	0.99	0.99	0.99	0.99	0.95	0.95	0.68	0.65	0.63	0.65	0.65	0.66
12.000	0.99	0.99	0.99	0.99	0.95	0.95	0.72	0.69	0.68	0.70	0.70	0.71
12.004	0.99	0.99	0.99	0.99	0.95	0.95	0.75	0.73	0.72	0.73	0.73	0.74
12.007	0.99	0.99	0.99	0.99	0.95	0.94	0.77	0.75	0.75	0.76	0.76	0.77
12.011	0.99	0.99	0.99	0.99	0.95	0.94	0.79	0.78	0.77	0.78	0.78	0.79
12.014	0.99	0.99	0.99	0.99	0.95	0.94	0.81	0.80	0.79	0.80	0.80	0.81
12.018	0.98	0.99	0.99	0.99	0.95	0.94	0.82	0.81	0.81	0.82	0.82	0.82
12.021	0.98	0.99	0.99	0.99	0.95	0.94	0.83	0.83	0.83	0.83	0.83	0.84
12.024	0.98	0.99	0.99	0.99	0.94	0.94	0.84	0.84	0.84	0.84	0.84	0.85
12.028	0.98	0.99	0.99	0.99	0.94	0.94	0.85	0.85	0.85	0.85	0.85	0.86

When controlling the carbon dosing using a sensor placed in the anoxic tanks, denitrification is improved. Nitrate concentration in the effluent decreases from 10.7 mg/l to 4.7 mg/l and total nitrogen from 12.7 mg/l and 7.8 mg/l. However, this decrease is not sufficient to meet the imposed discharge limits. The Monod expressions related to denitrification (Table 11.4) disclose that nitrate is not completely removed. Although the substrate, used in the denitrification, is almost depleted (orange and red cells with values close to zero) in the anoxic zones (DT01 and DT02), there is still some room for improvement.

Table 11.4. Substrate limitation (in the anoxic and aerobic zones), dissolved oxygen inhibition (in the aerobic zones) and phosphate limitation (in the last aerobic zones) of the denitrification visualized through the impact of the different Monod terms for the different sections of the activated sludge tank, averaged over the entire simulation period, using a colour-based system analysis tool.

AVERAGE	AN01	AN02	AN03	AN04	DT01	DT02	BT01	BT02	BT03	BT04	BT05	BT06	CA
Monod S_NH	1.00	1.00	1.00	1.00	0.99	0.99	0.96	0.96	0.95	0.93	0.93	0.92	0.90
Monod S_A	0.81	0.68	0.59	0.56	0.25	0.13	0.03	0.03	0.02	0.02	0.02	0.02	0.02
Monod S_F	0.85	0.78	0.67	0.55	0.16	0.14	0.13	0.12	0.12	0.15	0.16	0.18	0.20
Monod S_Alk	0.98	0.98	0.98	0.98	0.99	0.99	0.98	0.98	0.98	0.98	0.98	0.98	0.98
Monod S_PO	1.00	1.00	1.00	1.00	1.00	1.00	0.91	0.83	0.70	0.50	0.45	0.39	0.37
Monod S_NO	0.05	0.01	0.00	0.00	0.36	0.46	0.87	0.87	0.86	0.88	0.88	0.88	0.88
Inhibition S_O	1.00	1.00	1.00	1.00	0.98	0.95	0.23	0.33	0.49	0.08	0.09	0.12	0.03

In an attempt to further lower the nitrate concentrations the location of the sensor was altered towards the end of the aerobic zone. This decreased the nitrate concentration further to 3 mg/l. Unfortunately the total nitrogen concentration increased to 10.3 mg/l, caused by an increase of ammonium concentration from 0.4 mg/l (reference scenario) and 1.6 mg/l to 5.7 mg/l. The reason for this increased ammonium concentration is caused by the increased biological removal of phosphate. The dosing of carbon (from 11.6 m^3/d up to 20.3 m^3/d) causes a

stimulation of the biological phosphate removal by the phosphate accumulating organisms. The reduced concentration of phosphate results in a decreased rate of the nitrification (as is also demonstrated in the first example), which can be deduced from the significantly lower values for the Monod term of phosphate (Monod_S_PO) in the aerobic zones (Table 11.5).

Table 11.5. Effect of changing the sensor location on the substrate limitation (in the anoxic and aerobic zones), dissolved oxygen inhibition (in the aerobic zones) and phosphate limitation (in the last aerobic zones) of the denitrification visualized through the impact of the different Monod terms for the different sections of the activated sludge tank, averaged over the entire simulation period, using a colour-based system analysis tool.

AVERAGE	AN01	AN02	AN03	AN04	DT01	DT02	BT01	BT02	BT03	BT04	BT05	BT06	CA
Monod S_NH	1.00	1.00	1.00	1.00	1.00	0.99	0.99	0.99	0.99	0.98	0.98	0.98	0.98
Monod S_A	0.91	0.91	0.92	0.92	0.63	0.52	0.08	0.06	0.04	0.04	0.03	0.03	0.03
Monod S_F	0.84	0.72	0.57	0.43	0.12	0.12	0.14	0.12	0.11	0.16	0.17	0.20	0.23
Monod S_Alk	0.99	0.99	0.99	0.99	0.99	0.99	0.99	0.99	0.99	0.99	0.99	0.99	0.99
Monod S_PO	1.00	1.00	1.00	1.00	1.00	1.00	0.98	0.94	0.81	0.41	0.30	0.22	0.21
Monod S_NO	0.01	0.00	0.00	0.00	0.09	0.18	0.84	0.84	0.84	0.84	0.85	0.85	0.85
Inhibition S_O	1.00	1.00	1.00	1.00	0.99	0.96	0.12	0.22	0.49	0.05	0.05	0.05	0.03

11.6. CONCLUSIONS

A simple yet effective colour-based system analysis tool for activated sludge models was illustrated for supporting model analysis. The tool allowed expert modellers to make a fast system analysis given the large amount of simulation outputs and the complex interactions that occur within the treatment plant. The tool also facilitated discussion with and reporting for the non-expert modellers and proved to be a valuable tool in the decision-making process.

Chapter 12

Process optimization: taking decisions under model uncertainty

"Prediction is very difficult, especially about the future."
Niels Bohr

12.1. ABSTRACT

In the European Union, the Water Framework Directive (WFD) enforces a good ecological and chemical status of all surface waters, which is to be accomplished before 2015. Mathematical process models have proven to be a valuable tool in this optimization exercise. A model based scenario analysis was undertaken to evaluate measures that could be taken to reduce the yearly total nitrogen discharge by the wastewater treatment plant of Eindhoven. Based on the modelling results all stakeholders held an in-depth discussion. In this chapter the simulation results obtained during the scenario analysis, which was performed as pre-screening for the global optimization (i.e. taking into account the sewer system, the wastewater treatment plant and the river system), and how these are used in the decision process, are reported . The project revealed that increasing the mixed liquor suspended solids (MLSS) concentrations in the biological tanks has a beneficial effect on both nitrate (up to 34% improvement) and ammonium removal (up to 25% improvement). Also the relocation of recycle B proved to be a promising option (reducing effluent NO_3 concentrations up to 23%). From these results it was concluded by the Waterboard that in future scenarios the new location of recycle B was to be maintained as part of any new proposed measure. The interaction with the different stakeholders proved to be really valuable for all parties and increased the acceptance of the modelling results, as such reducing the uncertainty inherent to

the process of taking decisions. This satisfying approach will also be used in future model based optimization studies at the WWTP of Eindhoven.

Part of this chapter was published as:
Amerlinck, Y., T. Flameling, T. Maere, S. Weijers, and I. Nopens, 2013, Practical application of dynamic process models for wastewater treatment plant optimization: Work in progress: WEFTEC 2013.

12.2. SYMBOLS

$Q_{Biol,max}$	Maximum flow rate allowed to the biological tanks

12.3. INTRODUCTION

In the European Union, the Water Framework Directive (WFD) enforces a good ecological and chemical status of all surface waters, which is to be accomplished before 2015 (2000/60/EC). Exceptions are only allowed after proper justification, e.g. when it is technically infeasible or disproportionately costly to restore the water body to good status by 2015. Many surface waters throughout Europe still do not meet the WFD requirements due to discharges of combined sewer overflows (CSO) and effluents of wastewater treatment plants (WWTP). The extent of non-compliance and the need for measures were to be decided in 2012, based on the results of dedicated monitoring programs, established since 2009 (Commission reports, COM(2009) 156 final and COM(2012) 670 final). Mathematical models provide a valuable tool for guiding these decisions.
Waterboard De Dommel (Boxtel, The Netherlands) has been using models of the WWTP since the early 1990s. Since 2007 a cooperation was set up with Ghent University (BIOMATH) to model the WWTP of Eindhoven (The Netherlands). During the course of time these models have continuously been improved to be able to address more difficult model objectives. Although the model predictions have improved significantly over the course of time, there is still the need to take decisions under uncertainty as models are simplifications of reality and by definition contain a certain degree of uncertainty (Belia et al., 2009).
The latest version of the WWTP model has been developed within the frame of the award winning KALLISTO project. The integrated urban water system project KALLISTO (www.samenslimschoon.nl) is an innovation programme aiming for a

smart improvement of the surface water quality of the river Dommel by applying cost effective integrated system measures. The focus of the program is on protection of the aquatic environment from oxygen dips and ammonia peaks caused by the combined discharges of the WWTP effluent, 200 combined sewer overflows (CSO) and a storm water settling tank at the WWTP.
In KALLISTO, the waterboard applies an innovative combination of monitoring, modelling and controlling water flows and constructing adequate infrastructural and technical measures to meet the goals of the project. The program reasons from the impact on ecology of the river (immission based instead of emission based), and an integrated approach is followed in several respects; the wastewater system (WWTP and sewers) and river are viewed as a whole, peak loads (storm events) and seasonal effects are regarded simultaneously and the Waterboard optimises control measures and infrastructure simultaneously (Weijers et al., 2012).
The WWTP model has been integrated within a model of the integral urban water system (IUWS) in Eindhoven (Langeveld et al., 2013b). The Waterboard is using this integral urban water system model for the global optimization.
In this chapter the simulation results obtained during the scenario analysis of the WWTP, which also served as pre-screening for the global optimization with the IUWS model of Eindhoven (Benedetti et al., 2013), are reported and it is discussed how these results are used in the decision process.

12.4. MATERIAL AND METHODS

12.4.1. Scenarios

Several scenarios have been simulated to answer questions for possible upgrade options taking into account measures for both dry and rain weather. The scenario analysis was performed as pre-screening for the global optimization, i.e. one of the outcomes of this scenario analysis was which scenarios to account for during the integrated urban water system optimization.
Although the simulations did not provide a perfect match (specifically for nitrate removal) decisions had to be made to continue the Kallisto project within the given timeframe. In order to reduce the uncertainty related to the use of models, stakeholders were involved (Belia et al., 2009). The chosen approach to communicate the modelling results was based on a detailed discussion with the technologists of Waterboard De Dommel. As such, this entailed increasing the level of understanding both for the wastewater technologists and the modellers. This resulted in a greater confidence in the modelling results. During the discussions

focus was given to trends rather than absolute numbers, as such taking into account the limitations of the models.
The goal of the study was to evaluate whether measures could be taken to reduce the yearly total nitrogen discharge without expanding the volume of the activated sludge tanks and without compromising BOD and dissolved oxygen concentration in the effluent. As such the evaluation during dry weather flows focuses on effluent ammonium concentration, nitrate, total nitrogen, BOD and dissolved oxygen. Table 12.1 lists the different optimization scenarios for dry weather conditions. The table shows the measure ID, a description and the technical requirements to achieve it.

Table 12.1. Overview of the different scenarios for dry weather treatment selected to stimulate denitrification.

ID	MEASURE	TECHNICAL
1.1.1.	Increased MLSS concentrations	Increasing overflow height SST and lowering sludge wastage
1.2.1.	Location recycle B	Adjusting configurations
1.3.1.	Increasing COD to anoxic tank in addition to scenario 1.2.1.	Carbon addition
1.3.2.	Increasing COD to anoxic tank in addition to scenario 1.2.1.	Bypass PST

12.4.2. Scenario 1.1.1.

The objective of this scenario is the optimization of nitrogen removal (nitrification and denitrification) by the increase of the mixed liquor suspended solids MLSS concentration. In this scenario this was accomplished by increasing the overflow height (weir) of the secondary sedimentation tank (SST) and reducing the sludge wastage via the MLSS setpoint (Table 12.2). The maximum flow rate allowed to the biological tanks ($Q_{Biol,max}$) remained unchanged at 26,250 m³/h.

Table 12.2. An overview of the different values for the MLSS set point and the height of the secondary sedimentation tank SST executed for scenario 1.1.1.

#	MLSS set point	H SST
A	3.4 g/l	3 m
B	4.0 g/l	3 m
C	4.5 g/l	3 m
D	3.4 g/l	3.5 m
E	4.0 g/l	3.5 m
F	4.5 g/l	3.5 m
G	3.4 g/l	4 m
H	4.0 g/l	4 m
I	4.5 g/l	4 m

12.4.3. Scenario 1.2.1.

The objective of this scenario is the optimization of nitrogen removal (nitrification and denitrification) by the relocation of recyle B (see Table 12.3 and Figure 12.1).

The maximum flow rate allowed to the biological tanks ($Q_{Biol,max}$) remained unchanged at 26,250 m³/h.

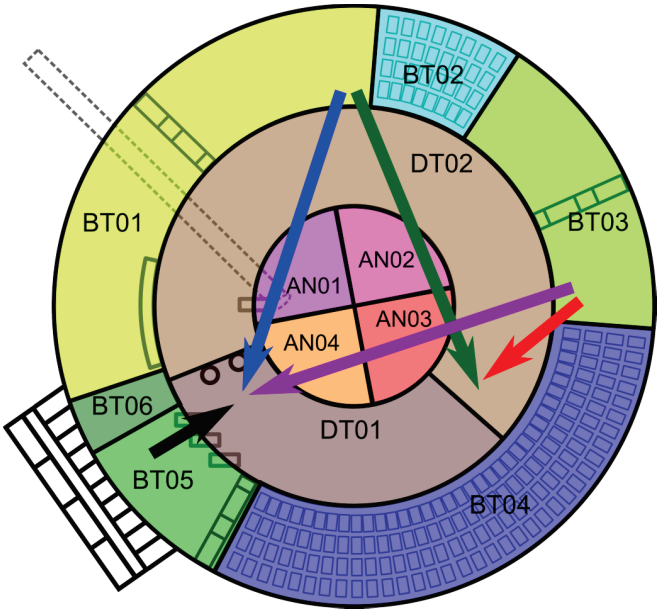

Figure 12.1. Scheme of the activated sludge tanks with possible relocation of recycle B (scenario 1.2.1) as listed in Table 12.3. The black arrow is the original location, the blue arrow shows relocation A, the green arrow shows relocation B, the purple arrow shows relocation C and the red arrow show the relocation D.

Table 12.3. An overview of the different options for the beginning and end of recycle B executed for scenario 1.2.1.

#	recycle B from outer ring	recycle B to middle ring
A	BT01	DT01
B	BT01	DT02
C	BT03	DT01
D	BT03	DT02

12.4.4. Scenario 1.3.1.

The objective of this scenario is the optimization of nitrogen removal (nitrification and denitrification) by the increase of the chemical oxygen demand (COD) load to the anoxic tank. In this scenario this was accomplished by chemical dosing in combination with a relocation of recycle B (Table 12.4 and Figure 12.2). The maximum flow rate allowed to the biological tanks ($Q_{Biol,max}$) remained unchanged at 26,250 m³/h.

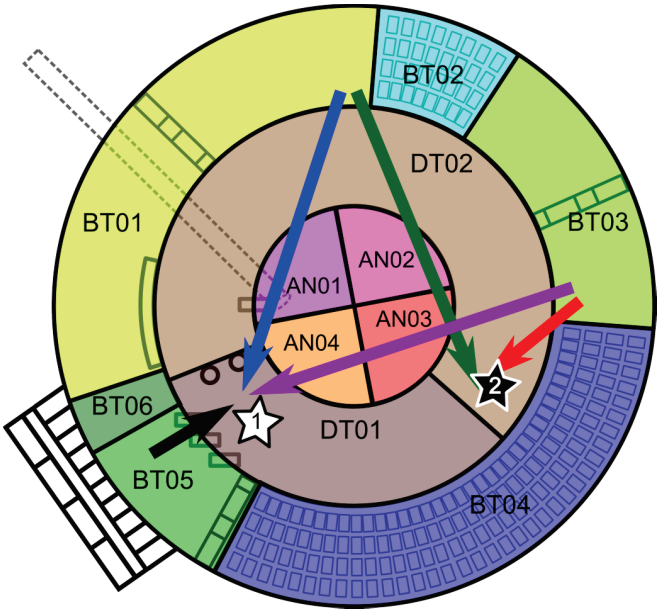

Figure 12.2. Scheme of the activated sludge tanks with two possible carbon dosing locations (large red/grey arrows) and possible relocation of recycle B (scenario 1.3.1) as listed in Table 12.4. The stars give the two possible locations for the carbon dosing.

Table 12.4. An overview of the different options for the location of the carbon dosing, the beginning and end of recycle B executed for scenario 1.3.1. The number between brackets refers to the dosing point as shown in Figure 12.2.

#	Carbon dosing in	recycle B from outer ring	recycle B to middle ring
A	DT01	BT05	DT01 (1)
B	DT01	BT01	DT01 (1)
C	**DT01**	**BT01**	**DT02 (2)**
D	**DT01**	**BT03**	**DT01 (1)**
E	DT01	BT03	DT02 (2)
F	DT02	BT05	DT01 (1)
G	DT02	BT01	DT01 (1)
H	DT02	BT01	DT02 (2)
I	DT02	BT03	DT01 (1)
J	DT02	BT03	DT02 (2)

12.4.5. Scenario 1.3.2.

The objective of this scenario is the optimization of nitrogen removal (nitrification and denitrification) by the increase of the COD load to the anoxic tank. In this scenario this increased load was accomplished by bypassing the PST without a relocation of recycle B (see Table 12.5 and Figure 12.3). The 2 degrees of freedom used are the percentage of bypass and the location where the bypass is introduced in the middle ring. The maximum flow rate allowed to the biological tanks ($Q_{Biol,max}$) remained unchanged at 26,250 m³/h.

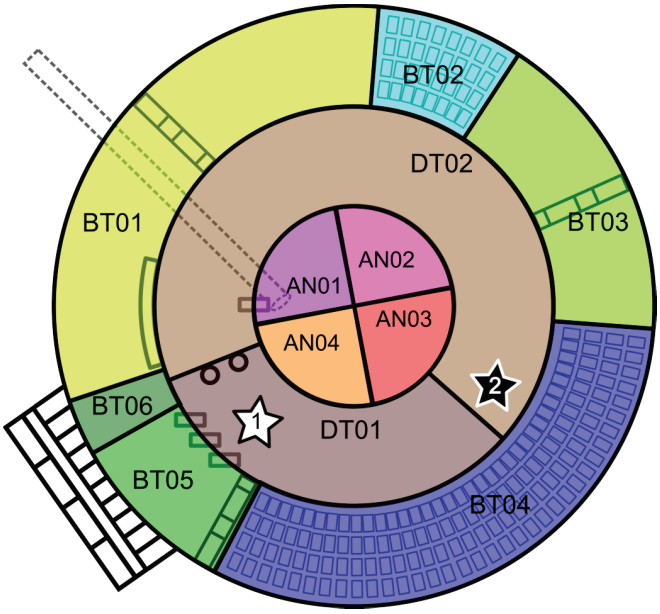

Figure 12.3. Scheme of the activated sludge tanks with two possible inlets for the PST bypass (black and white star) as listed in Table 12.5.

Table 12.5. An overview of the different options for the inlet location of the PST bypass and the amount of bypass executed for scenario 1.3.2.

#	Bypass to	Percentage of influent
A	DT01	0%
B	DT01	10%
C	DT01	20%
D	DT01	30%
E	DT01	40%
F	DT02	0%
G	DT02	10%
H	DT02	20%
I	DT02	30%
J	DT02	40%

12.5. RESULTS AND DISCUSSION

Figure 12.4 shows the results for dry weather scenario 1.1.1. Increasing the MLSS concentration (to 3.4 g/l, 4 g/l and 4.5 g/l) has a positive effect on both the nitrate (0.5, 19, 34% respectively) and ammonium removal (0.5, 14, 25% respectively) during dry weather. The model was unable to show a significant difference in effluent suspended solids when increasing the height of the clarifier. However, this is probably due to a limitation of the model, which was not designed for predicting this impact on the process performance.

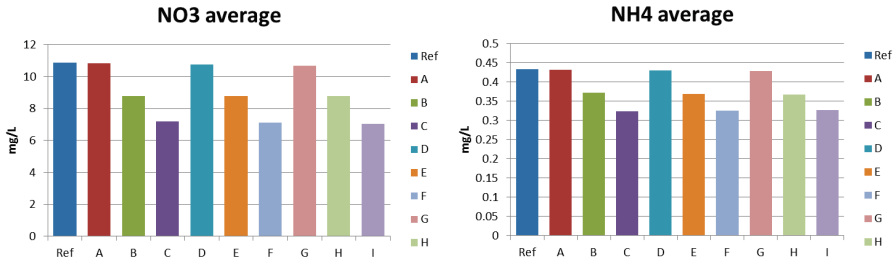

Figure 12.4. Results of the scenario analysis for scenario 1.1.1 for nitrate concentration (left) and ammonium concentration (right). Reference (MLSS 3.4 g/l – H 2.5 m), Scenario A (MLSS 3.4 g/l – H 3 m), Scenario B (MLSS 4 g/l – H 3 m), Scenario C (MLSS 4.5 g/l – H 3 m), Scenario D (MLSS 3.4 g/l – H 3.5 m), Scenario E (MLSS 4 g/l – H 3.5 m), Scenario F (MLSS 4.5 g/l – H 3.5 m), Scenario G (MLSS 3.4 g/l – H 4 m), Scenario H (MLSS 4 g/l – H 4 m) and Scenario I (MLSS 4.5 g/l – H 4 m).

Figure 12.5 shows the results for dry weather scenario 1.2.1. The relocation of the nitrate recycle (recycle B) has a positive effect on the nitrate removal (18, 20, 22, 23% reduction in NO_3 concentration) and a small negative effect on ammonium removal (0.7, 0.3, 0.1, 3.5% increase in NH_4 concentration) during dry weather. The optimal relocation is either option C or D, which are recycling from just before the summer package aeration. Thanks to the fact that the winter package aeration is not in use during dry weather, this significantly reduces the DO recirculation to the denitrification zone as these options take optimal use of the non-aerated zone in the outer ring for denitrification.

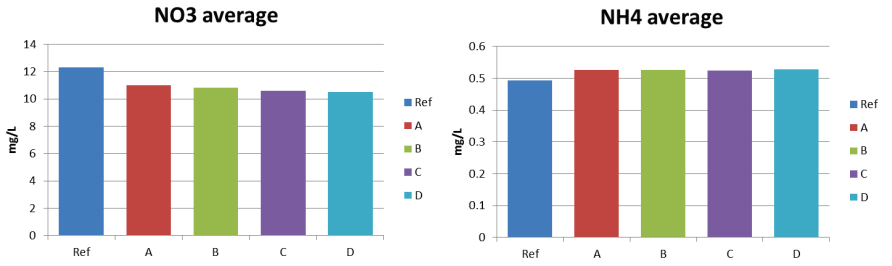

Figure 12.5. Results of the scenario analysis for dry weather scenario 1.2.1 regarding average nitrate concentration (left) and ammonium concentration (right). Reference (recycle B from outer ring section BT05 to middle ring section DT01), Scenario A (recycle B from outer ring section BT01 to middle ring section DT01), Scenario B (recycle B from outer ring section BT01 to middle ring section DT02), Scenario C (recycle B from outer ring section BT03 to middle ring section DT01) and Scenario D (recycle B from outer ring section BT03 to middle ring section DT02).

Figure 12.6 and Figure 12.7 show the results for dry weather scenario 1.3.1. The objective of this scenario is the optimization of nitrogen removal (nitrification and denitrification) by the increase of the COD load to the anoxic tank. The scenarios with chemical dosing and the original location of recycle B (scenario 1.3.1.A and

1.3.1.F) give the largest improvement in the removal of nitrate (about 57%). However, this comes with a very high consumption of chemicals (Figure 12.7). The other scenarios also give a large improvement of nitrate removal (between 52 and 54%) but with much lower carbon dosing (about 25 to 30% less). This leads to the conclusion that the same optimal recirculation location as found in scenario 1.2.1 leads to the best results in terms of denitrification performance and carbon dosage. During the discussions with the technologists, the simulations proved valuable to confirm their comprehension of the wastewater treatment plant and allowed the team to come up with a logic explanation of the observed behaviour. I.e. in the scenarios (A and F) with the current less optimal recirculation location more oxygen is recycled, which consumes the dosed carbon. In these scenarios the increase of denitrification is related to the increased sludge production and requires a higher amount of carbon source.

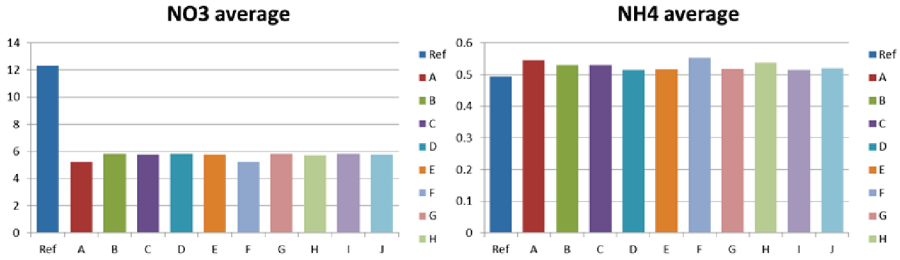

Figure 12.6. Results of the scenario analysis for the carbon dosing location and the relocation of the nitrate recycle (dry weather scenario 1.3.1) average nitrate concentration (left) and average ammonium concentration (right).

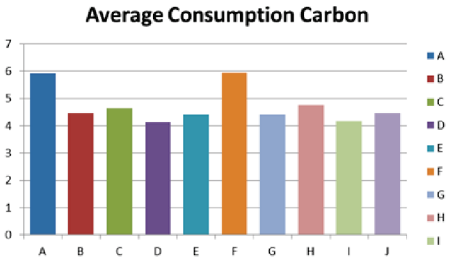

Figure 12.7. Results of the scenario analysis for the carbon dosing location and the relocation of the nitrate recycle (dry weather scenario 1.3.1) average carbon consumption.

Figure 12.8 shows the results of the dry weather scenario 1.3.2 where for some of the influent the PST is bypassed. An increase in percentage of influent that is bypassed increases the removal of nitrate. Bypassing to the second part of the anoxic tank gives another slight improvement of about 1%. Moreover, a slight improvement in ammonium removal is noticed. However, the improvements are significantly smaller compared to the other scenarios.

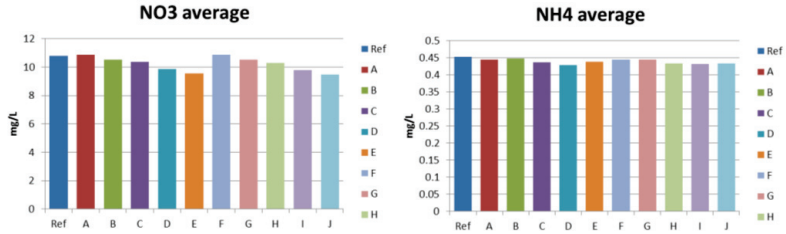

Figure 12.8. Results of the scenario analysis for dry weather scenario 1.3.2 regarding nitrate concentration (left) and ammonium concentration (right). Reference (No Bypass), Scenario A (Bypass of 0% to DT01), Scenario B (Bypass of 10% to DT01), Scenario C (Bypass of 20% to DT01), Scenario D (Bypass of 30% to DT01), Scenario E (Bypass of 40% to DT01), Scenario F (Bypass of 0% to DT02), Scenario G (Bypass of 10% to DT02), Scenario H (Bypass of 20% to DT02), Scenario I (Bypass of 30% to DT02) and Scenario J (Bypass of 40% to DT02).

12.6. CONCLUSIONS

A model based scenario analysis for the WWTP of Eindhoven was undertaken to evaluate measures that could be taken to reduce the yearly total nitrogen discharge to the river. Based on the modelling results, all stakeholders held an in-depth discussion, in this way increasing their confidence in the results. The project revealed that increasing the MLSS concentrations in the biological tanks has a beneficial effect on both nitrate (up to 34% improvement) and ammonium removal (up to 25% improvement). Also the relocation of recycle B revealed to be a promising option (reducing effluent NO_3 concentrations up to 23%). Even more in combination with the dosing of carbon (reducing effluent NO_3 concentrations up to 54%) or when partly bypassing the primary sedimentation tank (reducing effluent NO_3 concentrations up to 11%). One particular location of recycle B always gave the best performance. From these results it was concluded by the Waterboard that in future scenarios the new location of recycle B was to be maintained as part of any new proposed measure (no regret measure).

The interaction with the different stakeholders proved to be really valuable for all parties. The modellers increased their insight in the system and the related consequences for the model. The plant staff and managers found the discussions driven by the modelling results very fruitful in their understanding of the plant operation, which increased their confidence in the modelling results and helped them in designing future practical experiments at the plant. As such the interactions and discussions with all stakeholders proved a crucial factor in reducing the uncertainty for the decision making process.

PART VI

Conclusions and perspectives

Chapter 13

GENERAL CONCLUSIONS

"Science, my lad, is made up of mistakes, but they are mistakes which it is useful to make, because they lead little by little to the truth."
Jules Verne

13.1. Modelling wastewater treatment plants

One of the main challenges for the optimization of wastewater treatment plants, today, is the proper evaluation of all important performance indicators such as effluent quality (including priority pollutants), energy consumption and greenhouse gas emissions. Reducing the uncertainty in the simulation results is crucial in the general acceptance of and trust in modelling and can only be obtained when all relevant aspects are considered, as such avoiding sub optimal solutions. It is generally acknowledged that the largest uncertainties are located in the description of influent, hydraulics, gas-liquid mass transfers and primary and secondary settling.
This work has contributed to improving the balance in the WWTP models as such enhancing the quality of the model output. Indeed, more detail has been included in the sub-process models for influent characterization, primary sedimentation, oxygen transfer (aeration) and energy consumption (aeration blowers and pumps). Furthermore, the improvement of the simulation results for the WWTP of Eindhoven was demonstrated. In addition the models have been applied to describe observations at the plant which will allows support of decisions to be taken in the near future to make the plant WFD compliant.

13.2. Influent characterisation

In chapter 4, a measurement campaign was set up and samples were analysed using respirometric assays. Some hurdles regarding a better exploration of the impact of dilute wastewater conditions using respirometric assays are described and discussed.
Evaluating the performance of a wastewater treatment plant (WWTP) requires a good characterization of the biodegradable substrate entering the plant. As is generally acknowledged, the wastewater characterization under rain or storm weather conditions is significantly altered. This acknowledgment has, so far, not lead to a thorough investigation and evaluation of the influent characterisation during rain events. In this work some steps have been undertaken, but several factors are encountered that hamper the application of the respirometric assays for the influent fractionation, quantifying the biodegradable COD.
A first hurdle is the dependence of the yield of heterotrophs, of which an accurate value is required as a 10% mismatch leads to a variability of 18% in the estimation of biodegradable COD. In addition, the yield of heterotrophs is likely to change during storm events due to changed wastewater characteristics (e.g. first flush effects and dilution). However, the determination of the yield significantly extends the length of the analysis procedure, making its application difficult for high frequency measurements or measuring campaigns.
The low load conditions, due to the dilution effects during or after rain events, hampers the application of respirometric assays for influent fractionation as well. Attempts to improve the measurement have not been successful but indications are given that the evaluation of the assay output based on dynamic models (i.e. increasing the level of detail) will be needed to overcome the encountered hurdles.

13.3. Primary sedimentation

In chapters 5, 6 and 7 the modelling and mandatory data collection for primary sedimentation tanks have been addressed. Primary sedimentation tanks are often used as a preliminary step in wastewater treatment plants and have a significant impact on the subsequent processes caused by the considerable load reduction (50 to 70% of the suspended solids and 25 to 40% of the biochemical oxygen demand).
Primary sedimentation is a complex process involving flocculation, gravitational settling and drag. The gravitational settling in primary sedimentation tanks mainly occurs as discrete particle settling, of which the behaviour is independent of the

particle concentration, considerably different from secondary sedimentation tanks, but depends on the particle size distribution (and particle density distribution).
A literature review on modelling of primary sedimentation was conducted, taking into account a possible integration in the whole plant model of the WWTP of Eindhoven, and it was found that most modelling efforts are based on empirical relations and only a limited number of numerically more expensive models such as computational fluid dynamic (CFD) models are applied.
The empirical models, however, do not succeed in describing the high scatter present in primary sedimentation tank removal efficiency data, which is caused by the complexity of the process. The CFD models contribute much more detail but often fail to include the settling process in a coherent manner. In addition they are too complex to apply within a whole plant modelling context.
An excellent compromise is the so-called, phenomenological models such as the model of Bachis et al. (2012). These models are promising as they provide sufficient detail to model the impact of particle velocity distributions. In this work the model of Bachis et al. (2012) has been integrated within a rigorous discretization scheme as proposed by Bürger et al. (2011). The model was further extended with a differentiation between organic and inorganic matter, which is deemed crucial for description of the succeeding biological treatment.
For the evaluation of the primary sedimentation tank performance at the WWTP of Eindhoven, data was collected in collaboration with Waterboard The Dommel and comprised routinely collected data from January 5, 2011 till June 14, 2013 as well as data from 3 dedicated measurement campaigns. The analysis of the data showed the inconsistent variability in removal efficiencies between organic and inorganic matter, but as well for inert COD and biodegradable COD. In addition, some unexpected phenomena were observed, i.e. an increase in concentrations of soluble COD, NH_4, PO_4 and inorganic suspended solids.
The increase of ammonium and phosphate and the decrease of nitrate observed during the measurement campaign on May 6, 2014, was linked to the presence of both ordinary heterotrophic and phosphate accumulating organisms in the wastewater, by the application of a modified version of ASM2d, modelling the biological reactions.
On the other hand, the unexpected increase of inorganic suspended solids noticed during the measurement campaign on September 2, 2014, was associated to the formation of the precipitate hydroxylapatite and a consequent removal of phosphate, applying a physical-chemical model implemented in the modelling software PHREEQC.
Finally the impact of the sedimentation process on the whole WWTP of Eindhoven was modelled and implemented in the modelling software WEST (mikebyDHI). It

was proven that the primary sedimentation tanks definitely affect the denitrification but may also affect the nitrification. Moreover, the increased accuracy in modelling the PST demonstrated once again that uncalled calibration efforts can be avoided. The latter leads to a model with a higher predictive power.

13.4. Aeration and consumption of energy

In chapter 8, 9 and 10 more detailed models for the main energy consuming processes in WWTP, i.e. aeration and pumping, are extended and applied. For aeration, both the process implications and the energy consumption is being modelled. The approach for the modelling of aeration blower energy consumption is similar to the modelling of the pumping energy consumption, which is discussed as well.

An extensive measurement campaign with off-gas tests was performed at the WWTP of Eindhoven to provide more information on the performance and behaviour of the aeration system. A high spatial and temporal variability in the oxygen transfer efficiency was observed, indicating the need to grasp this behaviour in the aeration models. Applying this newly gathered system knowledge in the aeration model resulted in an improved fit of the dissolved oxygen concentrations. Moreover, an important consequence of this was that ammonium predictions could be improved by resetting the ammonium half-saturation coefficient for autotrophs to its default value. This again proved the importance of balancing sub-models with respect to the need for model calibration as well as model predictive power.

A new dynamic model for a more accurate prediction of aeration energy costs in activated sludge systems, equipped with submerged air distributing diffusers (producing coarse or fine bubbles) connected via piping to blowers, has been developed, calibrated and demonstrated for the WWTP of Mekolalde (Spain). The new model proved to give an accurate prediction of the real energy consumption by the blowers and captures the trends better than the constant average power consumption models currently being used. This enhanced prediction of energy peak demand, which dominates the price setting of energy, illustrates that the dynamic model is preferably used in multi-criteria optimization exercises for minimizing the energy consumption.

A new dynamic model for a more accurate prediction of pumping costs in wastewater treatment has been developed to restore the balance in the coupled sub-models. The model is calibrated using two case studies, for which the model proved

to predict the measured data of energy consumption. The model is also more accurate compared to other approaches to quantify energy consumption thus far, which paves the way towards 'global' process optimisation and new, improved control strategies for energy reduction at WWTPs.

13.5. Simulation Methodology

In chapter 11, 12 and 13 the application of the simulation methodology is explained. The simulation methodology comprises a section on calibration and one on process optimization under uncertainty. In general, the application of mathematical tools, such as global sensitivity analysis, mass balances and color based evaluation methods is encouraged.

The calibration methodology focusses on restoring the balance of the sub process models by improving the level of detail rather than force-fitting bio-kinetic parameters, as such maintaining the predictive quality of the model under varying process conditions. The calibration methodology was demonstrated on the WWTP of Eindhoven, improving the aeration and the primary sedimentation tank model, and gave excellent results for dissolved oxygen, ammonium and nitrate. Work is on-going for the short term rain weather and the long-term validation, for which the modelling work on the secondary clarifiers and a better characterization of mixing seems crucial.

A model based process optimization study for the WWTP of Eindhoven was reported, where the interactions and discussions with all stakeholders proved a crucial factor in reducing the uncertainty for the decision making process.

In addition to other tools such as mass balances, a simple yet effective colour-based system analysis tool for activated sludge models was proposed and illustrated for supporting model analysis. The tool allowed expert modellers to make a fast system analysis given the large amount of simulation outputs and the complex interactions that occur within the treatment plant. The tool also facilitated discussion with and reporting for the non-expert modellers and proved to be a valuable tool in the decision-making process.

In summary, this PhD has considerably extended the modelbase of less studied parts of the treatment plant allowing for better predictions of effluent quality and energy requirements. Moreover, it provided tools for model investigation and whole-plant model development. This can now serve as a solid basis for whole plant optimisation and controller development.

Chapter 14

PERSPECTIVES AND FUTURE WORK

"Whenever you find yourself on the side of the majority, it is time to pause and reflect."
Mark Twain

14.1. Influent characterisation

A lot of work has been done in the characterisation of wastewater in view of modelling activated sludge systems, however, little work has been performed on the characterisation during storm events. Several suggestions arise from the work performed here.
First, the characterisation of the yield of heterotrophs for the carbonaceous matter in storm water needs attention. As it is recognized that wastewater is different under these conditions this will lead to a difference in yield. This is important not only for modelling, but also for the plant performance and operational costs (aeration demand and sludge production). This suggestion might eventually lead to extended models incorporating different components for dry and storm weather. One might envision that this could end up with completely different activated sludge models, where the components are characterised using gas or liquid chromatography or even UV-VIS spectrophotometry.
Second, the investigation of the possibility of concentrating the wastewater samples by membrane filtration might be a route to explore. Although it looks straightforward, attention will need to be addressed on the impact of pore size of the membranes and the pressure (or vacuum) applied to the filtering.
Third, the combination of the characterisation in view of activated sludge modelling preceded by primary sedimentation tanks needs attention. This entails linking the particle size with biodegradability, which is currently a rather fuzzy method.

14.2. Primary sedimentation

Modelling of primary sedimentation has been revived, however, a lot of work needs to be accomplished. It is suggested to use the PSVD model implemented in the Bürger et al. (2011) model structure as basis and extend it with additional processes.

First, including the hydraulic retention time for soluble components, which will allow the modelling of the observed plug flow behaviour at the beginning of a storm event. I.e. the wastewater present in the PST with dry weather concentrations, i.e. high ammonium concentrations, is pushed into the biological treatment at the increased wet weather flow rate, leading to an ever higher load before the storm water dilution kicks in.

Second, linking the description of the particle settling velocity to the distributions of the particle characteristics (size and density). This will require additional measurements for the determination of the particle size and density distributions.

Third, the inclusion of biological and chemical reactions, allowing to more accurately describe the phenomena observed during the measurement campaign.

Fourth, modelling the flocculation behaviour and its impact on the settling process needs to be further investigated. This is not only true for regular primary sedimentation, but also for new technological approaches such as high rate systems.

Finally, re-integrating hindered and compression settling to propose a 'standard' model for sedimentation tanks, which allows the description of primary and secondary sedimentation tanks would be a useful addition to the current state of the art.

14.3. Aeration and consumption of energy

Despite the improvement the model by Rosso et al. (2005) introduced, it could and needs to be further improved. The linking of the α-factor to only the sludge age (SRT) and the airflow rate is questionable and lacks rigour in describing the physical phenomena behind. Indeed, considering the SRT is a global WWTP characteristic and aeration (oxygen transfer and the α-factor) is a local parameter influenced by local physics, using this as single predictor is too short-sighted. Actually the US EPA (1989) mentions the change of the α-factor over the length of the aeration tank, for which only one SRT is applicable.

First suggestion would be to study in more detail the correction factors applied for non-standard conditions. The temperature factor has not been studied at all, the α-

factor is a lumped factor and the β-factor is based on existing corrections for salt concentrations and temperature but these have not been developed nor tested for the wastewater matrix.
Second, many of the factors (surfactants, viscosity, floc volume) influencing the α-factor, have an impact on the formation and shape of the air bubbles. As such an evaluation on the drivers and the impact of bubble coalescence will yield a lot of information. In this evaluation, bubble column tests in combination with modelling frameworks such as population balance models (Nopens et al., 2015) will have a definite added value.
Third, the application of the aeration blower and pumping energy consumption models for other plants is need to verify and validate its applicability. Moreover, the implementation into the BSM framework would contribute to the application of the presented models.

14.4. Simulation Methodology

A few suggestions could be envisioned with regard to the simulation methodology.
First, in view of calibration, the use of optimal experimental design (OED), for lab or pilot scale tests would be a great advantage. For example the application of OED would be beneficial for the calibration of the sedimentation tank models and the enhanced biological phosphorus removal (EBPR) model. For the latter, standard phosphate uptake and release tests have proven to be too short in time to estimate a number of the relevant parameters (own work).
Second, in view of process optimization and the reduction of uncertainty, applying ensemble modelling (Bates and Granger, 1969), i.e. simulating multiple models with different model structures, is really valuable. Applying ensemble modelling allows for the assessment of model structure uncertainty, this in constrast with most commonly applied uncertainty assessment methods (e.g. Monte Carlo based) where the model structure is assumed to be perfect. Applying ensemble modelling for studying EBPR at the WWTP of Eindhoven, next to the modified ASM2d model, the bio-P model of TUD (Van Veldhuizen et al., 1999) and the UCT-Pho model (Hu et al., 2007) could be applied. When these different models give small variations in output the uncertainty is small for the simulated period at hand (and vice versa).

14.5. Restoring the balance in modelling the WWTP of Eindhoven

Although a lot of work has been done already in improving the detail for the different sub processes of the model of the Eindhoven WWTP, some suggestions are made that are not described in this work here.

First, improving the modelling of the hydraulics using compartmental models (Alvarado et al., 2012; Rehman et al., 2015). At this moment the number of tanks in series has been determined by expert judgement but should be derived from tracer tests and computational fluid dynamics. This improved modelling of the hydraulics will increase the model performance for rain weather events.

Second, calibrating the Bürger-Diehl (2011) model for secondary settling tanks, including the compression processes. This calibration is crucial for the further application in the whole plant model. After the calibration, finally the whole plant model can benefit from the better model structure, which is important in view of modelling storm events.

Third, evaluating the use of the biological phosphorus model applying global sensitivity analysis and calibrating the model using optimal experimental design (De Pauw, 2005).

Finally, a model based feasibility study on resource recovery and the impact on the wastewater treatment plant could be conducted. This includes the modelling of the potential struvite recovery from the sludge treatment facility in Mierlo.

These suggestions will contribute to WFD compliance and beyond this to the energy neutrality and concept of a WWTP becoming a WRRF or factory of resources.

Bibliography

Adamsson, A., V. Stovin, and L. Bergdahl, 2003, Bed shear stress boundary condition for storage tank sedimentation: Journal of Environmental Engineering-Asce, v. 129, p. 651-658.

Akca, L., C. Kinaci, and M. Karpuzcu, 1993, A model for optimum design of activated-sludge plants: Water Research, v. 27, p. 1461-1468.

Alarie, R. L., E. A. McBean, and G. J. Farquhar, 1980, SIMULATION MODELING OF PRIMARY CLARIFIERS: Journal of the Environmental Engineering Division-Asce, v. 106, p. 293-309.

Alvarado, A., S. Vedantam, P. Goethals, and I. Nopens, 2012, A compartmental model to describe hydraulics in a full-scale waste stabilization pond: Water Research, v. 46, p. 521-530.

Amerlinck, Y., T. Flameling, T. Maere, S. Weijers, and I. Nopens, 2014, Modelling dissolved air flotation as pre-treatment for reaching low P effluent with activated sludge: IWA Specialist Conference - Global Challenges: Sustainable Wastewater Treatment and Resource Recovery.

Amerlinck, Y., J. Roels, C. Thoeye, and L. Benedetti, 2009, Model-based optimization in view of energy savings of the WWTP of Oostende: 1st IWA BeNeLux Regional Young Water Professionals Conference.

Annesini, M. C., M. Beccari, and G. Mininni, 1979, Solids removal efficiency of primary settling tanks in municipal wastewater treatment plants: Water Air and Soil Pollution, v. 12, p. 441-447.

Anthony, J. W., R. A. Bideaux, K. W. Bladh, and M. C. Nichols, 2009, Handbook of Mineralogy, Mineralogical Society of America, Chantilly, VA 20151-1110, USA. http://www.handbookofmineralogy.org/.

APHA, 1992, Standard methods for the examination of water and wastewater: Washington, DC, USA.

Ast, T., M. DiBara, C. Hatcher, J. Turgeon, and M. O. Wizniak, 2008, Benchmarking Wastewater Facility Energy Performance Using ENERGY STAR® Portfolio Manager: Proceedings of the Water Environment Federation, v. 2008, p. 7322-7339.

Austin, D., and J. Nivala, 2009, Energy requirements for nitrification and biological nitrogen removal in engineered wetlands: Ecological Engineering, v. 35, p. 184-192.

Bachis, G., T. Maruéjouls, S. Tik, Y. Amerlinck, I. Nopens, P. Lessard, and P. A. Vanrolleghem, 2014, Modelling and characterisation of primary settlers in view of whole plant modelling and resource recovery: 4th IWA/WEF Wastewater treatment Modelling seminar.

Bachis , G., B. Vallet, T. Maruéjouls, L. Clouzot, P. Lessard, and P. A. Vanrolleghem, 2012, Particle classes-based model for sedimentation in urban wastewater systems: IWA Particle Separation Conference.

Bandyopadhyay, B., and A. E. Humphrey, 2009, Dynamic measurement of the volumetric oxygen transfer coefficient in fermentation systems.: Biotechnology and bioengineering, v. 104, p. 841-853.

Barker, P. S., and P. L. Dold, 1997, General model for biological nutrient removal activated-sludge systems: model presentation: Water Environment Research, v. 69, p. 969-984.

Barnett, M. W., M. K. Stenstrom, and J. F. Andrews, 1998, Dynamics and control of wastewater systems: Lancaster, Pennyslvania, U.S.A., CRC, Press.

Bates, J. M., and C. W. J. Granger, 1969, Combination of forecasts: Operational Research Quarterly, v. 20, p. 451-&.

Beal, C. M., A. S. Stillwell, C. W. King, S. M. Cohen, H. Berberoglu, R. P. Bhattarai, R. L. Connelly, M. E. Webber, and R. E. Hebner, 2012, Energy Return on Investment for Algal Biofuel Production Coupled with Wastewater Treatment: Water Environment Research, v. 84, p. 692-710.

BEE, B. o. E. E., 2006, Guide Books 3: Energy Efficiency in Electrical Utilities., Government of India, Ministry of Power, New Delhi, India.

Belia, E., Y. Amerlinck, L. Benedetti, B. Johnson, G. Sin, P. Vanrolleghem, K. Gernaey, S. Gillot, M. Neumann, L. Rieger, A. Shaw, and K. Villez, 2009, Wastewater treatment modelling: dealing with uncertainties: Water Science and Technology, v. 60, p. 1929-1941.

Benedetti, L., D. J. Batstone, B. De Baets, I. Nopens, and P. A. Vanrolleghem, 2008, Global sensitivity analysis of biochemical, design and operational parameters of the Benchmark Simulation Model no. 2: International Congress on Environmental Modelling and Software.

Benedetti, L., J. Langeveld, A. F. van Nieuwenhuijzen, J. de Jonge, J. de Klein, T. Flameling, I. Nopens, O. van Zanten, and S. Weijers, 2013, Cost-effective solutions for water quality improvement in the Dommel River supported by sewer-WWTP-river integrated modelling: Water Science and Technology, v. 68, p. 965-973.

Benson, B. B., and D. Krause Jr, 1984, The concentration and isotopic fractionation of oxygen dissolved in freshwater and seawater in equilibrium with the atmosphere: Limnology and oceanography, v. 29, p. 620-632.

Bernier, M., and B. Bourret, 1999, Pumping energy and variable frequency drives: Ashrae Journal, v. 41, p. 37-40.

BIPM, I., I. IFCC, and I. IUPAC, 1993, OIML, Guide to the Expression of Uncertainty in Measurement. International Organisation for Standardization, Geneva, Switzerland, ISBN 92-67-10188-9.

Bixio, D., G. Parmentier, D. Rousseau, F. Verdonck, J. Meirlaen, P. A. Vanrolleghem, and C. Thoeye, 2002, A quantitative risk analysis tool for design/simulation of wastewater treatment plants: Water Science and Technology, v. 46, p. 301-307.

Bixio, D., P. van Hauwermeiren, and C. Thoeye, 2000, Impact of primary treatment technologies on BNR: the case study of the STP of Ghent, Watermatex.

Boehnke, B., R. Schulze-Rettmer, and S. W. Zuckut, 1998, Cost-effective reduction of high-strength wastewater by adsorption-based activated sludge technology: Water-Engineering & Management, v. 145, p. 31-34.
Boogaard, F., F. van de Ven, J. Langeveld, and N. van de Giesen, 2014, Stormwater Quality Characteristics in (Dutch) Urban Areas and Performance of Settlement Basins: Challenges, v. 5, p. 112-122.
Box, G. E., and G. M. Jenkins, 1976, Time series analysis: forecasting and control: Oakland, CA: Holden-Day.
Boyce, M. P., 2002, Centrifugal compressors: a basic guide, The Boyce consultancy group, Texas, USA, p. 560.
Brent, R. P., 1973, Algorithms for minimization without derivatives: New York, USA, Prentice-Hall.
Bunn, S., 2007, Greenhouse Gas Reduction as an Additional Benefit of Optimal Pump Scheduling for Water Utilities: Proceedings of the Water Environment Federation, v. 2007, p. 1243-1252.
Böhnke, B., 1989, Bemessung der Stickstoffelimination in der Abwasserreinigung-Ergebnisse eines Erfahrungsaustausches der Hochschulen: Korrespondenz Abwasser, v. 9, p. 1046.
Bürger, R., S. Diehl, S. Farås, and I. Nopens, 2012, On reliable and unreliable numerical methods for the simulation of secondary settling tanks in wastewater treatment: Computers & Chemical Engineering, v. 41, p. 93-105.
Bürger, R., S. Diehl, and I. Nopens, 2011, A consistent modelling methodology for secondary settling tanks in wastewater treatment: Water Research, v. 45, p. 2247-2260.
Camp, T. R., and A. A. Estrada, 1953, Studies of Sedimentation Basin Design [with Discussion]: Sewage and Industrial Wastes, p. 1-14.
Campolongo, F., J. Cariboni, and A. Saltelli, 2007, An effective screening design for sensitivity analysis of large models: Environmental Modelling & Software, v. 22, p. 1509-1518.
Cao, Y. C., and A. Pawlowski, 2012, Sewage sludge-to-energy approaches based on anaerobic digestion and pyrolysis: Brief overview and energy efficiency assessment: Renewable & Sustainable Energy Reviews, v. 16, p. 1657-1665.
Chebbo, G., and M. C. Gromaire, 2009, VICAS-An Operating Protocol to Measure the Distributions of Suspended Solid Settling Velocities within Urban Drainage Samples: Journal of Environmental Engineering-Asce, v. 135, p. 768-775.
Choubert, J. M., L. Rieger, A. Shaw, J. Copp, M. Sperandio, K. Sorensen, S. Ronner-Holm, E. Morgenroth, H. Melcer, and S. Gillot, 2013, Rethinking wastewater characterisation methods for activated sludge systems - a position paper: Water Science and Technology, v. 67, p. 2363-2373.
Christoulas, D. G., P. H. Yannakopoulos, and A. D. Andreadakis, 1998, An empirical model for primary sedimentation of sewage: Environment International, v. 24, p. 925-934.
Cierkens, K., S. Plano, L. Benedetti, S. Weijers, J. de Jonge, and I. Nopens, 2012, Impact of influent data frequency and model structure on the quality of WWTP model calibration and uncertainty: Water Science & Technology, v. 65, p. **9**.

CIRIA, 1973, Cost-effective sewage: Treatment - the creation of an optimizing model. Report 46,2, London, CIRIA (Construction Industry Research and Information Association).

Coderre, A., 1999, Simulation du comportement d'unités de décantation primarie: évaluation du modèle de Takacs et al. (1991), Essai de maitrise, Université Laval, Québec.

Copp, J. B., 2002, The COST simulation benchmark—description and simulator manual: Luxembourg, Office for Official Publications of the European Communities.

Copp, J. B., H. Spanjers, and P. A. Vanrolleghem, 2002, Respirometry in Control of the Activated Sludge Process: Benchmarking Control Strategies: Scientific and Technical report, v. 11, IWA Publishing.

Corominas, L., L. Rieger, I. Takacs, G. Ekama, H. Hauduc, P. A. Vanrolleghem, A. Oehmen, K. V. Gernaey, M. C. M. van Loosdrecht, and Y. Comeau, 2010, New framework for standardized notation in wastewater treatment modelling: Water Science and Technology, v. 61, p. 841-857.

Cosenza, A., G. Mannina, P. A. Vanrolleghem, and M. B. Neumann, 2014, Variance-based sensitivity analysis for wastewater treatment plant modelling: Science of the Total Environment, v. 470, p. 1068-1077.

Coulson, J. M., J. F. Richardson, and J. R. Backhurst, 1999, Coulson & Richardson's Chemical Engineering: Fluid Flow, Heat Transfer and Mass Transfer, Elsevier Science & Tech.

Crittenden, J. C., R. R. Trussell, D. W. Hand, K. J. Howe, and G. Tchobanoglous, 2005, MWH's Water Treatment: Principles and Design: Hoboken, New Jersey, john Wiley & Sons, Inc. .

Dammel, E. E., and E. D. Schroeder, 1991, Density of activated-sludge solids: Water Research, v. 25, p. 841-846.

Danckwerts, P. V., 1951, Significance of Liquid-Film Coefficients in Gas Absorption: Industrial \& Engineering Chemistry, v. 43, p. 1460-1467.

Davidson, J. M., and T. L. Benson, 2003, Guidelines and procedures for pumping station assessments: Proceedings of the Water Environment Federation, v. 2003, p. 385-409.

de Haas, D. W., M. C. Wentzel, and G. A. Ekama, 2000, The use of simultaneous chemical precipitation in modified activated sludge systems exhibiting biological excess phosphate removal Part 1: Literature review: Water Sa, v. 26, p. 439-452.

De Pauw, D., 2005, Optimal experimental design for calibration of bioprocess models: a validated software toolbox.

De Pauw, D. J. W., and P. A. Vanrolleghem, 2006, Practical aspects of sensitivity function approximation for dynamic models: Mathematical and Computer Modelling of Dynamical Systems, v. 12, p. 395-414.

Delgado Diaz, S., L. Vera Pena, E. Gonzalez Cabrera, M. Martinez Soto, L. M. Vera Cabezas, and L. R. Bravo Sanchez, 2012, Effect of previous coagulation in direct ultrafiltration of primary settled municipal wastewater: Desalination, v. 304, p. 41 - 48.

Devisscher, M., G. Ciacci, L. Fe, L. Benedetti, D. Bixio, C. Thoeye, G. De Gueldre, S. Marsili-Libelli, and P. A. Vanrolleghem, 2006, Estimating costs and benefits of advanced control for wastewater treatment plants - the MAgIC methodology: Water Science and Technology, v. 53, p. 215-223.

Dircks, K., P. Pind, H. Mosbaek, and H. Mogens, 1999, Yield determination by respirometry - The possible influence of storage under aerobic conditions in activated sludge: Water SA, v. 25, p. 69-74.

Dold, P., and M. Fairlamb, 2001, Estimating oxygen transfer KLa, SOTE and air flow requirements in fine bubble diffused air systems: Proceedings of the Water Environment Federation, v. 2001, p. 780-791.

Donckels, B., 2009, Optimal experimental design to discriminate among rival dynamic mathematical models, Ghent University.

Drtil, M., P. Németh, and I. Bodik, 1993, Kinetic constants of nitrification: Water Research, v. 27, p. 35-39.

Dulekgurgen, E., S. Dogruel, O. Karahan, and D. Orhon, 2006, Size distribution of wastewater COD fractions as an index for biodegradability: Water Research, v. 40, p. 273-282.

Ekama, G. A., P. L. Dold, and G. v. R. Marais, 1986, Procedures for determining influent COD fractions and the maximum specific growoth rate of heterotrophs in activated sludge systems: Water Science & Technology, v. 18, p. 91-114.

El-Din, A., and D. Smith, 2002a, A combined transfer-function noise model to predict the dynamic behavior of a full-scale primary sedimentation tank: Water Research, v. 36, p. 3747 - 3764.

El-Din, A., and D. Smith, 2002b, Modeling a Full-Scale Primary Sedimentation Tank Using Artificial Neural Networks: Environmental Technology, v. 23, p. 479-496.

Escritt, L. B., 1972, Sewerage and Sewage Disposal, v. 2: London, McDonald and Evans Ltd.

Fabiyi, M. E., and R. Novak, 2008, Evaluation of the Factors that Impact Successful Membrane Biological Reactor Operations at High Solids Concentration: Proceedings of the Water Environment Federation, v. 2008, p. 503-512.

Fall, C., N. A. Flores, M. A. Espinoza, G. Vazquez, J. Loaiza-Návia, M. C. van Loosdrecht, and C. M. Hooijmans, 2011, Divergence Between Respirometry and Physicochemical Methods in the Fractionation of the Chemical Oxygen Demand in Municipal Wastewater: Water Environment Research, v. 83, p. 162-72.

Fenu, A., J. Roels, T. Wambecq, K. De Gussem, C. Thoeye, G. De Gueldre, and B. Van De Steene, 2010, Energy audit of a full scale MBR system: Desalination, v. 262, p. 121-128.

Flameling, A. G., B. A. H. Reitsma, M. J. Weijs, L. P. A. ter Beke, H. J. Marsman, M. Hoogenraad, and T. P. de Graaf, 2003, Definitief ontwerp RWZI Eindhoven, Waterschap de Dommel, p. 121.

Flores-Alsina, X., M. Arnell, Y. Amerlinck, L. Corominas, K. V. Gernaey, L. Guo, E. Lindblom, I. Nopens, J. Porro, A. Shaw, L. Snip, P. A. Vanrolleghem, and U. Jeppsson, 2014, Balancing effluent quality, economic cost and greenhouse gas

emissions during the evaluation of (plant-wide) control/operational strategies in WWTPs: Science of The Total Environment, v. 466–467, p. 616-624.
Funamizu, N., and T. Takakuwa, 1994, Simulation of the operating-conditions of the municipal waste-water treatment-plant at low-temperatures using a model that includes the IAWPRC activated-sludge model: Water Science and Technology, v. 30, p. 105-113.
Garcia, H. E., and L. I. Gordon, 1992, Oxygen solubility in seawater - beter fitting equations: Limnology and Oceanography, v. 37, p. 1307-1312.
Garcia-Ochoa, F., and E. Gomez, 2009, Bioreactor scale-up and oxygen transfer rate in microbial processes: An overview: Biotechnology Advances, v. 27, p. 153-176.
Gatti, M. N., F. García-Usach, A. Seco, and J. Ferrer, 2010, Wastewater COD characterization: analysis of respirometric and physical-chemical methods for determining biodegradable organic matter fractions: Journal of Chemical Technology & Biotechnology, v. 85, p. 536-544.
Germain, E., F. Nelles, A. Drews, P. Pearce, M. Kraume, E. Reid, S. J. Judd, and T. Stephenson, 2007, Biomass effects on oxygen transfer in membrane bioreactors: Water Research, v. 41, p. 1038-1044.
Gernaey, A. K., B. Petersen, J.-p. Ottoy, and P. Vanrolleghem, 2001a, Activated sludge monitoring with combined respirometric–titrimetric measurements: Water Research, v. 35, p. 1280-1294.
Gernaey, K., I. Nopens, D. Vrecko, J. Alex, and J. Dudley, 2006, An updated proposal for including further detail in the BSM2 PE calculation, [internal BSM2 taskgroup document].
Gernaey, K., B. Petersen, D. Dochain, and P. A. Vanrolleghem, 2002, Modeling aerobic carbon source degradation processes using titrimetric data and combined respirometric-titrimetric data: Structural and practical identifiability: Biotechnology and Bioengineering, v. 79, p. 754-767.
Gernaey, K., P. A. Vanrolleghem, and P. Lessard, 2001b, Modeling of a reactive primary clarifier: Water Science and Technology, v. 43, p. 73-81.
Gernaey, K. V., U. Jeppsson, P. A. Vanrolleghem, and J. B. Copp, 2014, Benchmarking of Control Strategies for Wastewater Treatment Plants, IWA Publishing.
Gernaey, K. V., and S. B. Jørgensen, 2004, Benchmarking combined biological phosphorus and nitrogen removal wastewater treatment processes: Control Engineering Practice, v. 12, p. 357-373.
Gillot, S., S. Capela-Marsal, M. Roustan, and A. Héduit, 2005, Predicting oxygen transfer of fine bubble diffused aeration systems—model issued from dimensional analysis: Water Research, v. 39, p. 1379-1387.
Gillot, S., and A. Heduit, 2008, Prediction of alpha factor values for fine pore aeration systems: Water Science and Technology, v. 57, p. 1265-1269.
Gillot, S., and A. Héduit, 2000, Effect of air flow rate on oxygen transfer in an oxidation ditch equipped with fine bubble diffusers and slow speed mixers: Water Research, v. 34, p. 1756-1762.
Goel, R., T. Mino, H. Satoh, and T. Matsuo, 1999, MOdeling hydrolysis processes considering intracellular storage: Water Science and Technology, v. 39, p. 97-105.

Grasso, D., K. Subramaniam, M. Butkus, K. Strevett, and J. Bergendahl, 2002, A review of non-DLVO interactions in environmental colloidal systems: Reviews in Environmental Science and Biotechnology, v. 1, p. 17-38.

Guisasola, A., G. Sin, J. A. Baeza, J. Carrera, and P. Vanrolleghem, 2005, Limitations of ASM1 and ASM3: a comparison based on batch oxygen uptake rate profiles from different full-scale wastewater treatment plants: Water Science and Technology, v. 52, p. 69-77.

Gujer, W., 2006, Activated sludge modelling: past, present and future: Water Science and Technology, v. 53, p. 111-119.

Hartel, L., and H. J. Popel, 1992, A Dynamic secondary clarifier model including processes of sludge thickening: Water Science and Technology, v. 25, p. 267-284.

Hauduc, H., S. Gillot, L. Rieger, T. Ohtsuki, A. Shaw, I. Takacs, and S. Winkler, 2009, Activated sludge modelling in practice: an international survey: Water Science and Technology, v. 60, p. 1943-1951.

Hauduc, H., L. Rieger, A. Oehmen, M. C. M. van Loosdrecht, Y. Comeau, A. Heduit, P. A. Vanrolleghem, and S. Gillot, 2013, Critical review of activated sludge modeling: State of process knowledge, modeling concepts, and limitations: Biotechnology and Bioengineering, v. 110, p. 24-46.

He, C., J. Marsalek, and Q. Rochfort, 2004, Numerical modelling of enhancing suspended solids removal in a CSO facility: Water Quality Research Journal of Canada, v. 39, p. 457-465.

Henderson, K. J., and D. J. Reardon, 2004, How overdesign leads to high energy costs and simple techniques to optimize energy usage: Proceedings of the Water Environment Federation, v. 2004, p. 368-374.

Henkel, J., P. Cornel, and M. Wagner, 2011, Oxygen transfer in activated sludge - new insights and potentials for cost saving: Water Science and Technology, v. 63, p. 3034-3038.

Henze, M., 1992, Characterization of wastewater for modelling of activated sludge processes: Water Science & Technology, v. 25, p. 1-15.

Henze, M., 2008, Biological Wastewater Treatment: Principles, Modeling, and Design, IWA Pub.

Henze, M., W. Gujer, T. Mino, and M. van Loosdrecht, 2000, Activated Sludge Models: *ASM1, ASM2, ASM2d and ASM3*: IWA Scientific and Technical Report: London, IWA Publishing.

Heynderickx, P. M., and J. Defrancq, 2013, Fysisch-chemische processen van de milieusanering: partim lucht en water, p. 280.

Higbie, R., 1935, The rate of adsorption of a pure gas into a still liquid during short periods of exposure: Trans. Am. Inst. Chem. Eng, v. 31, p. 365-389.

Hu, Z. R., M. C. Wentzel, and G. A. Ekama, 2007, A general kinetic model for biological nutrient removal activated sludge systems: Model development: Biotechnology and Bioengineering, v. 98, p. 1242-1258.

Hulsbeek, J. J. W., J. Kruit, P. J. Roeleveld, and M. C. M. van Loosdrecht, 2002, A practical protocol for dynamic modelling of activated sludge systems: Water Science and Technology, v. 45, p. 127-136.

International Organization for Standardization, 2002, Air Intake Filters, ISO 5011:2002, International Organization for Standardization, Geneva, Switzerland.

International Organization for Standardization, 2011, ISO 11885:2007, Water quality – Determination of selected elements by inductively coupled plasma optical emission spectrometry (ICP-OES).

Jeppsson, U., M. N. Pons, I. Nopens, J. Alex, J. B. Copp, K. V. Gernaey, C. Rosen, J. P. Steyer, and P. A. Vanrolleghem, 2007, Benchmark simulation model no 2: general protocol and exploratory case studies: Water Science and Technology, v. 56, p. 67-78.

Kappeler, J., and W. Gujer, 1992, Estimation of kinetic parameters of heterotrophic biomass under aerobic conditions and characterization of wastewater for activated sludge modelling: Water Science & Technology, v. 25, p. 125-139.

Kempton, S., R. M. Sterritt, and J. N. Lester, 1987, Heavy-metal removal in primary sedimentation. 2. The influence of metal speciation and particle-size distribution: Science of the Total Environment, v. 63, p. 247-258.

Kim, Y., K. Han, and W. Lee, 2003, Removal of organics and calcium hardness in liner paper wastewater using UASB and CO2 stripping system: Process Biochemistry, v. 38, p. 925-931.

Kim, Y. H., S. H. Yeom, J. Y. Ryu, and B. K. Song, 2004, Development of a novel UASB/CO2-stripper system for the removal of calcium ion in paper wastewater: Process Biochemistry, v. 39, p. 1393-1399.

Kynch, G. J., 1952, A theory of sedimentation: Trans. Faraday Soc., v. 48, p. 166-176.

Laboratory, R. R. E., 1989, Design Manual: Fine Pore Aeration Systems, U.S. Environmental Protection Agency, Office of Research and Development, Center for Enviromental Research Information.

Lagarde, F., M.-H. Tusseau-Vuillemin, P. Lessard, A. Héduit, F. Dutrop, and J.-M. Mouchel, 2005, Variability estimation of urban wastewater biodegradable fractions by respirometry: Water Research, v. 39, p. 4768-4778.

Langeveld, J. G., L. Benedetti, J. J. M. de Klein, I. Nopens, Y. Amerlinck, A. van Nieuwenhuijzen, T. Flameling, O. van Zanten, and S. Weijers, 2013a, Impact-based integrated real-time control for improvement of the Dommel River water quality: Urban Water Journal, v. 10, p. 312-329.

Langeveld, J. G., L. Benedetti, J. J. M. de Klein, I. Nopens, Y. Amerlinck, A. van Nieuwenhuijzen, T. Flameling, O. van Zanten, and S. Weijers, 2013b, Impact-based integrated real-time control for improvement of the Dommel River water quality: Urban Water Journal (Accepted).

Lesouef, A., M. Payraudeau, F. Rogalla, and B. Kleiber, 1992, OPTIMIZING NITROGEN REMOVAL REACTOR CONFIGURATIONS BY ON-SITE CALIBRATION OF THE IAWPRC ACTIVATED-SLUDGE MODEL: Water Science and Technology, v. 25, p. 105-123.

Lessard, P., and M. B. Beck, 1988, Dynamic Modeling of Primary Sedimentation: Journal of Environmental Engineering, v. 114, p. 753-769.

Lessard, P., and M. B. Beck, 1991, Dynamic simulation of storm tanks: Water Research, v. 25, p. 375-391.

Liptak, B. G., 2005, Instrument Engineers' Handbook, Fourth Edition, Volume Two: Process Control and Optimization, Taylor & Francis.

Liu, X. F., and M. H. Garcia, 2011, Computational Fluid Dynamics Modeling for the Design of Large Primary Settling Tanks: Journal of Hydraulic Engineering-Asce, v. 137, p. 343-355.

Lyn, D. A., A. I. Stamou, and W. Rodi, 1992, Density currents and shear-induced flocculation in sedimentation tanks: Journal of Hydraulic Engineering-Asce, v. 118, p. 849-867.

Maere, T., L. Benedetti, M. Janssen, S. Weijers, and I. Nopens, 2008, Use of an automated calibration methodology and scenario analysis for WWTP optimization: the Haaren case: Proceedings of SIDISA08, Simposio Internazionale di Ingegneria Sanitaria Ambientale.

Maere, T., L. Benedetti, and I. Nopens, 2009, An update on mixing and pumping costs of BSM-MBR : a benchmark simulation model for membrane bioreactors to compare control strategies: IWA BeNeLux Regional Young Water Professionals Conference, 1st, Abstracts.

Maere, T., B. Verrecht, S. Moerenhout, S. Judd, and I. Nopens, 2011, BSM-MBR: A benchmark simulation model to compare control and operational strategies for membrane bioreactors: Water Research, v. 45, p. 2181-2190.

Maiza, M., A. Bengoechea, P. Grau, W. De Keyser, I. Nopens, D. Brockmann, J. P. Steyer, F. Claeys, G. Urchegui, and E. Ayesa, 2011, A multi-layer modelling software framework supporting the design of automatic control solutions in WWTPs: 8th IWA Symposium on Systems Analysis and Integrated Assessment (Watermatex 2011).

Majone, M., K. Dircks, and J. J. Beun, 1999, Aerobic storage under dynamic conditions in activated sludge processes. The state of the art: Water Science & Technology, v. 39.

Martín de la Vega, P. T., M. A. Jaramillo, and E. Martínez de Salazar, 2013, Upgrading the biological nutrient removal process in decentralized WWTPs based on the intelligent control of alternating aeration cycles: Chemical Engineering Journal, v. 232, p. 213-220.

Maruejouls, T., P. A. Vanrolleghem, G. Pelletier, and P. Lessard, 2012, A phenomenological retention tank model using settling velocity distributions: Water Research, v. 46, p. 6857-6867.

Matko, T., N. Fawcett, A. Sharp, and T. Stephenson, 1996, Recent Progress in the Numerical Modelling of Wastewater Sedimentation Tanks: Process Safety and Environmental Protection, v. 74, p. 245 - 258.

Mazzolani, G., F. Pirozzi, and G. d'Antonoi, 1998, A generalized settling approach in the numerical modeling of sedimentation tanks: Water Science and Technology, v. 38, p. 95-102.

McCarty, P. L., 2007, Thermodynamic electron equivalents model for bacterial yield prediction: Modifications and comparative evaluations: Biotechnology and Bioengineering, v. 97, p. 377-388.

Melcer, H., 2003, Methods for Wastewater Characterization in Activated Sludge Modelling, Water Environment Research Foundation.

mikebyDHI, WEST.

Monod, J., 1942, Recherches sur la Croissance des Cultures Bactériennes (2nd edn.) Hermann, Paris.
Monteith, H., Y. Kalogo, and N. Louzeiro, 2007, Achieving stringent effluent limits takes a lot of energy!: Proceedings of the Water Environment Federation, v. 2007, p. 4343-4356.
Montgomery, J. M., 1985, Water treatment: principles and design: Canada, John Wiley & Sons, Inc., 696 p.
Morris, M. D., 1991, Factorial sampling plans for preliminary computational experiments: Technometrics, v. 33, p. 161-174.
Mwaikambo, L. Y., and M. P. Ansell, 2001, The determination of porosity and cellulose content of plant fibers by density methods: Journal of Materials Science Letters, v. 20, p. 2095-2096.
Nelder, J. A., and R. Mead, 1965a, A simplex method for function minimization: Computer Journal, v. 7, p. 308-313.
Nelder, J. A., and R. Mead, 1965b, A simplex method for function minization: computer journal v. 7, p. 308-313.
Niemann, K., and H. Orth, 2001, Control measures for wastewater treatment plants during storm flow: Water Science and Technology, v. 43, p. 309-314.
Nopens, I., 2005, Modelling the Activated Sludge Flocculation Process: a Population Balance Approach, 279 p.
Nopens, I., 2010, Modelling and control of Wastewater treatment plants: Department of Applied Mathematics, Biometrics and Process Control Research unit BIOMATH, UGent, (Course note of 1st/2nd Mater Bio-Science engineering).
Nopens, I., L. Benedetti, U. Jeppsson, M. N. Pons, J. Alex, J. B. Copp, K. V. Gernaey, C. Rosen, J. P. Steyer, and P. A. Vanrolleghem, 2010, Benchmark Simulation Model No 2: finalisation of plant layout and default control strategy: Water Science and Technology, v. 62, p. 1967-1974.
Nopens, I., E. Torfs, J. Ducoste, P. A. Vanrolleghem, and K. V. Gernaey, 2015, Population balance models: a useful complementary modelling framework for future WWTP modelling: Water Science and Technology, v. 71, p. 159-167.
Orhon, D., E. Ates, S. Sozen, and E. U. Cokgor, 1997, Characterization and COD fractionation of domestic wastewaters: Environmental Pollution, v. 95, p. 191-204.
Orhon, D., G. Insel, and O. Karahan, 2007, Respirometric assessment of biodegradation characteristics of the scientific pitfalls of wastewaters: Water Science and Technology, v. 55, p. 1-9.
Orhon, D., and D. Okutman, 2003, Respirometric assessment of residual organic matter for domestic sewage: Enzyme and Microbial Technology, v. 32, p. 560-566.
Otterpohl, R., 1995, Dynamische Simulation zur Unterstützung der Planung und des Betriebes kommunaler Kläranlagen, Ges. zur Förderung d. Siedlungswasserwirtschaft an d. RWTH Aachen.
Otterpohl, R., and M. Freund, 1992, Dynamic models for clarifiers of activated sludge plants with dry and wet weather flows: Water Science and Technology, v. 26, p. 1391-1400.

Paraskevas, P., G. Kolokithas, and T. Lekkas, 1993, A complete dynamic model of primary sedimenation: Environmental Technology, v. 14, p. 1037-1046.
Parkhurst, D. L., and C. A. J. Appelo, 2013, Description of Input and Examples for PHREEQC Version 3--a Computer Program for Speciation, Batch-reaction, One-dimensional Transport, and Inverse Geochemical Calculations.
Pasztor, I., P. Thury, and J. Pulai, 2008, Chemical oxygen demand fractions of municipal wastewater for modeling of wastewater treatment: International Journal of Environmental Science & Technology, v. 6, p. 51-56.
Peavy, H. S., D. R. Rowe, and G. Tchobanoglous, 1985, Environmental engineering New York, McGraw-Hill, Inc. .
Perry, R. H., D. W. Green, and J. O. Maloney, 1997, Perry's Chemical Engineers' Handbook, McGraw-Hill Book Company.
Petersen, B., 2000, Calibration, identificability and optimal experimental design of activated sludge models: PhD Thesis, Ghent University, Belgium, p. 362.
Petersen, B., P. Vanrolleghem, K. Gernaey, and M. Henze, 2002, Evaluation of an ASM1 model calibration procedure on a municipal–industrial wastewater treatment plant: Journal of Hydroinformatics, v. 4, p. 15-38.
Phillips, H. M., K. E. Sahlstedt, K. Frank, J. Bratby, W. Brennan, S. Rogowski, D. Pier, W. Anderson, M. Mulas, J. B. Copp, and N. Shirodkar, 2009, Wastewater treatment modelling in practice: a collaborative discussion of the state of the art: Water Science and Technology, v. 59, p. 695-704.
Racault, Y., A. E. Stricker, A. Husson, and S. Gillot, 2011, Monitoring the variations of the oxygen transfer rate in a full scale membrane bioreactor using daily mass balances: Water Science and Technology, v. 63, p. 2651-2657.
Ratkovich, N., W. Horn, F. P. Helmus, S. Rosenberger, W. Naessens, I. Nopens, and T. R. Bentzen, 2013, Activated sludge rheology: A critical review on data collection and modelling: Water Research, v. 47, p. 463-482.
Rehman, U., T. Maere, M. Vesvikar, Y. Amerlinck, M. Arnaldos, and I. Nopens, 2014, Hydrodynamic – biokinetic model integration applied to a full-scale WWTP, IWA World Water Congress & Exhibition, Lisbon, Portugal.
Rehman, U., M. Vesvikar, T. Maere, L. Guo, P. A. Vanrolleghem, and I. Nopens, 2015, Effect of sensor location on controller performance in a wastewater treatment plant: Water Science and Technology, v. 71, p. 700-708.
Reitsma, B. A. H., P. Telkamp, and H. J. Marsman, 2007, Proceshandboek RWZI Eindhoven, tweede druk, Waterschap de Dommel, p. 196.
Remy, C., M. Boulestreau, and B. Lesjean, 2014, Proof of concept for a new energy-positive wastewater treatment scheme: Water Science and Technology, v. 70, p. 1709-1716.
Ribes, J., J. Ferrer, A. Bouzas, and A. Seco, 2002, Modelling of an Activated Primary Settling Tank Including the Fermentation Process and VFA Elutriation: Environmental Technology, v. 23, p. 1147-1156.
Rieger, L., S. Gillot, G. Langergraber, and A. Shaw, 2012, Good Modelling Practice: Guidelines for Use of Activated Sludge Models, Iwa Publishing.
Riffat, R., 2013, Fundamentals of wastewater treatment and engineering United states, CRC Press, Taylor & Francis group. IWA publishing

Roeleveld, P. J., and M. C. M. van Loosdrecht, 2002, Experience with guidelines for wastewater characterisation in The Netherlands: Water Science and Technology, v. 45, p. 77-87.
Ronteltap, M., M. Maurer, and W. Gujer, 2007, Struvite precipitation thermodynamics in source-separated urine: Water Research, v. 41, p. 977-984.
Rooks, J. A., and A. K. Wallace, 2003, Energy efficiency of variable speed drive systems, Conference Record of the 2003 Annual Pulp and Paper Industry Technical Conference: Ieee Conference Record of Annual Pulp and Paper Industry Technical Conference: New York, Ieee, p. 160-163.
Ros, M., M. Dular, and P. A. Farkas, 1988, Measurement of respiration of activated sludge Water Research, v. 22, p. 1405-1411.
Rosenberger, S., K. Kubin, and M. Kraume, 2002, Rheology of Activated Sludge in Membrane Bioreactors: Engineering in Life Sciences, v. 2, p. 269--275.
Rossman, L. A., 2000, EPANET users manual 2.0., Cincinnati, USA, USEPA.
Rosso, D., R. Iranpour, and M. K. Stenstrom, 2005, Fifteen years of offgas transfer efficiency measurements on fine-pore aerators: Key role of sludge age and normalized air flux: Water Environment Research, v. 77, p. 266-273.
Rosso, D., J. A. Libra, W. Wiehe, and M. K. Stenstrom, 2008, Membrane properties change in fine-pore aeration diffusers: Full-scale variations of transfer efficiency and headloss: Water Research, v. 42, p. 2640-2648.
Rosso, D., and M. K. Stenstrom, 2005, Comparative economic analysis of the impacts of mean cell retention time and denitrification on aeration systems: Water Research, v. 39, p. 3773-3780.
Rosso, D., and M. K. Stenstrom, 2006, Surfactant effects on α-factors in aeration systems: Water Research, v. 40, p. 1397-1404.
Saltelli, A., M. Ratto, T. Andres, F. Campolongo, J. Cariboni, D. Gatelli, M. Saisana, and S. Tarantola, 2008, Global sensitivity analysis: the primer, John Wiley & Sons.
Saul, A. J., and D. R. Ellis, 1992, Sediment depostion in storage tanks: Water Science and Technology, v. 25, p. 189-198.
Schilperoort, R. P. S., 2011, Monitoring as a Tool for the Assessment of Wastewater Quality Dynamics, Technical University of Delft, The Netherlands.
Schuler, A. J., and H. Jang, 2007, Microsphere addition for the study of biomass properties and density effects on settleability in biological wastewater treatment systems: Water Research, v. 41, p. 2163-2170.
Segev, R., D. Hasson, and R. Semiat, 2011, Improved high recovery brackish water desalination process based on fluidized bed air stripping: Desalination, v. 281, p. 75-79.
Shiba, S., and Y. Inoue, 1975, Dynamic response of settling basins: Journal of the Environmental Engineering Division-Asce, v. 101, p. 741-755.
Sierp, F., 1967, Die Gewerblichen und industriellen Abwässer. Entstehung, Schädlichkeit, Verwertung, Reinigung und Beseitigung. 3.Aufl, Springer.
Silva, C., S. Quadros, P. Ramalho, H. Alegre, and M. J. Rosa, 2014, Translating removal efficiencies into operational performance indices of wastewater treatment plants: Water Research, v. 57, p. 202 - 214.

Sin, G., D. J. W. De Pauw, S. Weijers, and P. A. Vanrolleghem, 2008, Developing a framework for continuous use of models in daily management and operation of WWTPs: a life cycle approach: Water Science and Technology, v. 57, p. 1301-1307.

Smith, R., 1969, Preliminary Design of Wastewater Treatment Systems: Journal of the Sanitary Engineering Division, v. 95, p. 31.

Sollfrank, U., and W. Gujer, 1991, Characterisation of domestic wastewater for mathematical modelling of the activated sludge process Water Science & Technology, v. 23, p. 1057-1066.

Sophonsiri, C., and E. Morgenroth, 2004, Chemical composition associated with different particle size fractions in municipal, industrial, and agricultural wastewaters: Chemosphere, v. 55, p. 691-703.

Spanjers, H., P. A. Vanrolleghem, G. Olsson, and P. L. Dold, 1998, Respirometry in Control of the Activated Sludge Process: Principles: Scientific and Technical reports, v. 7: London, IWA Publishing, 48 p.

Sperandio, M., V. Urbain, P. Ginestet, M. J. Audic, and E. Paul, 2001, Application of COD fractionation by a new combined technique: comparison of various wastewaters and sources of variability: Water Science and Technology, v. 43, p. 181-190.

Spérandio, M., and E. Paul, 2000, Estimation of wastewater biodegradable COD fractions by combining respirometric experiments in various So/Xo ratios: Water Research, v. 34, p. 1233-1246.

Stenstrom, M. K., and R. G. Gilbert, 1981, Effects of alpha, beta and theta factor upon the design, specification and operation of aeration systems: Water Research, v. 15, p. 643-654.

Stenstrom, M. K., S.-Y. Leu, and P. Jiang, 2006, Theory to Practice: Oxygen Transfer and the New ASCE Standard: Proceedings of the Water Environment Federation, v. 2006, p. 4838-4852.

Stephenson, T., and J. N. Lester, 1987, Heavy metal behavior during the activated sludge process. 2. Insoluble metal removal mechanisms: Science of the Total Environment, v. 63, p. 215-230.

Stricker, A. E., P. Lessard, A. Heduit, and P. Chatellier, 2003, Observed and simulated effect of rain events on the behaviour of an activated sludge plant removing nitrogen: Journal of Environmental Engineering and Science, v. 2, p. 429-440.

Strotmann, U. J., A. Geldern, A. Kuhn, C. Gendig, and S. Klein, 1999, Evaluation of a respirometric test method to determine the heterotrophic yield coefficient of activated sludge bacteria: Chemosphere, v. 38, p. 3555-3570.

Stumwohrer, K., N. Matsche, and S. Winkler, 2003, Influence of changes of the wastewater composition on the applicability of UV-absorption measurements at combined sewer overflows: Water Science and Technology, v. 47, p. 73-78.

Subcommittee, A. S. C. E. O. T. S., 1997, Standard Guidelines for In-Process Oxygen Transfer Testing (ASCE 18-96), American Society of Civil Engineers.

Takamatsu, M., M. Barrett, and R. J. Charbeneau, 2009, Hydraulic model for sedimentation in storm-water detention basins: Journal of Environmental Engineering, v. 136, p. 527-534.

Takamatsu, M., M. E. Barrett, and R. J. Charbeneau, 2012, Alternative Approach to Evaluate Sedimentation Performance of Stormwater Detention Basins Using a Nondimensionalized Time Scale: Journal of Environmental Engineering-Asce, v. 138, p. 809-814.

Takács, I., G. G. Patry, and D. Nolasco, 1991, A dynamic model of the clarification-thickening process: Water Research, v. 25, p. 1263-1271.

Tay, J. H., 1982, Development of a settling model for primary settling tanks: Water Research, v. 16, p. 1413-1417.

Tchobanoglous, G., F. L. Burton, Metcalf, Eddy, and H. D. Stensel, 2004, Wastewater Engineering: Treatment and Reuse, McGraw-Hill.

Tebbutt, T. H. Y., 1979, Primary sedimentation of wastewater: Journal Water Pollution Control Federation, v. 51, p. 2858-2867.

The Engineering Toolbox, 2005, Air pressure and altitude above sea level, http://www.engineeringtoolbox.com/air-altitude-pressure-d_462.html.

Thomas, V. K., B. Chambers, and W. Dunn, 1989, Optimization of aeration efficiency - A design procedure for secondary-treatment using a hybrid aeration system: Water Science and Technology, v. 21, p. 1403-1419.

Torfs, E., T. Maere, R. Bürger, S. Diehl, and I. Nopens, 2015, Impact on sludge inventory and control strategies using the benchmark simulation no. 1 with the Bürger-Diehl settler model: Water Science & Technology, v. 71, p. 11.

U.S. Department of Energy, 2008, Motor tip sheet #11: Adjustable Speed Drive Part-Load Efficiency, p. 2.

Ulanicki, B., J. Kahler, and B. Coulbeck, 2008, Modeling the efficiency and power characteristics of a pump group: Journal of Water Resources Planning and Management-Asce, v. 134, p. 88-93.

US EPA, R. R. E. L., 1989, Design Manual: Fine Pore Aeration Systems, U.S. Environmental Protection Agency, Office of Research and Development, Center for Enviromental Research Information.

Van Hoey, S., P. Seuntjes, J. van der Kwast, and I. Nopens, 2014, A qualitative model structure sensitivity analysis method to support model selection: Journal of Hydrology, v. 519, Part D, p. 3426 - 3435.

Van Veldhuizen, H. M., M. C. M. Van Loosdrecht, and J. J. Heijnen, 1999, Modelling biological phosphorus and nitrogen removal in a full scale activated sludge process: Water Research, v. 33, p. 3459-3468.

Vanrolleghem, P., 2002, Principles of respirometry in activated sludge wastewater treatment: Proceedings International Workshop on Recent Development in Respirometry for Wastewater Treatment Plant Monitoring and Control. Tawain: Taipei.

Vanrolleghem, P., H. Spanjers, B. Petersen, P. Ginestet, and I. Takacs, 1999, Estimating (combinations of) activated sludge model NO. 1 parameters and components by respirometry: Water Science & Technology, v. 39, p. 195-214.

Vanrolleghem, P. A., G. Insel, B. Petersen, G. Sin, D. De Pauw, I. Nopens, H. Dovermann, S. Weijers, and K. Gernaey, 2003, A comprehensive model calibration procedure for activated sludge models: Proceedings of the Water Environment Federation, v. 2003, p. 210-237.

Vanrolleghem, P. A., and H. Spanjers, 1998, A hybrid respirometric method for more reliable assessment of activated sludge model parameter: Water Science and Technology, v. 37, p. 237-246.
Vieira, T. S., J. R. Siqueira, A. D. Bueno, R. E. M. Morales, and V. Estevam, 2015, Analytical study of pressure losses and fluid viscosity effects on pump performance during monophase flow inside an ESP stage: Journal of Petroleum Science and Engineering, v. 127, p. 245-258.
VITO, 2012, Compendium voor analyse van water, Bepaling van de geselecteerde elementen met inductief gekoppeld plasma atomaireemissiespectrometrie (WAC/III/B/010), Belgisch staatsblad (19 april 2012).
Voshel, D., and J. G. Sak, 1968, Effect of primary effluent suspended solids and bod on activated sludge production: Journal Water Pollution Control Federation, v. 40, p. R203-&.
Wadley, S., and C. A. Buckley, 1997, Chemical speciation self-study work manual Pollution Research Group, Department of Chemical Engineering, University of Natal
Wagner, M., P. Cornel, and S. Krause, 2002, Efficiency of Different Aeration Systems in Full Scale Membrane Bioreactors: Proceedings of the Water Environment Federation, v. 2002, p. 434-443.
Walski, T. M., T. E. Barnard, E. Harold, L. B. Merritt, N. Walker, and B. E. Whitman, 2004, Wastewater collection system modeling and design.
Walski, T. M., D. V. Chase, D. A. Savic, W. Grayman, S. Beckwith, and E. Koelle, 2003, Advanced Water Distribution Modeling and Management.
Wambecq, T., A. Fenu, K. De Gussem, G. Parmentier, G. De Gueldre, and B. Van de Steene, 2013, The impact of horizontal water velocity on the energy consumption of a full-scale wastewater treatment plant: Water and Environment Journal, v. 27, p. 247-252.
Wang, L. K., Y. T. Hung, and N. K. Shammas, 2007, Advanced Physicochemical Treatment Processes, Humana Press.
WEF, 2009a, Design of Municipal Wastewater Treatment Plants MOP 8, Fifth Edition, McGraw-Hill Education.
WEF, 2009b, Energy Conservation in Water and Wastewater Facilities - MOP 32, McGraw-Hill Education.
WEF, 2013, Wastewater Treatment Process Modeling, MOP 31, 2nd Edition, WEF Press, 388 p.
Weijers, S. R., J. de Jonge, O. van Zanten, L. Benedetti, J. Langeveld, H. W. Menkveld, and A. F. van Nieuwenhuijzen, 2012, KALLISTO: cost effective and integrated optimization of the urban wastewater system Eindhoven: Water Practice & Technology, v. 7.
Weiss, R. F., 1970, The solubility of nitrogen, oxygen and argon in water and seawater: Deep Sea Research and Oceanographic Abstracts, v. 17, p. 721 - 735.
Wentzel, M. C., M. F. Ubisi, M. T. Lakay, and G. A. Ekama, 2002, Incorporation of inorganic material in anoxic/aerobic-activated sludge system mixed liquor: Water Research, v. 36, p. 5074-5082.
Whitman, W. G., 1962, The two film theory of gas absorption: International Journal of Heat and Mass Transfer, v. 5, p. 429 - 433.

Yoshikawa, M., Y. Hoshino, and N. Iwata, 2013, Role of seed settleability and settling velocity in water for plant colonization of river gravel bars: Journal of Vegetation Science, v. 24, p. 712-723.

Young, J. C., and R. M. Cowan, 2004, Respirometry for Environmental Science and Engineering, SJ Enterprises.

Zahreddine, P., L. Dufresne, J. Wheeler, S. Couture, D. Reardon, and K. Henderson, 2010, Energy Conservation Measures for Municipal Wastewater Treatment Innovative Technologies and Practices: Proceedings of the Water Environment Federation, v. 2010, p. 3359-3384.

Appendix A

The whole plant model of Eindhoven

Figure A.1 gives an overview of the layout of the whole plant model of the WWTP of Eindhoven, comprising all the important treatment steps at the plant, i.e. including the implementation of the controls. Table A.1 gives an overview of the used sub-models.

Table A.1. Overview of the process units and the corresponding models for the EHV-10 model (including controllers) ordered as in the treatment scheme.

Name	WEST Model name	Purpose of the model
in	Eindhoven_fract2	Influent and fractionation model
SF01	Flow	Measurement influent flow rate
SQI01	EffluentQualityIndex	Measurement water quality parameters in the influent – model construction
M01	TwoCombiner	Combining influent and recycle from rain buffer tank
Q_Biology	AbsTwoSplitter	Split flow biology and rain buffer tank
SF02	Flow	Measurement flow rate to rain buffer tank
RB_PST	PrimaryPointSettler	Rain buffer tank model part 1 - removal suspended solids – model construction
RB_Buffer	PumpedVolumeBuffer_Eindhoven	Rain buffer tank model part 2 –storage, recycle and overflow
P_RRB	AbsTwoSplitter	Recycle to influent pumps from rain buffer tank
C_RRB	Raintank_Eindhoven	Flow rate control to influent pumps from rain buffer tank
M02	TwoCombiner	Combining normal emptying and removed sludge
L_RRB	DifferentialLoopBreaker	Model artefact: numerical solution solving solve sets
PST	Tay4	Sand trap and Primary sedimentation tank
SF03	Flow	Measurement flow rate after PST
M03	TwoCombiner	Combining flow from PST and recirculation A
D_Al	Alum	Alum dosing
C_Al	OperatorDelayed	Control alum dose based on effluent PO_4 measurements
D_Fe	IronHydroxide	Iron dosing
M04	ThreeCombiner	Combining mainstream with dosed metal salts
TC_TG	MEChemical	Chemical phosphate removal
AN01	FixVolumeASU	Anaerobic tank – compartiment 1
AN02	FixVolumeASU	Anaerobic tank – compartiment 2
AN03	FixVolumeASU	Anaerobic tank – compartiment 3
AN04	FixVolumeASU	Anaerobic tank – compartiment 4
M05	ThreeCombiner	Combining flow from the anaerobic tank to denitrification tank, RAS and recirculation B
M06	TwoCombiner	Combining internal recirculation denitrification tank and flow from anaerobic tank

DT1	FixVolumeASU	Denitrification tank – compartiment 1
DT2	FixVolumeASU	Denitrification tank – compartiment 2
P_RecA_IRDT	AbsThreeSplitter	Splitting recirculation A, internal recirculation denitrification tank and flow from denitrification tank to aerated tanks
C_RecA	Linear_Saturation	Control recirculation A
L_DT	DifferentialLoopBreaker	Model artefact: numerical solution solving solve sets
L_RecA	DifferentialLoopBreaker	Model artefact: numerical solution solving solve sets
SOD01	OD	Measurement oxygen demand in flow from denitrification tank to the aerated tank
M07	TwoCombiner	Combining flow from denitrification tank to the aerated tank and internal recirculation aerated tank
SOD02	OD	Measurement oxygen demand in the aerated tank
BT01	FixVolumeASU	Aerated tank – compartiment 1
BT02	FixVolumeASU	Aerated tank – compartiment 2 (with winter aeration package)
A_WP	Irvine_Aeration_model_Carbon_foot_print	Winter aeration package
C_Q_Air WP	OnOffBand	Control airflow rate winter aeration package
BT03	FixVolumeASU	Aerated tank – compartiment 3
BT04	FixVolumeASU	Aerated tank – compartiment 4 (with summer aeration package)
A_ZP	Irvine_Aeration_model_Carbon_foot_print	Summer aeration package
C_NH4	PID_AntiWindup_Saturation	Ammonium control
C_Q_Air ZP	PID_AntiWindup_Saturation	Control airflow rate summer aeration package
BT05	FixVolumeASU	Aerated tank – compartiment 5
P_RecB	AbsTwoSplitter	Combining recirculation B
C_RecB	PI_Saturation_recB_EHV	Control recirculation B
L_RecB	DifferentialLoopBreaker	Model artefact: numerical solution solving solve sets
BT06	FixVolumeASU	Aerated tank – compartiment 6
IR_BT	AbsTwoSplitter	Internal recirculation aerated tank
L_BT	DifferentialLoopBreaker	Model artefact: numerical solution solving solve sets
CA	FixVolumeASU	Cascade after aerated tank
SST	BurgerDoubleExponential	Secondary sedimentation tank
C_RAS	ConstantRatioWithOffset_Saturation	Control underflow rate of SST
M08	TwoCombiner	Combining effluent activated sludge tanks and overflow rain buffer tank
SPO401	PO4	PO_4 measurement in the effluent
SQI02	EffluentQualityIndex	Measurement water quality parameters in the effluent – model construction
P_WAS	AbsTwoSplitter	Sludge wastage pump
C_WAS	PI_Saturation	Control sludge wastage
SQI03	EffluentQualityIndex	Measurement water quality parameters in the sludge wastage – model construction
L_RAS	DifferentialLoopBreaker	Model artefact: numerical solution solving solve sets

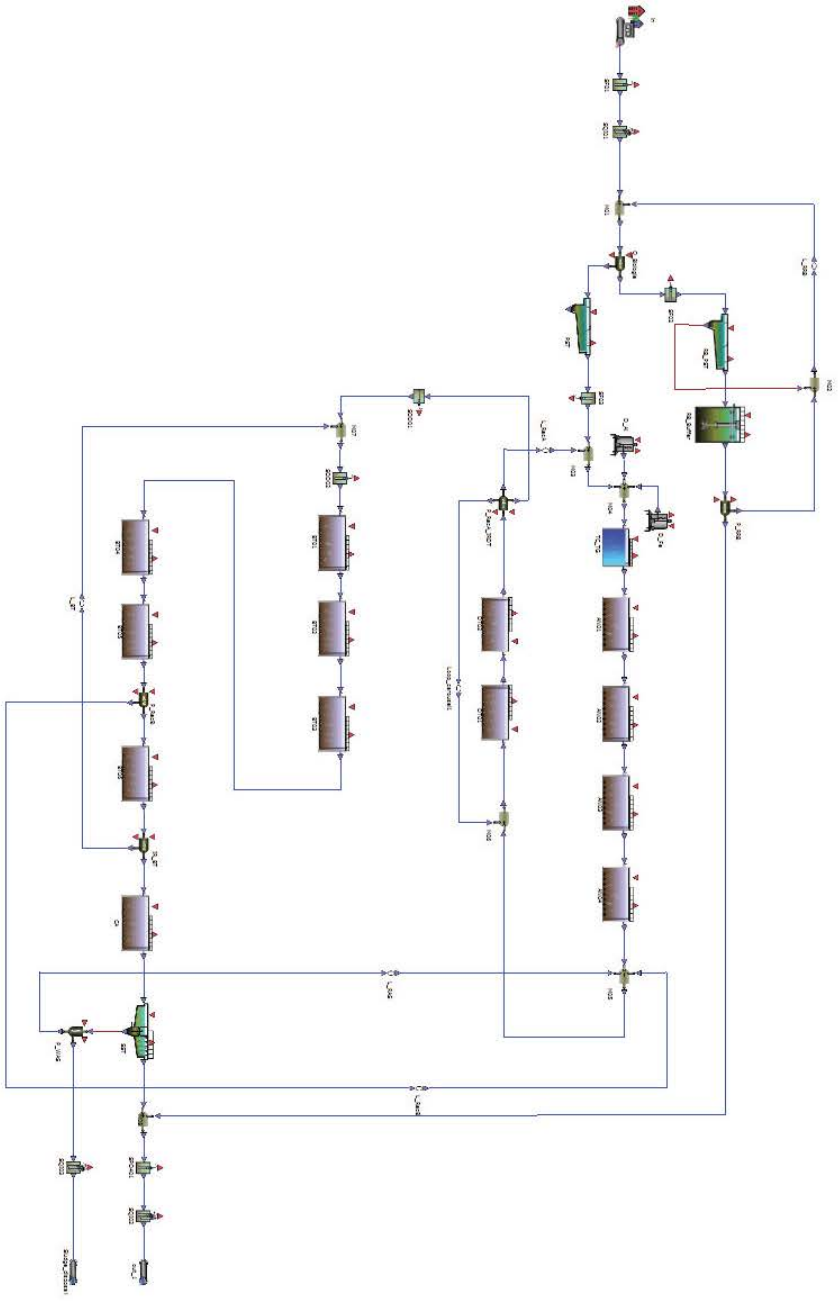

Figure A.1. Layout of the WWTP of Eindhoven model.

Biokinetic model

The ASM2d model (Henze et al., 2000) forms the basis of the biokinetic model used in the whole plant model of the WWTP of Eindhoven. A first extension is the adaptation to make the lysis of biomass dependent on the environmental factors (anaerobic, anoxic or aerobic) (Gernaey and Jørgensen, 2004). The second extension is the inclusion of a particulate inorganic fraction (Wentzel et al., 2002), which was necessary for the calculation of the removal efficiencies of the primary sedimentation tanks using the new improved model. The Gujer matrix of the biokinetic model is presented in tables A.2 to A.15.

Table A.2. Stoichiometric matrix for the soluble components.

	Soluble Components									
Processes	S_U	S_{O2}	S_{N2}	S_F	S_{VFA}	S_{AI}	S_{NOx}	S_{PO4}	S_{NHx}	S_{Alk}
AerHydrol	f_{SU}			1 - f_{SU}				$v_{SPO4,1}$	$v_{SNHx,1}$	$v_{SAlk,1}$
AnHydrol	f_{SU}			1 - f_{SU}				$v_{SPO4,2}$	$v_{SNHx,2}$	$v_{SAlk,2}$
AnaerHydrol	f_{SU}			1 - f_{SU}				$v_{SPO4,3}$	$v_{SNHx,3}$	$v_{SAlk,3}$
Fermentation				- 1	1			$v_{SPO4,4}$	$v_{SNHx,4}$	$v_{SAlk,4}$
AerGrowthOnSVFA		$v_{SO2,5}$			- 1 / Y_{OHO}			$v_{SPO4,5}$	$v_{SNHx,5}$	$v_{SAlk,5}$
AerGrowthOnSF		$v_{SO2,6}$		- 1 / Y_{OHO}				$v_{SPO4,6}$	$v_{SNHx,6}$	$v_{SAlk,6}$
AnGrowthOnSVFADenitrif			$v_{SN2,7}$		- 1 / Y_{OHO}		$v_{SNOx,7}$	$v_{SPO4,7}$	$v_{SNHx,7}$	$v_{SAlk,7}$
AnGrowthOnSFDenitrif			$v_{SN2,8}$	- 1 / Y_{OHO}			$v_{SNOx,8}$	$v_{SPO4,8}$	$v_{SNHx,8}$	$v_{SAlk,8}$
LysisOfHetero								$v_{SPO4,9}$	$v_{SNHx,9}$	$v_{SAlk,9}$
GrowthOfAuto		$v_{SO2,10}$					$v_{SNOx,10}$	$v_{SPO4,10}$	$v_{SNHx,10}$	$v_{SAlk,10}$
LysisOfAuto								$v_{SPO4,11}$	$v_{SNHx,11}$	$v_{SAlk,11}$
StorageOfXPAOStor					- 1			$v_{SPO4,12}$		$v_{SAlk,12}$
AnStorageOfXPAOPP			$v_{SN2,13}$				$v_{SNOx,13}$	- 1		$v_{SAlk,13}$
AnGrowthOnXPAOStorDenitrif			$v_{SN2,14}$				$v_{SNOx,14}$	$v_{SPO4,14}$	$v_{SNHx,14}$	$v_{SAlk,14}$
AerStorageOfXPAOPP		$v_{SO2,15}$						- 1		$v_{SAlk,15}$
AerGrowthOnXPAOStor		$v_{SO2,16}$						$v_{SPO4,16}$	$v_{SNHx,16}$	$v_{SAlk,16}$
LysisOfXPAO								$v_{SPO4,17}$	$v_{SNHx,17}$	$v_{SAlk,17}$
LysisOfXPAOStor					1					$v_{SAlk,18}$
LysisOfXPAOPP								1		$v_{SAlk,19}$
Precipitation								- 1		$v_{SAlk,20}$
Redissolution								1		$v_{SAlk,21}$
Aeration		1								

Table A.3. Stoichiometric matrix for the particulate components.

Processes	Particulate Components										
	X_U	X_{CB}	X_{OHO}	X_{PAO}	$X_{PAO,PP}$	$X_{PAO,Stor}$	X_{ANO}	XTSS	X_{MEOH}	X_{MEP}	X_{Ig}
AerHydrol		- 1						$v_{XTSS,1}$			
AnHydrol		- 1						$v_{XTSS,2}$			
AnaerHydrol		- 1						$v_{XTSS,3}$			
Fermentation											
AerGrowthOnSVFA			1					$v_{XTSS,5}$			
AerGrowthOnSF			1					$v_{XTSS,6}$			
AnGrowthOnSVFADenitrif			1					$v_{XTSS,7}$			
AnGrowthOnSFDenitrif			1					$v_{XTSS,8}$			
LysisOfHetero	f_{XU}	1 - f_{XU}	- 1					$v_{XTSS,9}$			
GrowthOfAuto							1	$v_{XTSS,10}$			
LysisOfAuto	f_{XU}	1 - f_{XU}					- 1	$v_{XTSS,11}$			
StorageOfXPAOStor					- Y_{PO4}	1		$v_{XTSS,12}$			
AnStorageOfXPAOPP					1	- $Y_{PAO,Stor}$		$v_{XTSS,13}$			
AnGrowthOnXPAOStorDenitrif				1		- 1 / Y_{PAO}		$v_{XTSS,14}$			
AerStorageOfXPAOPP					1	- $Y_{PAO,Stor}$		$v_{XTSS,15}$			
AerGrowthOnXPAOStor				1		- 1 / Y_{PAO}		$v_{XTSS,16}$			
LysisOfXPAO	f_{XU}	1 - f_{XU}		- 1				$v_{XTSS,17}$			
LysisOfXPAOStor						- 1		- 0.6			
LysisOfXPAOPP					- 1			- 3.23			
Precipitation								1.42	- 3.45	4.87	
Redissolution								- 1.42	3.45	- 4.87	
Aeration											

Table A.4. Stoichiometric coefficients for nitrates, nitrites and ammonium.

	S_{NOx}		S_{NHx}
$v_{SNOx,7}$	- (1 - Y_{OHO}) / (2.86 * Y_{OHO})	$v_{SNHx,1}$	- (1 - f_{SU}) * $i_{N,SF}$ - f_{SU} * $i_{N,SU}$ + $i_{N,XCB}$
$v_{SNOx,8}$	- (1 - Y_{OHO}) / (2.86 * Y_{OHO})	$v_{SNHx,2}$	- (1 - f_{SU}) * $i_{N,SF}$ - f_{SU} * $i_{N,SU}$ + $i_{N,XCB}$
$v_{SNOx,10}$	1 / Y_{ANO}	$v_{SNHx,3}$	- (1 - f_{SU}) * $i_{N,SF}$ - f_{SU} * $i_{N,SU}$ + $i_{N,XCB}$
$v_{SNOx,13}$	- $Y_{PAO,Stor}$ / 2.86	$v_{SNHx,4}$	$i_{N,SF}$
$v_{SNOx,14}$	- (1 - Y_{PAO}) / (2.86 * Y_{PAO})	$v_{SNHx,5}$	- $i_{N,BM}$
		$v_{SNHx,6}$	- ((- 1 / Y_{OHO}) * $i_{N,SF}$ + $i_{N,BM}$)
		$v_{SNHx,7}$	- $i_{N,BM}$
		$v_{SNHx,8}$	- ((- 1 / Y_{OHO}) * $i_{N,SF}$ + $i_{N,BM}$)
		$v_{SNHx,9}$	- (f_{XU} * $i_{N,XU}$ + (1 - f_{XU}) * $i_{N,XCB}$ - $i_{N,BM}$)
		$v_{SNHx,10}$	- $i_{N,BM}$ - 1 / Y_{ANO}
		$v_{SNHx,11}$	$i_{N,BM}$ - $i_{N,XU}$ * f_{XU} - $i_{N,XCB}$ * (1 - f_{XU})
		$v_{SNHx,14}$	- $i_{N,BM}$
		$v_{SNHx,16}$	- $i_{N,BM}$
		$v_{SNHx,17}$	- (f_{XU} * $i_{N,XU}$ + (1 - f_{XU}) * $i_{N,XCB}$ - $i_{N,BM}$)

Table A.5. Stoichiometric coefficients for phosphate.

	S_{PO4}
$v_{SPO4,1}$	$-(1-f_{SU}) * i_{P,SF} - f_{SU} * i_{P,SU} + i_{P,XCB}$
$v_{SPO4,2}$	$-(1-f_{SU}) * i_{P,SF} - f_{SU} * i_{P,SU} + i_{P,XCB}$
$v_{SPO4,3}$	$-(1-f_{SU}) * i_{P,SF} - f_{SU} * i_{P,SU} + i_{P,XCB}$
$v_{SPO4,4}$	$i_{P,SF}$
$v_{SPO4,5}$	$-i_{P,BM}$
$v_{SPO4,6}$	$-((-1/Y_{OHO}) * i_{P,SF} + i_{P,BM})$
$v_{SPO4,7}$	$-i_{P,BM}$
$v_{SPO4,8}$	$-((-1/Y_{OHO}) * i_{P,SF} + i_{P,BM})$
$v_{SPO4,9}$	$-(f_{XU} * i_{P,XU} + (1-f_{XU}) * i_{P,XCB} - i_{P,BM})$
$v_{SPO4,10}$	$-i_{P,BM}$
$v_{SPO4,11}$	$i_{P,BM} - i_{P,XU} * f_{XU} - i_{P,XCB} * (1-f_{XU})$
$v_{SPO4,12}$	Y_{PO4}
$v_{SPO4,14}$	$-i_{P,BM}$
$v_{SPO4,16}$	$-i_{P,BM}$
$v_{SPO4,17}$	$i_{P,BM} - i_{P,XU} * f_{XU} - i_{P,XCB} * (1-f_{XU})$

Table A.6. Stoichiometric coefficients for alkalinity.

	S_{Alk}
$v_{SAlk,1}$	(1 / 14) * Stoichiometry[AerHydrol][S_{NHx}] - (1.5 / 31) * Stoichiometry[AerHydrol][S_{PO4}]
$v_{SAlk,2}$	(1 / 14) * Stoichiometry[AerHydrol][S_{NHx}] - (1.5 / 31) * Stoichiometry[AerHydrol][S_{PO4}]
$v_{SAlk,3}$	(1 / 14) * Stoichiometry[AerHydrol][S_{NHx}] - (1.5 / 31) * Stoichiometry[AerHydrol][S_{PO4}]
$v_{SAlk,4}$	(1 / 14) * Stoichiometry[Fermentation][S_{NHx}] - (1.5 / 31) * Stoichiometry[Fermentation][S_{PO4}] - (1 / 64) * Stoichiometry[Fermentation][S_{VFA}]
$v_{SAlk,5}$	(1 / 14) * Stoichiometry[AerGrowthOnSVFA][S_{NHx}] - (1.5 / 31) * Stoichiometry[AerGrowthOnSVFA][S_{PO4}] - (1 / 64) * Stoichiometry[AerGrowthOnSVFA][S_{VFA}]
$v_{SAlk,6}$	(1 / 14) * Stoichiometry[AerGrowthOnSF][S_{NHx}] - (1.5 / 31) * Stoichiometry[AerGrowthOnSF][S_{PO4}]
$v_{SAlk,7}$	(1 / 14) * Stoichiometry[AnGrowthOnSVFADenitrif][S_{NHx}] - (1.5 / 31) * Stoichiometry[AnGrowthOnSVFADenitrif][S_{PO4}] - (1 / 14) * Stoichiometry[AnGrowthOnSVFADenitrif][S_{NOx}] - (1 / 64) * Stoichiometry[AnGrowthOnSVFADenitrif][S_{VFA}]
$v_{SAlk,8}$	(1 / 14) * Stoichiometry[AnGrowthOnSFDenitrif][S_{NHx}] - (1.5 / 31) * Stoichiometry[AnGrowthOnSFDenitrif][S_{PO4}] - (1 / 14) * Stoichiometry[AnGrowthOnSFDenitrif][S_{NOx}]
$v_{SAlk,9}$	(1 / 14) * Stoichiometry[LysisOfHetero][S_{NHx}] - (1.5 / 31) * Stoichiometry[LysisOfHetero][S_{PO4}]
$v_{SAlk,10}$	(1 / 14) * Stoichiometry[GrowthOfAuto][S_{NHx}] - (1 / 14) * Stoichiometry[GrowthOfAuto][S_{NOx}]
$v_{SAlk,11}$	(1 / 14) * Stoichiometry[LysisOfAuto][S_{NHx}] - (1.5 / 31) * Stoichiometry[LysisOfAuto][S_{PO4}]
$v_{SAlk,12}$	- (1.5 / 31) * Stoichiometry[StorageOfXPAOStor][SPO4] - (1 / 64) * Stoichiometry[StorageOfXPAOStor][SVFA] - (1 / 31) * Stoichiometry[StorageOfXPAOStor][$X_{PAO,PP}$]
$v_{SAlk,13}$	- (1.5 / 31) * Stoichiometry[AnStorageOfXPAOPP][S_{PO4}] - (1 / 14) * Stoichiometry[AnStorageOfXPAOPP][S_{NOx}] - (1.01 / 31) * Stoichiometry[AnStorageOfXPAOPP][$X_{PAO,PP}$]
$v_{SAlk,14}$	(1 / 14) * Stoichiometry[AnGrowthOnXPAOStorDenitrif][S_{NHx}] - (1.5 / 31) * Stoichiometry[AnGrowthOnXPAOStorDenitrif][S_{PO4}] - (1 / 14) * Stoichiometry[AnGrowthOnXPAOStorDenitrif][SNOx]
$v_{SAlk,15}$	- (1.5 / 31) * Stoichiometry[AerStorageOfXPAOPP][S_{PO4}] - (1 / 31) * Stoichiometry[AerStorageOfXPAOPP][$X_{PAO,PP}$]
$v_{SAlk,16}$	(1 / 14) * Stoichiometry[AerGrowthOnXPAOStor][S_{NHx}] - (1.5 / 31) * Stoichiometry[AerGrowthOnXPAOStor][S_{PO4}]
$v_{SAlk,17}$	(1 / 14) * Stoichiometry[LysisOfXPAO][S_{NHx}] - (1.5 / 31) * Stoichiometry[LysisOfXPAO][S_{PO4}]
$v_{SAlk,18}$	- (1 / 64)
$v_{SAlk,19}$	- (1.5 / 31) * Stoichiometry[LysisOfXPAOPP][S_{PO4}] - (1 / 31) * Stoichiometry[LysisOfXPAOPP][$X_{PAO,PP}$]
$v_{SAlk,20}$	- (1.5 / 31) * Stoichiometry[Precipitation][S_{PO4}]
$v_{SAlk,21}$	- (1.5 / 31) * Stoichiometry[Redissolution][S_{PO4}]

Table A.7. Stoichiometric coefficients for total suspended solids

	X_{TSS}
$v_{XTSS,1}$	$- i_{TSS,XCB}$
$v_{XTSS,2}$	$- i_{TSS,XCB}$
$v_{XTSS,3}$	$- i_{TSS,XCB}$
$v_{XTSS,5}$	$i_{TSS,BM}$
$v_{XTSS,6}$	$i_{TSS,BM}$
$v_{XTSS,7}$	$i_{TSS,BM}$
$v_{XTSS,8}$	$i_{TSS,BM}$
$v_{XTSS,9}$	$- i_{TSS,BM} + f_{XU} * i_{TSS,XU} + (1 - f_{XU}) * i_{TSS,XCB}$
$v_{XTSS,10}$	$i_{TSS,BM}$
$v_{XTSS,11}$	$- i_{TSS,BM} + i_{TSS,XU} * f_{XU} + i_{TSS,XCB} * (1 - f_{XU})$
$v_{XTSS,12}$	$- Y_{PO4} * 3.23 + 0.6$
$v_{XTSS,13}$	$3.23 - Y_{PAO,Stor} * 0.6$
$v_{XTSS,14}$	$i_{TSS,BM} - (1 / Y_{PAO}) * 0.6$
$v_{XTSS,15}$	$3.23 - Y_{PAO,Stor} * 0.6$
$v_{XTSS,16}$	$i_{TSS,BM} - (1 / Y_{PAO}) * 0.6$
$v_{XTSS,17}$	$f_{XU} * i_{TSS,XU} + (1 - f_{XU}) * i_{TSS,XCB} - i_{TSS,BM}$

Table A.8. Kinetic switching functions.

Name	Equation
$Monod_{SAlk}$	$C[S_{Alk}] / (K_{Alk} + C[S_{Alk}])$
$Monod_{SAlk,ANO}$	$C[S_{Alk}] / (C[S_{Alk}] + K_{Alk,AUT})$
$Competition_{SVFA,SF}$	$C[S_{VFA}] / (C[S_F] + C[S_{VFA}])$
$Competition_{SF,SVFA}$	$C[S_F] / (C[S_F] + C[S_{VFA}])$
$Monod_{SVFA}$	$C[S_{VFA}] / (K_{VFA} + C[S_{VFA}])$
$Monod_{SF}$	$C[S_F] / (K_F + C[S_F])$
$Monod_{SF,Ferm}$	$C[S_F] / (K_{fe} + C[S_F])$
$Monod_{SNHx}$	$C[S_{NHx}] / (K_{NHx} + C[S_{NHx}])$
$Monod_{SNHx,ANO}$	$C[S_{NHx}] / (C[S_{NHx}] + K_{NHx,ANO})$
$Inhibition_{SNOx}$	$K_{NOx} / (K_{NOx} + C[S_{NOx}])$
$Monod_{SNOx}$	$C[S_{NOx}] / (K_{NOx} + C[S_{NOx}])$
$Inhibition_{SO2}$	$K_{O2} / (K_{O2} + C[S_{O2}])$
$Monod_{SO2}$	$C[S_{O2}] / (K_{O2} + C[S_{O2}])$
$Monod_{SO2,ANO}$	$C[S_{O2}] / (C[S_{O2}] + K_{O2,AUT})$
$Monod_{SPO4}$	$C[S_{PO4}] / (K_P + C[S_{PO4}])$
$Monod_{SPO4,PAO}$	$C[S_{PO4}] / (C[S_{PO4}] + K_{PS})$
$Monod_{XCB}$	$(C[XC_B] / C[X_{OHO}]) / (K_{X,Temp} + C[XC_B] / C[X_{OHO}])$
$Monod_{XPAO,Stor}$	$(C[X_{PAO,Stor}] / C[X_{PAO}]) / (K_{PAO,Stor} + C[X_{PAO,Stor}] / C[X_{PAO}])$
$Inhibition_{XPAO,PP}$	$(K_{MAX} - C[X_{PAO,PP}] / C[X_{PAO}]) / (K_{IPP} + K_{MAX} - C[X_{PAO,PP}] / C[X_{PAO}])$
$Monod_{XPAO,PP}$	$(C[X_{PAO,PP}] / C[X_{PAO}]) / (K_{PP} + C[X_{PAO,PP}] / C[X_{PAO}])$

Table A.9. Kinetic matrix.

Processes	RATES
AerHydrol	$k_{h,Temp} * Monod_{SO2} * Monod_{XCB} * C[X_{OHO}]$
AnHydrol	$k_{h,Temp} * n_{NOx,Hyd} * Inhibition_{SO2} * Monod_{SNOx} * Monod_{XCB} * C[X_{OHO}]$
AnaerHydrol	$k_{h,Temp} * n_{fe} * Inhibition_{SO2} * Inhibition_{SNOx} * Monod_{XCB} * C[X_{OHO}]$
Fermentation	$Q_{fe,Temp} * Inhibition_{SO2} * Inhibition_{SNOx} * Monod_{SF,Ferm} * Monod_{SAlk} * C[X_{OHO}]$
AerGrowthOnSVFA	$mu_{OHO,Temp} * Monod_{SO2} * Monod_{SVFA} * Competition_{SVFA,SF} * Monod_{SNHx} * Monod_{SPO4} * Monod_{SAlk} * C[X_{OHO}]$
AerGrowthOnSF	$mu_{OHO,Temp} * Monod_{SO2} * Monod_{SF} * Competition_{SF,SVFA} * Monod_{SNHx} * Monod_{SPO4} * Monod_{SAlk} * C[X_{OHO}]$
AnGrowthOnSVFADenitrif	$mu_{OHO,Temp} * n_{NOx,Het} * Inhibition_{SO2} * Monod_{SVFA} * Competition_{SVFA,SF} * Monod_{SNHx} * Monod_{SNOx} * Monod_{SPO4} * Monod_{SAlk} * C[X_{OHO}]$
AnGrowthOnSFDenitrif	$mu_{OHO,Temp} * n_{NOx,Het} * Inhibition_{SO2} * Monod_{SF} * Competition_{SF,SVFA} * Monod_{SNHx} * Monod_{SNOx} * Monod_{SPO4} * Monod_{SAlk} * C[X_{OHO}]$
LysisOfHetero	$b_{H,Temp} * (Monod_{SO2} + n_{NOx,Het,d} * Inhibition_{SO2} * Monod_{SNOx}) * C[X_{OHO}]$
GrowthOfAuto	$mu_{ANO,Temp} * Monod_{SO2,ANO} * Monod_{SNHx,ANO} * Monod_{SPO4} * Monod_{SAlk,ANO} * C[X_{ANO}]$
LysisOfAuto	$b_{ANO,Temp} * (Monod_{SO2} + n_{NOx,ANO,d} * Inhibition_{SO2} * Monod_{SNOx}) * C[X_{ANO}]$
StorageOfXPAOStor	$Q_{PAO,Stor,Temp} * Monod_{SVFA} * Monod_{SAlk} * Monod_{XPAO,PP} * Inhibition_{SO2} * Inhibition_{SNOx} * C[X_{PAO}]$
AnStorageOfXPAOPP	$n_{NOx,PAO} * Q_{PAO,PP,Temp} * Monod_{SNOx} * Monod_{SPO4,PAO} * Monod_{SAlk} * Monod_{XPAO,Stor} * Inhibition_{SO2} * Inhibition_{XPAO,PP} * C[X_{PAO}]$
AnGrowthOnXPAOStorDenitrif	$n_{NOx,PAO} * mu_{PAO,Temp} * Monod_{SNOx} * Monod_{SNHx} * Monod_{SAlk} * Monod_{SPO4} * Monod_{XPAO,Stor} * Inhibition_{SO2} * C[X_{PAO}]$
AerStorageOfXPAOPP	$Q_{PAO,PP,Temp} * Monod_{SO2} * Monod_{SPO4,PAO} * Monod_{SAlk} * Monod_{XPAO,Stor} * Inhibition_{XPAO,PP} * C[X_{PAO}]$
AerGrowthOnXPAOStor	$mu_{PAO,Temp} * Monod_{SO2} * Monod_{SNHx} * Monod_{SAlk} * Monod_{SPO4} * Monod_{XPAO,Stor} * C[X_{PAO}]$
LysisOfXPAO	$b_{PAO,Temp} * (Monod_{SO2} + n_{NOx,P,d} * Inhibition_{SO2} * Monod_{SNOx}) * Monod_{SAlk} * C[X_{PAO}]$
LysisOfXPAOStor	$b_{PAO,Stor,Temp} * (Monod_{SO2} + n_{NOx,P,d} * Inhibition_{SO2} * Monod_{SNOx}) * Monod_{SAlk} * C[X_{PAO,Stor}]$
LysisOfXPAOPP	$b_{PAO,PP,Temp} * (Monod_{SO2} + n_{NOx,P,d} * Inhibition_{SO2} * Monod_{SNOx}) * Monod_{SAlk} * C[X_{PAO,PP}]$
Precipitation	$k_{PRE} * C[S_{PO4}] * C[X_{MEOH}]$
Redissolution	$k_{RED} * C[X_{MEP}] * (C[S_{Alk}] / (K_{ALK,ANO} + C[S_{Alk}]))$
Aeration	$k_L a_{Actual} * (S_{O2,Saturation} - C[S_{O2}])$

Table A.10. Temperature correction functions.

Name	Equation
$b_{ANO,Temp}$	$b_{ANO} * pow(\theta_{bANO}, T_{Actual} - T_{Ref})$
$b_{OHO,Temp}$	$b_{OHO} * pow(\theta_{bOHO}, T_{Actual} - T_{Ref})$
$b_{PAO,Temp}$	$b_{PAO} * pow(\theta_{bPAO}, T_{Actual} - T_{Ref})$
$b_{PAO,Stor,Temp}$	$b_{PAO,Stor} * pow(\theta_{bPAO,Stor}, T_{Actual} - T_{Ref})$
$b_{PAO,PP,Temp}$	$b_{PAO,PP} * pow(\theta_{bPAO,PP}, T_{Actual} - T_{Ref})$
$k_{h,Temp}$	$k_h * pow(\theta_{kh}, T_{Actual} - T_{Ref})$
$K_{NHx,ANO,Temp}$	$K_{NHx,ANO} * pow(10, (0.051 * T_{Actual} - 1.158))$
$K_{X,Temp}$	$K_X * pow(\theta_{KX}, T_{Actual} - T_{Ref})$
$mu_{ANO,Temp}$	$mu_{ANO} * pow(\theta_{muANO}, T_{Actual} - T_{Ref})$
$mu_{OHO,Temp}$	$mu_{OHO} * pow(\theta_{muOHO}, T_{Actual} - T_{Ref})$
$mu_{PAO,Temp}$	$mu_{PAO} * pow(\theta_{muPAO}, T_{Actual} - T_{Ref})$
$Q_{PAO,Stor,Temp}$	$Q_{PAO,Stor} * pow(\theta_{QPAO,Stor}, T_{Actual} - T_{Ref})$
$Q_{PAO,PPP,Temp}$	$Q_{PAO,PP} * pow(\theta_{QPAO,PP}, T_{Actual} - T_{Ref})$
$Q_{fe,Temp}$	$Q_{fe} * pow(\theta_{Qfe}, T_{Actual} - T_{Ref})$
$S_{O2,Saturation}$	$14.65 - 0.41 * T_{Actual} + 0.00799 * T_{Actual}^2 - 0.0000778 * T_{Actual}^3$

Table A.11. Kinetic parameters: half saturation indices.

Name	Value	Unit	Description
K_{VFA}	4	mg/l	Saturation index for S_{VFA}
K_{Alk}	0.1	mg/l	Saturation index for alkalinity
$K_{Alk,ANO}$	0.5	mg/l	Saturation index of autotrophs for alkalinity
K_F	4	mg/l	Saturation/inhibtion index for growth on S_F
K_{IPP}	0.02	mg/l	Inhibition index for $X_{PAO,PP}$ storage
K_{MAX}	0.34	-	Maximum ratio of $X_{PAO,PP}/X_{PAO}$
K_{NHx}	0.05	mg/l	Saturation index for ammonium (nutrient)
$K_{NHx,ANO}$	1	mg/l	Saturation index of autotrophs for ammonium
K_{Nox}	0.5	mg/l	Saturation/inhibition index fir nitrate
K_{O2}	0.2	mg/l	Saturation/inhibition index for oxygen
$K_{O2,ANO}$	0.5	mg/l	Saturation/inhibition index of autotrophs for oxygen
K_P	0.01	mg/l	Saturation index for phosphorus (nutrient)
$K_{PAO,Stor}$	0.01	mg/l	Saturation index for PAO,Stor
$K_{PAO,PP}$	0.01	mg/l	Saturation index for poly-phosphate
K_{PS}	0.2	mg/l	Saturation index for phosphorus in PP storage
K_X	0.1	mg/l	Saturation index for particulate COD
K_{fe}	4	-	Saturation index for fermentation on S_F

Table A.12. Kinetic parameters: rate constants.

k_{PRE}	1	1/d	Rate constant for P precipitation
k_{RED}	0.6	1/d	Rate constant for P redissolution
k_h	3	1/d	Hydrolysis rate constant
mu_{ANO}	1	1/d	Maximum growth rate
mu_{OHO}	6	1/d	Maximum growth rate on substrate
mu_{PAO}	1	1/d	Maximum growth rate
$Q_{PAO,Stor}$	3	1/d	Rate constant for storage of PHA (base: $X_{PAO,PP}$)
$Q_{PAO,PP}$	1.5	1/d	Rate constant for storage of PP
Q_{fe}	3	1/d	Maximum rate for fermentation
b_{ANO}	0.15	1/d	Decay rate
b_{OHO}	0.4	1/d	Rate constant for lysis and decay
b_{PAO}	0.2	1/d	Rate constant for lysis of X_{PAO}
$b_{PAO,Stor}$	0.2	1/d	Rate constant for lysis of $X_{PAO,Stor}$
$b_{PAO,PP}$	0.2	1/d	Rate constant for lysis of $X_{PAO,PP}$

Table A.13. Kinetic parameters: reduction factors.

$n_{NO,ANO,d}$	0.33	-	Anoxic reduction factor for decay of autotrophs
$n_{NO,Het}$	0.8	-	Reduction factor for denitrification
$n_{NO,Het,d}$	0.5	-	Anoxic reduction factor for decay of heterotrophs
$n_{NO,Hyd}$	0.6	-	Anoxic hydrolysis reduction factor
$n_{NO,PAO}$	0.6	-	Amount of PAO organisms active under anoxic conditions
$n_{NO,P,d}$	0.33	-	Anoxic reduction factor for decay of PAO, PP and PHA
n_{fe}	0.4	-	Anaerobic hydrolysis reduction factor

Table A.14. Kinetic parameters: temperature correction.

T_{Ref}	20	°C	Reference temperature of the activated sludge
θ_{KX}	0.896	-	Temperature correction factor for K_X
$\theta_{QPAO,Stor}$	1.041	-	Temperature correction factor for $Q_{PAO,Stor}$
$\theta_{QPAO,PP}$	1.041	-	Temperature correction factor for $Q_{PAO,PP}$
θ_{Qfe}	1.072	-	Temperature correction factor for Q_{fe}
θ_{bANO}	1.116	-	Temperature correction factor for b_{ANO}
θ_{bOHO}	1.072	-	Temperature correction factor for b_{OHO}
θ_{bPAO}	1.072	-	Temperature correction factor for b_{PAO}
$\theta_{bPAO,Stor}$	1.072	-	Temperature correction factor for $b_{PAO,Stor}$
$\theta_{bPAO,PP}$	1.072	-	Temperature correction factor for $b_{PAO,PP}$
θ_{kh}	1.041	-	Temperature correction factor for k_h
θ_{muANO}	1.111	-	Temperature correction factor for mu_{ANO}
θ_{muOHO}	1.072	-	Temperature correction factor for mu_{OHO}
θ_{muPAO}	1.041	-	Temperature correction factor for mu_{PAO}

Table A.15. Stoichiometric parameters.

Name	Value	Unit	Description
Y_{ANO}	0.24	-	Yield For Autotrophic Biomass
Y_{OHO}	0.625	-	Yield For Heterotrophic Biomass
Y_{PAO}	0.625	-	Yield coeff (biomass/PHA)
$Y_{PAO,Stor}$	0.2	-	PHA requirement for PP storage
Y_{PO4}	0.4	-	PP requirement (S_{PO4} release) per PHA stored
f_{SU}	0	-	Fraction of inert COD in particulate substrate
f_{XU}	0.1	-	Fraction of inert COD generated in biomass lysis
$i_{N,BM}$	0.07	-	Nitrogen content of biomass
$i_{N,SF}$	0.03	-	Nitrogen content of soluble substrate S_F
$i_{N,SU}$	0.01	-	Nitrogen content of inert soluble COD S_U
$i_{N,XU}$	0.02	-	Nitrogen content of inert particulate COD X_U
$i_{N,XCB}$	0.04	-	Nitrogen content of slowly biodegradable COD XC_B
$i_{P,BM}$	0.02	-	Phosphorus content of biomass
$i_{P,SF}$	0.01	-	Phosphorus content of soluble substrate S_F
$i_{P,SU}$	0	-	Phosphorus content of inert soluble COD S_U
$i_{P,XU}$	0.01	-	Phosphorus content of inert particulate COD X_U
$i_{P,XCB}$	0.01	-	Phosphorus content of slowly biodegradable COD XC_B
$i_{TSS,BM}$	0.9	-	TSS to biomass ratio
$i_{TSS,XU}$	0.75	-	TSS to X_U ratio
$i_{TSS,XCB}$	0.75	-	TSS to XC_B ratio

Aeration model

The aeration model is based on the theory developed by Boyle et al. (1989). An extension was made using a statistical correlation between αSOTE and the system SRT and the air flux according to Rosso et al (2005).

The value of K_La (Equation A.1) is calculated as a function of airflow rate and the oxygen transfer efficiency (Boyle et al. 1989).

$$k_L a = \frac{\rho_{Air} \cdot Q_{Air} \cdot Y_i \cdot OTE}{(\beta \cdot C_S^* - C_0) \cdot V} \quad \text{(A.1)}$$

Where ρ_{Air} is the density of air [kg/m^3], Q_{air} is the airflow rate [m^3/d], Y_i is the inlet mole fraction of oxygen [-], OTE is the oxygen transfer efficiency [%], C_0 is the dissolved oxygen concentration in the aerated tank [g O_2/m^3], β is the oxygen saturation concentration correction factor [-], C_s^* is the oxygen saturation concentration [g O_2/m^3] and V is the volume of the aerated tank [m^3].

The oxygen transfer efficiency can be deduced from the standard oxygen transfer efficiency (Equation A.2).

$$OTE = \alpha SOTE \cdot \frac{\beta \cdot C_S^* - C_0}{C_{s20}} \cdot \theta^{(T-20)} \quad \text{(A.2)}$$

Where θ is the temperature correction factor [-] and T is the water temperature [°C].

Rosso et al. (2005) identified sludge age and air flux to be the key process parameters for aeration modelling and proposed a statistical correlations for αSOTE (Equation A.3).

$$\alpha SOTE = A \cdot \log \chi - B \quad \text{(A.3)}$$

Where A and B are calibration parameters [-] χ is the ratio of SRT over normalized air flow rate [-] (equation A.4).

$$\chi = \frac{SRT}{Q_{N,air}} \quad \text{(A.4)}$$

Where $Q_{N,air}$ is the resulting normalized airflow rate [1/d]

$$Q_{N,air} = \frac{Q_{air}}{a_{spec} \cdot N_d \cdot Z} \quad \text{(A.5)}$$

where Q_{air} is the airflow rate [m^3/d], a_{spec} is the diffuser specific area [m^2], N_d is the total number of diffusers [-] and Z is the diffuser submergence depth [m].

The pressure correction for the saturation concentration is calculated according to equation

$$C_S^* = C_{sT} \cdot \frac{\rho_s \cdot H \cdot f + p_{site} - p_{w,site}}{p_{atm} - p_{w,std}} \quad \text{(A.6)}$$

Where C^*_s is the corrected oxygen saturation concentration [mg/l], C_{sT} is the standard oxygen saturation concentration in clean water [g/l], p_{site} is the atmospheric pressure at test site [Pa], p_{atm} is the atmospheric pressure at standard conditions [101325 Pa], $p_{w,site}$ is the saturated water vapor pressure at test site [Pa], $p_{w,std}$ is the saturated water vapour pressure at standard temperature [2300 Pa], f is a correction factor for averaging over the entire depth of the reactor [0.4 – 0.5, -], H is the depth of the tank [m] and ρ_s is the density of the sludge [kg/m^3].

The calculation (Equation 9) of standard oxygen saturation concentration in clean water is adopted from standard methods (APHA, 1992).

$$C_{sT} = 14.65 - 0.41 \cdot T + 0.0049 \cdot T^2 + 0.0000778 \cdot T^3 \quad \text{(A.7)}$$

Where T is the temperature of the water [°C].

Hydraulic model for the activated sludge tanks

The hydraulics of the activated sludge tanks are modelled using a tanks-in-series approach (Figure A.2). The inner ring (anaerobic tank) is represented by 4 completely stirred tank reactors (CSTR), mimicking the four physical compartments available. The middle ring (denitrification tank) is represented by 2 CSTRs and the outer ring by 6 CSTRs (Figure A.2).

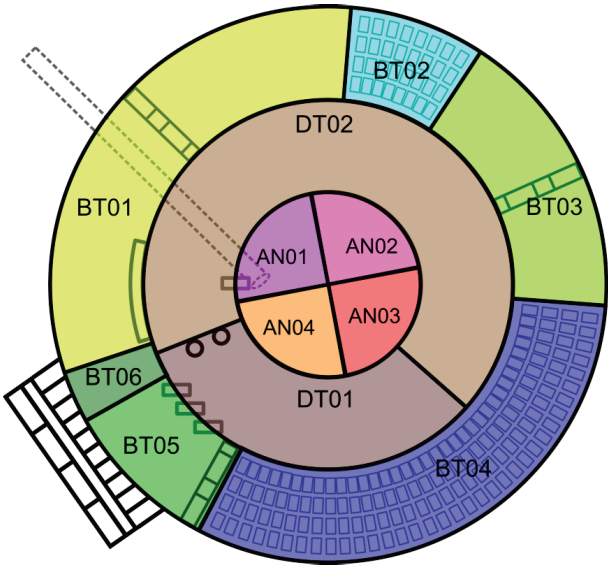

Figure A.2. Overview of the mapping of the tanks-in-series model on the layout of the activated sludge tanks.

Primary sedimentation tank model

The model of Tay (1982)was extended to reflect the difference in removal efficiency between COD (containing only organic fractions) and TSS (containing both inorganic and organic fractions). The settling characteristics are specified based on the half-removal time (T_A), which is the time at which 50% of the influent suspended solids is removed.

$$X_r = \frac{S_0 - S}{S} = \frac{t_r}{T_A + t_r} \quad \text{(A.8)}$$

Where S_0 is the suspended solids concentration in the influent to the settling tank [mg/l], S is the suspended solids concentration in the effluent of the settling tank [mg/l], t_r is the hydraulic retention time in the settling tank [d] and T_A is the half-removal time [d].

The half removal times for the organic and inorganic fractions are calculated according to equations A.9 and A.11, respectively.

$$T_{A,XCOD} = \frac{V_{Clar}}{Q_{In,DW}} * \frac{f_{ns,XCOD}}{(1-f_{ns,XCOD})} \quad \text{(A.9)}$$

Where $T_{A,XCOD}$ the half-removal time for the particulate COD [d], V_{Clar} is the volume of the primary sedimentation tank [m³], $Q_{In,DW}$ is the average incoming flow rate during dry weather conditions [m³/d] and $f_{ns,XCOD}$ (Equation A.10) is the non-settleable fraction for the particulate COD [-].

$$f_{ns,XCOD} = \frac{(1-ER_{XCOD})}{f_{Out,DW}} \quad \text{(A.10)}$$

Where ER_{XCOD} is the removal efficiency for the particulate COD [-] and $f_{Out,DW}$ is the fraction of the incoming flow rate going to the effluent [-].

$$\boldsymbol{T_{A,XIg} = \frac{V_{Clar}}{Q_{In,DW}} * \frac{f_{ns,XIg}}{(1-f_{ns,XIg})}} \quad \text{(A.11)}$$

Where $T_{A,XIg}$ the half-removal times for the particulate inorganic fraction [d], V_{Clar} is the volume of the primary sedimentation tank [m³] and $f_{ns,XIg}$ (Equation A.12) is the non-settleable fraction for the particulate inorganic fraction [-].

$$f_{ns,XIg} = \frac{(1-ER_{XIg})}{f_{Out,DW}} \quad \text{(A.12)}$$

Where ER_{XIg} is the removal efficiency for the particulate inorganic fraction [-].

Secondary settling model

The secondary settling model is an implementation (Torfs et al., 2015) of the Bürger-Diehl model introduced by Bürger et al. (2011). The model is based on the conservation of mass, which can be cast into the following one-dimensional (1D) partial differential equation (PDE) of nonlinear convection–diffusion type for the solids concentration as a function of depth z and time t (Equation A.13).

$$\frac{\partial C_{TSS}}{\partial t} + \frac{\partial}{\partial z}F(C_{TSS}, z, t) = \frac{\partial}{\partial z}\left(\{d_{comp}(C_{TSS}) + d_{disp}(z, Q_{In}(t)\}\frac{\partial C_{TSS}}{\partial z}\right) + \frac{Q_{In}(t)C_{TSS,In}(t)}{A_{Clar}}\delta(z) \quad \text{(A.13)}$$

Where C_{TSS} is the concentration of solids [mg/l], $C_{TSS,In}$ is the influent concentration of solids [mg/l], d_{comp} is the is the compression function as defined in Bürger et al. (2011) [m²/d],d_{disp} is the dispersion function as defined in Bürger et al. (2011) [m²/d] and Q_{In} is the influent flow rate and A_{Clar} is the surface area of the tank. The second term on the left-hand side models discrete settling combined with the bulk flux. The first term on the right side describes dispersion and the second term is a singular source term for the influent.

Discretization, for which 20 layers have been selected as a compromise between complexity and accuracy, of the mathematical model is developed according to Bürger et al. (2011).

Chemical phosphate removal

The model is an implementation of the model of Briggs (de Haas et al., 2000), which applies an empirical relation (Equation A.14) between the chemical removal

of phosphorus and the metal, iron (Fe) or aluminium (Al) dosing. This relation is determined by the precipitation equilibria of the metal-hydroxides and the metal-phosphate salts and is limited by the solubility product of the metal-phosphate salts.

$$P_{Out} = a_1 P_{In} * e^{-a_2 \frac{Me^{\circ}}{P_{In}}} \quad \text{(A.14)}$$

Where a_1 and a_2 are empirical parameters [-], P_{in} is the influent phosphate concentration [mol/l], P_{Out} is the effluent phosphate (PO_4) concentration [mol/l] and Me^0 concentration of dosed metal.

The concentration of phosphate in the effluent is limited, firstly, by the concentration of metal dosed, i.e. the maximal quantity of phosphate that precipitates is determined by its stoichiometry (Equation A.15). Secondly the effluent concentration of PO_4 is also limited by the solubility product of the metal-phosphate salts.

$$r\,Me^{3+} + PO_4^{3-} + (3r-3)H_2O \leftrightarrows Me_rPO_4(OH)_{3r-3} + (3r-3)H^+ \quad \text{(A.15)}$$

Where r is the stoichiometric coefficient [-].

For the model of the WWTP of Eindhoven, values 1.1 and 1.42 for a_1 and a_2 respectively are adopted, being typical values for municipal wastewater proposed by (de Haas et al., 2000). For the stoichiometric coefficient r the value of 1.2 is selected.

Appendix B

Data for the influent fractionation of the WWTP of Roeselare

Table 14.1. Influent Data of the WWTP of Roeselare on February 24th, 2014.

Quantity	Unit	Analysis 1	Analysis 2	Analysis 2	Average	Stdev	Stdev (%)
Q	m^3/h	1900					
COD_{tot}	mg/l	191.00	174.00	172.00	179.00	10.44	5.83
COD_{ff}	mg/l	101.00	104.00	102.00	102.33	1.53	1.49
BOD_{10}	mg/l	50.70	53.50		52.10	1.98	3.80
BOD_5	mg/l	42.30	45.10		43.70	1.98	4.53
k_{BOD}	mg/l	0.34	0.34		0.34	0.00	1.46
BOD_{tot}	mg/l	52.63	54.41		53.52	1.26	2.35
TP_{tot}	mg/l	2.28	2.36	2.32	2.32	0.04	1.72
TP_{ff}	mg/l	0.07	0.07	0.08	0.07		
PO_4	mg/l	1.74	1.74	1.71	1.73	0.02	1.00
TN_{tot}	mg/l	25.20	24.20	24.00	24.47	0.64	2.63
TN_{ff}	mg/l	19.50	12.90	15.70	16.03	3.31	20.66
TSS	g/l	0.08	0.06		0.07	0.02	25.81
VSS	g/l	0.14	0.18		0.16	0.03	19.21
NH_4	mg/l	10.70	9.98	11.40	10.69	0.71	6.64
NO_3	mg/l	3.16	3.15	3.12	3.14	0.02	0.66
pH		7.90	7.91	7.93	7.91	0.02	0.19
TSS (AS)	g/l	3.36			3.36	N.A.	N.A.
VSS (AS)	g/l	2.10			2.10	N.A.	N.A.
COD_{tot} (eff)	mg/l	31.80	22.40	22.80	25.67	5.32	20.71
COD_{ff} (eff)	mg/l	20.30	20.90	19.90	20.37	0.50	2.47
BOD_5 (eff)	mg/l	21.90			21.90	N.A.	N.A.
BOD_{10} (eff)	mg/l	11.50			11.50	N.A.	N.A.
k_{BOD} (eff)	mg/l	0.28			0.28	N.A.	N.A.
BOD_{tot} (eff)	mg/l	12.38			12.38	N.A.	N.A.
Kj-N	mg/l	22.04	21.05	20.88	21.32	0.63	2.94
bCOD	mg/l	61.92	64.01		62.97	1.48	2.35
S_{VFA}	mg/l	50.47	51.97	51.29	51.24	0.75	1.47
S_U	mg/l	18.27	18.81	17.91	18.33	0.45	2.47
S_B	mg/l	82.73	85.19	84.09	84.00	1.23	1.47
S_F	mg/l	32.26	33.22	32.80	32.76	0.48	1.47
XC_B	mg/l	-20.81	-21.18		-21.04	0.26	-1.24
X_U	mg/l	110.81	91.18		97.70	13.88	14.21
S_{NH4}	mg/l	10.70	9.98	11.40	10.69	0.71	6.64
S_{NO3}	mg/l	3.16	3.15	3.12	3.14	0.02	0.66
S_{PO4}	mg/l	1.74	1.74	1.71	1.73	0.02	1.00

Table 14.2. Influent Data of the WWTP of Roeselare on March 3rd, 2014.

Quantity	Unit	Analysis 1	Analysis 2	Analysis 2	Average	Stdev	Stdev (%)
Q	m^3/h	Not Available					
COD_{tot}	mg/l	52.20	53.90	52.10	52.73	1.01	1.92
COD_{ff}	mg/l	18.80	17.30	16.40	17.50	1.21	6.93
BOD_{10}	mg/l	Missing data	Missing data	Missing data	Missing data	Missing data	Missing data
BOD_5	mg/l	Missing data	Missing data	Missing data	Missing data	Missing data	Missing data
k_{BOD}	mg/l	Missing data	Missing data	Missing data	Missing data	Missing data	Missing data
BOD_{tot}	mg/l	Missing data	Missing data	Missing data	Missing data	Missing data	Missing data
TP_{tot}	mg/l	1.01	1.07	0.94	1.01	0.06	6.41
TP_{ff}	mg/l	0.07	0.06	0.06	0.06		
PO_4	mg/l	0.72	0.91	0.70	0.78	0.12	15.09
TN_{tot}	mg/l	10.40	8.11	8.93	9.15	1.16	12.69
TN_{ff}	mg/l	7.31	7.02	7.23	7.19	0.15	2.08
TSS	g/l	0.02	0.03		0.03	0.01	24.01
VSS	g/l	0.11	0.09		0.10	0.02	16.97
NH_4	mg/l	2.42	2.49	2.55	2.49	0.07	2.62
NO_3	mg/l	2.32	2.19	2.17	2.23	0.08	3.66
pH		7.58	7.60	7.59	7.59	0.01	0.13
TSS (AS)	g/l	3.04			3.04	N.A.	N.A.
VSS (AS)	g/l	1.90			1.90	N.A.	N.A.
COD_{tot} (eff)	mg/l	32.20	30.70	29.40	30.77	1.40	4.55
COD_{ff} (eff)	mg/l	15.20	16.30	15.70	15.73	0.55	3.50
BOD_5 (eff)	mg/l	Missing data	Missing data	Missing data	Missing data	Missing data	Missing data
BOD_{10} (eff)	mg/l	Missing data	Missing data	Missing data	Missing data	Missing data	Missing data
k_{BOD} (eff)	mg/l	Missing data	Missing data	Missing data	Missing data	Missing data	Missing data
BOD_{tot} (eff)	mg/l	Missing data	Missing data	Missing data	Missing data	Missing data	Missing data
Kj-N	mg/l	8.08	5.92	6.76	6.92	1.09	15.73
bCOD	mg/l	Missing data	Missing data	Missing data	Missing data	Missing data	Missing data
S_{VFA}	mg/l	3.12	1.60	1.38	2.04	0.95	46.47
S_U	mg/l	13.68	14.67	14.13	14.16	0.50	3.50
S_B	mg/l	5.12	2.63	2.27	3.34	1.55	46.47
S_F	mg/l	2.00	1.03	0.89	1.30	0.61	46.47
XC_B	mg/l	Missing data	Missing data	Missing data	Missing data	Missing data	Missing data
X_U	mg/l	Missing data	Missing data	Missing data	Missing data	Missing data	Missing data
S_{NH4}	mg/l	2.42	2.49	2.55	2.49	0.07	2.62
S_{NO3}	mg/l	2.32	2.19	2.17	2.23	0.08	3.66
S_{PO4}	mg/l	0.72	0.91	0.70	0.78	0.12	15.09

Table 14.3. Influent Data of the WWTP of Roeselare on March 24th, 2014.

Quantity	Unit	Analysis 1	Analysis 2	Analysis 2	Average	Stdev	Stdev (%)
Q	m^3/h	974					
COD_{tot}	mg/l	196.00	194.00	197.00	195.67	1.53	0.78
COD_{ff}	mg/l	54.20	49.50	49.70	51.13	2.66	5.20
BOD_{10}	mg/l	50.70	50.70		50.70	0.00	0.00
BOD_5	mg/l	39.50	40.90		40.20	0.99	2.46
k_{BOD}	mg/l	0.35	0.35		0.35	0.00	0.71
BOD_{tot}	mg/l	50.46	50.25		50.36	0.15	0.31
TP_{tot}	mg/l	3.04	3.09	3.02	3.05	0.04	1.18
TP_{ff}	mg/l	<0,05	<0,05	<0,05	<0,05		
PO_4	mg/l	2.57	2.50	2.59	2.55	0.05	1.85
TN_{tot}	mg/l	26.80	27.20	24.40	26.13	1.51	5.79
TN_{ff}	mg/l	23.80	22.80	22.70	23.10	0.61	2.63
TSS	g/l	0.10	0.10		0.10	0.00	0.00
VSS	g/l	0.16	0.18		0.17	0.02	11.65
NH_4	mg/l	13.50	13.10	13.20	13.27	0.21	1.57
NO_3	mg/l	1.87	1.85	1.84	1.85	0.02	0.82
pH		8.17	8.16	8.16	8.16	0.01	0.07
TSS (AS)	g/l	3.30	3.55	3.55	3.47	0.15	4.23
VSS (AS)	g/l	2.12	2.13		2.13	0.00	0.13
COD_{tot} (eff)	mg/l	36.70	38.20	36.00	36.97	1.12	3.04
COD_{ff} (eff)	mg/l	21.30	15.90	16.90	18.03	2.87	15.93
BOD_5 (eff)	mg/l	3.40	4.50		3.95	0.78	19.69
BOD_{10} (eff)	mg/l	5.10	7.60		6.35	1.77	27.84
k_{BOD} (eff)	mg/l	0.29	0.29		0.29	0.00	0.00
BOD_{tot} (eff)	mg/l	8.34	8.33		8.34	0.00	0.04
Kj-N	mg/l	24.93	25.35	22.56	24.28	1.50	6.20
bCOD	mg/l	59.37	59.11		59.24	0.18	0.31
S_{VFA}	mg/l	21.37	21.47	21.04	21.29	0.22	1.05
S_U	mg/l	19.17	14.31	15.21	16.23	2.59	15.93
S_B	mg/l	35.03	35.19	34.49	34.90	0.37	1.05
S_F	mg/l	13.66	13.72	13.45	13.61	0.14	1.05
XC_B	mg/l	24.34	23.92		24.34	0.29	1.21
X_U	mg/l	117.46	120.58		120.19	2.20	1.83
S_{NH4}	mg/l	13.50	13.10	13.20	13.27	0.21	1.57
S_{NO3}	mg/l	1.87	1.85	1.84	1.85	0.02	0.82
S_{PO4}	mg/l	2.57	2.50	2.59	2.55	0.05	1.85

Table 14.4. Influent Data of the WWTP of Roeselare on April 7th, 2014.

Quantity	Unit	Analysis 1	Analysis 2	Analysis 2	Average	Stdev	Stdev (%)
Q	m^3/h	730					
COD_{tot}	mg/l	209.00	202.00	205.00	205.33	3.51	1.71
COD_{ff}	mg/l	62.60	56.00	49.80	56.13	6.40	11.40
BOD_{10}	mg/l	69.00	70.50		69.75	1.06	1.52
BOD_5	mg/l	56.40	62.00		59.20	3.96	6.69
k_{BOD}	mg/l	0.36	0.37		0.37	0.01	2.51
BOD_{tot}	mg/l	70.71	70.02		70.37	0.49	0.70
TP_{tot}	mg/l	3.29	3.24	3.20	3.24	0.05	1.39
TP_{ff}	mg/l	<0,05	<0,05	<0,05	<0,05		
PO_4	mg/l	2.44	2.52	2.49	2.48	0.04	1.63
TN_{tot}	mg/l	31.50	31.10	31.60	31.40	0.26	0.84
TN_{ff}	mg/l	26.30	24.00	27.30	25.87	1.69	6.54
TSS	g/l	0.06	0.06		0.06	0.00	1.21
VSS	g/l	0.25	0.20		0.23	0.03	14.89
NH_4	mg/l	21.50	21.10	21.40	21.33	0.21	0.98
NO_3	mg/l	0.42	0.41	0.42	0.42	0.00	0.48
pH		7.97	7.96	7.96	7.96	0.01	0.07
TSS (AS)	g/l	3.69	3.56	3.58	3.61	0.07	1.95
VSS (AS)	g/l	2.26	2.12		2.19	0.09	4.32
COD_{tot} (eff)	mg/l	38.10	35.80	34.80	36.23	1.69	4.67
COD_{ff} (eff)	mg/l	32.20	28.90	29.00	30.03	1.88	6.25
BOD_5 (eff)	mg/l	4.80	2.00		3.40	1.98	58.23
BOD_{10} (eff)	mg/l	7.60	3.90		5.75	2.62	45.50
k_{BOD} (eff)	mg/l	0.29	0.29		0.29	0.00	0.04
BOD_{tot} (eff)	mg/l	8.32	8.31		8.31	0.01	0.15
Kj-N	mg/l	31.09	30.69	31.18	30.99	0.26	0.85
bCOD	mg/l	83.19	82.38		82.78	0.58	0.70
S_{VFA}	mg/l	20.51	18.29	14.46	17.75	3.06	17.25
S_U	mg/l	28.98	26.01	26.10	27.03	1.69	6.25
S_B	mg/l	33.62	29.99	23.70	29.10	5.02	17.25
S_F	mg/l	13.11	11.70	9.24	11.35	1.96	17.25
XC_B	mg/l	49.57	52.39		53.68	1.99	3.70
X_U	mg/l	96.83	93.61		95.52	2.27	2.38
S_{NH4}	mg/l	21.50	21.10	21.40	21.33	0.21	0.98
S_{NO3}	mg/l	0.42	0.41	0.42	0.42	0.00	0.48
S_{PO4}	mg/l	2.44	2.52	2.49	2.48	0.04	1.63

Table 14.5. Influent Data of the WWTP of Roeselare on April 14th, 2014.

Quantity	Unit	Analysis 1	Analysis 2	Analysis 2	Average	Stdev	Stdev (%)
Q	m^3/h	680					
COD_{tot}	mg/l	234.00	218.00	210.00	220.67	12.22	5.54
COD_{ff}	mg/l	59.60	60.50	56.80	58.97	1.93	3.27
BOD_{10}	mg/l	71.90	69.00		70.45	2.05	2.91
BOD_5	mg/l	60.60	56.40		58.50	2.97	5.08
k_{BOD}	mg/l	0.33	0.32		0.33	0.01	1.53
BOD_{tot}	mg/l	75.43	71.47		73.45	2.81	3.82
TP_{tot}	mg/l	3.65	3.61	3.50	3.59	0.08	2.17
TP_{ff}	mg/l	0.07	0.06	0.06	0.06		
PO_4	mg/l	2.84	2.76	2.71	2.77	0.07	2.37
TN_{tot}	mg/l	32.10	30.20	27.50	29.93	2.31	7.72
TN_{ff}	mg/l	21.80	16.50	20.80	19.70	2.82	14.29
TSS	g/l	0.05	0.04		0.04	0.00	9.43
VSS	g/l	0.50	0.19		0.35	0.22	64.58
NH_4	mg/l	21.60	21.40	21.60	21.53	0.12	0.54
NO_3	mg/l	0.53	0.53	0.54	0.53	0.00	0.50
pH		8.11	8.10	8.08	8.10	0.02	0.19
TSS (AS)	g/l	4.38	4.36	4.26	4.33	0.06	1.41
VSS (AS)	g/l	3.14	2.99		3.07	0.11	3.50
COD_{tot} (eff)	mg/l	32.90	29.70	29.00	30.53	2.08	6.81
COD_{ff} (eff)	mg/l	29.80	26.00	28.60	28.13	1.94	6.90
BOD_5 (eff)	mg/l	4.50	3.10		3.80	0.99	26.05
BOD_{10} (eff)	mg/l	7.60	5.60		6.60	1.41	21.43
k_{BOD} (eff)	mg/l	0.29	0.29		0.29	0.00	0.02
BOD_{tot} (eff)	mg/l	8.32	8.32		8.32	0.00	0.02
Kj-N	mg/l	31.57	29.67	26.97	29.40	2.31	7.86
bCOD	mg/l	88.75	84.08		86.41	3.30	3.82
S_{VFA}	mg/l	20.00	22.63	18.95	20.52	1.90	9.25
S_U	mg/l	26.82	23.40	25.74	25.32	1.75	6.90
S_B	mg/l	32.78	37.10	31.06	33.65	3.11	9.25
S_F	mg/l	12.78	14.47	12.11	13.12	1.21	9.25
XC_B	mg/l	55.97	46.98		52.77	6.36	12.04
X_U	mg/l	118.43	110.52		108.93	5.59	5.14
S_{NH4}	mg/l	21.60	21.40	21.60	21.53	0.12	0.54
S_{NO3}	mg/l	0.53	0.53	0.54	0.53	0.00	0.50
S_{PO4}	mg/l	2.84	2.76	2.71	2.77	0.07	2.37

Summary

In the European Union, the Water Framework Directive enforces a good ecological and chemical status of all surface waters, which is to be accomplished by 2015. Mathematical models provide a valuable tool for guiding the decisions towards meeting the requirements set forth by the Water Framework Directive. In order to meet those requirements, one of the main challenges for the optimization of wastewater treatment plants, today, is the proper evaluation of all important performance indicators such as effluent quality (including priority pollutants) but also energy consumption and greenhouse gas emissions. In order to come to an optimal solution, all relevant aspects need to be considered, as such reducing the uncertainty in the model outcome. It is generally acknowledged that the largest uncertainties are located in the description of influent, hydraulics, gas-liquid mass transfers and primary and secondary settling.
Regardless this importance of the different sub-processes, wastewater treatment plant (WWTP) models, to date, show a clear unbalance in the modelling of the different sub-processes, i.e. the models consist of highly detailed biokinetic models but often lack detail of other critical processes carrying a considerable uncertainty. Improving the balance in the WWTP models basically comes down to move from total ignorance towards quantifiable or scenario uncertainty. Moving away from total ignorance is pursued by incorporating more detail in the important processes. As such, the objective of this work is to include more detail in the sub-process models for influent characterization, primary sedimentation, oxygen transfer (aeration) and energy consumption (aeration blowers and pumps) and showing its impact on the results and calibration of the biokinetic model.

In the second part influent characterisation under dilute circumstances is investigated. A good characterization of the biodegradable substrate entering the plant, especially under storm or rain weather conditions, is required in view of the evaluation of the performance of a WWTP. A first hurdle to be taken towards this characterization is the determination of the yield of heterotrophs, which is likely to change during storm events due to changed wastewater characteristics (e.g. first flush effects and dilution). However, the determination of the yield significantly extends the length of the analysis procedure, making its application difficult for high frequency measurements or measuring campaigns. A second hurdle, is that

low load conditions, due to the dilution effects during or after rain events, hampers the application of respirometric assays for influent fractionation as well. Attempts to improve the measurement have not been successful but indications are given that the evaluation of the assay output based on dynamic models (i.e. increasing the level of detail) will be needed to overcome the encountered hurdles.
In the third part the modelling of primary sedimentation tanks (PST) is investigated. PSTs are often used as a preliminary step in WWTPs and have a significant impact on the subsequent processes. A literature review on primary sedimentation tank models was conducted and it was found that most modelling efforts are based on empirical relations. These empirical models, however, do not succeed in describing the high scatter present in primary sedimentation tank removal efficiency data. A promising approach, to understand the driving forces for this high scatter, is the so-called, phenomenological models, which are models that incorporate more mechanistic knowledge about the process. In this work the phenomenological model of Bachis et al. (2012) has been integrated within a rigorous discretization scheme as proposed by Bürger et al. (2011). The model was further extended with a differentiation between organic and inorganic matter, which is considered to be crucial for the description of the succeeding biological treatment.
For the evaluation of the primary sedimentation tank performance at the WWTP of Eindhoven, data was collected in collaboration with Waterboard The Dommel and comprised routinely collected data as well as data from 3 dedicated measurement campaigns. Modelling the biochemical reactions, by the application of a modified version of ASM2d implemented in the modelling software WEST, enabled to link the unexpected increase of ammonium and phosphate observed during the measurement campaign on May 6, 2014, to the presence of both ordinary heterotrophic and phosphate accumulating organisms in the wastewater. Applying a physical-chemical model implemented in the modelling software PHREEQ-C, supported the hypothesis of the formation of a precipitate (hydroxylapatite) and a consequent removal of phosphate, contributing to the unexpected increase of inorganic suspended solids noticed during the measurement campaign on September 2, 2014. Finally the impact of the sedimentation process on the whole WWTP of Eindhoven was modelled and implemented in the modelling software WEST. It was proven that the primary sedimentation tanks definitely affect the denitrification but may also affect the nitrification.
In the fourth part, aeration and energy consumption is studied. An extensive measurement campaign with off-gas tests at the WWTP of Eindhoven revealed a high spatial and temporal variability in the oxygen transfer efficiency. Applying this newly gathered system knowledge in the aeration model resulted in an

improved fit of the dissolved oxygen concentrations. Moreover, an important consequence of this was that ammonium predictions could be improved by resetting the ammonium half-saturation coefficient for autotrophs to its original value.
Both for aeration energy and pumping energy consumption, a new dynamic model, which includes a detailed description of the system and pump or blower, gave improved predictions of the dynamics compared to the simpler constant average power consumption models currently used.

The study on modelling the sub-processes demonstrated that improving the balance in sub-model details results in improved predictive quality of the model under varying process conditions. As such a simulation methodology should in first instance focus on improving the balance of details in the sub-models rather than force-fitting bio-kinetic parameters. In conclusion, this PhD has considerably extended the model library of less studied parts of the treatment plant allowing for better predictions of effluent quality and energy requirements.

Samenvatting

De Kaderrichtlijn Water is een Europese richtlijn die oplegt dat de lidstaten een goede ecologische en chemische waterkwaliteit moeten bereiken vanaf 2015. Wiskundige modellen leveren daarbij een waardevol instrument om de noodzakelijke beslissingen te ondersteunen. Om aan deze beslissingen te nemen is de grootste uitdaging de grondige evaluatie van alle belangrijke indicatoren zoals effluent kwaliteit (inclusief micropolluenten) maar ook energie verbruik en de uitstoot van broeikasgassen. Om daarbij een optimale oplossing te vinden moeten alle relevante processen in rekening gebracht worden, om zodoende de onzekerheid in de modelvoorspellingen te verminderen. Het is algemeen aanvaard dat de grootste onzekerheid zich bevindt in de beschrijving van het influent, de hydraulica, de gas-vloeistof overgangen en de voor- en nabezinking.
Ondanks het belang van deze verschillende deelprocessen, bevatten modellen van rioolwaterzuiveringsinstallaties (RWZI) een duidelijk onevenwicht in de modellering van de verschillende onderdelen. In veel gevallen bestaan deze modellen uit heel gedetailleerde biokinetische modellen maar ontbreken er details van andere kritische processen waaraan een grote onzekerheid verbonden is.
De balans in de RWZI modellen verbeteren betekent eigenlijk het verschuiven van totale onwetendheid naar kwantificeerbare of scenario onzekerheid. Het vermijden van de totale onwetendheid wordt bereikt door meer detail toe te voegen aan de beschrijving van de deelprocessen. Zodoende is het doel van dit werk het toevoegen van meer detail in de modellen van de influent karakterisering, voorbezinking, zuurstofoverdracht (beluchting) en energie verbruik (luchtcompressors en pompen) en het aantonen van de impact op de resultaten en de kalibratie van het biokinetisch model.

In het tweede deel wordt influent karakterisering van verdunde afvalstromen onderzocht. Een goed karakterisering van het biologisch afbreekbaar substraat dat op de installatie toekomt, in het bijzonder bij storm- of regenweeromstandigheden, is noodzakelijk met het oog op de evaluatie van de prestaties van een RWZI. Een eerste hindernis daarbij is de bepaling van de groei opbrengstcoëfficiënt van heterotrofe biomassa die hoogst waarschijnlijk veranderd tijdens een storm door de veranderende afvalwaterkarakteristieken (bijvoorbeeld door het ‘first flush’ effect en verdunningseffecten). De bepaling van de groei opbrengstcoëfficiënt betekent

echter een significante verlenging van de analyse procedure wat de toepassing bij hoogfrequente metingen of meetcampagnes. Een tweede hindernis is dat het verdunde afvalwater tijdens of na regengebeurtenissen de toepassing van respirometrie bemoeilijken. Pogingen om de metingen te verbeteren waren niet succesvol maar het onderzoek gaf aanwijzingen dat het gebruik van dynamische modellen (m.a.w. het verhogen van het detailniveau) noodzakelijk lijkt om deze moeilijkheden te overwinnen.

In het derde deel wordt de modellering van voorbezinktanks (VBT) onderzocht. VBTs worden vaak gebruik als voorbereidende stap in een RWZI en hebben een aanzienlijke invloed op de daarop volgende processen. A literatuur studie over VBT modellen toonde aan dat de meest gebruikte modellen empirisch van aard zijn. Deze empirische modellen kunnen echter de hoge spreiding in de data van VBT verwijderingspercentages niet verklaren. Een veelbelovende benadering om de drijvende krachten van deze hoge spreiding te verklaren zijn de zogenaamde fenomenologische modellen. Dit zijn modellen die kennis van de mechanismen in het proces in rekening brengen. In dit werk werd het fenomenologisch model van Bachis et al. (2012) geïntegreerd in een wiskundig geldig discretisatie schema zoals voorgesteld door Bürger et al. (2011). Het model werd verder uitgebreid met het onderscheid tussen organisch en anorganisch materiaal. Dit wordt als cruciaal beschouwd voor de beschrijving van de daarop volgende biologische zuivering. Voor de evaluatie van de werking van de VBTs op de RWZI van Eindhoven, werd data verzameld in samenwerking met het waterschap de Dommel. Deze data verzameling omvatte routinematig verzamelde data alsook 3 specifieke meetcampagnes. Het modelleren van de biochemische reacties, door het toepassen van een aangepast ASM2d model geïmplementeerd in de software WEST, maakte het mogelijk om de onverwachte toename van ammonium en fosfaat, tijdens de meetcampagne op 6 mei 2014, te verklaren met de reacties van in het afvalwater aanwezig heterotrofe en fosfaat accumulerende micro-organismes. Het toepassen van een fysisch-chemisch model geïmplementeerd in de software PHREEQ-C, ondersteunde dan weer de hypothese van de vorming van een neerslag (hydroxyapatite) en de daaraan gekoppelde verwijdering van fosfaat die bijdraagt aan de onverwachte toename van anorganisch zwevende stoffen tijdens de meetcampagne op 2 september 2014. Ten laatste werd de impact op de volledige WZI van Eindhoven gemodelleerd en geïmplementeerd in de software WEST. Daarmee werd de invloed van de VBTs op de denitrificatie maar ook op de nitrificatie aangetoond.

In het vierde deel wordt beluchting en energie verbruik bestudeerd. Een uitgebreide meetcampagne op de WZI van Eindhoven, met gas metingen aan het water oppervlak van de reactor, onthulden hoge ruimtelijke en tijdelijke variaties in

zuurstofoverdracht efficiëntie. Het toepassen van deze nieuw verworven systeem kennis in het beluchtingsmodel leidde tot een verbeterde overeenkomst tussen model en gemeten opgeloste zuurstof concentraties. Een belangrijk gevolg was daarbij dat de voorspellingen van de ammonium concentraties verbeterd konden worden door de ammonium half-verzadigingscoëfficiënt terug op zijn originele waarde te zetten.
Voor zowel het energie verbruik van de beluchtingscompressoren en de pompen geeft een nieuw ontwikkeld dynamisch model, dat een gedetailleerde beschrijving van de systeem- en compressor- of pompcurves berekent, een verbeterde voorspelling van de dynamiek in het energieverbruik in vergelijking met de eenvoudigere constante-gemiddelde-energie-verbruik modellen die tegenwoordig vaak gebruikt worden.

Deze studie over de meer gedetailleerde modellering van de deelprocessen toonde aan dat het verbeteren van het evenwicht in detail van de model onderdelen de voorspellende kwaliteiten onder verschillende procesomstandigheden verbeterde. Daarmee rekening houdend zou een simulatie methodologie in eerste instantie de focus moeten leggen op het verbeteren van het evenwicht van de details in de verschillende model onderdelen eerder dan in het geforceerd aanpassen van de biokinetische parameters. Tot besluit, dit doctoraatswerk heeft bijgedragen tot een aanzienlijke uitbreiding van de beschikbare modellen van de tot op heden minder bestudeerde delen van de WZI en zodoende tot het verbeteren van de kwaliteit van de model voorspellingen betreffende effluent kwaliteit en energie vereisten.

Curriculum vitae

Personal details

Address	Kervijnstraat 14	Date of Birth	1 October 1974
	8531 Bavikhove	Place of Birth	Kortrijk
Phone	Tel. 0032 492 627 993	Nationality	Belgian
Email	yamerlinck@live.be	Civil status	Married, 3 children

Professional career

BIOMATH (2011-)

Ghent University, Faculty of Bioscience Engineering, Department of Mathematical modelling, Statistics and Bioinformatics, Research Group BIOMATH.

Research Assistant

Optimization of wastewater treatment using mathematical modelling to describe the multidisciplinary aspects of a complex system taking into account physics, chemistry, biology and economics.

MOSTforWATER NV (2007-2011)

Co-founder and member of the Board of Directors.

An international SME created as spin-off of Ghent University and as spin-out of HEMMIS NV. Baekeland Fonds II (a seed capital fund) and VINNOF ('Vlaams Innovatie fonds' or Enterprise Flanders) are amongst the major shareholders.

Management

Member of the management committee that takes strategic and day-today decisions on marketing, human resources, planning and finances.

Senior Consultant

Acquisition, management and execution of modelling projects worldwide. Some examples are the European (FP7) funded projects AquaFit4Use (http://www.aquafit4use.eu/) and ADD Control, update of the wastewater treatment model library of VEOLIA (France), modelling of the industrial wastewater treatment plant of Beldem in view of savings on operational costs for Cofely Services (Belgium) and modelling of a special sensor of Hitachi (Japan).

HEMMIS NV (1999-2006)
An SME active on the crossroad of environmental legislation/technology and IT.

International customer support
> Worldwide customer support and training for the modelling and simulation software WEST.

Marketing and sales
> Participation in conferences and exhibitions and the organization of promotion campaigns.

LEVI STRAUSS (1997-1998)
Wastewater treatment engineer and operator.

Education

PhD (2011-)
Doctoral school of Bioscience Engineering, Ghent University, Ghent.

Post graduate program (2007-2008)
Business management, EHSAL Management School, Brussels.

Industrial Engineer (1992-1996)
Chemistry with option Environment, University College West-Vlaanderen (Provinciale Industriële Hogeschool Kortrijk), Kortrijk.

Key Qualifications

International experience
A Broad international experience gained during attending and presenting on conferences, giving training courses (China, France, Japan, South-Africa, USA…), writing proposals for project funding and commercial meetings resulted in a large professional network.

Experienced lecturer of Courses
Teaching
> Ghent University, Assisting in the course 'Modeling and simulation of biological systems', academic year 2011-2012.

International workshops
Some examples:

Lecturer Workshop: “Advanced Hands-On Workshop on Whole Wastewater Treatment Plant Modelling “, WEFTEC 2008, Chicago, USA. Chair: Leiv Rieger, Université Laval, Co-Chair: Bruce R. Johnson, CH2M HILL.
Lecturer Training seminar: Modélisation et simulation des stations d’épurations, 23 and 24 February 2004, in collaboration with Prof. Jean-Luc Vasel (Unité Assainissement et Environnement, Fondation Universitaire Luxembourgeoise) and Prof. Peter Vanrolleghem (BIOMATH, Ghent University).
Lecturer Workshop: Modelling Aquatic systems: WISA conference 2003, Cape Town, South-Africa in collaboration with Kitty Foxon (University of Kwazulu- Natal), Sven Sotemann (University of Cape Town) and Enrico Remigi (Politecnico di Milano).

Languages

Languages	Speaking	Reading	Writing
English	5	5	5
French	4	4	3
Spanish	1	1	1
German	1	1	1
Dutch	*	*	*

Grade skill 1-5 (1 = basic, 5 = excellent, * = mother tongue)

Other

Thesis students

I have tutored the thesis work of several national and international students.

Reviewer

Water Research
Water Science & Technology

Contributions to scientific and technical reports

IWA Task Group on Benchmarking of Control Strategies for Wastewater Treatment Plants
IWA Task Group on Design and Operations Uncertainty (DOUTGroup)
IWA Task Group on the use of water quality and process models for minimizing wastewater utility greenhouse gas footprints (GHG)
IWA Task Group on a Generalized Physico-Chemical Modelling Framework

References

A1

Arnaldos, M., Y. Amerlinck, U. Rehman, T. Maere, S. Van Hoey, W. Naessens, and I. Nopens, 2014, From the Affinity Constant to the Half-Saturation Index:

Understanding Conventional Modeling Concepts in Novel Wastewater Treatment Processes: Water Research, v. In Press, Accepted Manuscript, p. 458-470.
Barrera, E. L., H. Spanjers, K. Solon, Y. Amerlinck, I. Nopens, and J. Dewulf, 2014, Modeling the anaerobic digestion of cane-molasses vinasse: extension of the Anaerobic Digestion Model No. 1 (ADM1) with sulfate reduction for a very high strength and sulfate rich wastewater: Water Research, p. 42-54.
De Keyser, W., Y. Amerlinck, G. Urchegui, T. Harding, T. Maere, and I. Nopens, 2014, Detailed dynamic pumping energy models for optimization and control of wastewater applications: Journal of Water and Climate Change, v. 5, p. 299-314.
Flores-Alsina, X., M. Arnell, Y. Amerlinck, L. Corominas, K. V. Gernaey, L. Guo, E. Lindblom, I. Nopens, J. Porro, A. Shaw, L. Snip, P. A. Vanrolleghem, and U. Jeppsson, 2014, Balancing effluent quality, economic cost and greenhouse gas emissions during the evaluation of (plant-wide) control/operational strategies in WWTPs: Science of The Total Environment, v. 466–467, p. 616-624.
Holguin-Gonzalez, J. E., P. Boets, G. Everaert, I. S. Pauwels, K. Lock, S. Gobeyn, L. Benedetti, Y. Amerlinck, I. Nopens, and P. L. M. Goethals, 2014, Development and assessment of an integrated ecological modelling framework to assess the effect of investments in wastewater treatment on water quality: Water Science & Technology, v. 70, p. 10.
Langeveld, J., I. Nopens, R. Schilperoort, L. Benedetti, J. de Klein, Y. Amerlinck, and S. Weijers, 2013, On data requirements for calibration of integrated models for urban water systems: Water Science and Technology, v. 68, p. 728-736.
Langeveld, J. G., L. Benedetti, J. J. M. de Klein, I. Nopens, Y. Amerlinck, A. van Nieuwenhuijzen, T. Flameling, O. van Zanten, and S. Weijers, 2013, Impact-based integrated real-time control for improvement of the Dommel River water quality: Urban Water Journal, v. 10, p. 312-329.
Batstone, D. J., Y. Amerlinck, G. Ekama, R. Goel, P. Grau, B. Johnson, I. Kaya, J. P. Steyer, S. Tait, I. Takacs, P. A. Vanrolleghem, C. J. Brouckaert, and E. Volcke, 2012, Towards a generalized physicochemical framework: Water Science and Technology, v. 66, p. 1147-1161.
Guo, L., J. Porro, K. R. Sharma, Y. Amerlinck, L. Benedetti, I. Nopens, A. Shaw, S. W. H. Van Hulle, Z. Yuan, and P. A. Vanrolleghem, 2012, Towards a benchmarking tool for minimizing wastewater utility greenhouse gas footprints: Water Science and Technology, v. 66, p. 2483-2495.
Belia, E., Y. Amerlinck, L. Benedetti, B. Johnson, G. Sin, P. Vanrolleghem, K. Gernaey, S. Gillot, M. Neumann, L. Rieger, A. Shaw, and K. Villez, 2009, Wastewater treatment modelling: dealing with uncertainties: Water Science and Technology, v. 60, p. 1929-1941.

Vanhooren, H., J. Meirlaen, Y. Amerlinck, F. Claeys, H. Vangheluwe, and P. Vanrolleghem, 2003, WEST: modelling biological wastewater treatment.: Journal of Hydroinformatics, v. 5, p. 23.

C1

Y. Amerlinck, G. Bellandi, A. Amaral, S. Weijers I. Nopens, 2015, Detailed off-gas measurements for improved modelling of the aeration performance at the WWTP of Eindhoven: 2nd New Developments in IT & Water Conference.

Amerlinck, Y., K. Cierkens, and I. Nopens, 2015, Application of a colour-based system analysis tool at the WWTP of Eindhoven: 2nd New Developments in IT & Water Conference.

Amerlinck, Y., K. Cierkens, and I. Nopens, 2014, A simple yet efficient colour-based system analysis tool for ASM: 4th IWA/WEF Wastewater Treatment Modelling seminar.

Amerlinck, Y., K. Cierkens, T. Flameling, S. Weijers, and I. Nopens, 2014a, A practical and sound calibration procedure applied to the WWTP of Eindhoven: IWA World Water Congress & Exhibition.

Amerlinck, Y., T. Flameling, T. Maere, S. Weijers, and I. Nopens, 2014, Modelling dissolved air flotation as pre-treatment for reaching low P effluent with activated sludge: IWA Specialist Conference - Global Challenges: Sustainable Wastewater Treatment and Resource Recovery.

Bachis, G., T. Maruéjouls, S. Tik, Y. Amerlinck, I. Nopens, P. Lessard, and P. A. Vanrolleghem, 2014, Modelling and characterisation of primary settlers in view of whole plant modelling and resource recovery: 4th IWA/WEF Wastewater treatment Modelling seminar.

Rehman, U., T. Maere, M. Vesvikar, Y. Amerlinck, M. Arnaldos, and I. Nopens, 2014, Hydrodynamic – biokinetic model integration applied to a full-scale WWTP, IWA World Water Congress & Exhibition, Lisbon, Portugal.

Amerlinck, Y., T. Flameling, T. Maere, S. Weijers, and I. Nopens, 2013, Practical application of dynamic process models for wastewater treatment plant optimization: Work in progress: WEFTEC 2013.

Torfs, E., P. Vlasschaert, Y. Amerlinck, R. Bürger, S. Diehl, S. Faras, and I. Nopens, 2013, Towards improved 1-D settler modelling: calibration of the Bürger model and case study: WEFTEC 2013.

Amerlinck, Y., W. De Keyser, G. Urchegui, and I. Nopens, 2012, A generic extension to a dynamic pumping energy model for wastewater applications: Ecotechnologies for Wastewater Treatment 2012 International Conference.

Amerlinck, Y., W. De Keyser, G. Urchegui, and I. Nopens, 2012, Realistic Dynamic Pumping Energy Models for Wastewater Applications WEFTEC 2012, p. 16.

Flores-Alsina, X., M. Arnell, Y. Amerlinck, L. Corominas, K. V. Gernaey, L. Guo, E. Lindblom, I. Nopens, J. Porro, and A. Shaw, 2012, Balancing effluent quality, economical cost and greenhouse gas emissions during the evaluation of plant-wide wastewater treatment control strategies: IWA Conference on Nutrient Removal and Recovery, p. 23-25.

Guo, L., P. A. Vanrolleghem, Y. Amerlinck, and I. Nopens, 2011, Plant-wide inspection of integrated N2O pathway models: 8th International IWA symposium System Analysis and Integrated Assessment.

Martinez, A. A., Y. Amerlinck, S. Vedantam, P. Goethals, and I. Nopens, 2011, Biokinetic modeling of a WSP in combination with a rigorous, yet simple mixing model: Waste Stabilisation Ponds, 9th IWA Specialist conference.

Porro, J., L. S. Guo, K. Sharma, L. Benedetti, S. Van Hulle, P. A. Vanrolleghem, Y. Amerlinck, Z. Yuan, A. Shaw, and I. Nopens, 2011, Towards a benchmarking tool for minimizing wastewater utility greenhouse gas footprints, 8th International IWA Symposium on Systems Analysis and Integrated Assessment in Water Management (WATERMATEX2011). San Sebastian, Spain.

Benedetti, L., A. van Nieuwenhuijzen, J. de Jonge, Y. Amerlinck, S. Plano, I. Nopens, and S. Weijers, 2010, Wet-weather Treatment Upgrade Scenarios with Sensitivity and Uncertainty Analysis at the Eindhoven WWTP: WEFTEC 2010, p. 2443-2459.

Kinnear, D., I. Nopens, M.-L. Pellegrin, T. Maere, D. Nolasco, R. Glassen, G. Insel, Y. Amerlinck, E. Bailey, E. Belia, I. Takacs, D. Houweling, P. Causey, R. Giardina, S. Murthy, P. Vanrolleghem, J. Barnard, H. Melcer, P. Krauth, R. Reardon, and J. B. Neethling, 2010, Membrane Bioreactor Life-Cycle Cost Assessment Simulation: Digital Game-Based Learning: WEFTEC 2010, p. 4336-4345.

Porro, J., Y. Amerlinck, D. Eberle, J. Daw, R. Smith, E. Becker, and I. Nopens, 2010, Using a Process Modeling and LCA Approach for Balancing Energy, Operating Costs, Greenhouse Gases, and Water Environment: WEFTEC 2010, p. 1973- 1978.

Porro, J., Y. Amerlinck, A. Shaw, P. A. Vanrolleghem, Z. Yuan, M. Kampschreur, K. Chandran, and I. Nopens, 2010, The use of dynamic water quality and process models for minimizing wastewater utillity greenhouse gas footprints: IWA Water and Energy conference.

Amerlinck, Y., J. Roels, C. Thoeye, and L. Benedetti, 2009, Model-based optimization in view of energy savings of the WWTP of Oostende: 1st IWA BeNeLux Regional Young Water Professionals Conference.
Belia, E., Y. Amerlinck, L. Benedetti, B. Johnson, G. Sin, and P. A. Vanrolleghem, 2008, Modelling accuracy: dealing with uncertainties: 1st IWA/WEF Wastewater Treatment Modelling Seminar.
Nopens, I., D. Kinnear, L. Benedetti, Y. Amerlinck, K. Gernaey, J. Comas, J. McCorquodale, P. Van Driessche, K. Essemiani, and J. De Clercq, 2008, Recent advances in clarifier modelling: 1st IWA/WEF Wastewater Treatment Modelling Seminar.
Russell, D. L., J. Dudley, and Y. Amerlinck, 2003, The US and EU's Different Approach to the Control of Waste Discharges: WEFTEC 2003, p. 710 - 729.
Amerlinck, Y., S. Gillot, and P. A. Vanrolleghem, 2001, Benchmarking WWTP control strategies with robustness and economic measures as performance criteria: WEFTEC 2001, p. 269-276.